Catalytic Activity Study of Double-Metal Cyanide Complexes for Biodegradable Polymers Synthesis

Thesis Submitted to AcSIR
for the Award of the Degree of

Doctor of Philosophy

in

Chemical Sciences

By

Joby Sebastian

(AcSIR Roll No.: 10CC11J26052)

Under the Guidance of
Dr. D. Srinivas

CSIR- National Chemical Laboratory
Pune- 411008, India

May 2015

CERTIFICATE

This is to certify that the thesis entitled ***"Catalytic Activity Study of Double-Metal Cyanide Complexes for Biodegradable Polymers Synthesis"*** submitted by ***Mr. Joby Sebastian***, for the degree of ***Doctor of Philosophy*** in ***Chemical Sciences***, was carried out under my supervision at Catalysis and Inorganic Chemistry Division, CSIR-National Chemical Laboratory, Pune – 411 008, India under Academy of Scientific and Innovative Research (AcSIR), New Delhi. Such material obtained from other sources has been duly acknowledged in the thesis.

Date: **Dr. D. Srinivas**

Place: Pune Research Guide

DECLARATION

I hereby declare that the work described in the thesis entitled ***"Catalytic Activity Study of Double-Metal Cyanide Complexes for Biodegradable Polymers Synthesis"*** submitted for the degree of ***Doctor of Philosophy*** in ***Chemical Sciences*** to the Academy of Scientific and Innovative Research (AcSIR), New Delhi, has been carried out by me at the Catalysis and Inorganic Chemistry Division, CSIR-National Chemical Laboratory, Pune–411008, India under the supervision of ***Dr. D. Srinivas***. I further declare that the material obtained from other sources has been duly acknowledged in this thesis. The work is original and has not been submitted in part or full by me for any other degree or diploma to this or any other university.

Date: **Mr. Joby Sebastian**

Place: Pune Research Scholar

..... dedicated to my parents

No one has ever been given more loving and unconditional support than I have been given by you.

Acknowledgements

To my great delight I would like to express my heart-felt gratitude to Dr. D. Srinivas for providing me the admirable opportunity to take the first step in scientific research under his guidance. I thank him for his excellent guidance, constant encouragement, and sincere advice when I was both on and off the road. His suggestions always added a third dimension to everything I subsequently read. I consider very fortunate for my association with him which has given a decisive turn and a significant boost in my career.

I thank Dr. Sourav Pal, Director and D. Sivaram (Ex-director), CSIR-NCL, Pune for giving me the opportunity to work in this institute and exploit all the infrastructural facilities needed for my research work.

I thank the Council of Scientific and Industrial Research, New Delhi for the research fellowship.

I am grateful to Dr. A. P. Singh (Ex-head), Catalysis division, for letting me to access all the divisional facilities for the research work.

I am lucky enough to have critical suggestions and timely help from Dr. P. Wadgaonkar, Dr. C. V. Rode, Dr. P. A. Joy, Dr. N. N. Joshi, Dr. C.V. Avadhani, Dr. B.B Idage and Dr.(Mrs.) S.B.Idage. Their interest, positive approach and stable support have always been a source of encouragement to me.

I sincerely thank Mrs. D. A. Dhoble, Mrs. P. Purohit, Mr. S. Menon, Dr. M. G. Kulkarni and Central NMR facility for help in polymer characterization. I also express my gratitude to Dr. R. Nandini Devi, Dr. S.B Umbarkar, Dr. C. V. V. Satyanarayana, Ms. Violet Samuel, Dr. S. P. Mirajkar, Dr. (Mrs.) S. S. Deshpande, Mr. R. K. Jha, Dr. R. S. Somani (CSIR-CSMCRI, Bhavnagar, India) for help in catalyst characterization. Many thanks to Mr. P. K. Purushothaman, Mr. Madhu and Mr. Milind for their help and cooperation in official matters during these years.

Many thanks to my labmates, Dr. Jithendra, Dr. Anuj, Dr. Bhogesh, Dr. Mehejabeen, Unni, Devadutta, Sagar, Anthony, Vikram and Sreenavya for their patience, friendship, humour, arguments, understanding, discussions and of course, for enduring my eloquence.

I miss if did not thank many people who accompanied and accommodated me. Thanks to Rahul, Sabarish, Vishal, Poonam, Chitra, Ravindra, Dr. Thushara, Dr. Edwin, Raja Ambal, Devaraji, Dr. Narasimha, Nishita, Dr. Deepa, Anup, Pavan, Ashok, Lenin, Mohan, Ashish, Dr. Ajay, Dr. Prakash, Narendra, Anjani, Sanoop, Srikant, Dhanraj, Pravin Shinde, Prajitha, Sreekuttan and Sarath.

Thanks to Sr. Arpitha, Sr. Gildas and Sr. Modhini for keeping me in your prayers all the time and encouraging me with spiritual words ("I can do all this through him who gives me strength", Philippians 4:13).

So much love and thanks to my parents, my brother and his family for their continuing understanding and sacrifice in support of my education. Their support and love encouraged me to look optimistically into the future even in my stressful times.

Joby Sebastian

Abbreviations

AA	Adipic acid
BET	Brunauer, Emmett and Teller
BJH	Barrett-Joyner-Halenda
^{13}C	Carbon (atomic weight = 13)
CHO	Cyclohexene oxide
CMM	Couple-monomer methodology
CP-MAS	Cross polarization- magic angle spinning
DB	Degree of branching
DEPT	Distortionless enhanced polarization transfer
DMC	Double metal cyanide
DMM	Double monomer methodology
DSC	Differential scanning calorimetry
DRIFT	Diffuse reflectance infrared Fourier transform spectroscopy
EDX	Energy dispersive X-ray analysis
F_{CO2}	Percentage incorporation of CO_2
FTIR	Fourier transform infrared spectroscopy
G	Glycerol
GPC	Gel permeation chromatography
^{1}H	Hydrogen (atomic weight = 1)
HMBC	Heteronuclear multiple quantum correlation
HP	Hyperbranched polymers
HRTEM	High resolution transmission electron microscopy
HSQC	Heteronuclear single quantum correlation
MALDI-TOF	Matrix assisted laser desorption/ ionization time- of- flight mass spectrometry
MBL	α-methylene-γ- butyrolactone
MMA	Methylmethacrylate
MMBL	γ-methyl-α-methylene-γ-butyrolactone
M_n	Number average molecular weight
M_w	Weight average molecular weight
NMR	Nuclear magnetic resonance spectroscopy
NOE	Nuclear overhauser effect

PC	Propylene carbonate
PCHC	Poly(cyclohexene carbonate)
PDI	Polydispersity index
PEG	Polyethylene glycol
PO	Propylene oxide
PMMA	Polymethylmethacrylate
PPC	Poly(propylene carbonate)
SA	Succinic acid
SEM	Scanning electron microscopy
SMM	Single monomer methodology
t-BuOH	Tert-butanol
T_g	Glass transition
TG	Thermogravimetry
TOF	Turn over frequency
TPD	Temperature programmed desorption
XRD	X-ray diffraction
η	Viscosity

Table of Contents

Chapter-1: General Introduction 1

1.1. Introduction 2
1.1.1. Classification of biodegradable polymers 2
1.1.2. Mechanism of biodegradation 3
1.2. Biodegradable polymers from renewables 4
1.3. Hyperbranched polymers 7
1.3.1. Applications of HPs 8
1.3.2. History of HPs 9
1.3.3. Synthetic methodologies of HPs 10
1.3.4. The $A_2 + B_3$ methodology 10
1.3.5. Catalysts for $A_2 + B_3$ polymerization 11
1.4. Carbon dioxide utilization 13
1.4.1. Conditions for using CO_2 as a reactant 15
1.4.2. Aliphatic polycarbonates 17
1.4.2.1. History of polycarbonates 17
1.4.2.2. Catalysis in copolymerization of CO_2 and epoxides 19
1.4.2.3. Thermal and mechanical properties of polycarbonates 23
1.4.2.4. Applications of polycarbonates 24
1.5. Double-metal cyanides 24
1.5.1. Structural evolution in DMCs 25
1.5.2. Applications of DMCs 28
1.5.3. DMCs in polycarbonate synthesis 28
1.5.3.1. DMCs in PPC synthesis 28
1.5.3.2. DMCs in PCHC synthesis 30
1.6. Scope and objectives of the present work 31
1.7. Organization of thesis 31
1.8. References 33

Chapter-2: Experimental Methods and Characterization Techniques 40

2.1. Introduction 41
2.2. Catalyst preparation 41
2.2.1. Fe-Zn DMC catalysts 41

2.2.1.1. Fe-Zn-0 41
2.2.1.2. Fe-Zn-1 42
2.2.1.3. Fe-Zn-2 42
2.2.1.4. Fe-Zn-3 42
2.2.1.5. Fe-Zn-4 42
2.2.1.6. Fe-Zn-5 42
2.2.1.7. Fe-Zn-6 43
2.2.1.8. Fe-Zn-7 43
2.2.1.9. Fe-Zn-8 43
2.2.2. Co-Zn DMC catalysts 43
2.2.2.1. Co-Zn-0 43
2.2.2.2. Co-Zn-1 43
2.2.2.3. Co-Zn-2 44
2.2.2.4. Co-Zn-3 44
2.2.2.5. Co-Zn-4 44
2.2.2.6. Co-Zn-4-1 45
2.2.2.7. Co-Zn-4-2 45
2.3. Characterization techniques 45
2.3.1. X-ray diffraction 45
2.3.2. Fourier transform infrared spectroscopy 46
2.3.3. Raman spectroscopy 46
2.3.4. N_2 / CO_2 physisorption 47
2.3.5. Thermogravimetry 48
2.3.6. Scanning electron microscopy 49
2.3.7. High resolution transmission electron microscopy 50
2.3.8. Nuclear magnetic resonance spectroscopy 50
2.3.9. Temperature-programmed desorption 51
2.4. Reaction procedure 52
2.4.1. Synthesis of hyperbranched polyesters 52
2.4.2. Copolymerization of CHO and CO_2 52
2.4.3. Copolymerization of PO and CO_2 53
2.4.4. Terpolymerization of PO, CHO and CO_2 54
2.5. Product analysis 54

2.5.1. Hyperbranched polyesters 54
2.5.1.1. Nuclear magnetic resonance spectroscopy 54
2.5.1.2. Inherent viscosity 56
2.5.1.3. Matrix assisted laser desorption/ ionization time-of-flight mass spectrometry 57
2.5.2. PCHC/ PPC/ Terpolymer 57
2.5.2.1. Nuclear magnetic resonance spectroscopy 57
2.5.2.2. Gel permeation chromatography 60
2.5.2.3. Differential scanning calorimetry 61
2.5.2.4. Thermogravimetry 62
2.5.2.5. Fourier transform infrared spectroscopy 62
2.5.2.6. X-ray diffraction 62
2.6. References 62

Chapter-3: Synthesis of Hyperbranched Polyesters from Glycerol and Diacids over Fe-Zn DMC Catalysts 64

3.1. Introduction 65
3.2. Experimental 66
3.3. Results and discussion 67
3.3.1. Structural characterization 67
3.3.1.1. XRD 67
3.3.1.2. FTIR 68
3.3.1.3. N_2–physisorption 71
3.3.1.4. SEM 71
3.3.1.5. HRTEM 71
3.3.1.6. DRIFT spectroscopy of adsorbed pyridine 74
3.3.1.7. NH_3-TPD 74
3.3.2. Catalytic activity 75
3.3.2.1. Effect of reaction temperature 79
3.3.2.2. Effect of reaction time 80
3.3.2.3. Effect of molar ratio of reactants 81
3.3.3. Product characterization 82
3.3.3.1. 2D NMR 82
3.3.3.2. MALDI-TOF 82

3.3.3.3. FTIR 85
3.3.3.4. EDX 85
3.3.4. Catalyst reusability 86
3.3.5. Reaction mechanism 88
3.4. Conclusions 90
3.5. References 90

Chapter-4: Copolymerization of Cyclohexene Oxide and Carbon Dioxide over Co-Zn DMC Catalysts 92

4.1. Introduction 93
4.2. Experimental 95
4.3. Results and discussion 96
4.3.1. Structural characterization 96
4.3.1.1. XRD 96
4.3.1.2. FTIR 98
4.3.1.3. Raman spectroscopy 102
4.3.1.4. CP-MAS NMR 104
4.3.1.5. TG- FTIR 104
4.3.1.6. TG 104
4.3.1.7. EDX 107
4.3.1.8. DRIFT spectroscopy of adsorbed pyridine 107
4.3.1.9. NH_3-TPD 109
4.3.1.10. SEM 109
4.3.2. Catalytic activity 109
4.3.2.1. Effect catalyst quantity 115
4.3.2.2. Effect reaction temperature 116
4.3.2.3 Effect of reaction pressure 116
4.3.2.4. Effect reaction time 116
4.3.3. Product characterization 118
4.3.3.1. ^{13}C NMR 118
4.3.3.2. FTIR 118
4.3.3.3. TG 119
4.3.3.4. DSC 119
4.3.3.5. XRD 119

4.3.4. Reusability 121
4.3.5. Structure activity correlations 121
4.3.5.1. Structure of DMC complexes 121
4.3.5.2. Reaction mechanism 122
4.4. Conclusions 124
4.5. References 124

Chapter-5: Copolymerization of Propylene Oxide & CO_2 and Terpolymerization of Propylene Oxide, Cyclohexene Oxide & CO_2 over Co-Zn DMC Catalysts 126

5.1. Introduction 127
5.2. Experimental 129
5.3. Results and discussion 129
5.3.1. Structural characterization 129
5.3.2. Catalytic activity 130
5.3.2.1. Structure- activity correlations 134
5.3.2.2. Reaction mechanism 136
5.3.3. Product characterization 136
5.3.3.1. ^{13}C NMR 136
5.3.3.2. TG 138
5.3.3.3. DSC 138
5.4. Conclusions 138
5.5. Terpolymerization of CHO, PO and CO_2 138
5.5.1. Catalytic activity 139
5.5.2. Product characterization 143
5.5.2.1. ^{1}H NMR 143
5.5.2.2. DSC 145
5.5.2.3. ^{13}C NMR 146
5.5.2.4. TG 147
5.5.2.5. XRD 149
5.5.3. Effect of reaction parameters 149
5.5.3.1. Effect of reaction temperature 149
5.5.3.2. Effect of reaction pressure 149
5.5.3.3. Effect of catalyst quantity 151
5.5.3.4. Effect of reaction time 151

5.5.3.5. Effect of molar ratio of epoxides 153
5.5.4. Reaction mechanism 153
5.6. Conclusions 154
5.7. References 155

Chapter-6: Summary and Conclusions 157

List of Publications and Patents 162

List of Figures

Fig. No.	Figure Caption	Page No.
1.1.	Global bio-based biodegradable plastics market for 2016	2
1.2.	2-Glutaric acid and its derivates from biomass as monomers for polyesters/amides	5
1.3.	Members of the dendritic family	8
1.4.	Current research and technologies ordained towards the capture, storage and chemical transformations of CO_2	14
1.5.	Number of scientific publications on aliphatic polycarbonates in past decades	18
1.6.	Single site homogeneous catalysts of polycarbonates synthesis: (a) tetraphenylporphyrin AlOMe, (b) zinc β-diiminate acetate and (c) (salen)Cr(III)Cl.	20
1.7.	Structure of (a) cubic $Zn_3[Co(CN)_6]_2$, (b) porous framework of $Zn_2[Fe(CN)_6]$ $2H_2O$ and (c) cavity at the surface of hexagonal zinc hexacyanometallates	27
1.8.	Tentative structure of Fe-Zn DMC catalyst	29
2.1.	^{13}C NMR (top) and DEPT (bottom) spectra of Glycerol-Succinic acid hyperbranched polyester	55
2.2.	^{1}H NMR spectrum of PCHC	58
2.3.	^{1}H NMR spectrum of PPC	59
2.4.	^{1}H NMR spectrum of terpolymer	60
3.1.	XRD patterns of Fe-Zn DMC catalysts	68
3.2.	Representative FTIR spectra of Fe-Zn-4, Fe-Zn-5 and Fe-Zn-6 catalysts	70
3.3.	N_2-physisorption isotherms (top) and pore size distributions (bottom) of Fe-Zn-4, Fe-Zn-5 and Fe-Zn-6	72
3.4.	SEM images of (a) Fe-Zn-0, (b) Fe-Zn-1, (c) Fe-Zn-2, (d) Fe-Zn-3, (e) Fe-Zn-4, (f) Fe-Zn-5, (g) Fe-Zn-6, (h) Fe-Zn-7 and (i) Fe-Zn-8	73
3.5.	HRTEM of Fe-Zn-4 showing mesopores	74
3.6.	Py-DRIFT spectrum of Fe-Zn-4 recorded at 150 °C	75
3.7.	NH_3-TPD profile of Fe-Zn-4	75

3.8.	Dependence of catalytic activity on total acidity (top) and average crystallite size (bottom) of Fe-Zn DMC catalysts	78
3.9.	Thermogravimetric analysis of Fe-Zn-4 and Fe-Zn-5	80
3.10.	2D NMR spectra of G-SA polymer	83
3.11.	MALDI-TOF spectra of G-SA (top) and G-AA (bottom) polymers	84
3.12.	FTIR spectrum of G-SA polymer	86
3.13.	EDX spectrum of G-SA polymer	86
3.14.	XRD (top) and FTIR (bottom) of fresh and reused Fe-Zn-4	87
3.15.	Tentative reaction mechanism of polyesterification over Fe-Zn DMC catalyst	89
4.1.	XRD patterns of Co-Zn DMC complexes. Peaks due to cubic (♦) and monoclinic (*) phases are marked	97
4.2.	XRD patterns: (a) Co-Zn-4, $ZnCl_2$ and $K_3[Co(CN)_6]$, (b) Co-Zn-x and Co-Zn-xa (before and after thermal activation, respectively, at 180 °C for 2 h) and (c) as-synthesized Co-Zn-4 (i), after thermal treatment at 180 °C for 2 h (ii) and after thermal activation at 180 °C for 4 h (iii)	99
4.3.	FTIR spectra of Co-Zn DMC catalysts	101
4.4.	FTIR (left) and Raman (right) spectra in the ν(C≡N) region in DMC catalysts	102
4.5.	CP-MAS spectra of Co-Zn DMC catalysts	103
4.6.	(a) TG-FTIR of Co-Zn-1 at various temperatures and (b) TG curves of various Co-Zn DMC catalysts	105
4.7.	(a) DRIFT spectroscopy of adsorbed pyridine and (b) NH_3-TPD of Co-Zn-4	108
4.8.	SEM images of Co-Zn DMC catalysts: (a) Co-Zn-0, (b) Co-Zn-1, (c) Co-Zn-2, (c) Co-Zn-3 and (d) Co-Zn-4	110
4.9.	Time on stream activity of Co-Zn DMC catalysts	113
4.10.	CO_2 adsorption isotherms of Co-Zn-1, Co-Zn-2 and Co-Zn-4	114
4.11.	Effect of reaction parameters on the induction period of Co-Zn-4: (a) catalyst quantity, (b) reaction temperature and (c) reaction pressure.	117
4.12.	Inverse-gated ^{13}C NMR spectrum of PCHC synthesized over Co-Zn-4. Inset shows the polymer produced	118
4.13.	FTIR spectrum of PCHC	119

4.14.	(a) TG, (b) DSC and (c) XRD of PCHC	120
4.15.	XRD of fresh and recycled Co-Zn-4	121
4.16.	Reaction mechanism for copolymerization of CHO and CO_2 over Co-Zn-4	123
5.1.	Time on stream activity of Co-Zn DMCs for the copolymerization of PO and CO_2	133
5.2.	Tentative reaction mechanism of copolymerization of PO and CO_2	135
5.3.	Inverse-gated ^{13}C NMR spectrum of PPC synthesized over Co-Zn-2	136
5.4.	(a) TG and (b) DSC of PPC synthesized over Co-Zn-2	137
5.5.	Time on stream activity of Co-Zn DMCs for the terpolymerization	142
5.6.	^{1}H NMR spectrum of terpolymers obtained over Co-Zn DMCs in the carbonate and ether regions. (a) PPC + PCHC and polymers obtained using (b) Co-Zn-1, (c) Co-Zn-2, (d) Co-Zn-3 and (e) Co-Zn-4. Inset shows produced polycarbonates	144
5.7.	DSC of terpolymers produced over (a) Co-Zn-1, (b) Co-Zn-2, (c) Co-Zn-3 and (d) Co-Zn-4	146
5.8.	Inverse-gated ^{13}C NMR spectra of (a) physical blend and terpolymers synthesized over (b) Co-Zn-1, (c) Co-Zn-2, (d) Co-Zn-3 and (e) Co-Zn-4	147
5.9.	TG of terpolymers synthesized over (a) Co-Zn-1, (b) Co-Zn-2, (c) Co-Zn-3 and (d) Co-Zn-4	148
5.10.	PXRD of terpolymers synthesized over (a) Co-Zn-1, (b) Co-Zn-2, (c) Co-Zn-3 and (d) Co-Zn-4	148
5.11.	Effect of reaction parameters on induction period of Co-Zn-4 DMC catalyst. (a) temperature, (b) CO_2 pressure, (c) catalyst quantity and (d) mol% of PO	152
5.12.	(a) Effect of mol% of PO on output mol% of PPC and (b) wt% of PC produced	152
5.13.	Tentative reaction mechanism for terpolymerization of PO, CHO and CO_2	154

List of Schemes

Scheme No.	Scheme Caption	Page No.
1.1.	Polymerization of polar vinyl monomers	5
1.2.	Low energy processes for the conversion of CO_2	17
1.3.	Synthesis procedures of aliphatic polycarbonates	19
2.1.	Synthesis of hyperbranched polyesters from glycerol and succinic acid	52
2.2.	Copolymerization of CHO and CO_2	53
2.3.	Copolymerization of PO and CO_2	53
2.4.	Terpolymerization of PO, CHO and CO_2	54

List of Tables

Table No.	Table Caption	Page No.
1.1.	Statistics of CO_2 discharge from industries	13
1.2.	Figures of CO_2 utilization in various chemical syntheses	15
1.3.	Thermal and mechanical properties of different polycarbonates	23
2.1.	Various branching segments of hyperbranched polyester and their chemical shifts	56
3.1.	Nomenclature of DMC catalysts and the complexing and co-complexing agents used in their synthesis	67
3.2.	Physicochemical characteristics of Fe-Zn DMC catalysts	69
3.3.	Catalytic activity of Fe-Zn DMC: Polyesterification of glycerol with succinic acid	76
3.4.	Effect of reaction parameters on the catalytic activity of Fe-Zn-4	81
3.5.	Suggested branched segments of G-SA and G-AA polymers	85
4.1.	Physicochemical properties of Co-Zn DMC catalysts	106
4.2.	Catalytic activity of Co-Zn DMC catalysts for polycarbonate synthesis	111
4.3.	Influence of reaction parameters on the catalytic activity of Co-Zn-4	115
5.1.	Catalytic activity of Co-Zn DMCs for PO/CO_2 copolymerization	131

5.2.	Catalytic activity of Co-Zn DMCs for the terpolymerization of PO, CHO and CO_2	140
5.3.	Effect of reaction parameters on catalytic activity of Co-Zn-4 during terpolymerization	150

Chapter - 1

General Introduction

1.1. Introduction

The remarkable development in the field of science and technology has brought out many advanced materials to the world. Among them, polymers with their incredulous tunable properties compared to conventional materials dominate every aspects of day today life. Their fascinating physical properties of strength and light weight made them more versatile. At the same time, their attained durability raised concerns about environmental pollution. This predicament has led to the concept of degradable polymers [1]. Biodegradable polymers are macromolecules of any class such as linear, cross-linked, chain branched or dendrimers that break down after their targeted purpose into environmentally friendly natural products consisting of gases like CO_2 and N_2, water, biomass and inorganic salts by microorganisms or by any natural forces such as light, heat or stress. Scientific innovations and developments are now focussing on the implementation of the concept of biodegradable polymers in every field of polymer application [2]. Fig. 1.1 shows the global forecast of the application of bio-based, biodegradable polymers for the year of 2016, where major attention has been given to packaging due to littering problems [3].

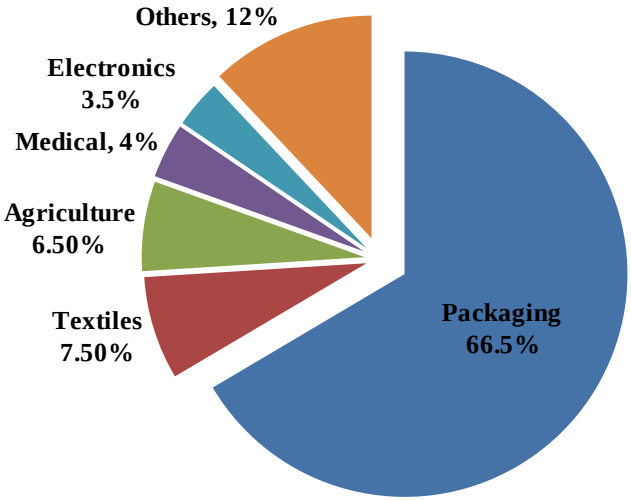

Fig. 1.1. Global bio-based, biodegradable plastics market for 2016 [3].

1.1.1. Classification of biodegradable polymers

Biodegradable polymers are classified mainly into two families based on their origin: (a) natural polymers - polymers from natural resources and (b) synthetic polymers - polymers synthesized from crude oil. Natural polymers are further sub-divided into six classes, based on the chemical point of view [4]. They are,

1. Polysaccharides (starch, cellulose, lignin and chitin),
2. Proteins (gelatine, casein, wheat gluten, silk and wool),

3. Lipids (plant oils including castor oil and animal fats),
4. Polyesters produced by microorganisms or by plants (polyhydroxyalkanoates, poly-3-hydroxybutyrate),
5. Polyesters from renewables (polylactate), and
6. Miscellaneous polymers (natural rubber, composites, etc).

Synthetic biodegradable polymers are classified into four categories [4], viz.,

1. Aliphatic polyesters (polygylcolate, polybutylene succinate and polycaprolactone),
2. Aromatic polyesters or blends of aliphatic and aromatic polyesters (polybutylene succinate terephthalate, polyesters containing hydrolysis sensitive groups such as ethers, amides and aliphatic chains),
3. Polyvinylalcohols, and
4. Modified polyolefins (polyethylene or polypropylene with specific chemical agents sensitive to temperature or light for easy degradation).

In addition, biodegradable polymers are more specifically categorized based on their chemical composition, synthesis method, processing method, economic importance, application, etc [4]. Each of these classifications provides different useful information.

1.1.2. Mechanism of biodegradation

Most of the petroleum-based (synthetic) polymers are carbon and hydrogen rich. Due to this inbuilt hydrophobicity, they are inert towards microorganisms. In order for that the carbon nutrients in polymer to be made available for biological cells, these polymers are first introduced to a set of various chemical transformations which allows surface erosion by oxidative enzymes. Most often, this initiation step is favoured by normal abiotic mechanisms of organic (hydrolysis) and physical (auto oxidation) chemistry. Hydrolysis is favoured in polymers with hetero atoms such as polyesters, polyamides and polyurethanes. Most synthetic biodegradable polymers consist of hydrolysable groups in their backbone. Auto oxidation is the principle initiation step for degradation in high carbon chain polymers [2, 5, 6]. The main factors influencing the biodegradability of synthetic polymers are: (i) presence of hydrolysable and/or oxidisable linkages, (ii) presence of suitable substituents, (iii) right kind of stereo-configuration, (iv) balance of hydrophobicity and hydrophilicity, and (v) conformational flexibility. At the same time, rate of biodegradation is governed by the morphology of the polymer. A diffuse mode of degradation is observed for hydrolysable polymers where the amorphous region of the polymer degrades first followed by the crystalline and highly cross-linked regions as these regions are less accessible to the degradants [7].

1.2. Biodegradable polymers from renewables

Synthetic and semi-synthetic polymers are conventionally prepared from monomers derived from the downstream processing of non-renewable fossil resources. The dwindling nature of petroleum resources has now directed the research in both academia and industry towards renewable resources as alternatives. Use of renewable feedstock for chemical production has several advantages which include: (i) lesser dependence on fossil feedstock, (ii) renewable nature of the raw material, (iii) carbon neutrality, (iv) eco-friendliness, (v) employment to rural population, (vi) economic growth of the country and (vii) possibility of having new building blocks for novel applications [8]. Thus, synthesis of biodegradable polymers from renewables represents a smart practice in terms of developing benign and sustainable chemical processes. Among the four classes of synthetic biodegradable polymers, aliphatic polyesters are well recommended over the others since their hydrolytic or enzymatic cleavage results in easily metabolisable hydroxyl-carboxylic acids [9]. Among renewable resources, biomass represents an abundant and carbon-neutral resource for biodegradable polymers. Statistics explains that out of the 200 billion tons/year of biomass produced by photosynthesis, only 3.5% is used by mankind [10]. This gives an opportunity for experimentalists to design new chemical transformations from biomass to diverse monomers for polymer synthesis. Bozell et al [11] has conceptualized a reaction scheme for the production of 2-ketoglutaric acid and their derivatives as feedstock monomers to fabricate various aliphatic polyesters and polyamides as shown in Fig. 1.2. The reaction profile makes use of enzymatic and chemical pathways for the monomer generation. The well-known citric acid cycle was the central process adopted for degradation of biomass into 2-ketoglutatric acid (produced as intermediate in the metabolic process of cellular respiration). By the assistance of chemical transformations, making use of catalysts, 2-ketoglutaric acid is then derivatized into different monomers for the design of various aliphatic polyesters and polyamides [11].

Another most promising and widely utilized biodegradable polymer from biomass is polylactic acid. The monomer, lactic acid is obtained from corn or sugar beets by the enzymatic or chemical processes. These polyesters are now commercialized as a replacement for non-biodegradable polyolefin based polymers. Further, polylactic acid is completely recyclable and its physical and mechanical properties are well tunable by modification of the main chain architecture (through branching, cross-linking, etc.) [12].

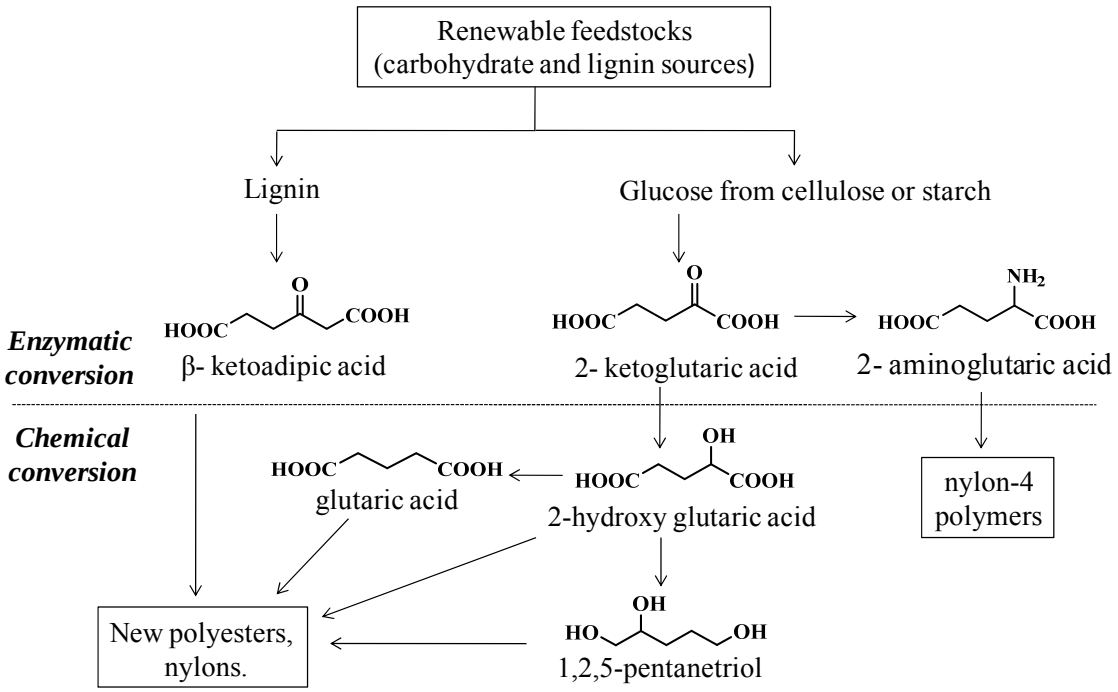

Fig. 1.2. 2-Glutaric acid and its derivates from biomass as monomers for polyesters/amides.

Polymethylmethacrylate (PMMA) containing pendent ester groups is one of the most studied transparent thermoplastics for light weight or shatter resistant applications. PMMA is now available in more specified *iso*, *syndio* and *actactic* forms finely controlled by the choice of catalyst system used. Conventionally, it is prepared from methylmethacrylate (MMA) molecules [13]. A sustainable substitute for non-renewable MMA is vinylbutyrolactones. Vinylbutyrolactones are renewable and biomass-derived, of which α-methylene-γ-butyrolactone (MBL, Tulipalin A) is isolated from tulip flowers [14] (Scheme 1.1). A methyl derivative of MBL, γ-methyl-α-methylene-γ-butyrolactone (MMBL) is currently synthesized by Dupont from biomass derived levulinic acid in a two step process [15]. These PMBL and PMMBL polymers contain pendent cyclic ester groups instead of linear ones found in PMMA. This gives them better durability, higher refractive index and higher glass transition temperature than PMMA to be used as environmentally friendly thermoplastic elastomers [14, 15].

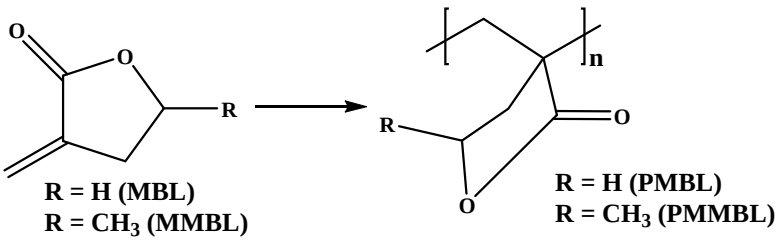

Scheme 1.1. Polymerization of polar vinyl monomers.

Recently, non-edible plant oils have been documented as another practical source of renewable feedstock for the polymer industry. Vegetable oils are composed of triglycerides and their hydrolysis gives glycerol (1 mol) and fatty acids (3 moles). Both these molecules are considered as monomers for the synthesis of biodegradable polymers. The fatty acids generally found in vegetable oils are palmitic acid, stearic acid (saturated) and oleic acid, linoleic acid & linolenic acid (unsaturated). Saturated acids containing one functional group does not constitute as monomers for polymerization. Unsaturated acids with one or more double bonds can be either homopolymerized or can be copolymerized to biopolymers, biocomposites and biocoatings [16]. Ricinoleic acid, a derivative of linoleic acid found in castor oil (one double bond is hydrolysed) is another interesting monomer as it contains three different functional groups (one -OH, one -COOH and one double bond). It can be either homopolymerized to get aliphatic polyester or polyricinoleic acid, or copolymerized with other suitably selected monomers containing -OH, -COOH and double bond to get novel, biodegradable polymers [17-20]. Biopolyamides prepared from castor oil are now commercially available from companies like Arkema (Rilsan-PA11), Rhodia (Technyl-eXten) and BASF (Ultramid-Balance) [21].

Hydrolysis and transesterification of triglycerides (biodiesel process) generate huge amount of glycerol as by-product. For every 9 kg of biodiesel produced, 1 kg of glycerol is generated as side product. Wide industrialization of biodiesel produces glycerol in excess as compared to its current consumption in food, pharmaceutical, cosmetics, and many other industries [22]. Glycerol was recognized by US department of energy as one of the top 12 building blocks from biomass in 2004 [23]. Although there are plenty of chemical transformations available for glycerol utilization (e.g. oxidation, reduction, hydrogenolysis, etc.), polymerization of glycerol to polyethers and polyesters represents an efficient and sustainable way to exploit this renewable feedstock. Rokicki et al [24] synthesized hyperbranched polyglycerols by the ring opening polymerization of glycerol carbonate using trimethlylolpropane as the initiator. The monomer glycerol carbonate was prepared by the transesterification of glycerol with dimethyl carbonate. Hyperbranched polyglycerols are used as amphiphilic material for biomedical applications such as drug carriers, molecular labels or probe moieties and hydrogels, after esterification of the terminal -OH group with hydrophobic groups [25, 26]. Glycerol has also been used for the synthesis of hyperbranched polyesters by the reaction with aliphatic diacids such as succinic, adipic and sebacic acids [27]. Dendritic polyesters composed of glycerol and succinic acid are used as a cover for linear laceration in eye treatment [28].

Incorporation of carbon dioxide (CO_2) into polymeric matrixes like the synthesis of polycarbonates represents another sustainable process for the effective utilization of this green house gas feedstock to biodegradable polymers of great environmental adaptability. Copolymerization of CO_2 with epoxides like propylene oxide (PO) and cyclohexene oxide (CHO) is a thriving field in academic research. Polycarbonates find various applications as environmentally friendly packaging materials, lithographic applications, binder for ceramics, adhesives, etc [29]. Another efficient way to make use of this feedstock is to synthesize cyclic carbonates. Ring-opening polymerization of these cyclic carbonates into aliphatic polycarbonates of novel properties and applications is a practicing scheme around the world. Brignou et al [30] suggested the synthesis 7-membered cyclic carbonates from biomass derived levulinic and itaconic acids monomers for the ring-opening polymerization to biodegradable aliphatic polycarbonates.

1.3. Hyperbranched polymers

Branching is a common and important phenomenon in cosmos. It is universal and ranges from light years (Crab Nebula) to kilometers (river basins) to macro meters (trees, nerves) to micro meters and down to nanometers (nervures, proteoglycan). It is an effective and efficient way of the transfer, dissipation and distribution of energy and mass. Today polymers are available in various architectures such as linear, chain-branched, cross-linked, cyclic, star-like, ladder-like, dendritic, comb-like, cyclic brush-like, sheet-like, tubal and supramolecular interlocked. Except linear, cyclic and interlocked polymers, all others possess branching, highlighting its significance in macromolecular chemistry. Hyperbranched polymers (HPs) are randomly branched polymeric architectures belonging to the fourth major class of polymers - dendritic polymers [31, 32]. Dendritic family consists of eight sub-classes: (a) dendrons and dendrimers, (b) linear - dendritic hybrids, (c) dendronized polymers, (d) dendrigrafts, (e) hyperbranched polymers, (f) hyperbranched polymer brushes, (g) hyperbranched polymer - grafted linear macromolecules and (h) hypergrafts or hyperbranched polymer - star macromolecules (Fig. 1.3). The main structural disparity between dendrimers and HPs is the following. Dendrimers (a, b, c and d sub-classes) are 3-dimensional globular molecules with highly symmetric structures and 100% degree of branching (DB), while HPs (e, f, g and h sub-classes) are 3-dimensional ellipsoidals with asymmetric structure and DB ranging from 40 to 60%. Although, they are structurally different, their functional groups and chemical properties like solubility and reactivity are similar. Dendrimers are synthesized based on the convergent and divergent methodologies

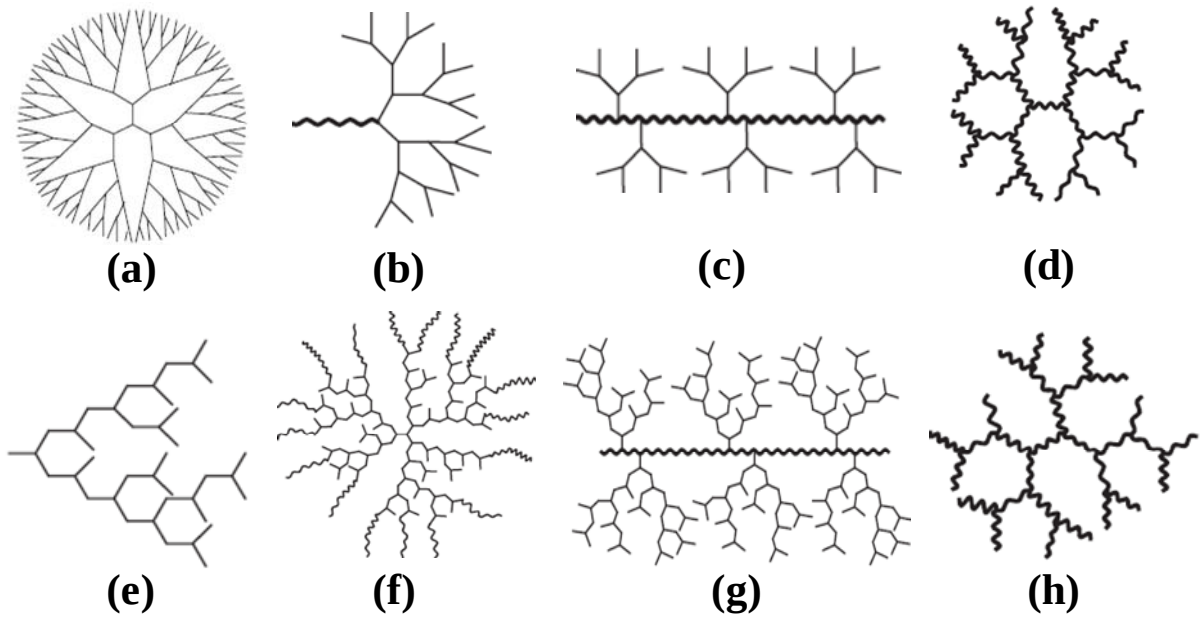

Fig. 1.3. Members of the dendritic family: (a) dendrimer, (b) linear dendritic hybrid, (c) dendronized polymer, (d) dendrigraft, (e) hyperbranched polymer, (f) hyperbranched polymer brushes, (g) hyperbranched grafted polymer and (h) hypergraft [31].

which involve protection of functional groups, its deprotection and chromatographic separation in each synthesis step. HPs, on the other hand, are usually synthesized by a single step with purification by simple precipitation. Due to these advantages and scaling up opportunities, HPs are finding increased scientific attention than dendrimers [31]. HPs have high level of solubility and compatibility, low solution viscosity, resistance to aggregate even in concentrated solutions, ability to function as nano containers for substances encapsulated inside, weak dependence of hydrodynamic volume on molecular weight and lump of free ends of chains with functional groups on their periphery for post modifications [33, 34]. HPs derived from renewables broaden their versatility and acceptance as novel and environmentally friendly polymeric materials of great potential.

1.3.1. Applications of HPs

On the basis of their unique structure-derived properties, HPs find promising applications as additives, coatings, gene/drug carriers, nano reactors, nano capsules, sensors, electron/energy/light harvesting, catalysts, etc [31]. HPs can be used to encapsulate guest molecules in their cavities. In this regard, drugs, dyes, metal complexes and inorganic nano particles have been successfully hosted by amphiphilic HPs such as hyperbranched polyglycerol, poly(amidoamine), poly(sulfoneamine) and poly(ester amide) [35, 36]. HPs can also be designed to trap selective molecules from mixtures and release them under certain

conditions (pH and light). This extends their applicability for sequestration of harmful and waste molecules in the context of environmental protection. Regardless of their irregular structures and randomly branched units, HPs show supra-molecular self assembly behaviours. Supramolecular self assemblies of HPs of macroscopic to nano scale have been achieved in various morphologies and with different functions. Multi-arm HP vesicles are used as model membranes to mimic the fusion and fission behaviours of cells [37]. Supramolecular self assembly of dye loaded hyperbranched poly(amidoamine) as large honey comb-like films was used for strong fluorescence [38]. Hyperbranched poly(amidoamine) modified with phenylalanine has been used as a substitute for poly(amidoamine) dendrimer as it shows non-toxicity and high efficiency in gene transfection [39]. Several commercialized HPs such as poly(ethlyeneimine), Boltorn (hyperbranched aliphatic polyester), Hybrane (hyperbranched polyesteramide) and polyglycerol have been studied as gene and drug delivery carriers for biomedical applications [31].

1.3.2. History of HPs

The historical background of HPs goes back to 19th century when Berzelius prepared a branched resin by the condensation of tartaric acid with glycerol [40]. Inspired by this, in 1901, Watson reported an aromatic branched ester from glycerol and phthalic anhydride/phthalic acid. Later, Callahan, Arsem, Dawson and Howell pursued this reaction in detail and their experimental conclusions are still conducive even today for the chemical/physical behaviours of these polymerizations [41]. Kienle et al [41] found that the specific viscosity of these branched polymers was low as compared to values reported by Staudinger for synthetic linear polymers, such as polystyrene. After 8 years, Baekeland industrialized the first commercial synthetic plastic (phenolic polymers) through Bakelite Company [42]. The cross-linked phenolic polymers were obtained by the polymerization of soluble resole precursor made from formaldehyde and phenol. Prior to gelation, these polymers had a random hyperbranched structure. In the 1940s, Flory [43] introduced the concept of 'degree of branching (DB)' and 'highly branched species' for these monomer polymerizations on the foundation of statistical mechanics. These calculations were based on the polycondensation of bifunctional A_2 monomer with trifunctional B_3 monomers without considering the gelation (cross-linking) phenomenon. Later, in 1952, Flory [44] modified his theory and stated that highly branched polymers can be synthesized without gelation by polycondensation of a monomer containing one A functional group and two or more B functional groups (AB_n monomer, $n \geq 2$). Based on Flory's theory, in 1982, Kricheldorf et al [45] synthesized highly branched polyesters without gelation by copolymerization of AB and

AB_2 type monomers. But, it was in 1980, when Kim and Websters [46] coined the name 'hyperbranched polymers' to these dendrimeric architectures. Since then, there has been a revolution in scientific publications in this field.

1.3.3. Synthetic methodologies of HPs

HPs are synthesized by two methodologies: (a) single monomer methodology (SMM) and (b) double monomer methodology (DMM). SMM is adopted from a single monomer of AB_n type, where A and B represent two different functionalities and $n \geq 2$. The main advantage of SMM is that gelation (cross-linking between different HPs) is completely avoided during the synthesis [32]. One of the major disadvantages of SMM is that most of the monomers are not commercially available and have to be synthesized on requirement. A broad spectrum of HPs including hyperbranched polyphenylenes [47] polyethers [48] polyesters [49] polyamides [50], polycarbonates [51], poly(ether ketone)s [52], polyurethanes [53], polycarbosilanes [54], polyamides [55], and poly(acetophenone)s [56] have been successfully synthesized via one-step polycondensation of AB_n type monomers.

The DMM, on the other hand, is based on copolymerization of two dissimilar monomers having different functionalities of A_x and B_y, where $y > x$ [32]. A large library of these monomers is commercially available which makes the synthesis process flexible for preparing different HPs with various combinations of the monomers. One major drawback of DMM is that the method is highly prone to gelation and in some cases, it is unavoidable. Therefore, the reaction has to be quenched before the critical gelation point. In most of the cases, gelation is avoided by a crucial control of reaction parameters such as reaction temperature, reaction time and molar ratio of monomers. A new philosophy known as couple-monomer methodology (CMM) was developed by Yan and Gao and Aharoni and Edwards [57]. It was based on the non-equal reactivity of functional groups in specific monomers. Here, the two monomers, preferentially A_2 and B_3 would generate one type of AB_2 intermediate *in situ* in the initial stage of polymerization, and this will follow the SMM to generate HPs without gelation.

1.3.4. The A_2 + B_3 methodology

The first intentional preparation of HPs *via* the A_2 + B_3 approach was reported independently by the groups of Fréchet [60] and Kakimoto [58]. But, it was recognized as a new method to prepare highly cross-linked polymeric materials owing to its uncontrolled gelation behaviour [42]. This has initiated a serious research on this type of reactions. Eventually, Kakimoto and Fréchet concluded that soluble HPs can be obtained without cross-linking by either of the following ways, stopping the polymerization by precipitation, end-

capping prior to the critical point of gelation, by the slow addition of monomer, or by using special catalysts and condensation agents [59].

Although the A_2 + B_3 strategy to HPs inherits some potential advantages over the conventional AB_2 approach, such as facile preparation and commercial availability of monomers, it still holds the major drawback of uncontrollable gelation, especially under conditions of relatively high monomer concentration and high reaction temperature. This strongly limits the wide application of A_2 + B_3 approach in large scale manufacturing. Gelation can be circumvented by two ways: (a) the reaction must be performed under low monomer concentration i.e., through slow monomer addition or (b) the polymerization must be stopped prior to the critical gelation point. A new methodology with the merits of commercial availability of monomers and lack of incidence of gelation was then highly appreciated. In this regard, Flory [59] has developed a gelation theory for the ideal polymerization of A_2 and B_3 monomers. It is based on three assumptions: (1) equal reactivity of all A or B groups at any given stage of the reaction, (2) no side reactions and the reaction is restricted to the condensation of A and B groups only and (3) no intra-molecular cyclization and chain termination in the process. If any of the above criteria becomes invalid during polymerization, gelation can be avoided.

1.3.5. Catalysts for A_2 + B_3 polymerization

Catalysts were an important part of the wide research in HPs. A more popular homogeneous catalysis was practiced due to their strict selectivity regimes. Emrick et al [60] applied the A_2 + B_3 approach to synthesize aliphatic hyperbranched polyethers using 1,2,7,8-diepoxyoctane as the A_2 monomer and 1,1,1-tris(hydroxymethyl)ethane as the B_3 monomer with tetra-n-butylammonium chloride (Bu_4NCl, 5 mol% based on A_2 monomer) as the homogeneous nucleophilic catalyst. The nucleophilic attack of the chloride ion on the less hindered terminal carbon of epoxide led to the formation of a secondary alkoxide. An equilibrium was then established through the rapid proton exchange from one of the -OH of B_3 monomer to secondary alkoxide of A_2 monomer. This leads to the formation of a new primary alkoxide from B_3 monomer. Nucleophilic attack of these primary alkoxides of B_3 monomer on epoxide rings of A_2 monomer resulted in the propagation of polymer and finally to the formation of aliphatic hyperbranched polyethers. They continued this catalytic approach for the direct polymerization of 1,4-butanediol and triepoxide under a variety of reaction conditions. The phenomenon of gelation was indispensable in these situations but was controllable. Size exclusion chromatography revealed that the polydispersity index (PDI) of the soluble polymers isolated before the critical gelation point was extremely broad

(M_w/M_n > 20). The product was not fully characterized due to the separation difficulties from residual monomers and catalyst [61].

Murtuza et al [62] have synthesized hyperbranched polyethylene oligomers, by a combination of an early or late transition metal complex, $TiCl_4$ or $TaCl_5$ with an excess of aluminium alkyl compound AlR_xCl_{3-x}. The transition metal alkyl species formed *in situ* initially catalyzed the formation of short alkenes, principally 1-hexene followed by cationic oligomerization of these alkenes on Lewis acidic sites to form hyperbranched architectures. The hyperbranched and globular dendrimer-like polyolefins were novel and had drastically different properties compared to the conventional linear polyolefins. They can be used as additives in lubricating oils. Minor amounts of branched polyolefins can impart both detergent and dispersant properties when blended into fuels. With their transparency, non-toxicity and low viscosity they can potentially serve as base materials for formulations of pharmaceutical agents and personal care items. Schömer et al [63] synthesized a thermo-responsive aliphatic hyperbranched polyether polyols by the anionic polymerization of two commercially available monomers propylene oxide (latent A_2 monomer) and glycidol (latent B_3 monomer). The polymerization was initiated by potassium salt of 1,1,1-tris(hydroxymethyl)propane. The initiator, ring opens one of the epoxide to form a secondary alkoxide. In the subsequent step, a proton exchange from glycidol (intra molecular or intermolecular) generates a primary alkoxide and the propagation continues with the formation of hyperbranched structure with glycerol as the branching unit. De et al [64] synthesized a hyperbranched epoxy polymer from castor oil-modified hyperbranched polyester polyol and *in situ* generated glycidyl ether epoxy of bisphenol-A using sodium methoxide, *para*-toulene sulfonic acid and sodium hydroxide as catalyst in a three step process. In the first step, castor oil was treated with excess glycerol to generate monoglycerides (A_2 monomer). In the second step it was reacted with 2,2-bis(hydroxyl methyl) propionic acid (BB'_2 monomer) to get hyperbranched polyester. In the third step, this hyperbranched polyester was post modified with bisphenol-A and epichlorohydrin to generate hyperbranched epoxide. The hyperbranched epoxy polymer shows outstanding toughness, elasticity and biodegradability for its use as thermosetting plastic. The same group has synthesized a vegetable oil based hyperbranched polyesteramide from N,N'-bis(2-hydroxyethyl)castor oil fattyamide, maleic anhydride, phthalic anhydride and isophthalic acid as A_2 monomers and diethanol amine as B_3 monomer. These novel theromsets with better properties are used as biodegradable surface coating materials [65]. Stumbé et al [66] synthesized aliphatic hyperbranched polyester derived from renewables like glycerol (B_3

monomer) and succinic and adipic acid (A_2 monomer) using dibutyltin oxide as the homogeneous catalyst. The resulting hyperbranched polyesters were oligomers with a maximum DB of only 48%. Attempts to improve the DB by changing the reaction parameters resulted in gelation. Wyatt et al [27] studied this reaction in aprotic solvents like dimethylsulfoxide and N,N-dimethylformamide to control the gelation using titanium (IV) butoxide as the homogeneous catalyst. These polyesters find application in biomedical field, as cosmetics, food additives, surfactants and lubricants.

Although there are plenty of reports on the successful synthesis of various aliphatic HPs using homogeneous mineral acid or base catalysis, a little or no attention was given to the applicability of heterogeneous catalysts for any of these polymerizations. Given that the homogeneous catalysts have high specificity and homogeneity in chemical transformations, synthesis of new HPs will continue to depend on homogeneous catalysis. At the same time an introduction of heterogeneous catalyst with the advantage of easy handling, less corrosion and easy separation for these known reactions is recommended.

1.4. Carbon dioxide utilization

Total dependence on fossil fuels (petroleum, coal and gas) for energy generation will continue to pile up green house CO_2 in atmosphere. US department of energy has estimated a 15% increase of CO_2 concentration in atmosphere since the beginning of 21st century [67]. Table 1.1 shows the statistics of CO_2 emission from various industries.

Table 1.1. Statistics of CO_2 discharge from industries [68]

Industrial sector	**Metric tonnes of CO_2/y produced**
Oil refineries	850- 900
Liquefied natural gas sweetening	25- 30
Ammonia	160
Ethene and other	155
Ethene oxide	10- 15
Fermentation	> 200
Cement	> 1000
Iron and steel	~ 900

While CO_2 capture and storage is one option of its sequestration, its conversion to valuable chemicals and materials is most attractive. The feasibility of this concept depends on

the availability of CO_2 and the economics of the process. There are several incentives for producing chemicals from CO_2. They include [69],

1. CO_2 is a cheap and nontoxic feedstock. It is a convenient replacement for toxic chemicals such as $COCl_2$ and isocyanates.
2. Transformation of CO_2 into chemicals is innovative and can result in novel material compositions such as polymers.
3. New schemes for the production of existing chemicals would be more efficient by CO_2 utilization.
4. CO_2 utilization would have some positive impact in reducing the green house effect.

Sources of CO_2 for chemical conversions are natural reservoirs, natural gas processing plants and, ethylene oxide, ammonia and hydrogen production plants. But the major contribution would be from fossil fuelled power plants. Conventionally CO_2 is used in four major processes: (i) urea production (~ 5.2 million metric tons/year), (ii) refrigeration (~ 1.5 million metric tons/year), (iii) beverages (~ 0.75 million metric tons/year) and (iv) enhanced oil recovery (~ 6 - 7 million metric tons/year) [67]. Figure 1.4 portrays a graphical abstract of the current research and processes for CO_2 utilization. Today, the amount of CO_2 converted to chemicals is two orders of magnitude larger than carbon capture and sequestration in its infancy stage (roughly 4-5 metric tons/year of CO_2). Table 1.2 shows the figures of CO_2 utilization in various industrial chemical processes [68].

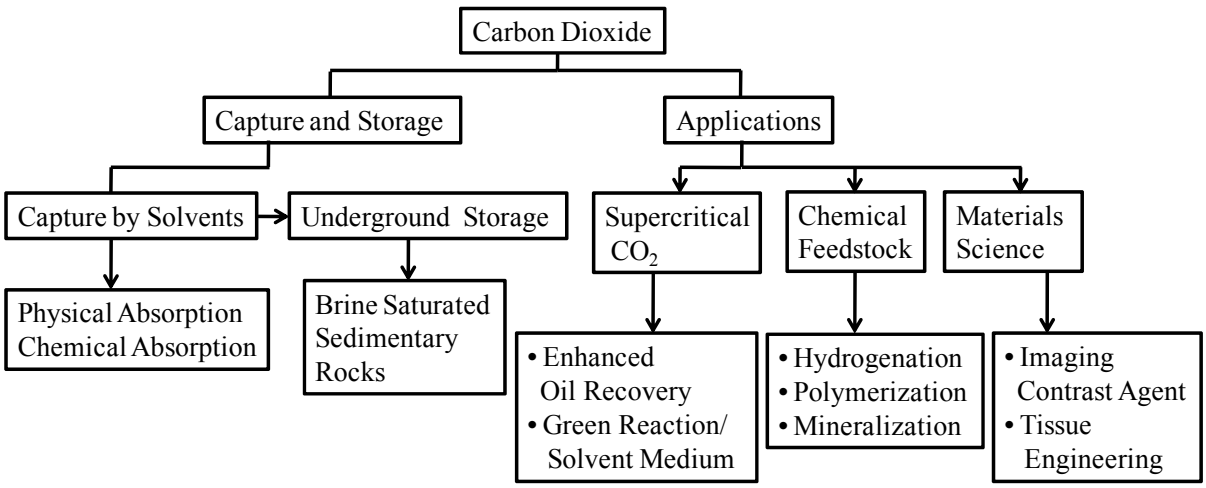

Fig. 1.4. Current research and technologies ordained towards the capture, storage and chemical transformations of CO_2 [70].

Table 1.2. Figures of CO_2 utilization in various chemical syntheses [68].

Compound	Actual Production (Mt/y)[a]	CO_2 used (Mt/y)	2016 forecast (Mt/y)	CO_2 needed (Mt/y)
Urea	**155**	**114**	**180**	**132**
Methanol	**50**	**8**	**60**	**10**
Dimethyl ether	*11.4*	*3*	*>20*	*>5*
Methyl *tert*-butyl ether	*30*	*1.5*	*40*	*3*
Formaldehyde	*21*	*3.5*	*25*	*5*
Carbonates	**0.2**	**0.005**	**> 2**	**0.5**
Polycarbonates	**4**	**0.1**	**5**	**1**
Carbamates	**5.3**	**0**	**> 6**	**1**
Polyurethans	**> 8**	**0**	**10**	**0.5**
Acrylates	**2.5**	**0**	**3**	**1.5**
Formic acid	**0.6**	**0**	**1**	**0.9**
Inorganic carbonates	**200**	**50**	**250**	**70**
Calcium carbonate	*114*			
Soda Solvay	*50*			
Total		**172**		**207**
Technological		**28**		**80**
Algae for biodiesel	**0.005**	**0.010**	**1**	**2**

Bold values represent the total and italics the sub-partial. [a]Metric tons per year.

1.4.1. Conditions for using CO_2 as a reactant

The proposal of new technologies for the effective utilization of CO_2 must consider the following criteria [71],

1. There should be a reduction in overall CO_2 emitted in the new process,
2. The new process must be less energetic and material intensive as compared to the existing one,
3. More safer and working conditions must be employed and,
4. The new process must be economically viable.

Industrially, CO_2 is used for four economically favourable chemical processes [72]: (a) urea synthesis, (b) salicylic acid production by 'Kolbe-Schmitt' process, (c) cyclic carbonates production and (d) methanol synthesis *via* water gas-shift reaction. The major reason for the limited use of CO_2 in chemical process is due to its low energy content and

high stability. Thermodynamically, the -TΔS makes only a little contribution for driving a chemical reaction involving CO_2. Hence, the deciding factor for the reaction is the enthalpy, ΔH. Consequently, for the feasibility of a reaction, ΔH should be either negative or small positive. Thus, the execution of a chemical reaction involving CO_2 at ambient conditions has to make use of less stable reactants such that the products are more stable than the reactants. Another smart approach to this scenario is the use of catalysts for the activation of CO_2, because catalysts can reduce the activation energy of the reaction. This aspect is highly desirable for keeping the reaction conditions near ambient [72].

The energetic of CO_2 utilization depends upon two possibilities: (i) CO_2 can be incorporated totally without any change in oxidation state, termed as low energy process, and (ii) reduction in the oxidation state of CO_2 to a state required for the targeted compound, termed as high energy process. Examples for both processes are annotated below [73].

Low energy processes: Carboxylates - RCOOH(R), lactones, linear esters, carbamates - RR′NCOOR″, carbonates - $(RO)_2CO$, ureas - $(RHN)_2CO$, polymers like polycarbonates and polyurethanes, inorganic carbonates and hydrogen carbonates belong to the this category. For the energetic to be favourable, CO_2 is reacted with highly reactive electron-rich molecules such as H_2O, OH^-, RR′NH, RR′R″C^-, olefins, alkynes and dienes under mild conditions (< 273 K).

High energy processes: HCOOH, CO, H_2CO, CH_3OH, CH_4, hydrocarbons and similar compounds are of this class. Energy is needed in all these processes and is provided in many different forms: electrons (electrochemical reduction), hydrogen (hydrogenation reactions), metals (reaction with Group-1 metals) and radiations (splitting of CO_2 into CO and ½O_2 at high energy).

Conversion of CO_2 to fuels by high energy processes using fossil fuels as energy supplier would discharge more CO_2 to the atmosphere than converted. Therefore, the low energy processes making use of highly reactive molecules like epoxide, dienes and amines are the centre of attraction. An advantage of this approach is that some of these processes not only reduce the amount of CO_2 emitted but also avoid the use of toxic and energy intensive chemicals like CO and $COCl_2$ (Scheme 1.2). Although there are different ways for the low energy utilization of CO_2, synthesis of polymers from CO_2 for material applications have some advantages over others. If a chemical is made from CO_2, the used CO_2 will be regenerated within short times. This recycle rate would be slow for polymers as they are durable at least for few decades [71]. Hence, the synthesis of aliphatic polycarbonates from

epoxides and CO_2 represents a sustainable low energy process for the utilization of CO_2 to environmentally adaptable polymers for various applications.

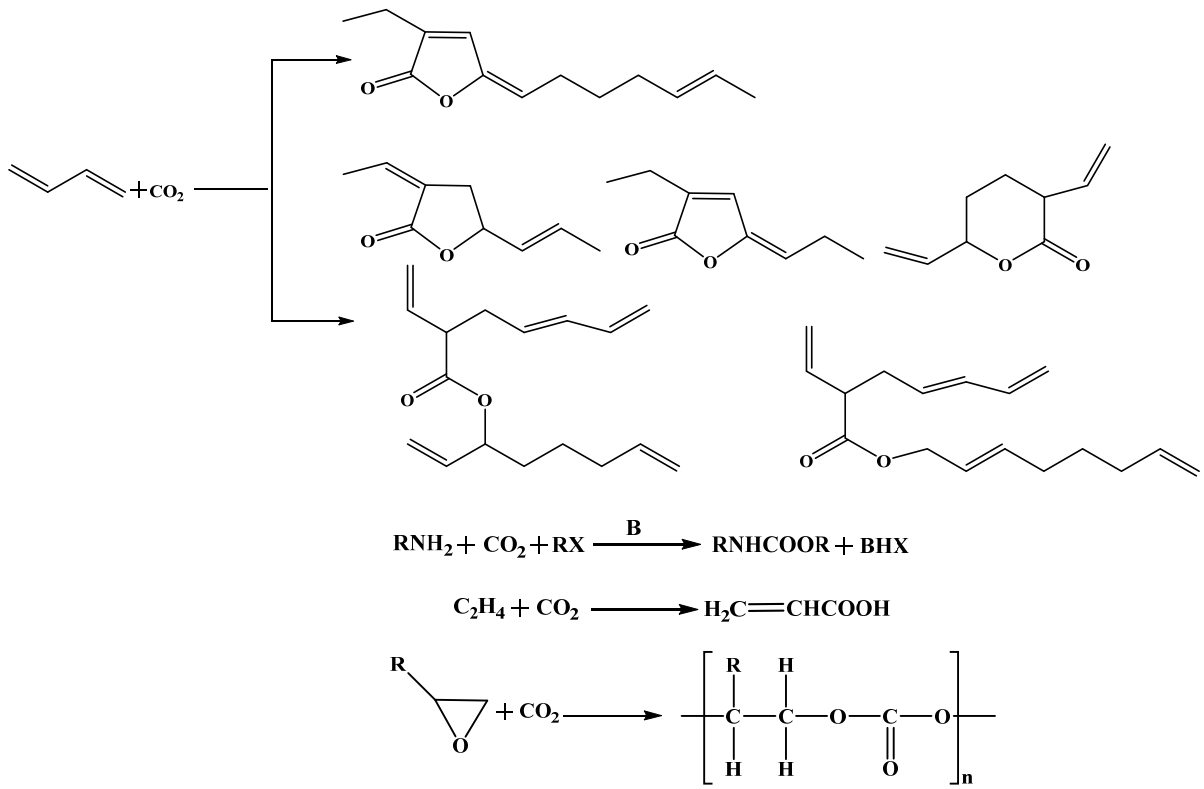

Scheme 1.2. Low energy processes for the conversion of CO_2.

1.4.2. Aliphatic polycarbonates

1.4.2.1. History of polycarbonates

The first synthesis of a 'polycarbonate' was reported by Enihorn [74] in 1898, who prepared an aromatic polycarbonate by reacting hydroquinone, resorcinol and catechol with $COCl_2$ in pyridine solution. Hydroquinone and resorcinol produced linear crystalline and amorphous polycarbonates with melting points of 280 and 200 °C, respectively. Followed by this discovery, Bischoff and Hedenstroem [75] synthesized the same polycarbonates by transesterification of aromatic diols with diphenyl carbonate. The transesterification concept avoided the use of toxic $COCl_2$. In 1930, Carothers and van Natta [76] prepared aliphatic polycarbonates by two synthetic routes: (a) transesterification of aliphatic dihydroxylic compounds with diethyl carbonate and (b) ring-opening polymerization of cyclic carbonates of aliphatic dihydroxylic compounds. Aliphatic polycarbonates were low melting and low crystalline as compared to aromatic polycarbonates of earliest discoveries. The first commercial synthesis of polycarbonates from allyl ester of diethylene glycol carbonate was commissioned by Pittsburgh Plate Glass Company in 1941 [77]. Extensive research was

continued in the synthesis of aromatic polycarbonates because of their excellent physical and mechanical properties. A renaissance in research for aliphatic polycarbonates occurred in 1990's (Fig. 1.5), where these polymers were recognized as alternatives for films, packaging, and rigid plastics applications. As compared to aromatic polycarbonates, the industrial applications of aliphatic polycarbonates were limited as macromonomers for the production of polyurethanes and other copolymers due to their low molecular weights [78].

Initial studies on aliphatic polycarbonates were devoted on improving their thermal stability and mechanical properties. At the same time, increasing concerns about green house effect have directed the research on CO_2 and its incorporation in aliphatic polycarbonates [78, 79]. Today, the more demand for biodegradable and biocompatible polymers for various biomedical applications revived the interest in aliphatic polycarbonates in which their degradability, low glass-transition temperatures (T_g) and elasticity, which were considered as major weaknesses have turned into highly desirable advantages over many other polymers [80]. Fig. 1.5 shows the number of scientific publications on polycarbonates over the past decades.

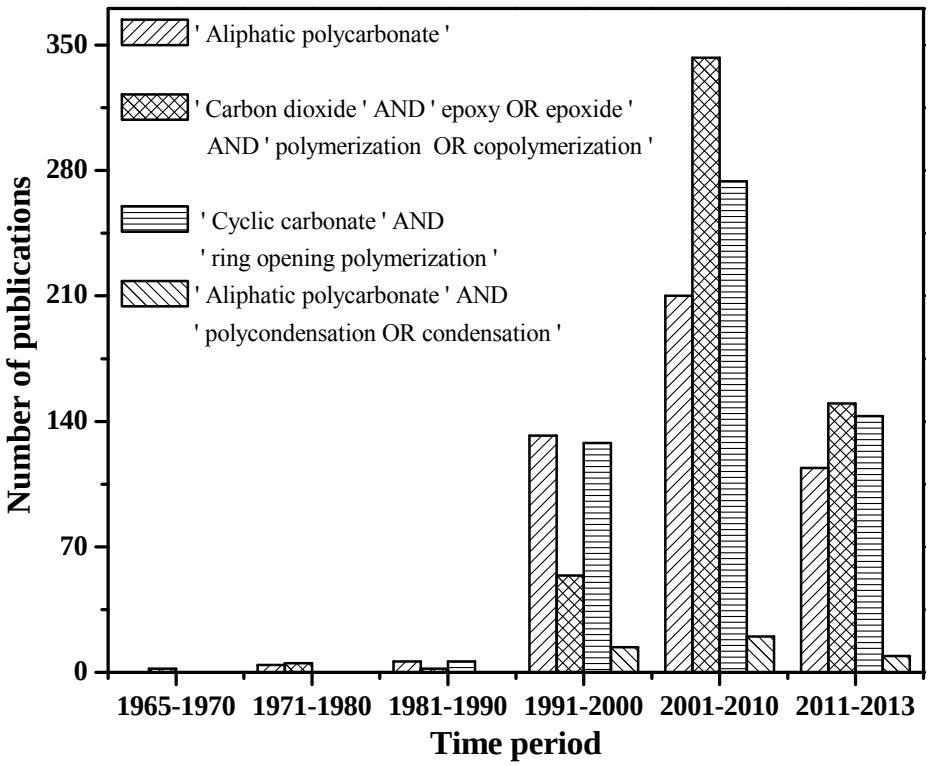

Fig. 1.5. Number of scientific publications on aliphatic polycarbonates in past decades [78].

Aliphatic polycarbonates are generally prepared by three synthesis routes: (a) polycondensation of polyols with dialkyl carbonate (Scheme 1.3(a)), (b) copolymerization of

CO_2 with epoxides (Scheme 1.3(b)) and (c) ring-opening polymerization of cyclic carbonates (Scheme 1.3(c)). In all these processes, CO_2 has been used either directly or indirectly as a monomer or reagent [78]. Significant progress has been made to improve each method over the last two decades where special interest was given to the direct utilization of CO_2 by copolymerization.

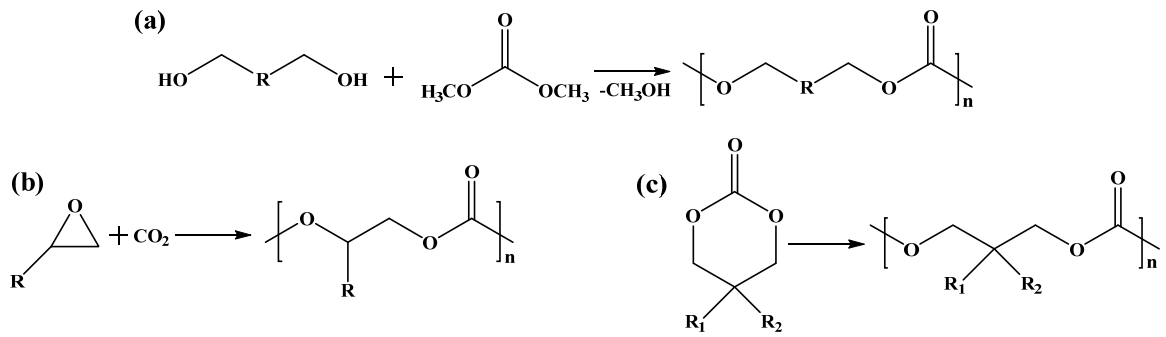

Scheme 1.3. Synthesis procedures of aliphatic polycarbonates.

1.4.2.2. Catalysis in copolymerization of CO_2 and epoxides

The report by Stevens [81] in 1966 was the earliest on the copolymerization of an epoxide viz., ethylene oxide and CO_2. The discussed process was carried out in presence of polyhydric phenols preferably ethylene glycol *via* base catalysis. The polymerization at elevated temperature and high pressure incorporated only few carbonate units as compared to the ether units. Later, in 1969, Inoue et al [82] reported the first metal catalyzed copolymerization of CO_2 and propylene oxide (PO) over a heterogeneous catalyst system composed of 1:1 mixture of $ZnEt_2$ and H_2O. The polymerization produced 11.8 wt% (with respect to PO) of methanol insoluble alternating polycarbonate. Thereafter, various modifications (different monohydric and polyhydric alcohols instead of H_2O) of catalyst systems have been proposed by different groups for improved activity [83]. Of all the various formulations of zinc catalysts available today, zinc glutarate is considered as the most active catalyst (T = 60 °C, P_{CO2} = 51.7 bar, t = 40 h, 64 g polymer/g catalyst, 99% methanol insoluble fraction, number average molecular weight (M_n) = 143000, polydispersity index (PDI) = 2.4, < 1% ethers). The catalyst is synthesized by the reaction of $Zn(OH)_2$ or ZnO with dicarboxylic acid in toluene [84]. Single crystal analysis of the catalyst showed a layered structure of zinc ions with bridging dicarboxylates between the layers [85]. This catalyst was commercialized (Empower Materials) for the synthesis of poly(ethylene carbonate) owing to its inexpensive synthetic reagents and robust nature [86].

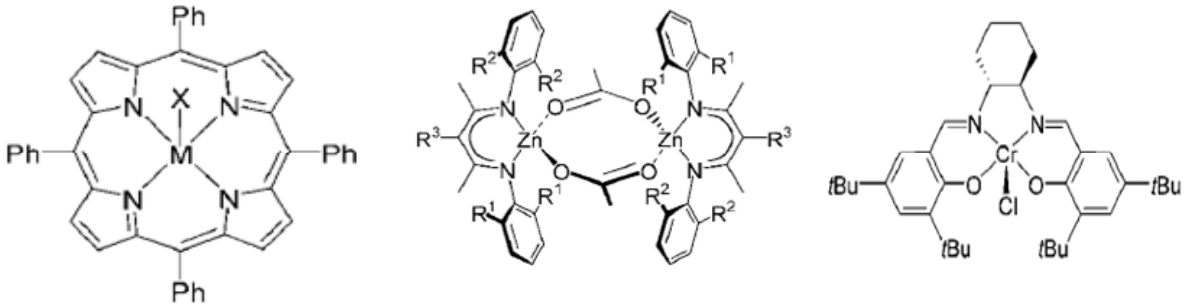

(a) **(b)** **(c)**

Fig. 1.6. Single site homogeneous catalysts of polycarbonates synthesis: (a) tetraphenylporphyrin AlOMe, (b) zinc β-diiminate acetate and (c) (salen)Cr(III)Cl.

Although research on aliphatic polycarbonates by epoxide ring opening was well accepted and focussed on heterogeneous catalysts in its early stages, the mechanism of catalytic action was not clearly addressed due to the heterogeneity of active centres and lack of experimental techniques. A mechanistic investigation on the mode of action of catalyst was then initiated by Inoue [87] in 1978 with the design of a well defined homogeneous single site aluminium based porphyrin catalyst (Fig. 1.6 (a)). The porphyrin ligand was inspired from the natural fixation of CO_2 by chlorophyll containing porphyrin ligand. The aluminium tetraphenylporphyrin with an Al-OMe bond in presence 1-methylimidazole as co-catalyst was used for the copolymerization of PO and CO_2. The polymerization was very slow at 20 °C resulting only 9% of PO conversion with a CO_2 incorporation of 10 mol% and a molecular weight (M_n) of 3700 (PDI = 1.1). However, the studies revealed that the copolymerization takes place in two steps of which the first step is the attack of epoxide at the metal centre to form a metal alkoxide bond and the second step is the attack of CO_2 to change the metal alkoxide to metal carbonate bond. Hence, catalysts with metal alkoxide or metal carbonate bonds were regarded as the active centres for the copolymerization. There after a number of scientific results and comprehensive reviews were published on homogeneous catalysts discussing their activities and modes of action of catalysts during copolymerization [29, 88]. These studies showed that only few metals are active for the copolymerization. They include Al, Cr, Co, Mg, Li, Zn, Cu and Cr. Invoking the idea from heterogeneous zinc glutatrate catalyst, a number of possibilities with homogeneous single site Zn catalysts were also extensively subjected to the activity studies. Well defined monomeric and dimeric zinc catalysts were proved as efficient catalysts for the copolymerization of cyclohexene oxide (CHO) and CO_2. These include reports of sterically encumbering bis-phenoxide derivatives of zinc (T = 80 °C, P_{CO2} = 55 bar, t = 69 h, 91 mol% CO_2

incorporation, M_n = 38000, PDI = 4.5) [88], a highly fluorinated zinc carboxylate (T = 100 °C, P_{CO2} = 137.8 bar, t = 24 h, 93 mol% CO_2 incorporation, M_n = 17030, PDI = 6.4) [89] and zinc β-diiminate complexes (T = 50 °C, P_{CO2} = 6.8 bar, t = 2 h, 96 mol% CO_2 incorporation, M_n = 31000, PDI = 1.1) [90]. Among these, the β-diiminate complex suggested by Cheng et al [90] showed a breakthrough activity towards the copolymerization of CHO and CO_2 (Fig. 1.6 (b)). In this complex, Zn is tetrahedral and the two aryl groups are perpendicular to the plane of N-Zn-N. The complex exists as acetate bridged dimer in the solid state. The catalyst displayed high sensitivity towards steric and electronic effects modulating the active Zn centre. For instance, when R_1 = CN and R_2 & R_3 = Me and ^{i}Pr, respectively, the catalyst displayed a turnover frequency (TOF) of 2290 h^{-1} at 50 °C. When R_1 = H and R_2 = R_3 = Et, a corresponding TOF of 239 h^{-1} was observed. Likewise, subtle changes in the nature of the β-diiminate ligand had led to efficient catalysis of other epoxides, viz., PO [91] and limonene oxide [92] with CO_2 to selectively afford polycarbonates. Kinetic studies on the copolymerization of CHO and CO_2 on these diiminate complexes concluded a bimetallic mechanism in which one Zn centre coordinates and activate the epoxide while the other one provide the propagating carbonate species to ring-open the epoxide [90].

To date, the most active catalysts reported for the copolymerization of CO_2 and epoxides are the (salen)Cr(III)Cl (Fig. 1.6 (c)) or Co(III)-based catalysts with some sort of added onium salt as co-catalyst. Here, the Lewis acidic metal centre activates the epoxide which is subsequently attacked by the carbonate anion generated from the onium salt. Cohen et al [93] studied a set of (salcy)CoX (where X is halide or carboxylate) for the alternating copolymerization of PO and CO_2. The catalysts were found to be highly active in producing poly(propylene carbonate) (PPC) with no detectable amount of cyclic carbonate in a living behaviour. PPCs were highly regio regular with 99 mol% carbonate linkages and with narrow molecular weight distributions (T = 22 °C, P_{CO2} = 13.7 bar, t = 1 h, M_n = 26800, PDI = 1.13). The study also revealed that the addition of a co-catalyst bis(triphenylphosphine)iminium chloride (PPNCl) leads to an iso-enriched PPC with 94 mol% head-tail connectivity with a TOF of 620 h^{-1}. The (R,R)-(salcy)CoOBzF_5 co-catalyst showed the highest TOF of 1100 h^{-1} with 99 mol% polycarbonate selectivity and 96 mol% head-tail linkages (M_n = 2200, PDI = 1.15). Nakano et al [94] designed a (salcy)Co(III) complex containing two acetate ligands and a piperidinyl and piperidinium arms attached to the (salcy) ligand for the copolymerization of PO and CO_2 with the aim to completely suppress the formation of cyclic carbonate. This was achieved by the piperidinium arm which controls the nucleophilicity of the propagating chain by protonation. The protonated anionic chain is not nucleophilic

enough for the backbiting reaction to form the cyclic byproduct. Copolymerization with this Co(III) catalyst yielded 38% of PPC with a TOF of 254 h^{-1}(T = 25 °C, P_{CO2} = 14 bar, M_n = 12600, PDI = 1.13, monomer/catalyst = 2000) with only 1% of cyclic carbonate production. This new design of the catalyst excluded the addition of co-catalyst as used by Cohen et al [93]. Here, the single catalyst itself functioned as both catalyst and co-catalyst. Inspired by this catalyst and co-catalyst combination at single molecule, Noh et al [95] designed a cobalt salen complex containing quaternary ammonium salts attached at the 5th position of two phenyl rings of the (salen) ligand. The designed catalyst was highly active for the copolymerization of PO and CO_2 even at a monomer/catalysts ratio of 25000. The catalyst showed the highest TOF (3300 h^{-1}) at 80 °C (94 % selective to PPC, M_n = 71000, PDI = 1.25). This has been regarded as the most active catalyst for PO and CO_2 copolymerization to date. These single (salen)Co(III) complexes have several advantages over the catalyst-co-catalyst binary systems. They include: (a) extremely low amount of catalyst as compared to the monomer, (b) the polymerizations are immortal in nature so that the reversible chain transfer phenomena in presence of chain transfer agents like H_2O or alcohol will not affect the PDI of the polymer, (c) the appended amine parts are able to attract the anionic polymer chain preventing it from the backbiting reaction to form cyclic carbonates and (d) these single functioned catalysts prevent the reduction of active Co(III) to inactive Co(II) [96].

Terpolymerization of CO_2 and epoxides or other reagents was also attempted with these homogeneous catalysts. Kröger et al [97] reported the terpolymerization of CO_2 with CHO and lactide with an aminoimido zinc acetate catalyst. The reaction with a CHO : lactide ratio of 1.5 : 1 produced polymer containing 10 mol% CO_2 incorporation and 90 mol% lactide incorporation (TOF = 26 h^{-1}). Shi et al [98] reported the terpolymerization of CO_2, CHO and PO with a binary catalyst system containing a chiral tetradentate Schiff-base cobalt complex (SalenCo-2,4-dinitropheoxy) catalyst and a bulky ionic PPNCl as co-catalyst. The catalyst system was highly efficient in producing terpolymers with narrow polydispersity (CHO: PO = 1:1, M_n = 24400, PDI = 1.24) and with > 99 mol% carbonate linkages. The terpolymer showed only single T_g at 69 °C and it was adjustable by changing the ratio of PO and CHO. Li et al [99] has reported the terpolymerization of CO_2 with PO and CHO by a bifunctional single component cobalt salen complex. Incorporation of PPC units in poly(cyclohexene carbonate) (PCHC) has reduced its brittleness and improved the mechanical properties. T_g of the terpolymer was easily adjustable between 40 to 119 °C by changing the epoxide molar ratios (CHO: PO = 1:1, M_n = 65200, PDI = 1.17, T_g = 69.5 °C).

Table 1.3. Thermal and mechanical properties of different polycarbonates [100].

Properties	PPC	PCHC	Terpolymer PPC : PCHC = 20:80
M_w	28900	33800	35200
PDI	3.83	4.23	5.27
Glass transition (T_g) (°C)	22- 30	99- 111	93- 100
T_g inflection point (°C)	28	105	97
Activation energy of T_g (kJ/mol)	290	366.2	336.4
Activation entropy (J/mol/K)	679	654	617
Degradation temperature from DSC (°C)	253	308	296
Initial decomposition temperature , TG (°C)	235 (air) 238 (N_2)	282 (air) 290 (N_2)	265 (air) 276 (N_2)
Modulus (MPa)	212	2460	2080
Tensile strength (MPa)	9	11.8	13.5
Strain break (%)	8	0.5	0.7

1.4.2.3. Thermal and mechanical properties of polycarbonates

Physical properties of aliphatic polycarbonates are very much depending on their molecular weight and the micro structure. Table 1.3 shows the thermal and mechanical properties of PPC, PCHC and a terpolymer of both [100]. The polymers were synthesized over a zinc adipate catalyst of Empower Materials composition. Polycarbonates of the study were completely amorphous with only 3-5 mol% randomly distributed ether linkages. Molecular weights of the polymers were in the range of 30,000 with a broad distribution (PDI = 3-5). PPC showed the lowest glass transition temperature (T_g) ranging between 20-30 °C. T_g increases with increase in chain stiffness and is high for PCHC. T_g was influenced by crystallinity, microstructural defect content and co-monomer content of the polymer. Incorporation of PPC in PCHC to synthesize a terpolymer of both has resulted a reduction in T_g as compared to pure PCHC. The activation energies and activation of entropies of T_g calculated from dynamic mechanical analysis followed the same trend as that of T_g values relating to the rigidity of the polymer chain. It is also clear from the table that the initial decomposition temperature of polycarbonates increases with the amount of hydrocarbon content which is high for PCHC. In conclusion, the T_g of the polymer depends on a combined

effect of free volume associated with the side chains (which hinder the intermolecular dipolar interactions) and the stiffness of the polymer backbone. At the same time, the degradation temperature depends on a combined effect of the hydrocarbon unit and the stiffness of the polymer. The mechanical properties of the polymer depend upon T_g which in turn depends upon the structure of the polymer. PCHC and the terpolymer are brittle as it is clear from the elastic modulus of the polymer, which is very high compared to PPC and their strain break is less than 1%. While PPC behaves comparatively elastomeric with low elastic modulus with a strain break of 8%. Addition of a third monomer helps to achieve polymer with desired properties.

1.4.2.4. Applications of polycarbonates

Aliphatic polycarbonates are relatively new material to the field of polymer science. The utility of these materials for various applications is governed by their thermal and mechanical properties. Relatively unimpressive thermal and mechanical properties of these polycarbonates along with their high cost hamper them for general applicability. PPC is used as a mid segment in polyurethanes to improve its properties. PPC containing ~ 80 mol% ether linkages shows good solubility in supercritical CO_2, shown by a polymer other than fluorinated polymers [101]. Low molecular weight PPC polyols are used in a wide variety of coating applications such as metal can linings, wood finishing and protective finishes for automotive industry, as surfactants for enhanced oil recovery, foams and adhesives. High molecular weight PPCs are used as thermoplastics, in electronic processing and as low temperature cleanly decomposing binders [102]. PCHCs possessing higher T_g (~ 115 °C) show properties similar to polystyrene. Also the higher decomposition temperature (~ 300 °C) helps them for melt processing. Their clean burning recommends them as sealants and for lithographic process for the construction of pores in micro-fluidic devices [101]. More efficient and economic catalytic mediated production of these polymeric materials will reduce their cost and increase the availability for new applications.

1.5. Double metal cyanides

Double metal cyanides (DMC) are inorganic coordination polymers with frameworks containing metal cyanide moieties. Chemically they are Prussian blue analogues. Prussian blue was accidently discovered by Diesbach in 1704 [103]. Ever since this breakthrough, this bright coloured pigment was in great demand by industries such as paints, lacquers, printing inks, laundry chalks and arts. Prussian blue exists in two forms of which the insoluble form exits as ferric ferrocyanide with a molecular formula $Fe^{III}_4[Fe^{II}(CN)_6]_3.xH_2O$, where x = 14-16, and the soluble form exits as $KFe^{III}[Fe^{II}(CN)_6]$. Keggin et al [104] solved the crystal

structure of the soluble form to a face centred cubic lattice in which the high spin Fe(III) and the low spin Fe(II) ions are octahedrally surrounded by -NC and -CN ligands. This makes -CN a bridging ligand. The K^+ ions occupy the interstitial sites as charge balancers. Single crystal analysis of the insoluble form also revealed a primitive cubic lattice structure. But it was found that one-fourth of the $Fe(CN)_6$ is missing from their lattice points. So the valencies of Fe(III) are satisfied by water molecules instead of missing -NC ligands (Fe^{III} becomes oxophilic). In addition to that ~ 8 H_2O molecules are occupying the interstitial sites held by hydrogen bonds with the coordinated H_2O molecules. The average coordination composition at Fe(III) was estimated by neutron diffraction to be $FeN_{4.5}O_{1.5}$. The space group symmetry of Prussian blue was assigned to *Fm3m* [105]. The blue colour of the complex is due to the charge transfer between $[Fe^{II}(CN)_6]^{4-}$ and Fe^{III} ions. In the ground state most of the electrons are localized on the $[Fe^{II}(CN)_6]^{4-}$ ions [106].

1.5.1. Structural evolution in DMCs

DMCs are Prussian blue analogues with a general formula $M^A{}_m[M^B(CN)_6]_n.xH_2O$ consisting of a three-dimensional cubic M^A-NC-M^B frame work with some M^B vacancies. These inorganic polymers offer a rich variation in their stoichiometries and hence, in their electronic properties. The number of these vacancies depends on the stoichiometry of the two metal atoms which in turn depends on their oxidation states. As discussed earlier the coordination sites of M^A are balanced by H_2O molecules due to M^B vacancies. The metal M^A can be Zn^{2+}, Fe^{2+}, Co^{3+}, Ni^{2+}, Mn^{2+}, Cr^{2+}, Co^{2+}, etc. and M^B can be Fe^{2+}, Fe^{3+}, Co^{3+}, Ni^{2+}, Mn^{2+}, Cr^{3+}, Pd^{2+}, etc. Based on this, several combinations of DMCs were prepared and subjected to detailed structural investigations. Weiser et al [107] found that the X-ray diffraction patterns of $Ti_3[Fe(CN)_6]_4$, Prussian blue, $Al_4[Fe(CN)_6]_3$, $Zn_3[Fe(CN)_6]_2$, $Cu_3[Fe(CN)_6]_2$, $Cd_3[Fe(CN)_6]_2$ are identical with respect to the position and relative intensities of diffraction lines. This indicates that these complexes crystallize in the same phase as that of Prussian blue. This also suggests that the $[Fe(CN)_6]$ ions are the main component in forming same crystalline structures with various M^B atoms.

In 1966, Herold [108] had patented a Fe-Zn and Co-Zn formulation of DMC as catalysts for polyether polyol synthesis ($M^A = Zn^{2+}$ and $M^B = Co^{3+}$). Apart from the merely aqueous precipitation of DMC, the patented synthesis was performed in presence of water soluble complexing agents (dioxane) since the removal of substantial amount or whole H_2O from the complex was found to be highly desirable in improving activity. The complexing agents shared the vacant valencies at Zn^{2+} along with H_2O molecules. This was a new recognition of DMCs as catalysts for chemical transformations. The molecular formula of

DMC was then modified as $M^A{}_m[M^B(CN)_6]_n.xH_2O.yR$, where R is a complexing agent, x and y can be a integer or fractional numbers. In 1975, the same group had specifically described the most active catalyst for the polymerization as $Zn_3[Co(CN)_6]_2$ $2.4(CH_3OCH_2CH_2OCH_3)$ $0.85ZnCl_2.4.4H_2O$ which contained excess of $ZnCl_2$ as a part of crystal structure along with the 1,2-dimethoxyethane as complexing agent. The modified catalyst not only produced high molecular weight polypropylene oxide but also showed good activity with low molecular weight hydroxyl initiators to produce polyether polyols [109].

In 1978, Mullica et al [110] determined the crystal structure of $Zn_3[Co(CN)_6]_2.12H_2O$ from three dimensional single crystal X-ray diffraction. Unlike Prussian blue analogues, this complex contained cobalt cyanide than iron cyanides. The crystal structure has assigned to a space group of *Fm3m* similar to the Prussian blues. The disordered structure contained 1.33 molecules in the unit cell and the divalent zinc atoms are linked to the Co atoms by the cyanide bridges (Fig. 1.7 (a)).

In 1985, Boxhoorn et al [111] initiated the studies on DMCs for molecular sieving applications. The studies were performed with $Zn_3[Co(CN)_6]_2$ complex with molecules such as n-hexane, 3-methyl pentane, 2,2-diemethyl butane, CO_2 and methane as probes. The adsorption properties of the complex was assigned to 33% vacancies due to missing $[Co(CN)_6]^{3-}$ ions. The pore openings of *ca.* 0.56 x 0.86 nm were large enough for the adsorption of n-hexane and 3-methyl pentane but not for 2,2-dimethyl butane. Adsorption studies on a $Zn[Fe(CN)_5NO]$ with cubic structure possessing zero vacancies found to be highly efficient in separating CO_2 from CH_4. In 1987, the same group has reported a rhombohedral and hexagonal modification of Co-Zn DMC for PO polymerization and the physical separation of CO_2 and CH_4 mixtures [113]. The rhombohedral modification had a molecular formula as $Zn_3[Co(CN)_6]_2$ $3H_2O$ and the hexagonal modification had a molecular formula as $Zn_2[Co(CN)_6](OH)$ $4H_2O$. The rhombohedral structural assignment was done in comparison of the isostructural behaviour with $K_2Zn_3[Fe(CN)_6]_2$ xH_2O reported by Gracereau et al [112] in 1979. The hexagonal structural assignment was solved by Boxhoorn group, the lattice parameters were a = 12.91 Å and c = 16.68 Å and the OH group was regarded as a bridging ligand between two zinc atoms. The rhombohedral modification showed little activity as compared to the cubic versions. The hexagonal form after modification with HCl and complexing agent showed very high activity for PO polymerization. For the sieving properties, the hexagonal modification showed comparable CO_2 adsorption as of cubic form while the rhombohedral modification showed inferior adsorption capacity as compared to the cubic form [113]. An incessant effort in modifying the molecular structure of DMCs was

continued afterwards to improve its catalytic activity for epoxide polymerization [114] and better sieving properties where more structural evolutions were obtained from the research on sieving properties.

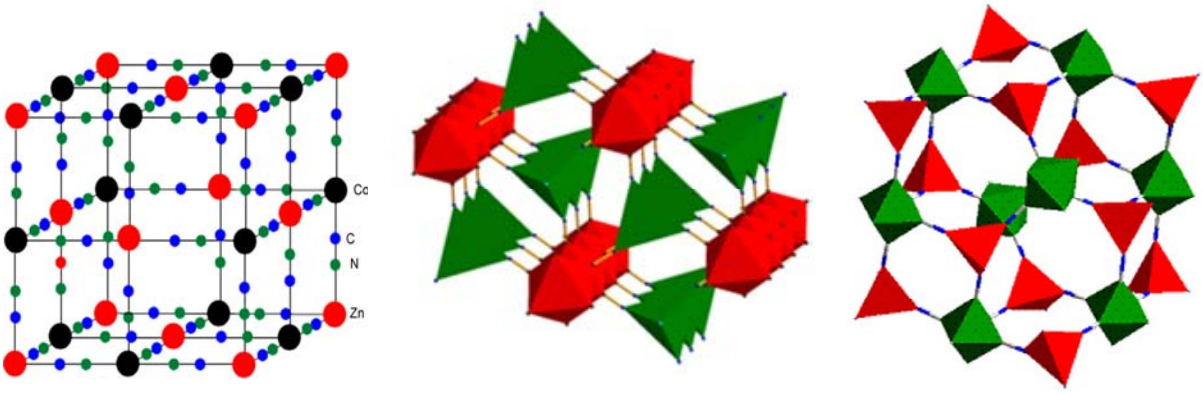

(a) **(b)** **(c)**

Fig. 1.7. Structure of (a) cubic $Zn_3[Co(CN)_6]_2$, (b) porous framework of $Zn_2[Fe(CN)_6]$ $2H_2O$ and (c) isolated cavity at the surface of hexagonal zinc hexacyanometallates.

Hernández et al [115] reported a typical coordination in hexacyanometallates and concluded that in hexagonal modification the zinc metal is tetrahedrally coordinated while it has an octahedral coordination in the cubic structures (Fig. 1.7 (b)). These coordination behaviours were extracted from the Rietveld analysis of powder X- ray diffractions. The identified zinc hexacyanoferrate(III), hexacyanocobaltate(III), hexacyanoiridiate(III) and mixed zinc-cesium hexacyanoferrate(II) existed as dimorphic, i.e., cubic and hexagonal (R3c) forms. The tetrahedral Zn was slightly distorted with an average N-Zn-N bond angle about 108°. The crystal structure contains large ellipsoidal cavities *ca* 1.5 x 0.9 x 0.8 nm communicated by elliptical windows of diameter 0.6 nm. In the cubic form, the N-Zn-N bond angle was close to 90° with a cavity (0.85 nm) of spherical shape. The tetrahedral coordination results in strong bond between CN ligand and Zn atom. The estimated Zn-NC distance in hexagonal form was 0.01 nm shorter than in the cubic form (0.2094 nm). Avila et al [116] reported Co, Ni, Cu, and Zn hexacyanoferrates(II) as prototype materials for hydrogen storage. The Zn form had a hexagonal (*P-3*) structure in which the Zn atom was tetrahedrally coordinated with three NC ligands and one H_2O (Fig. 1.7 (c)). The Cu and Ni complexes were found to be in cubic form (*Pm-3m*) and the Co modification was monoclinic ($P2_1/m$). The Ni and Cu modification showed higher H_2 adsorption in the hydrated form. Dehydration collapsed the crystal structure and reduced the H_2 adsorption. For the Zn prototype, no H_2 adsorption was observed due to their narrow channels. The Co form didn't show any H_2 adsorption after dehydration of crystal water. The CO_2 adsorption studies

showed the same trend as H_2 adsorption. Thallapally et al [117] studied the adsorption of gases like CO_2, N_2, SO_2, NO, H_2S and H_2O present in flue gases using a Co and Zn hexacyanocobaltate(III) complex. The complexes adsorbed 8-10 wt% of CO_2 at room temperature at 1 bar with a heat of adsorption lower than monoethanolamine scrubber. The SO_2, H_2S, NO adsorptions at the same conditions were 2.5, 2.7 and 1.2 mmol/g where cobalt modification showed better adsorption of SO_2 and H_2S. These DMCs were found to be stable even after exposure to the gases.

1.5.2. Applications of DMCs

Various formulations of DMCs find diverse applications in different fields and now-a-days DMC became a versatile material in all branches of science. The $(Ni^{II}_{0.22}Mn^{II}_{0.6}Fe^{II}_{0.18})_{1.5}[Cr^{III}(CN)_6]$ $7H_2O$ DMC is used as a double magnetic pole inversion magnet with changing temperature (-238 and -220 °C) [118]. Sato et al [119] studied the photo-induced magnetization in $K_{0.2}Co_{1.4}[Fe(CN)_6]$ $6.9H_2O$ to reveal an increase in critical temperature from -257 to -254 °C by illumination with red light. This property of DMC finds application in magneto-optical devices. DMC is also known as catalyst for β-amino alcohols synthesis where a Fe-Zn DMC with molecular formula $K_4Zn_4[Fe(CN)_6]_3$ $6H_2O.2$(tert-BuOH) was used as the catalyst [120]. Fe-Zn DMC catalyst with molecular formula $\{Zn_3[Fe_2(CN)_{10}](H_2O)_5.$(tert-BuOH)$\}.0.1ZnCl_2$ has used for the transesterification of dimethyl carbonate with different alcohols [121]. Nano Co-Zn DMC synthesized in presence of tert-BuOH as complexing agent and igepal as co-complexing agent in a reverse emulsion method was reported as efficient catalyst for hydroamination reactions [122]. A Fe-Zn DMC prepared with tert-BuOH as complexing agent and $EO_{20}PO_{70}EO_{20}$ as co-complexing agent was reported for Prins condensation reactions [123]. Fe-Zn DMC of molecular formula $K_4Zn_4[Fe(CN)_6]_3.6H_2O.2$(t-BuOH) has been used for the synthesis of biodiesel and biolubricants from vegetable oil by transesterification with methanol [124]. A tentative structure of this catalyst is shown in Fig. 1.8. In all these catalytic reactions the Lewis acidity of Zn^{2+} was regarded as the active centre. Recently a mixed Fe-Cu-Co DMC of molecular formula $FeCu_2[Co(CN)_6]_2.7.5H_2O$ has been reported for the aerobic oxidation of oximes to corresponding ketones [125].

1.5.3. DMCs in polycarbonate synthesis

1.5.3.1. DMCs in PPC synthesis

Co-Zn and Fe-Zn DMCs are well accepted catalysts for the copolymerization of epoxides and CO_2. The first use of DMC as a catalyst for the copolymerization was reported

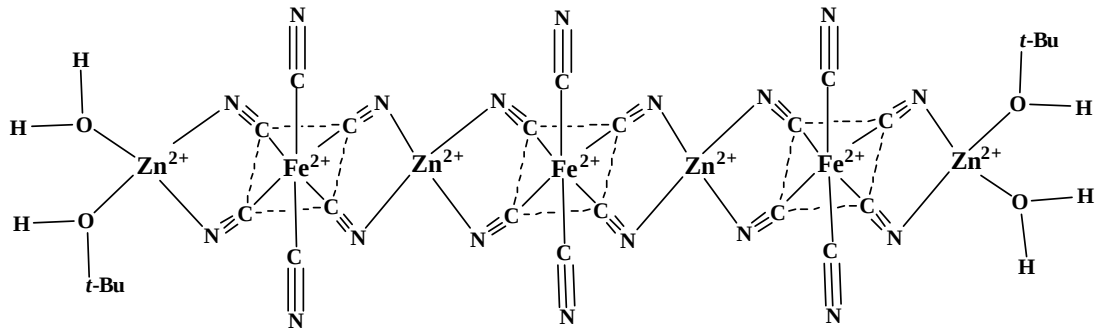

Fig. 1.8. Tentative structure of Fe-Zn DMC catalyst [124].

by Kruper et al [126] in 1985. The patent discussed the application of zinc hexacyanoferrate(III) for the copolymerization of ethylene oxide, PO, 1-butene oxide and CHO with CO_2. The catalyst prepared in presence of diglycolmethylether as the complexing agent produced polycarbonates with an M_n of 1500 - 30000 with a T_g between -15 to 25 °C. The polymer has incorporated 50-95 mol% CO_2 in the linear chain [126]. The first report on the use of Co-Zn modification of DMC for the copolymerization of PO and CO_2 was reported by Chen et al [127] in 2004. The $Zn_3[Co(CN)_6]_2$ DMC catalyst with polypropylene glycol of M_n = 400 as the initiator showed enhanced activity of over 1000 g polymer per gram of catalyst as compared to the $Zn_3[Fe(CN)_6]_2$ catalyst. The catalyst resulted 32 mol% of CO_2 incorporation in the polymer at 80 °C and 38 bar CO_2 in a 10 h reaction along with 12.2 wt% PC (M_n = 6050, PDI = 2.3). The latest advancements in DMC catalyzed copolymerization of PO and CO_2 include the following. Varghese et al [128] synthesized a new type of DMC catalyst of molecular formula $[ZnCl_2]_2[HCo(CN)_6][CH_3OH]$ to yield poly(propylene carbonate-co-propylene oxide) with high molecular weight (M_n ~ 40000) with a CO_2 incorporation of 60 mol% and a PDI of 1.8-2.2. The polymerizations were conducted at 65-90 °C for a period of 1-6 h at CO_2 pressures of 15-40 bars. Low molecular weight polymers (M_n ~ 2000) were also produced by feeding 1,10-decanediol as chain transfer agent. Gao et al [129] prepared a colourless oligo(carbonate-ether) diols from PO/CO_2 monomers using Co-Zn based DMC catalysts with different molecular weight polypropylene glycols as chain transfer agents. Oligo(carbonate-ether) of M_n= 6400 (PDI = 1.14-1.83) with CO_2 incorporation of 34.3 mol% were obtained over a period of 10 h at 90 °C and 40 bar CO_2. The amount of PC produced was < 8 wt%. Dong et al [130] used a combinatorial catalyst system comprising of Co-Zn DMC and a rare earth ternary complex for the synthesis of poly(ether carbonate)s *via* copolymerization of PO/CO_2. The catalyst systems produced poly(ether carbonate)s with 57.8 to 97.1 mol% of carbonate units with a M_n of 100000 (PDI = 4.64) at

40 bar CO_2 for 10 h at 70 ^oC. The synergetic effect between the two catalysts resulted enhancement in catalytic activity with reduction in PC (< 2 wt%). Zhang et al [131] employed a nano lamellar Co-Zn DMC catalysts of 100-500 nm edge length and 20-50 nm thickness to prepare PPC of M_n= 36500 (PDI = 2) with a CO_2 incorporation of 74.2 mol% at 40 ^oC for 10 h (P_{CO2} = 50 bar, W_{PC} = 5.6 wt%).

1.5.3.2. DMCs in PCHC synthesis

Yi et al [132] employed the first Co-Zn modification of DMC for the copolymerization of CO_2 and CHO. The authors used a nano Co-Zn DMC and a hybrid of Co-Zn and Fe-Zn DMC with $ZnCl_2$ and YCl_3 (50-100 nm). The catalyst showed a M_n of 5100 (PDI = 1.2) with a maximum of 59 mol% CO_2 incorporation at a CO_2 pressure of 6.8 bar. Thereafter, a number of publications came out which include the following. Chen et al [133] studied the activity of Co-Zn DMCs synthesized with different complexing agents. Among them, the complex with tert-butanol as complexing agent showed high conversion of 94% with 44.1 mol% of CO_2 incorporation over a reaction period of 2 h. The M_w and PDI varied from 9022 to 47250 and 1.62 to 3.4, respectively. Sun et al [134] employed an air stable hybrid catalyst of silicon dioxide/Co-Zn DMC with lamellar structure for the alternating copolymerization of CHO and CO_2. The hybrid catalyst produced 7.5 kg polymer/g of DMC with 47 mol% of CO_2 incorporation at 38 bar of CO_2 (100 °C, 3 h). The resultant polycarbonate was atactic with a M_n of 10,000 and PDI of 2-3. This group has further reported the mechanism of CHO/CO_2 polymerization through a combined kinetic study and electron spray ionization-mass spectrometry. These studies concluded that Zn-OH group in DMC catalyst is the active centre for polymerization; ether fractions in the polymer backbone were formed at the early stage of initiation forming head groups of the polymer. They reported 80.2 mol% of CO_2 incorporation in the polymer (40 bar, 50 °C, 5.3 h) [135]. Lee et al [136] studied the effect of co-complexing agents on Co-Zn DMCs for the copolymerization. The amount of CO_2 in the polymer varied between 14 and 63 mol% with the type of co-complexing agent used (M_n= 4500-11600 and PDI < 2). Dharman et al [137] applied a microwave induced copolymerization of CHO with CO_2 over Zn-Co catalyst. Microwave radiation removed the induction period of catalyst and this was attributed to higher activation of CHO by microwaves by its high polarization and high dielectric constant. The polymer was characterized with a M_n of 14500 (PDI = 1.5) and with a CO_2 incorporation of 75 mol%.

Apart from this, a one-pot terpolymerization of CO_2 with CHO and maleic anhydride over a Co-Zn has also been reported [138]. The polymerization resulted in poly(ester-

carbonates) with little amount of ether content (2.9-4.3 mol%). An excess of $ZnCl_2$ and tert-BuOH was found unavoidable in getting the highly active catalyst. The catalyst showed the highest activity of 12.7 kg polymer/g Zn for the reaction so far reported. Incorporation of maleic anhydride created an increase in the thermal properties of the polycarbonate.

1.6. Scope and objectives of the present work

In recent times, biodegradable polymers have attained great scientific interest because of their environmental adaptability and fast degradation. Catalysis has never been far away from the synthesis of these polymers. A well accepted homogeneous catalysis is primarily selected for their synthesis regardless of issues likes high moisture sensitivity, intricate handlings, corrosive nature and separation difficulties. Introduction of heterogeneous catalysts as a substitute can mitigate these problems to a great extent. However, it needs extensive structural characterization to correlate their critical structural features with catalytic activity. The main objective of this work is to employ heterogeneous DMC catalysts for the synthesis of biodegradable aliphatic hyperbranched polyesters and polycarbonates. A Fe-Zn DMC catalyst known for esterification and transesterification reactions was investigated, for the first time, in the synthesis of hyperbranched polyesters derived from glycerol (A_3 monomer) and diacid (succinic and adipic acid, B_2 monomer), renewable monomers. A Co-Zn DMC catalyst has been investigated for the copolymerization of CHO and/or PO with CO_2. This catalyst has also been investigated, for the first time, for the one-pot terpolymerization of CHO, PO and CO_2. One of the objectives of this study is to reveal the factors influencing the catalytic activity of Fe-Zn and Co-Zn DMC catalysts for polyesterification and polycarbonate synthesis through structure activity correlations.

1.7. Organization of thesis

The thesis is divided into six chapters. A brief description of each is given below.

Chapter 1 provides a general introduction about biodegradable polymers, hyperbranched polymers and polycarbonates, and the catalysis in synthesizing them. A historical structural evolution of DMC catalysts and their diverse applications is reported. The scope and objectives of the present work are also presented.

Chapter 2 describes the methodologies adopted for the synthesis of Fe-Zn and Co-Zn DMC catalysts and a detailed procedure for the polymerization reactions. A brief introduction to each characterization technique employed for the structural analysis of catalysts and polymers is also provided.

Chapter 3 presents the synthesis of hyperbranched polyesters derived from glycerol and diacids (succinic and adipic acid) over Fe-Zn DMC catalysts. Different DMC

compositions are synthesized by changing the complexing and co-complexing agent and varying the mode of addition of reagents. Activity studies and catalyst structure-activity correlations show that three critical parameters of Fe-Zn DMC influence the synthesis of hyperbranched polyesters of high degree of branching (DB) and controlled gelation. They include Lewis acidity (to initiate and catalyze the esterification reaction), hydrophobicity of the surface (to stabilize the active centres) and micro-meso porous architecture (to control the gelation). Influence of reaction parameters like temperature, reaction time and molar ratio of reactants on catalytic activity of Fe-Zn DMC is also investigated. The effect of chain length of acid monomer on DB and isolated yield of the polymer is also probed.

Chapter 4 deals with CO_2 utilization in polymer synthesis. Copolymerization of CO_2 with CHO over a set of structurally and compositionally different Co-Zn DMC catalysts prepared by two different synthetic procedures and their modifications are compared in terms of isolated yield and percentage incorporation of CO_2 in the polymers. Structure activity correlations reveal that the catalyst with monoclinic/rhombohedral crystal structure is more active than catalyst with cubic structure. Complexing agent is essential in inducing activity to catalysts. CO_2 adsorption indicates that higher the guest-host interactions lower is the induction period of catalysts. Excess of Cl^- ions in the catalyst structure increases Lewis acidity and improves the guest-host interactions. High density and strength of acid sites, low-crystal symmetry, moderate crystallinity, coordinated tert-butanol (complexing agent) and dispersed chloride ions are the critical parameters for high instant activity of Co-Zn DMC in copolymerization of CO_2 and CHO. Influence of reaction parameters on catalytic activity is also investigated.

Chapter 5 discusses the copolymerization of CO_2 and PO, and one-pot terpolymerization of PO, CHO and CO_2. Activity studies with the same set of structurally different Co-Zn catalysts show that the catalyst with highly crystalline cubic structure, less monoclinic impurity, high density of acid sites and less amount of complexing agent in its composition is more active and selective than the catalyst with monoclinic/rhombohedral crystal structure. Excess amount of alkali metal in catalyst structures causes higher selectivity towards cyclic carbonates. One-pot terpolymerization of PO, CHO and CO_2 on these set of Co-Zn DMC catalysts exhibits combined activity behaviour from their respective copolymerizations. Detailed structural analysis of the polymers shows that these catalysts produced block and terpolymers. The catalyst with monoclinic/rhombohedral crystal structure is highly active in producing an alternating terpolymer consisting of controlled fractions of propylene and cyclohexene carbonates. The catalyst with cubic structure produces a nearly

alternating terpolymer but it shows an induction period in the reaction and has no control on the composition of propylene and cyclohexene carbonate units in the terpolymer.

Chapter 6 provides an overall summary and conclusion of the work presented in the thesis.

By and large, this thesis describes the activity studies of Fe-Zn and Co-Zn DMC catalysts for the synthesis of two classes of biodegradable polymers: dendritic hyperbranched polymers derived from glycerol and diacids (succinic and adipic) and linear polycarbonates derived from CO_2 and epoxides (cyclohexene oxide and propylene oxide). In particular, this dissertation contributes to the fundamental understanding and advances the knowledge on the critical features of DMC catalysts for them to be active and selective in the investigated polymerization reactions.

1.8. References

[1] S. Maiti, Biodegradable Polymers: Polymer Recycle and Waste Management, Anusandhan Prakashan publications (2005).

[2] M. Vert, Biodegradable Polymers and Plastics, Royal Society of Chemistry (1992).

[3] www.plastemart.com.

[4] R. Smith, Biodegradable Polymers for Industrial Applications, Woodhead Publishing Limited and CRC Press LLC (2005).

[5] C.G. Pitt, Biodegradable Polymers and Plastics, Royal Society of Chemistry (1992).

[6] N. Grassie, G. Scott, Degradation and Stabilization of Polymers, Cambridge University Press (1985).

[7] G. Scott, D. Gilead, Degradable Polymers Principle and Applications, Chapman and Hall, London (1995).

[8] J.J. Bozel, Chemicals and Materials from Renewable Resources, ACS Symposium Series (2001) 784.

[9] C.M. Thomas, J.F. Lutz, Angew. Chem. Int. Ed. 50 (2011) 9244-9246.

[10] M. Poliakoff, P. Licence, Science 211 (2006) 810-812.

[11] J.J. Bozell, S. Kelley, W. Kang, D. Miller, M. Davis, Fuel Chemistry Division Preprints 47 (2002) 359-360.

[12] J.R. Hansen, H. Falsig, B. Jorgensen, C.H. Christensen, J. Chem. Technol. Biotechnol. 82 (2007) 329-333.

[13] E.Y.X. Chen, Chem. Rev. 109 (2009) 5157-5214.

[14] M.W.P.C. van Rossum, M. Alberda, L.H.W. Van der Plas, Phytochemistry 49 (1998)

723-729.

[15] L.E. Manzer, Appl. Catal. A: Gen. 272 (2004) 249-256.

[16] U. Biermann, J.O. Juergen, M.A.R. Meier, Macromol. Chem. Phys. 211 (2010) 854-862.

[17] H. Miyagawa, M. Misra, L.T. Drzal, A.K. Mohanty, Polymer 46 (2005) 445-453.

[18] M.Y. Krasko, A. Shikynov, A. Ezra, A.J. Domb, J. Polym. Sci. Part A: Polym. Chem. 41 (2003) 1059-1069.

[19] S. Matsumura, K. Takahashi, Makromol. Chem. Rapid Commun. 7 (1986) 369-373.

[20] M. Eissen, J.O. Metzger, E. Schmidt, U. Schneidewind, Angew. Chem. Int. Ed. 41 (2002) 414-436.

[21] V. Sharma, P.P. Kundu, Prog. Polym. Sci. 31 (2006) 983-1008.

[22] N. Pachauri, B. He, ASABE Annual International Meeting (2006).

[23] Department of Energy, U.S.A, Top Value Added Chemicals from Biomass, www1.eere.energy.gov/biomass/pdfs/ 35523.pdf, (2004).

[24] G. Rokicki, P. Rakoczy, P. Parzuchowski, M. Sobiecki, Green Chem.7 (2005) 529-539.

[25] H. Frey, R. Haag, Rev. Mol. Biotechnol. 90 (2002) 257-267.

[26] R. Knischka, P.J. Lutz, A. Sunder, R. Mülhaupt, H. Frey, Macromolecules 33 (2000) 315-320.

[27] V.T. Wyatt, G.D. Strahan, A. Nunez, J. Am. Oil Chem. Soc. 87 (2010) 1359-1369.

[28] N.R. Luman, T. Kim, M.W. Grinstaff, Pure Appl. Chem. 76 (2004) 1375-1385.

[29] M.R. Kember, A. Buchard, C.K. Williams, Chem. Commun. 47 (2011) 141-163.

[30] P. Brignou, M.P. Gil, O. Casagrande, J.F. Carpentier, S.M. Guillaume, Macromolecules 43 (2010) 8007-8017.

[31] D. Yan, C. Gao, H. Frey, Hyperbranched Polymers Synthesis Properties and Applications, John Wiley & Sons, Inc. Hoboken, New Jersey (2011).

[32] J.M.J. Fréchet, D.A. Tomalia, Dendrimers and Other Dendritic Polymers, West Sussex: Wiley, (2001).

[33] G.V. Korolev, M.M. Mogilevich, Three-dimensional Free Radical Polymerization: Cross-linked and Hyperbranched Polymers, Springer-Verlag, Berlin (2009).

[34] J.M. Spruell, C. Hawker, J. Chem. Sci. 2 (2011) 18-26.

[35] S.E. Stiriba, H. Kautz, H. Frey, J. Am. Chem. Soc. 124 (2002) 9698-9699.

[36] E. Burakowska, J.R. Quinn, S.C. Zimmerman, R. Haag, J. Am. Chem. Soc. 131

(2009) 10574-10580.

[37] Y.F. Zhou, D.Y. Yan, Angew. Chem. Int. Ed. 44 (2005) 3223-3226.

[38] C.H. Liu, C. Gao, D.Y. Yan, Angew. Chem. Int. Ed. 46 (2007) 4128-4131.

[39] X. Wang, H.J. He, J.Y. Wu, C. Gao, Y.H. Xu, Biomacromolecules 11 (2010) 245-251.

[40] R.H. Kienle, A.G. Hovey, J. Am. Chem. Soc. 51 (1929) 509-519.

[41] R.H. Kienle, P.A. Meulen, F.E. Petke, J. Am. Chem. Soc. 61 (1939) 2268-2271.

[42] G. Odian, Principles of Polymerization, 3rd Ed. New York, Wiley (1991).

[43] P.J. Flory, J. Am. Chem. Soc. 63 (1941) 3083-3090; P.J. Flory, J. Am. Chem. Soc. 63 (1941) 3091-3096; P.J. Flory, J. Am. Chem. Soc. 63 (1941) 3096-3100; P.J. Flory, J. Am. Chem. Soc. 69 (1947) 30-35.

[44] P.J. Flory, J. Am. Chem. Soc. 74 (1952) 2718-2723.

[45] H.R. Kricheldorf, Q.Z. Zang, G. Schwarx, Polymer 23 (1982) 1821-1829.

[46] Y.H. Kim, US Patent No 4,857,630 (1987); Y.H. Kim, O.W. Webster, J. Am. Chem. Soc. 112 (1990) 4592-4593.

[47] Y.H. Kim, O.W. Webster, Polym. Prep. 29 (2) (1988) 310-311.

[48] K.E. Uhrich, C. Hawker, J.M.J. Fréchet, S.R. Turner, Macromolecules 25 (1992) 4583-4587.

[49] P. Kambouris, C.J. Hawker, J. Chem Soc. Perkin Trans. 1 (1993) 2717-2727.

[50] G. Yang, M. Jikei, M. Kakimoto, Macromolecules 31 (1998) 5964-5966.

[51] D.H. Bolton, K.L. Wooley, Macromolecules 30 (1997) 1890-1896.

[52] C.J. Hawker, F. Chu, Macromolecules 29 (1996) 4370-4380.

[53] R. Spindler, J.M.J. Fréchet, Macromolecules 26 (1993) 4809-4813

[54] A. Muzafarov, M. Golly, M. Möller, Macromolecules 28 (1995) 8444-8446.

[55] L.J. Hobson, A.M. Kenwright, W.J. Feast, Chem. Commun. 19 (1997) 1877-1878.

[56] T.M. Londergan, Y. You, M.E. Thompson, W.P. Weber, Macromolecules 31 (1998) 2784-2788.

[57] D. Yan, C. Gao, Macromolecules 33 (2000) 7693-7699; S.M. Aharoni, S.F. Edwards, Macromolecules 22 (1989) 3361-3374.

[58] M. Jikei, S.H. Chon, M. Kakimoto, S. Kawauchi, T. Imase, J. Watanabe, Macromolecules 32 (1999) 2061-2064.

[59] P.J. Flory, Principles of Polymer Chemistry, Ithaca, NY, Cornell University Press (1953).

[60] T. Emrick, H.T. Chang, J.M.J. Fréchet, Macromolecules 32 (1999) 6380-6382

[61] T. Emrick, H.T. Chang, J.M.J. Fréchet, J. Polym. Sci. Part A: Polym. Chem. 38 (2000) 4850-4869.

[62] S. Murtuza, S.B. Harkins, G.S. Long, A. Sen, J. Am. Chem. Soc. 122 (2000) 1867-1872.

[63] M. Schömer, J. Seiwert, H. Frey, ACS Macro Lett. 1 (2012) 888-891.

[64] B. De, K. Gupta, M. Mandal, N. Karak, ACS Sustainable Chem. Eng. 2 (2014) 445-453.

[65] S. Pramanik, R. Konwarh, K. Sagar, B.K. Konwar, N. Karak, Prog. Org. Coat. 76 (2013) 689-697.

[66] J.F. Stumbé, B. Bruchmann, Macromol. Rapid Commun. 25 (2004) 921-924.

[67] U.S. Department of Energy, Carbon Dioxide and Climate, Office of Basic Energy Sciences (1984); W.M. Ayers, Catalytic Activation of Carbon Dioxide, American Chemical Society, Washington DC (1988).

[68] M. Aresta, A. Dibenedetto, A. Angelini, J. CO_2 Utiliz. 3 (2013) 65-73.

[69] H. Arakawa, M. Aresta, J.N. Armor, M.A. Barteau, E.J. Beckman, A.T. Bell, J.E. Bercaw, C. Creutz, G.A. Somorjai, P.C. Stair, B.R. Stults, W. Tumas, Chem. Rev. 101 (2001) 953-996.

[70] M. Abolhasani, A. Gnther, E. Kumacheva, Angew. Chem. Int. Ed. 53 (2014) 7992-8002.

[71] M. Aresta, Carbon Dioxide as Chemical Feedstock, Wiley-VCH Verlag GmbH & Co. KGaA, Weinheim (2010).

[72] H.J. Freund, M.W. Roberts, Surf. Sci. Rep. 25 (1996) 225-273.

[73] M. Aresta, E. Quaranta, I. Tommasi, P. Giannoccaro, A. Ciccarese, Gazz. Chim. Ital. 125 (1995) 509-538.

[74] A. Einhorn, Annalen 300 (1898) 135.

[75] C.A. Bischoff, A.V. Hedenstroem, Berichte 35 (1902) 3431.

[76] W.H. Carothers, F.J. van Natta, J. Am. Chem. Soc. 52 (1930) 314-326.

[77] S.G. Legrand, J.T. Bendler, Handbook of Polycarbonate Science and Technology, Marcel Dekker, Inc. New York (2000).

[78] J. Xu, E. Feng, J. Song, J. Appl. Polym. Sci. 131 (2014) 39822-39838.

[79] H. Sugimoto, S. Inoue, Pure Appl. Chem. 78 (2006) 1823-1834; G. Luinstra, A. Polym. Rev. 48 (2008) 192-219.

[80] J. Feng, R.X. Zhuo, X.Z. Zhang, Prog. Polym. Sci. 37 (2012) 211-236; S. Tempelaar, L. Mespouille, O. Coulembier, P. Dubois, A.P. Dove, Chem. Soc. Rev. 42 (2013) 1312-1336.

[81] H.C. Stevens, US Patent No. 3,248,415 (1966).

[82] S. Inoue, H. Koinuma, T. Tsuruta, J. Polym. Sci. Part B: Polym. Lett. 7 (1969) 287-292; S. Inoue, H. Koinuma, T. Tsuruta, Makromol. Chem. 130 (1969) 210-220.

[83] A. Rokicki, W. Kuran, J. Macromol. Sci. Rev. Macromol. Chem. C21 (1981) 135; W. Kuran, S. Pasynkiewicz, J. Skupinska, A. Rokicki, Makromol. Chem. 177 (1976) 11-20; P. Gorecki, W. Kuran, J. Polym. Sci. 23C (1985) 299-304.

[84] M. Ree, J.Y. Bae, J.H. Jung, T.J. Shin, J. Polym. Part A: Poly. Chem. 37 (1999) 1863-1876.

[85] Y.Q. Zheng, J.L. Liu, H.L. Zhang, Z. Kristallogr. 215 (4) (2000) NCS 1267-413; A. Rockicki, US Patent No. 4,943,677 (1990); S. Motika, US Patent No. 5,026,676 (1991).

[86] www.empowermaterials.com

[87] S. Inoue, J. Polym. Sci. Part A: Polym. Chem. 38 (2000) 2861-2871.

[88] D.J. Darensbourg, M.W. Holtcamp, Marcomolecules 28 (1995) 7577-7579.

[89] M. Super, E. Berluche, X. Costello, E.J. Beckman, Macromolecules 30 (1997) 368-372.

[90] M. Cheng, E.B. Lobkovsky, G.W. Coates, J. Am. Chem. Soc. 120 (1998) 11018-11019.

[91] S.D. Allen, D.R. Moore, E.B. Lobkovsky, G.W. Coates, J. Am. Chem. Soc. 124 (2002) 14284-14285.

[92] C.M. Byrne, S.D. Allen, E.B. Lobkovsky, G.W. Coates, J. Am. Chem. Soc. 126 (2004) 11404-11405.

[93] C.T. Cohen, T. Chu, G.W. Coates, J. Am. Chem. Soc. 127 (2005) 10869-10878.

[94] K. Nakano, T. Kamada, K. Nozaki, Angew. Chem. Int. Ed. 45 (2006) 7274-7277.

[95] E.K. Noh, S.J. Na, S. Sujith, S.W. Kim, B.Y. Lee, J. Am. Chem. Soc. 129 (2007) 8082-8083.

[96] D.J. Darensbourg, S.J. Wilson, Green Chem. 14 (2012) 2665-2671.

[97] M. Kröger, C. Folli, O. Walter, M. Döring, Adv. Synth. Catal. 348 (2006) 1908-1918.

[98] L. Shi, X.B. Lu, R. Zhang, X.J. Peng, C.Q. Zhang, J.F. Li, X.M. Peng, Macromolecules 39 (2006) 5679-5685.

[99] H. Li, Y. Niu, Polym. J. 43 (2011) 121-125.

[100] S.D. Thorat, P.J. Phillips, V. Semenov, A. Gakh, J. Appl. Polym. Sci. 89 (2003) 1163-1176.

[101] G.W. Coates, D.R. Moore, Angew. Chem. Int. Ed. 43 (2004) 6618-6639.

[102] Novomer, Catalyzing Green Chemistry, www.novomer.com.

[103] H. Holtzman, Ind. Eng. Chem. 37 (1945) 855-861.

[104] J.F. Keggin, F.D. Miles, Nature 137 (1936) 577-578.

[105] C.A. Lundgren, R.W. Murray, Inorg. Chem. 27 (1988) 933-939; F. Herren, P. Fischer, A. Ludi, W. Halg, Inorg. Chem. 19 (1980) 956-959.

[106] M.B. Robin, Inorg. Chem. 1 (1962) 337-342.

[107] H.B. Weiser, W.O. Milligan, J.B. Bates, J. Phys. Chem. 46 (1942) 99-111.

[108] R.J. Herold, US Patent No. 3,278,459 (1966).

[109] R.A. Livigni, R.J. Herold, O.C. Elmer, S.L. Aggarwal, ACS Symp. Seri. 6 (1975) 20-37.

[110] D.F. Mullica, W.O. Milligan, G.W. Beall, W.L. Reeves, Acta Cryst. B34 (1978) 3558-3561.

[111] G. Boxhoorn, J. Moolhuysen, J.G.F. Coolegem, R.A. van Santen, J. Chem. Soc. Chem. Commun. (1985) 1305-1307.

[112] P.P. Gracereau, E.G.A. Hardy, Acta Cryst. B35 (1979) 2843-2848.

[113] J. Kuyper, G. Boxhoorn, J. Catal. 105 (1987) 163-174.

[114] J. Hoffman, P. Gupta, H. Pielartzik, P. Ooms, W. Schafer, US Patent No. 5,998,327 (1999); H.R. Hinney, D.S. Wardius, US Patent No. 5,158,922 (1992); B.L. Khac, W. Chester, US Patent No. 5,789,626 (1998); B.L. Khac, W. Chester, US Patent No. 5,536,883 (1996).

[115] J.R. Hernández, E. Reguera, E. Lima, J. Balmaseda, R.M. García, H.Y. Madeira, J. Phys. Chem. Solid. 68 (2007) 1630-1642.

[116] M. Avila, L. Reguera, J.R. Hernández, J. Balmaseda, E. Reguera, J. Solid State Chem. 181 (2008) 2899-2907.

[117] P.K. Thallapally, R.K. Motkuri, C.A. Fernadez, B.P. McGrail, G.S. Behrooz, Inorg. Chem. 49 (2010) 4909-4915.

[118] S. Ohkoshi, Y. Abe, A. Fujishima, K. Hashimoto, Phys. Rev. Lett. 82 (1999) 1285-1288.

[119] O. Sato, T. Iyoda, A. Fujishima, K. Hashimoto, Science 272 (1996) 704-705.

[120] L. Saikia, J.K. Satyarthi, R. Gonnade, D. Srinivas, P. Ratnasamy, Catal. Lett. 123 (2008) 24-31.

[121] R. Srivastava, D. Srinivas, P. Ratnasamy, J. Catal. 241 (2006) 34-44.

[122] A. Peeters, P. Valvekens, R.P. Ameloot, G. Sankar, C.E.A. Kirschhock, D.E. De Vos, ACS Catal. 3 (2013) 597-607.

[123] M.V. Patil, M.K. Yadav, R.V. Jasra, J. Mol. Catal. A: Chem. 273 (2007) 39-47.

[124] P.S. Sreeprasanth, D. Srinivas, P. Ratnasamy, Appl. Catal. A: Gen. 314 (2006) 148-159.

[125] A.G. Ortiz, A. Grirrane, E. Reguera, H. García, J. Catal. 311 (2014) 386-382.

[126] W.J. Kruper, D.J. Swart, US Patent No. 4,500,704 (1985).

[127] S. Chen, Z. Hua, Z. Fang, G. Qi, Polymer 45 (2004) 6519-6524.

[128] J.K. Varghese, D.S. Park, J.Y. Jeon, B.Y. Lee, J. Polym. Sci. Part A: Polym. Chem. 51 (2013) 4811-4818.

[129] Y. Gao, Y. Qin, X. Zhao, F. Wang, X. Wang, J. Polym. Res. 19 (2012) 9878-9887.

[130] Y. Dong, X. Wang, X. Zhao, F. Wang, J. Polym. Sci. Part A: Polym Chem. 50 (2012) 362-370.

[131] X.H. Zhang, R.J. Wei, X.K. Sun, J.F. Zhang, B.Y. Du, Z.Q. Fan, G.R. Qi , Polymer 52 (2011) 5494-5502.

[132] M.J. Yi, S.H. Byun, C.S. Ha, D.W. Park, I. Kim, Solid State Ionics 172 (2004) 139-144.

[133] S. Chen, G.R. Qi, Z.J. Hua, H.Q. Yan, J. Polym. Sci. Part A: Polym. Chem. 42 (2004) 5284-5291.

[134] X.K. Sun, X.H. Zhang, F. Liu, S. Chen, B.Y. Du, Q. Wang, Z.Q. Fan, G.R. Qi, J. Polym.Sci. Part A: Polym. Chem. 46 (2008) 3128-3139.

[135] X.K. Sun, X.H. Zhang, R.J. Wei, B.Y. Du, Q. Wang, Z.Q. Fan, G.R. Qi, J. Polym. Sci.Part A: Polym. Chem. 50 (2012) 2924-2934.

[136] I.K. Lee, J.Y. Ha, C. Cao, D.W. Park, C.S. Ha, I. Kim, Catal. Today 148 (2009) 389-397.

[137] M.M. Dharman, J.Y. Ahn, M.K. Lee, H.L. Shim, K.H. Kim, I. Kim, D.W. Park, Green Chem. 10 (2008) 678-684.

[138] X.K. Sun, X.H. Zhang, S. Chen, B.Y. Du, Q. Wang, Z.Q. Fan, G.R. Qi, Polymer 51 (2010) 5719-5725.

Chapter - 2

Experimental Methods and Characterization Techniques

2.1. Introduction

This chapter describes the experimental methods involved in the synthesis of various compositionally different double-metal cyanide (DMC) catalysts, physicochemical characterization and reaction procedure for the synthesis of hyperbranched polyesters and polycarbonates. It also presents the methods for the purification and structural characterization of the polymers synthesized. Fe-Zn and Co-Zn DMC catalysts were synthesized by complexation of their respective precursor salts, $K_4[Fe(CN)_6].3H_2O$, $K_3[Co(CN)_6]$ and $ZnCl_2$ in presence of complexing [tert-butanol (t-BuOH), methanol or glycerol) and/or co-complexing agents (polyethylene glycol - PEG). Molecular weight of co-complexing agent was systematically varied (M_n = 300, 600, 1500 or 4000) to prepare different Fe-Zn DMC catalysts. Also the mode of reagent addition was altered to synthesize compositionally different Fe-Zn and Co-Zn DMC catalysts.

Catalysts of the present study were extensively characterized by various physical techniques like, X-ray powder diffraction (XRD), Fourier transform infrared spectroscopy (FTIR), Raman spectroscopy, N_2/CO_2 physisorption, thermogravimetry (TG), high resolution transmission electron microscopy (HRTEM), scanning electron microscopy (SEM), energy dispersive X-ray analysis (EDX), diffuse reflectance infrared Fourier transform spectroscopy of adsorbed pyridine (Py-DRIFT) and temperature-programmed desorption of ammonia (NH_3-TPD).

Structural analysis of hyperbranched polyesters was done using 1-dimensional proton nuclear magnetic resonance spectroscopy (^{1}H-NMR), inverse-gated ^{13}C-NMR spectroscopy with complementary distortionless enhanced polarization transfer (DEPT) technique, 2-dimensional spectroscopies like heteronuclear single quantum correlation spectroscopy (HSQC) and heteronuclear multiple quantum correlation spectroscopy (HMBC), and matrix assisted laser desorption/ionization time-of-flight mass spectrometry (MALDI-TOF). Aliphatic polycarbonates were characterized by ^{1}H-NMR, ^{13}C-NMR, FTIR, TG, differential scanning calorimetry (DSC) and gel permeation chromatography (GPC) techniques.

2.2. Catalyst preparation

2.2.1. Fe-Zn DMC catalysts

2.2.1.1 Fe-Zn-0

In a typical synthesis of Fe-Zn-0, solution 1 was prepared by dissolving 4.2 g of $K_4[Fe(CN)_6].3H_2O$ (0.01 mol; Merck, India) in 40 ml of deionized water. Solution 2 was prepared by dissolving 13.6 g of $ZnCl_2$ (0.1 mol; Merck, India) in 18 ml of deionized water. Solution 2 was added to solution 1 maintained at 50 °C while stirring over a period of 1 h. A

white precipitation occurred during the addition. The slurry was then aged for 1 h with continued stirring. The solid precipitate was then filtered, washed thoroughly with copious amount of deionized water to remove chloride ions and dried at 25 °C for 2 - 3 days to a constant weight (white coloured solid; yield = 3.9 g).

2.2.1.2 Fe-Zn-1

Fe-Zn-1 catalyst was prepared in presence of t-BuOH as complexing agent and PEG of number average molecular weight (M_n) 300 (PEG-300) as co-complexing agent [1]. In a typical synthesis, solution 1 was prepared by dissolving 4.2 g of $K_4[Fe(CN)_6].3H_2O$ (0.01 mol) in 40 ml of deionized water. Solution 2 was prepared by dissolving 13.6 g of $ZnCl_2$ (0.1 mol) in a mixture of deionized water (18 ml) and t-BuOH (20 ml). PEG-300 (15.0 g) was separately dissolved in 2 ml of deionized water and 40 ml of t-BuOH to prepare solution 3. Solution 2 was added slowly to solution 1 and equilibrated at 50 ^{o}C over a period of 1 h with vigorous stirring. White precipitation occurred during the addition. Then, solution 3 was added to this suspension over a period of 5 min and the stirring was continued for another 1 h. Solid cake formed was filtered, washed with 2 litres of deionized water to remove excess co-complexing agent, and dried at 25 °C for 2 - 3 days to a constant weight (yield = 3.7 g).

2.2.1.3. Fe-Zn-2

Fe-Zn-2 catalyst was prepared by the same procedure as that of Fe-Zn-1 except that co-complexing agent PEG-300 was replaced with PEG-600 (yield = 3.8 g).

2.2.1.4. Fe-Zn-3

Fe-Zn-3 catalyst was prepared by the same procedure as that of Fe-Zn-1 except that co-complexing agent PEG-300 was replaced with PEG-1500 (yield = 3.8 g).

2.2.1.5. Fe-Zn-4

Fe-Zn-4 DMC catalyst was prepared by the same procedure as that of Fe-Zn-1 except that co-complexing agent PEG-4000 was used instead of PEG-300 (yield = 3.7 g).

2.2.1.6. Fe-Zn-5

Fe-Zn-5 catalyst was prepared by the same procedure as that of Fe-Zn-4 but with a different mode of addition of reagents. In the modified synthesis, solution 1 was prepared by dissolving 4.2 g of $K_4[Fe(CN)_6].3H_2O$ (0.01 mol) in 40 ml of deionized water. Solution 2 was prepared by dissolving 13.6 g of $ZnCl_2$ (0.1 mol) in a mixture of deionized water (18 ml) and t-BuOH (20 ml). PEG-4000 (15.0 g) was separately dissolved in 2 ml of deionized water and 40 ml of t-BuOH to prepare solution 3. Solution 2 was added to solution 3 and this mixture was then added to solution 1 maintained at 50 °C over a period of 1 h with vigorous stirring. White precipitation occurred during the addition. The slurry was then aged at the same

temperature for 1 h. The solid cake formed was then filtered, washed with 2 litres of deionized water, and dried at 25 °C for 2 - 3 days to a constant weight (yield = 4.2 g).

2.2.1.7. Fe-Zn-6

Fe-Zn-6 DMC was prepared by the same procedure as that of Fe-Zn-4 but with a modification in the addition of reagent solutions. In the modified synthesis, solution 1 was added to solution 3 and equilibrated at 50 °C. To this mixture, solution 2 was added over a period of 1 h with vigorous stirring. White precipitation occurred during the addition. The slurry was then maintained at the same temperature for one more hour while stirring. Solid cake formed was then filtered, washed with 2 litres of deionized water, and dried at 25 °C for 2 - 3 days to a constant weight (yield = 4.1 g).

2.2.1.8. Fe-Zn-7

Fe-Zn-7 catalyst was synthesized by the same procedure as that of Fe-Zn-4 except that the complexing agent t-BuOH was replaced with methanol (yield = 3.7 g).

2.2.1.9. Fe-Zn-8

Fe-Zn-8 DMC was synthesized by the same procedure as that of Fe-Zn-4 except that the complexing agent t-BuOH was replaced with glycerol (yield = 4.0 g).

All Fe-Zn DMC catalysts were activated at 180 °C for 2 h prior to use in polymerizations and in characterizations.

2.2.2. Co-Zn DMC catalysts

2.2.2.1 Co-Zn-0

Co-Zn-0 DMC was prepared by complexation of $K_3[Co(CN)_6]$ with $ZnCl_2$ in the absence of complexing and/or co-complexing agent. In a typical synthesis, solution 1 was prepared by dissolving 4.0 g of $K_3[Co(CN)_6]$ (Aldrich Co.) in 70 ml of deionized water. Solution 2 was prepared by dissolving 12.5 g of $ZnCl_2$ (Merck, India) in 20 ml of deionized water. During the synthesis, solution 2 was added to solution 1 maintained at 50 °C over a period of 1 h. White precipitation occurred during the addition. After completing the addition, the slurry was aged at the same temperature for 1 h with stirring. The solid formed was filtered, washed with copious amount of deionized water and dried at 25 °C for 2 - 3 days to a constant weight (white coloured solid, yield = 3.7 g).

2.2.2.2 Co-Zn-1

Co-Zn-1 catalyst was prepared in the presence of t-BuOH as complexing agent and PEG- 4000 as co-complexing agent [1]. In a typical synthesis, solution 1 was prepared by dissolving 3.32 g of $K_3[Co(CN)_6]$ in 40 ml of deionized water. Solution 2 was prepared by dissolving 13.6 g of $ZnCl_2$ in a mixture of deionized water (18 ml) and t-BuOH (20 ml).

Solution 3 was prepared by dissolving 15.0 g of PEG-4000 in 2 ml of deionized water and 40 ml of t-BuOH. Solution 3 was warmed to get a transparent solution. During the synthesis, solution 2 was added to solution 1 maintained at 50 °C over a period of 1 h with vigorous stirring. White precipitation occurred during the addition. Then, solution 3 was added to this suspension over a period of 5 min and aged for 1 h with continued stirring. Solid cake formed was filtered, washed with deionized water (2 litres) and dried at 25 °C for 2 - 3 days to a constant weight (yield = 3.0 g).

2.2.2.3. Co-Zn-2

Co-Zn-2 DMC was prepared by the same procedure as that of Co-Zn-1 but with a modification in the mode of addition of reagent solutions. In a typical synthesis, solution 2 was mixed with solution 3 and this mixture was added to solution 1 maintained at 50 °C. The slurry was then aged for 1 h at 50 °C with stirring. Solid cake formed was separated by filtration, washed with deionized water (2 litres) and dried at 25 °C for 2 - 3 days to a constant weight (yield = 3.7 g).

2.2.2.4. Co-Zn-3

Co-Zn-3 DMC was prepared in the presence of complexing and co-complexing agents [2]. In a typical synthesis, solution 1 was prepared dissolving 4 g of $K_3[Co(CN)_6]$ in 70 ml of deionized water. Solution 2 was prepared by dissolving 12.5 g of $ZnCl_2$ in 20 ml of deionized water. Solution 3 was prepared by mixing 1 g of PEG-4000, 1 ml of t-BuOH and 100 ml of deionized water. Solution 2 was added to solution 1 maintained at 50 °C over a period of 1 h. To it, a mixture of t-BuOH and deionized water (1:1 volume ratio; 100 ml) was added immediately and stirred for another 10 min. Solution 3 was then added to this slurry and aged for 1 h at 50 °C while stirring. It was then filtered and suspended in PEG-4000 (1 g), t-BuOH (70 ml) and deionzed water (30 ml) mixture while stirring for 10 min at 50 °C. The solid cake was filtered and once again suspended in PEG-4000 (0.5 g) and t-BuOH (100 ml) solution at 50 °C while stirring for 10 min. Finally, it was filtered and dried at 25 °C for 2 - 3 days to a constant weight (yield = 3.8 g).

2.2.2.5. Co-Zn-4

Co-Zn-4 DMC was prepared by the same synthesis procedure as that of Co-Zn-3 with the modification that no co-complexing agent (PEG-4000) was used. In a typical synthesis, solution 2 was added to solution 1 maintained at 50 °C over a period of 1 h. To it, a mixture of 100 ml of t-BuOH and deionized water (1:1 volume ratio) was added and stirred for 10 min. Solution 3 containing t-BuOH (1 ml) and deionized water (100 ml) was then added and aged for 1 h. The solid formed was filtered, suspended in t-BuOH (70 ml) and deionzed water

(30 ml) mixture at 50 °C and stirred for 10 min. It was filtered and once again suspended solely in t-BuOH (100 ml) at 50 °C for 10 min while stirring. It was, then, filtered and dried at 25 °C for 2 - 3 days to a constant weight (yield = 3.7 g).

2.2.2.6. Co-Zn-4-1

This catalyst was prepared by the same procedure as that of Co-Zn-4 except that the second suspension step in t-BuOH (100 ml) was avoided (yield = 3.6 g).

2.2.2.7. Co-Zn-4-2

The catalyst was prepared by the same procedure as that of Co-Zn-4 except that after aging at 50 °C for 1 h, it was filtered and washed with 250 ml of deionized water. It was then suspended in t-BuOH (70 ml) and deionzed water (30 ml) mixture at 50 °C and stirred for 10 min. It was filtered and suspended solely in t-BuOH (100 ml) at 50 °C for 10 min while stirring. Finally, it was filtered and dried at 25 °C for 2 - 3 days to a constant weight (yield = 3.4 g).

All Co-Zn DMC catalysts were activated at 180 °C for 2 h prior to use in polymerizations and in characterizations.

2.3. Characterization techniques

2.3.1. X-ray diffraction

XRD is the most frequently used characterization technique to identify the phase purity (lattice parameters) and to estimate the crystallite sizes of solid crystalline materials [3]. The principle of XRD relies on the elastic scattering of X-rays by atoms in a periodic lattice. Constructively scattered monochromatic X-rays from different crystal planes produce a diffraction pattern. The lattice spacing (or inter planar spacing) of the material which is characteristic of compounds is calculated with the help of Bragg's relationship.

$$n\lambda = 2d\, sin\theta;\ \ n = 1, 2, \ldots$$

where λ is the wavelength of X-rays, d is the distance between two lattice planes, θ is the angle between incoming X-rays and the normal to the reflecting lattice plane, n is an integer known as order of reflection. Diffractions from large crystals are very narrow while for smaller crystallites line broadening becomes inevitable due to incomplete destructive interference in scattering directions where X-rays are out of phase. Crystallite sizes of materials are calculated with the help of Scherrer formula which relates crystal size to peak width as,

$$< L > = \frac{K\lambda}{\beta\, cos\theta}$$

where <*L*> is a measure for the dimension/size of the crystal in the direction perpendicular to the reflecting plane, λ is the X-ray wavelength, β is the peak width at half height, θ is the angle between the beam and the normal to the reflecting plane and *K* is a constant often taken as 0.95. In the present study, XRD of powdered samples were recorded in the 2θ range of 10-50° at a scan rate of 2°/min on a Philips X'Pert Pro diffractometer using Cu-K_α radiation (λ = 0.15406 nm) and a proportional counter detector. Catalyst powders in the forms of films were prepared on a glass plate and analyzed.

2.3.2. Fourier transform infrared spectroscopy

IR is considered as the first and the most important modern spectroscopic characterization technique. It found wide application in catalysis [3] as it provides information on structure, geometry and orientation of practically all molecules in the reaction mixture irrespective of their physical state. IR radiations excite vibrations in molecules of solid lattices by absorption. Transitions between vibrational levels of significant importance occur in the mid-IR region (200-4000 cm^{-1}). The vibrational frequency (ν) of a diatomic molecule is related to its force constant (*K*) and reduced mass (μ) as,

$$\nu = \frac{1}{2\pi}\sqrt{\frac{K}{\mu}} \qquad \mu = \frac{m_1\ m_2}{m_1 + m_2}$$

As per the equation, ν increases with increase in bond strength or force constant (*K*) and decreases with increase in masses (m_x) of atoms. This information is used to assign the bands in the spectrum of a molecule/sample. In the present study, FTIR spectra of DMC catalysts as KBr pellets (1 wt%) in the transmission mode were recorded on a Shimadzu 8201 PC spectrophotometer in the wavenumber region of 450 to 4000 cm^{-1} (100 scan accumulations) at a spectral resolution of 4 cm^{-1}.

DRIFT spectra of DMC catalysts adsorbed with pyridine (10 µl) were measured as loose powders on a Shimadzu 8201 PC spectrophotometer at different temperatures (50, 100, 150 and 200 °C; 100 scans and spectral resolution of 4 cm^{-1}). The produced spectra were subtracted by the standard reference spectrum of the sample unexposed to pyridine at the same temperature. The C-H stretching of adsorbed pyridine from 1200 to 1700 cm^{-1} was used to differentiate Lewis and Brönsted acid sites.

2.3.3. Raman spectroscopy

Raman spectroscopy is based on the inelastic scattering of photons, which lose energy by exciting vibrations in the sample [3, 4]. Photons from a monochromatic laser source are absorbed by the material and subsequently re-emitted. A Raman shift occurs when the

frequency of these re-emitted radiations is decreased (stokes lines) or increased (anti-stokes lines) due to bond vibrations. The Raman effect is induced by the molecular deformation which is determined by the polarizability factor α. The induced dipole moment (P) of the molecules is related to the electric field (E) of the incident monochromatic radiation and α, by the equation $P = \alpha E$. Upon interaction, molecules start vibrating with characteristic frequency which gives rise to Raman spectra for structural analysis. In the present study, FT-Raman spectra of catalysts were recorded on a Horiba JY LabRaman HR800 MicroRaman spectrometer using 630 nm wavelength generated by a He-Ne laser operating at 20 mV. The samples were prepared as loosely pressed circular discs on a glass plate for analysis.

2.3.4. N_2 / CO_2 physisorption

The most common method of measuring specific surface area and textural characteristics of catalytic materials is based on the theory developed by Brunauer, Emmett and Teller (BET), considering the multilayer adsorption [5]. The BET equation can be represented as:

$$\frac{P}{V(P_o - P)} = \frac{1}{C\,V_m} + \frac{(C-1)}{CV_m} \times \frac{P}{P_o}$$

where P is adsorption equilibrium pressure, P_o is saturation vapor pressure of the adsorbate (N_2) at the experimental temperature, V is volume of N_2 adsorbed at pressure P, V_m is volume of adsorbate required for monolayer coverage and C, a constant that is related to the heat of adsorption and liquefaction. The linear relationship between $P/V(P_o\text{-}P)$ and P/P_o is used to obtain the quantity of N_2 adsorbed. The monolayer volume, V_m is given by $1/(S+I)$, where S is the slope and is equal to $(C\text{-}1)/CV_m$ and I is the intercept equal to $1/CV_m$ [5]. The specific surface area of the catalyst (S_{BET}) is related to V_m, by the equation,

$$S_{BET} = \frac{V_m}{22414} \times N_a \times \sigma$$

where N_a is Avogadro number and σ is mean cross sectional area covered by one adsorbate molecule. The surface area of N_2 is taken as 0.162 nm^2. Several computational procedures are available for the derivation of pore size distribution of mesoporous samples from physisorption isotherms. Most popular among them is the Barrett-Joyner-Halenda (BJH) model, which is based on speculative emptying of the pores by a stepwise reduction of P/P_o, and allowance being made for the contraction of the multilayer in those pores already emptied by the condensate. The pore size distribution is usually expressed as a plot of $D_v \log d$ (cc/g) versus pore diameter (d) where D_v is the volume adsorbed in pore of diameter d. In the

present study, specific surface area, pore volume and pore diameter of DMC catalysts were determined at -196 °C using a Quantachrome USA (Autosorb-1C) instrument. Prior to N_2 adsorption, the samples (100 mg) in a quartz tube were evacuated at 180 °C for 3 h. After that the quartz cell was dipped in a liquid nitrogen container up to the sample level and then started passing N_2 through it. A reference alumina sample (supplied by Quantachrome, USA) was used to calibrate the instrument.

CO_2 adsorption isotherms were measured at 22 °C on an adsorption unit, ASAP 2020 (Micromeritics Inc., USA). Prior to these measurements, the catalyst sample (~ 0.2 g) was evacuated (1 x 10^{-3} mm Hg) at 180 °C for 10 h to clean the surface by removing water and any pre-adsorbed gas molecules. Required amount of CO_2 gas was then injected into the volumetric set-up to achieve a targeted set pressure (40-850 mm Hg). A minimum equilibrium interval of 10 s with a relative target tolerance of 5% of the targeted pressure and absolute target tolerance of 5 mm Hg was used to determine equilibrium sorption at each mentioned point. The isotherms were plotted as quantity of CO_2 adsorbed versus the partial pressure of CO_2. Further, the isotherms were analyzed by using the Dubinin-Astakhove model [6].

$$a_{ad} = a_o \times e^{-\left[\frac{RT}{E}\times ln(P_r)^{-1}\right]^n}$$

where a_{ad} is the amount of CO_2 adsorbed at a relative pressure P_r ($P = P_{eq}/P_r$), a_o is the limiting amount filling the micropores, E is characteristic energy, n is heterogeneity parameter, R is universal gas constant and T is temperature. The characteristic energy, E indicates average adsorption energy for CO_2 molecules on the catalyst surface.

2.3.5. Thermogravimetry

A TG experiment monitors the mass variation of a sample as a function of time or temperature in a controlled atmosphere under the run of a temperature program [7]. The technique is very useful for any reaction related to mass loss (drying, desorption, degradation etc.) or mass gain (wetting, adsorption etc.). In principle the sample is heated in a strict atmosphere (air/ inert) under a temperature program and the corresponding weight of the sample is recorded against time or temperature. Many parameters affect the signal, such as increasing the mass of the sample increases the reaction temperature and increasing the scanning rate also increases the temperature. So for better comparison, mass and scanning rate were kept constant. A thermogravimetric analyzer consists of a crucible generally made up of platinum or alumina connected to a balance and kept in a furnace with control over

temperature. Both the furnace and balance are important parts of a TG analyzer, compromise on the properties of furnace and balance will cause misinterpretation of data. In the present study, thermogravimetric measurements of DMC catalysts were carried out on a Seiko EXTAR 6000 microbalance with programmable temperature furnace. Each sample (5 - 10 mg) was out gassed by heating in a He flow (30 ml/min) from 25 to 1000 °C at 10 °C min^{-1}. The sequence of weight loss was used to predict the sequence of stability of different constituents in the catalyst structure and its decomposition temperature.

2.3.6. Scanning electron microscopy

SEM probes the morphological features of materials [3]. SEM scans over a sample surface with electrons as probe (5 - 50 eV) and detects the yield of either secondary or back-scattered electrons as a function of the position of primary beam. Contrast of the image depends upon the orientation of sample towards the detector. Parts of the surface facing the detector appear brighter than parts of the surface with their surface normal pointing away from the detector. Interaction between electron beam and sample produces different types of signals providing detailed information about the surface structure and morphology of the sample. When an electron from the beam encounters a nucleus in the sample, the resultant Coulombic attraction leads to a deflection in electron's path, known as Rutherford elastic scattering. A fraction of these electrons will be completely back scattered, re-emerging from the incident surface of the sample. Since the scattering angle depends on the atomic number of the nucleus, the primary electrons arriving at a given detector position can be used to produce images containing topological and compositional information. The major advantage of SEM is that bulk samples can also be directly studied by this technique. In the present study, SEM images of different catalysts were collected on a Leica STEREOSCAN 440, LEO Microscopy. The solid samples were spread over a carbon tape and then gold coated for good electrical conductance to produce quality images.

Chemical composition of the DMC catalysts, from sample rich region was estimated by energy dispersive X-ray analyzer FEI, Quanta 200 3D dual beam ESEM at 30 kV and with a resolution of 3 nm. The technique makes use of X-rays originated from the samples as a result of interaction of incident electron beam with the sample. The interaction of an electron with an atom produces two types of X-rays, X-ray emission characteristic of the atom and Bremsstrahlung. Element characteristic X-rays are produced when the incident electron ejects a bound electron from an atomic orbital. The core-ionized atom comes to ground state either by emitting characteristic X-rays or by Auger decay. The former is the basis for electron microprobe analysis for elemental detection.

2.3.7. High resolution transmission electron microscopy

HRTEM uses high energy electron beam to investigate morphological, compositional and crystallographic characteristics of materials [3]. A parallel high energy electron beam is allowed to impinge on samples and the transmitted electron beams are analyzed. The attenuation of the electron beam is dependent on the density and thickness of the material. The transmitted beam thus forms a two-dimensional projection of the sample mass which is subsequently magnified by electromagnetic lenses to produce bright field images. Dark-field images are obtained from diffracted electron beams, which are slightly off-angle from the transmitted beam. Typical operating conditions of a TEM instrument are 100 to 200 KeV electrons, 10^{-6} mbar vacuum, 0.3 nm resolution and magnification of 10^5 to 10^6. For HRTEM, the operating conditions are 100-300 KeV electrons, 10^{-6} mbar vacuum, 0.5 nm resolution and magnification of about 3 x 10^5 or 10^6. In the present study, HRTEM images of DMC catalysts were recorded on a FEI Technai F 30 instrument. Catalyst samples (0.001-0.005 g) were dispersed in methanol (5 ml) and sonicated for 0.5 h at room temperature. The highly dispersed catalyst particles (one drop) were casted on a copper grid (200 mesh, ICON Analytical) dried for 10 h at room temperature and then used for the analysis.

2.3.8. Nuclear magnetic resonance spectroscopy

NMR is a central method to analyze the structure of compounds, applied extensively in various branches of chemistry such as organic chemistry, inorganic chemistry and biochemistry [8]. NMR is the property of nucleus entirely concerned with nuclear spin (I). The nuclei of many elemental isotopes have a characteristic I. Some nuclei have integral spins (I = 1, 2, 3 .., e.g. ^{2}H, ^{10}B..), some have fractional spins (I = 1/2, 3/2, 5/2 .., e.g. ^{1}H, ^{13}C, ^{15}N..), and a some have no spin, (I = 0, e.g. ^{12}C, ^{16}O, ^{32}S, ..). Isotopes of particular interest are ^{1}H, ^{13}C, ^{19}F and ^{31}P, all of which have I = 1/2. The difference in energy between the two spin states depends on the external magnetic field strength. At a field equal to B_x, the formula for energy difference is given by $\Delta E = \mu B_x / I$ (μ is the magnetic moment of the nucleus in the field). Irradiation of a sample with radio frequency corresponding exactly to the spin state separation of a specific set of nuclei will cause excitation of those nuclei from lower spin state to higher spin state. The location of different NMR resonance signals depends on both the external magnetic field strength and the radio frequency and is expressed in terms of chemical shifts (δ ppm) with reference to tetramethyl silane (TMS). As compared to solution NMR which gives sharp signals, solid state NMR generally gives broad signals due to anisotropic or orientation dependent interactions. These anisotropic interactions can be suppressed by introducing artificial motion to the solid. This is achieved by rotating the

sample about an axis angled at 54.7° with respect to the external magnetic field. This technique is known as magic-angle spinning (MAS). In the present study, solid state ^{13}C NMR (MAS) of catalysts samples were done on a JEOL ECX-400 MHz spectrometer. Samples were finely powdered and packed tightly into rotors and introduced into the instrument for analysis (Acquisition time 0.1629 s, frequency 100.53 MHz, receiver gain 68, sweep width 50295.67 Hz, temperature 19.7 °C).

2.3.9. Temperature-programmed desorption

TPD deals with the adsorption of certain probe molecules on an activated material followed by the detection and quantification of its desorption from the surface in a linear temperature ramp. TPD is usually employed to characterize the acidic or basic properties of surfaces. The probe molecules generally used are NH_3, isopropyl ammine and pyridine for acidity measurements and CO_2/ SO_2 for basicity measurements. The three main steps in TPD experiment are the pre-treatment of the sample, adsorption of the probe molecule and desorption of the probe molecule. Desorption of NH_3 from a material surface by linear temperature ramp carries the information about the strength of acid sites in the analyte as desorption at lower temperature implies weaker acid sites whereas desorption at higher temperature implies stronger acid sites. The maximum temperature of desorption is selected based on the thermal stability of the material under scrutiny [7]. In the present study, NH_3-TPD measurements were done on a Micromeritics AutoChem 2910 instrument. In a typical analysis, 0.1 g of activated catalyst was accurately weighed in a U-shaped quartz tube. The catalyst was supported by a piece of quartz wool and mounted on the instrument. Prior to measurement, the catalyst was activated at 180 °C for Fe-Zn and 200 °C for Co-Zn DMCs for 0.5 h (10 °C/ min). It was then cooled to ambient temperature and adsorbed with a mixture of NH_3 in He (10 vol%) gas (30 ml/min, He flow 10 ml/ min) for 1 h. The catalyst was then heated to 100 °C (10 °C/ min) for 10 min to remove any physisorbed NH_3 under the flow of He (40 ml/ min). 10 min hold was then given to stabilize the base line. The analysis was carried out in the temperature range of 100 - 180 °/ 200 °C at a heating rate of 10 °C/ min (one measurement every 0.1 s) under the He flow of 30 ml/ min and kept at this temperature for 0.5 h. NH_3 concentration in the effluent was monitored with a gold-plated filament thermal conductivity detector. The amount of NH_3 desorbed was determined based on the area under the desorption peak.

2.4. Reaction procedure

2.4.1. Synthesis of hyperbranched polyesters

Polyesterification reactions were carried out in a glass, double-necked, round-bottom flask placed in a temperature-controlled oil bath (Scheme 2.1). No solvent was used during the polymerization. Known quantities of diacid (succinic acid - 1.77 g or adipic acid - 1.46 g) and glycerol (0.935 g) were charged into the reactor. The contents were flushed with dry N_2. Then, Fe-Zn DMC catalyst (3 wt% of total reactants) was added. Temperature was raised to 180 °C and the reaction was conducted for 1.5 h while stirring the contents vigorously using a magnetic stirrer and flushing with dry N_2. At the end, the contents were dissolved in acetone. The polymeric product and any left out starting material (glycerol and/or diacid) were completely miscible with acetone and remained in the liquid portion. The solid catalyst formed a separate phase which was removed by centrifugation (8000 rpm for 10 min)/ filtration from the liquid portion. Then, the polymer product was re-precipitated from the liquid portion by adding excess n-heptane. Reactants remained in acetone-heptane mixture. Product hyperbranched polyester was dried and then subjected to characterization.

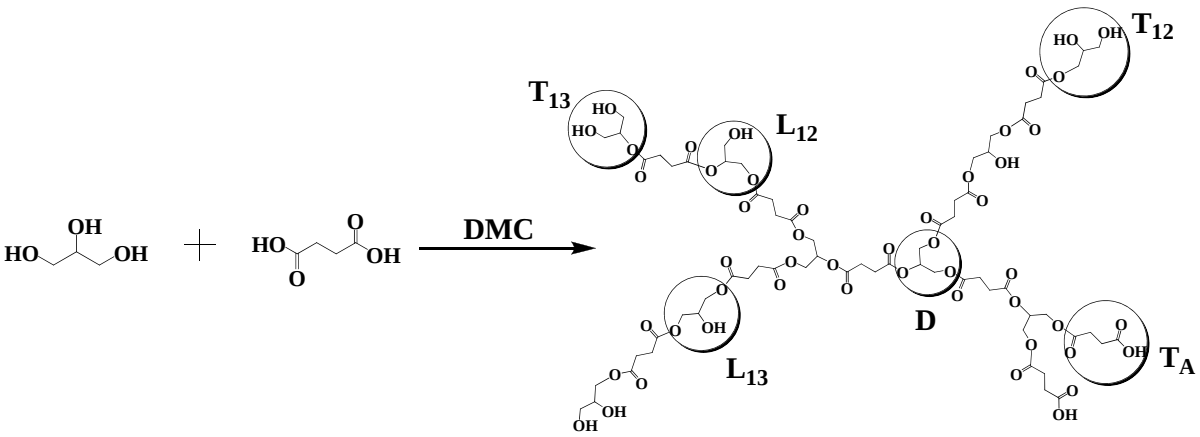

Scheme 2.1. Synthesis of hyperbranched polyesters from glycerol and succinic acid.

2.4.2. Copolymerization of CHO and CO_2

Co-polymerization of cyclohexene oxide (CHO) and CO_2 (Scheme 2.2) was carried out in a 100 ml stainless steel reactor (Parr Instrument Co., Parr 4871) equipped with a mechanical overhead stirrer, thermowell, gas inlet and outlet, liquid sampling valve, safety rupture disc, pressure gauge, transducer for digital pressure display and an automatic temperature control system. A volume of 10 ml each of CHO (Sigma Aldrich) and dried toluene (solvent, Thomas Baker, India) were charged into the reactor along with 0.25 g of Co-Zn DMC catalyst. The reactor was initially flushed twice with CO_2 and then pressurized

to 30 bar. The temperature was raised and maintained at 75 °C (2 °C/min) and the reaction was conducted for 11 h. At the end of the reaction, the reactor was depressurized slowly and the solid catalyst was separated by centrifugation (9000 rpm, 5 min) followed by decantation. The solvent toluene was removed over a rotary evaporator. The solid product was further purified by dissolving in dichloromethane, then re-precipitated from excess methanol (5 times the amount of dichloromethane) and dried at 50 °C. The superlated solution was purified by rotary evaporation and was liquid in nature. The polycarbonates thus obtained were subjected to analysis.

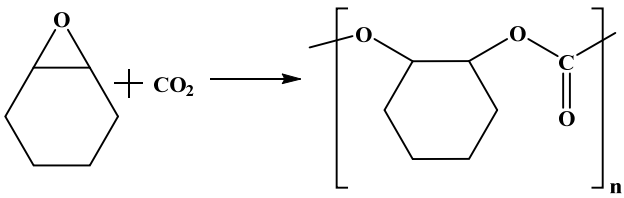

Scheme 2.2. Copolymerization of CHO and CO_2.

2.4.3. Copolymerization of PO and CO_2

Co-polymerization of propylene oxide (PO) and CO_2 (Scheme 2.3) was carried out in a 100 ml stainless steel reactor (Parr Instrument Co., Parr 4871). A volume of 10 ml each of PO (Merck, India) and dried toluene were charged into the reactor along with 0.25 g of Co-Zn DMC catalyst. The reactor was initially flushed with CO_2 twice and then pressurized to 30 bar. The temperature was raised and maintained at 85 °C (2 °C/min) and the reaction was conducted for 11 h. At the end of the reaction, the reactor was depressurized slowly and the solid catalyst was separated by centrifugation (9000 rpm, 5 min) followed by decantation. The solvent toluene was removed over a rotary evaporator. The elastomeric product was purified by dissolving in dichloromethane, then re-precipitating from excess methanol (5 times the amount of dichloromethane) and dried at 50 °C. The superalated solution was concentrated over a rotary evaporator and it was liquid in nature. Its composition is contained of oligomers of polyether and polycarbonate. Polypropylene carbonates thus obtained were subjected to characterization.

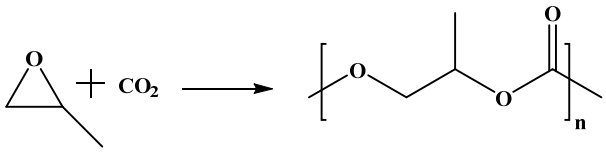

Scheme 2.3. Copolymerization of PO and CO_2.

2.4.4. Terpolymerization of PO, CHO and CO_2

Terpolymerization of CHO, PO and CO_2 (Scheme 2.4) was carried out in a 100 ml stainless steel reactor (Parr Instrument Co., Parr 4871). 1: 1 molar ratio of CHO (5.8 ml) and PO (4.2 ml), and 10 ml of dried toluene were charged into the reactor along with 0.226 g of Co-Zn DMC catalyst. Then, the reactor was flushed two times with CO_2 and pressurized to 30 bar. The temperature was raised to 85 °C at a ramp rate of 2 °C/min and maintained for 11 h. At the end of the reaction, the reactor was cooled and depressurized slowly. The catalyst was separated by centrifugation (9000 rpm, 5 min) followed by decantation. The solvent was removed over a rotary evaporator. The elasometric product was then purified by dissolving in dichloromethane and re-precipitating by adding excess methanol. The solid terpolycarbonate was dried at 50 °C. The superlated solution was concentrated by rotary evaporation and was viscous in nature. The polycarbonates thus obtained were subjected to characterization.

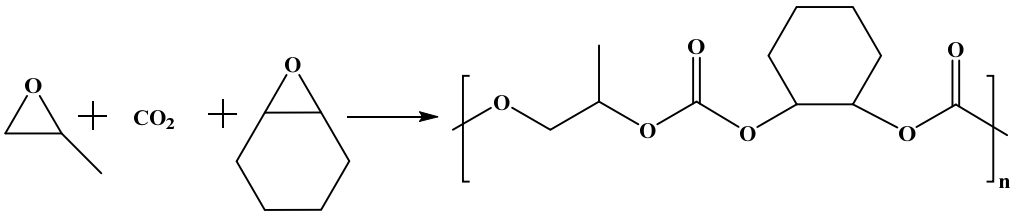

Scheme 2.4. Terpolymerization of PO, CHO and CO_2.

2.5. Product analysis

2.5.1. Hyperbranched polyesters

2.5.1.1. Nuclear magnetic resonance spectroscopy

Inverse-gated ^{13}C NMR spectroscopy (in DMSO) was used to estimate the degree of branching (DB) of hyperbranched polymers [9] (Scheme 2.1). Integration of carbon signals of normal spectra is not recommended for quantification purposes due to uneven nuclear Overhauser effect (NOE) enhancement of signals by decoupling and due to long longitudinal relaxation times. Hence, spectra for quantitative purposes are performed in inverse-gated decoupling mode. Here the ^{1}H decoupling is active during the acquisition, whereas it is switched off during the relaxation delay. In order to suppress the NOE-effect during the acquisition period, the relaxation delay is set to 10-times of relaxation time of ^{13}C [8]. In the present study, inverse-gated ^{13}C measurements were done on a Bruker Avance 500 MHz NMR spectrometer using the pulse program: Zgig 30 (acquisition time = 1.1 s, time delay = 5 s, number of scans = 4180). The various branching and linear segments of the polymer were assigned with the help of DEPT experiments. Table 1 shows the different branching segments

of hyperbranched polyesters and their ^{13}C NMR chemical shifts (Fig. 2.1). Branched segments in the product were also confirmed by 2D NMR spectroscopy. For HSQC, the following parameters were used: program = ctgp, acquisition time = 0.045 s (F2) and 0.0057 s (F1), spectral width = 9.997 ppm, receiver gain = 18400, O1 = 2496 Hz and O2 = 12106 Hz. In HMBC (program = gp12ndqf), the spectral parameters used were: acquisition time = 0.59397 s (F2) and 0.0047 s (F1), spectral width = 6.8947 ppm, receiver gain = 16,400, O1 = 1751.3 Hz and O2 = 13619.9 Hz.

Frey's equation [9] was used to calculate the degree of branching (DB):

$$DB = \frac{2D}{2D + L_{12} + L_{13}}$$

where D represents dendritic units with all the hydroxyl groups of glycerol got esterified, L_{12} and L_{13} represents linear segments with 1,2- and 1,3-hydroxyl groups of glycerol got esterified, T_{12} and T_{13} represents the terminal segments with only one hydroxyl group of glycerol got esterified and T_A represents the acid terminal groups (Scheme 2.1).

The acid terminal groups (T_A) are usually not considered in DB estimation. The DEPT spectra were used to differentiate between the methine and methylene carbons in the polymer (Fig. 2.1).

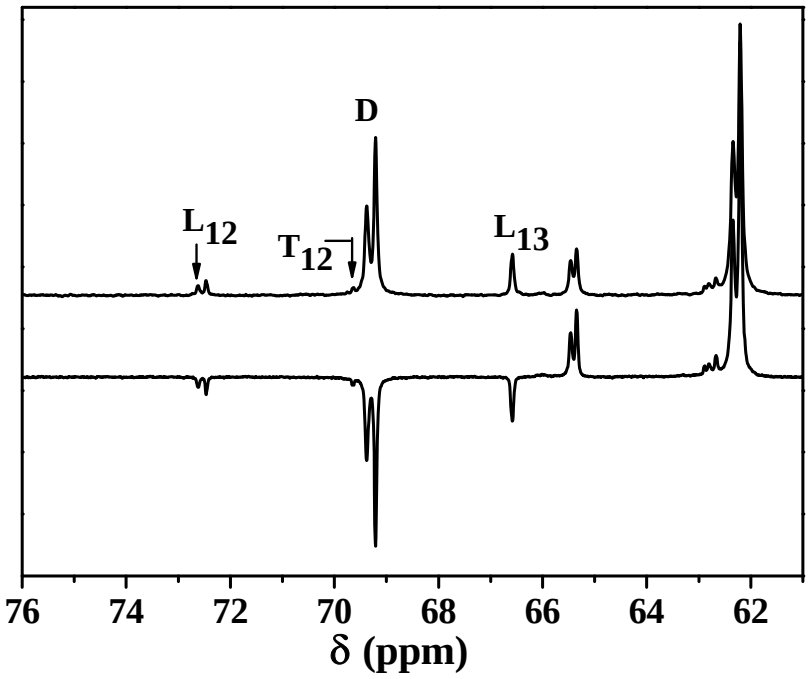

Fig. 2.1. ^{13}C NMR (top) and DEPT (bottom) spectra of Glycerol-Succinic acid hyperbranched polyester.

Table 2.1. Various branching segments of hyperbranched polyester and their chemical shifts.

Branching segment	Structure	Chemical shift (δ ppm)		
		a	b	c
L_{12}	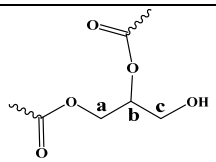	62.5	72.4	59.4
L_{13}	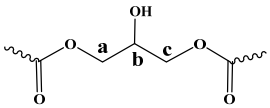	65.2	66.1	65.2
D	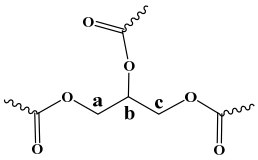	62.1	69.0	62.1
T_{12}	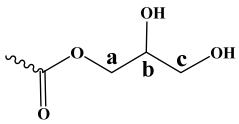	66.0	69.4	62.7
T_{13}	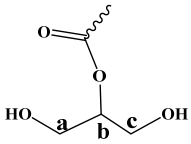	59.8	80.0	60.0

2.5.1.2. Inherent viscosity

The effect of DB on flow properties of polymer solution and its relation with cross-linking was analyzed by viscosity measurements. In general, viscosity measurements were done at sufficient dilutions such that the properties being measured are those of the 'isolated' molecule. Viscosity of a dilute polymer solution depends on various factors such as nature of the polymer, solvent, concentration of the polymer, average molecular weight, molecular weight distribution, temperature and rate of deformation. In viscosity measurements, the flow properties being observed are related to the hydrodynamic volume of the polymer. This hydrodynamic volume is the 'effective volume' in which the polymer occupies in solution [10]. In the case of hyperbranched polymers, as DB increases their hydrodynamic volume decreases due to compactness of branched structure. Since hydrodynamic volume of the polymer decreases with DB the viscosity of the solution decreases. For a highly cross-linked polymer, the individual polymer molecules are cross-linked to each other and which in turn increases the viscosity. In the present study, relative viscosity (η_{rel}) of the polymer was measured in tetrahydrofuran (THF) using an Ubbelhode viscometer immersed in a water bath at 29 °C (0.02 g polymer in 10 ml THF). The viscosity measurements were repeated three times and the average of the reading (time flow) was used for the calculation of η_{rel} by the equation,

$$\eta_{rel} = \frac{t}{t_s}$$

where t is the time of flow of polymer solution and t_s is the time of flow of solvent. Inherent viscosity (η_{inh}) is then calculated from η_{rel} as,

$$\eta_{inh} = \frac{\ln \eta_{rel}}{C}$$

where, C is the concentration of polymer solution [10].

2.5.1.3. Matrix assisted laser desorption/ ionization time -of- flight mass spectrometry

MALDI-TOF provides detection of various mass fragments present in macromolecules. The method is widely used to analyze different branching segments present in large biomolecules, in linear and branched polymeric architectures and to identify cyclic products. In MALDI analysis, the analyte is embedded in a matrix compound, usually a UV absorbing weak organic acid. This matrix solution is then supported on a conductive support and dried. The analyte containing matrix co-crystals are then irradiated with a nano second laser beam, for instance a UV radiation of 266 or 377 nm wavelength. The energies introduced are in the range of 1-5 x 10^7 W/cm^2. The laser energy generates vibrational oscillations in the co-crystals and results in its decomposition. The disintegrated ions are accelerated through an electric field and finally reach the detector. Ion masses as mass to charge ratio (m/z) are calculated by measuring their time of flight (TOF). TOF is longer for larger molecules. The spectrum is a plot of m/z versus their intensity where the charge is predominantly unity [11]. In the present study, mass spectra with automated tandem TOF fragmentation of hyperbranched polymers were acquired with a Voyager-DE STR (Applied Biosystems Voyager System 4383) in positive reflector mode with a laser intensity of 2324, accelerating voltage of 2 x 10^4 V and a number of laser shots of 50/spectrum. An aliquot (1 µl) of polymer solution (1 mg/l in acetone) was mixed with 24 µl of 2,5-dihydroxybenzoic acid (DHB) matrix solution (10 mg/ml, acetonitrile : water = 50 : 50 v/v). 1 µl of this resulting solution was then spotted on the MALDI plate for analysis.

2.5.2. PCHC/ PPC/ Terpolymer

2.5.2.1. Nuclear magnetic resonance spectroscopy

^{1}H NMR spectroscopy was used to calculate the percentage incorporation of CO_2 in different polycarbonates. For poly (cyclohexene carbonate) (PCHC), the measurements were done on a Bruker Avance 200 MHz spectrometer with a sweep width of 4138.95 Hz and an acquisition time of 7.9167 s using $CDCl_3$ as solvent (Fig. 2.2, Scheme 2.2).

Signals due to methine protons near to the carbonate linkages (δ = 4.2 to 4.6 ppm) and those near to the ether linkages (δ = 3.2 to 3.6 ppm) were integrated (A). The percentage incorporation of CO_2 (F_{CO2}) in the polymer was calculated using the formula [12],

$$F_{CO2} = \frac{A_{4.2-4.6}}{A_{4.2-4.6}+A_{3.2-3.6}} \times 100$$

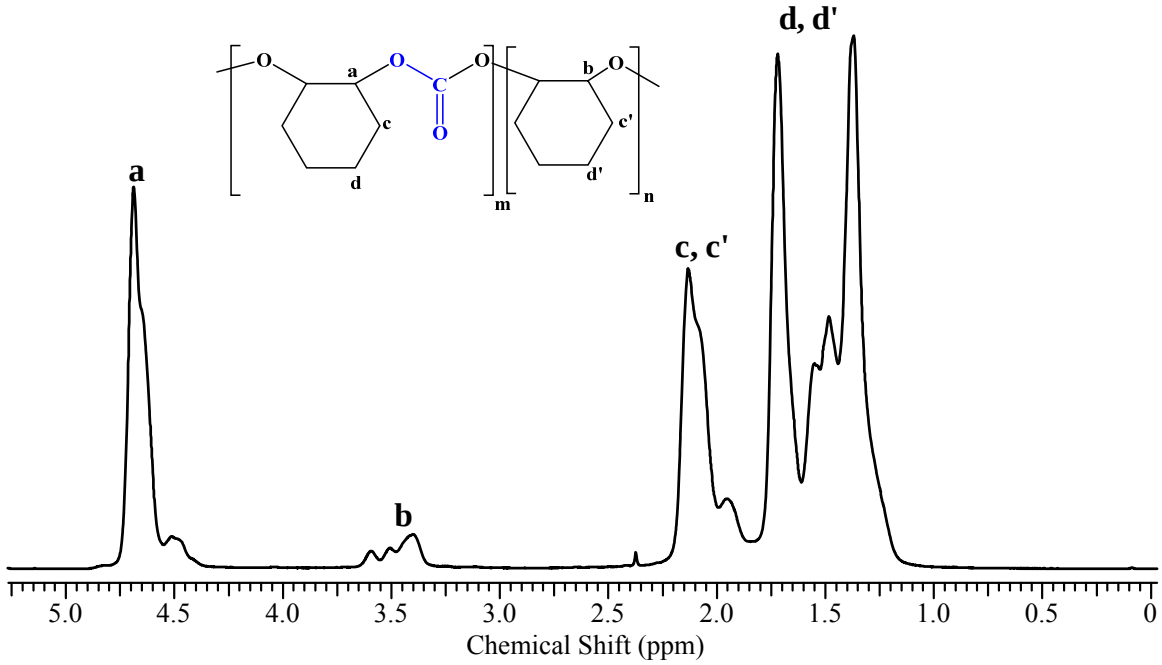

Fig. 2.2. ^{1}H NMR spectrum of PCHC.

Tacticity pattern of the polymer backbone was analyzed from the inverse-gated ^{13}C NMR spectra of PCHC in $CDCl_3$ recorded on a 500 MHz Bruker Avance spectrometer with a sweep width of 31249.05 Hz at 24.7 °C. In the spectrum, the m-centered tetrad (mmm/mmr/rmr) of carbonyl carbons corresponding to isotactic isomers appears at 153.8 ppm while that corresponding to syndiotactic isomers - the r-centred tetrads (rrr/rrm/mrm) appear at 153.1 to 153.3 ppm [13]. Integration of these signals provides the total distribution of tacticity in the polymer.

Percentage incorporation of CO_2 in poly(propylene carbonate) (PPC) was calculated by the integration of signals at 5.1 and 4.2 ppm (carbonate units), 3.5 ppm (ether linkages) and 4.5 ppm (cyclic carbonate) (Fig. 2.3, Scheme 2.3) using the formula reported by Chen et al [14].

$$F_{CO2} = \frac{(A_{5.1} + A_{4.2} - 2 \times A_{4.5})}{(A_{5.1} + A_{4.2} - 2 \times A_{4.5}) + A_{3.5}} \times 100$$

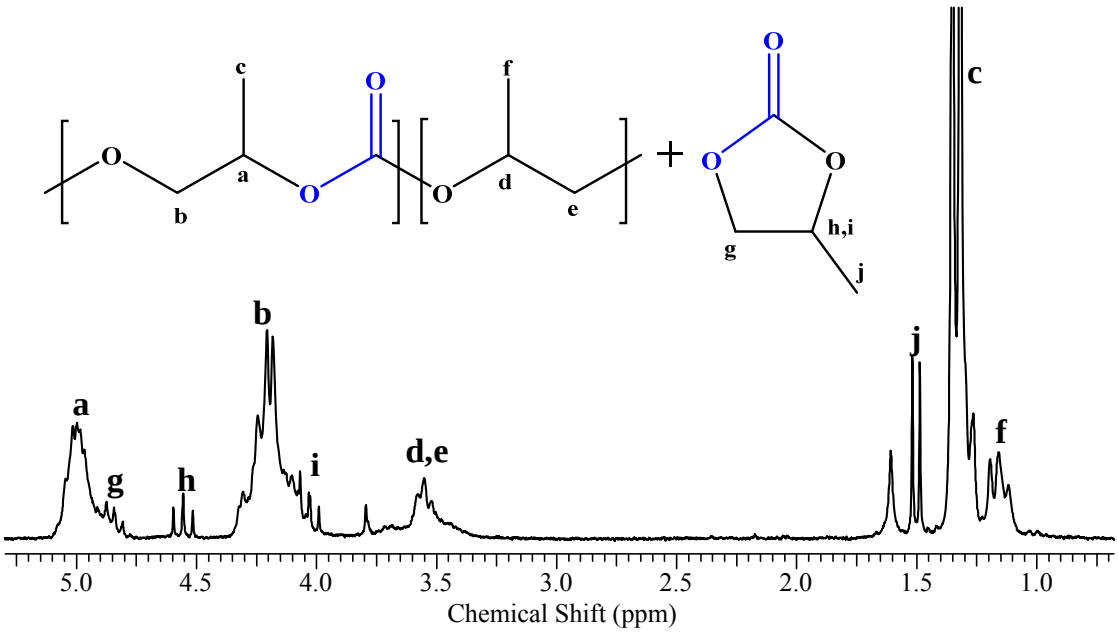

Fig. 2.3. ^{1}H NMR spectrum of PPC.

The amount of cyclic propylene carbonate (PC) was calculated by the integration of signals in the $–CH_3$ region (1.5 ppm, Fig. 2.3). The weight percentage (W_{PC}) of PC formed was calculated using the formula:

$$W_{PC} = \frac{102 \times A_{1.5}}{58 \times A_{1.14} + 102 \times (A_{1.33} + A_{1.50})} \times 100$$

where, $A_{1.14}$ and $A_{1.33}$ are integrated areas of $–CH_3$ protons of polyether and polycarbonate segments.

Configurational orientation of PPC was analyzed from inverse-gated ^{13}C NMR spectrum recorded on a 500 MHz Bruker Avance spectrometer in $CDCl_3$. Spectrum of PPC shows signals corresponding to head-head (HH), head-tail (HT) and tail-tail (TT) at 153.8-154.1, 154.3 - 154.5 and 154.8 ppm, respectively [15], in the carbonate region. Relative distribution of these segmental connections was calculated by the integration of signals.

Percentage incorporation of CO_2 in terpolymer was calculated by integration of signal near to carbonate units at 4.98 and 4.2 ppm (PPC units), 4.65 ppm (PCHC units) and ether units at 3.2 - 3.6 ppm for both propylene and cyclohexene units (Fig. 2.4, Scheme 2.4) as,

$$F_{CO2} = \frac{A_{5.1} + A_{4.2} + A_{4.6}}{A_{5.1} + A_{4.2} + A_{4.6} + A_{3.2-3.6}} \times 100$$

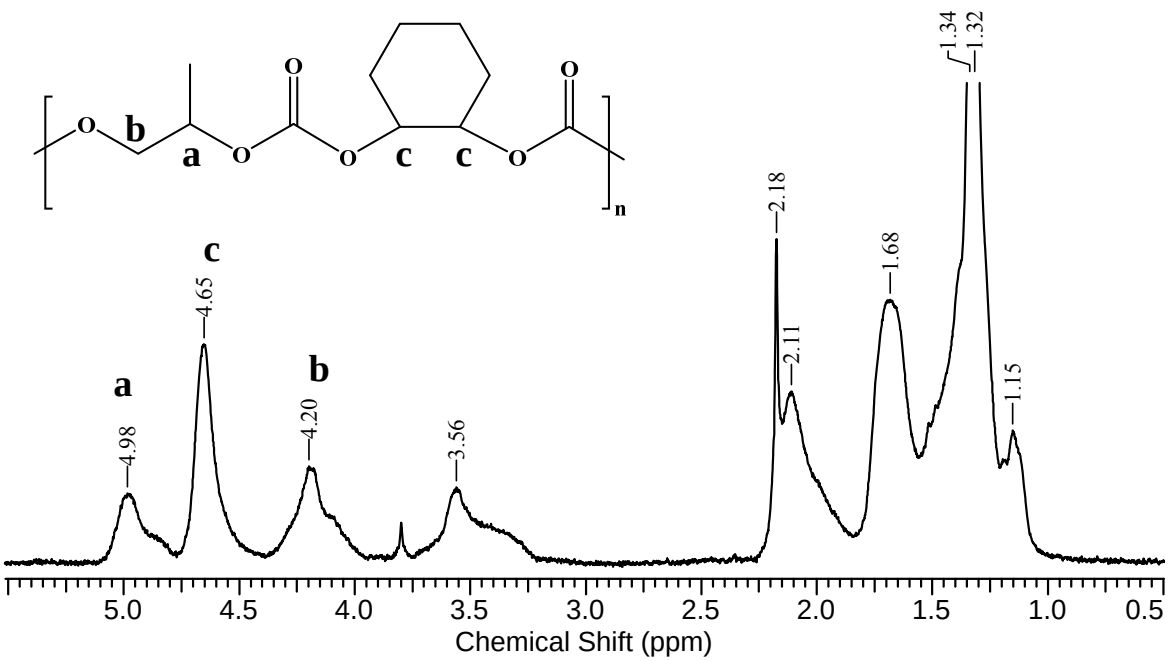

Fig. 2.4. ^{1}H NMR spectrum of terpolymer.

The tacticity pattern in the terpolymer was analyzed from inverse-gated ^{13}C NMR spectrum recorded at 500 MHz in comparison with the signal positions of PPC and PCHC as discussed earlier.

2.5.2.2. Gel permeation chromatography

Chromatography is a separation technique used for the isolation of components of a mixture based on the principle of partition of molecules between two phases, a stationary phase and a mobile phase. GPC is a type of liquid chromatography where the stationary phase is a solid and mobile phase is a liquid. The stationary phase is a gel consisting of particles of cross-linked polyamide/polystyrene containing pores or silica. The pore sizes of the stationary beads ranges from 5 to 10^5 nm. The mobile phase can be any solvent in which the components of mixture are soluble. Generally, the polymer samples are dissolved in a solvent and injected into the column containing the stationary beads. As the polymer solution advances through the column, smaller molecules occupy the pores of the stationary beads while the larger molecules because of their size restrictions remain in the mobile phase. As a result a partition of molecules based on their sizes originates. The bigger molecules then moves down the column towards the detector and get detected. This is followed by the elution of smaller molecules. Hence, the chromatogram is a plot of retention time versus intensity. The most common detectors used for GPC are based on differential refractive index, UV and evaporative light scattering of the mobile phase [16]. In the present study, the average molecular weight (M_w) and polydispersity index (PDI) of polycarbonates were

determined on a PL 220 HT gel permeation chromatograph (Polymer Chemistry Division, CSIR-NCL) equipped with Styragel columns at 25 °C using chloroform (Lichrosolv, Merck, India) as eluent with a refractive index detector. The sample concentration was 3 mg/ml with an injection volume of 100 µl. The columns were calibrated with monodisperse polystyrene standards of different molecular weights.

2.5.2.3. Differential scanning calorimetry

DSC measures the heat change associated with a chemical transformation as a function of temperature. The experiment records the difference in heat flow between the sample and the reference as a function of linear increase in temperature. Since DSC is at constant pressure, the heat flow (q) is equivalent to enthalpy (H) changes:

$$\left(\frac{dq}{dt}\right)_p = \frac{dH}{dt}$$

where dH/dt is the heat flow measured in mcal/s. Heat flow difference between the sample and reference is given by

$$\Delta\,\frac{dH}{dt} = \left(\frac{dH}{dt}\right)_{sample} - \left(\frac{dH}{dt}\right)_{reference}$$

This difference is positive for endothermic process (phase transitions) and negative for exothermic process (crystallization). The most important information obtainable from DSC is the temperature at which glass transition (T_g) occurs. T_g is the temperature at which amorphous polymers transforms from brittle, glass like form to a rubbery, flexible form. This is not a true phase transition but it accompanies a change in the local degrees of freedom of the polymer. At T_g, the specific heat (C_p), coefficient of thermal expansion, the free volume, and the dielectric constant changes rapidly. In other words, the mechanical properties of the polymer changes abruptly at this temperature and is regarded as an important property of the polymer for targeted applications. Heat capacities and changes in heat capacities can be determined from the shift in the baseline of the thermogram. Heat capacity is defined as,

$$C_p = \left(\frac{dq}{dT}\right)_p = \left(\frac{dH}{dT}\right)_p$$

In the DSC plot, T_g is identified as a drastic change in the base line implying a change in the heat capacity of the polymer. T_g is considered to be a second order transition since no enthalpy is associated with the process [7, 16]. In the present study, DSC analysis of polycarbonates were done on a DSCQ10 heat flux instrument (TA series, Polymer Science Divison, CSIR-NCL) in the temperature range -80 to 150 °C at 10 °C/ min. About 5 mg of

polymer is weighed accurately on an aluminium pan and sealed. It was then loaded in the instrument furnace along with a reference empty pan. The experiment was carried out under N_2 flow in the specified temperature program.

2.5.2.4. Thermogravimetry

The decomposition temperature of polycarbonates was analyzed by the TG analysis on a Diamond TG/ DTA instrument under He flow. About 6 mg of sample was taken on an aluminium pan. It was then mounted on a Seiko EXTAR 6000 microbalance with programmable temperature furnace. The experiment was carried out heating the sample in a He flow (30 ml/ min) from 25 to 500 °C at 10 °C/min. The decomposition temperature was determined by the sudden weight loss due to complete decomposition of the polymer in the thermogram.

2.5.2.5. Fourier transform infrared spectroscopy

FTIR spectra of polycarbonates were recorded in the transmittance mode as KBr pellets (1 wt% of polymer) on a Shimadzu 8201 PC spectrophotometer in the wavenumber region 450 to 4000 cm^{-1} with accumulation scans of 100 and spectral resolution of 4 cm^{-1}.

2.5.2.6. X-ray diffraction

XRD of solid PCHC and terpolymer was recorded in the 2θ range 10 - 50° at a scan rate of 2°/min on a Philips X'Pert Pro diffractometer using Cu K_α radiation (λ = 0.15406 nm) and a proportional counter detector. Materials in the forms of thick films were prepared on a glass plate and analyzed.

2.6. References

[1] P.S. Sreeprasanth, D. Srinivas, P. Ratnasamy, Appl. Catal. A 314 (2006) 148-159.

[2] B.L. Khac, W. Chester, US Patent No. 5,536,883 (1996).

[3] J.W. Niemantsverdriet, Spectroscopy in Catalysis, WILEY-VCH Verlag Gmbh & Co. KGaA, Weinheim (2007).

[4] J.M. Stencel, Raman Spectroscopy for Catalysis, Van Nostrand Reinnold, New York (1990).

[5] K.S.W. Sing, D.H. Everett, R.A.W. Haul, L. Moscou, R.A. Pierotti, J. Rouquerol, T. Siemieniewska, Pure & Appl. Chem. 57 (1985) 603-619.

[6] M.M. Dubinin, D.A. Cadenheat (Ed.), Progress in Surface Science and Membrane Science, Academic Press, New York (1975).

[7] J.C. Védrine, Characterization of Solid Materials and Heterogeneous Catalysts, WILEY-VCH Verlag Gmbh & Co. KGaA, Weinheim (2012).

[8] G. Gauglitz, T.V. Dinh, Handbook of Spectroscopy, WILEY-VCH, GmbH & Co. KGaA, Weinheim (2003).

[9] J.F. Stumbé, B. Bruchmann, Macromol. Rapid Commun. 25 (2004) 92-924.

[10] D.W.V. Krevelen, Properties of Polymers, Elsevier Sciences B V, Amsterdam (1994).

[11] H. Pasch, W. Schrepp, MALDI-TOF Mass Spectrometry of Synthetic Polymers, Springer- Verlag Berlin, Heidelberg (2003).

[12] M.J. Yi, S.H. Byun, C.S. Ha, D.W. Park, I. Kim, Solid State Ionics 172 (2004) 139-144.

[13] K. Nakano, K. Nozaki, T. Hiyama, Macromolecules 34 (2001) 6325-6332.

[14] S. Chen, Z. Xiao, M. Ma, J. Appl. Polym. Sci. 107 (2008) 3871-3877.

[15] S. Chen, Z. Hua, Z. Fang, G. Qi, Polymer 45 (2004) 6519-6524.

[16] F. Stelle, Handbook of Instrumental Techniques for Analytical Chemistry, Prentice Hall PTR, New Jersey (1997).

Chapter - 3

Synthesis of Hyperbranched Polyesters from Glycerol and Diacids over Fe-Zn DMC Catalysts

3.1. Introduction

Hyperbranched polymers (HPs) represent a sub-class of dendritic polymers with branch on branch topology. These three-dimensional ellipsoidal architectures possess a degree of branching (DB) ranging from 40 - 60% which is significantly low as compared to their three-dimensional globular dendrimeric analogues with 100% DB. Regardless of this demerit HPs inherit some advantages over dendrimers which include one-step synthesis procedure and easy purification by precipitation as compared to multi-step synthetic procedures including protection, deprotection and chromatographic separations for dendrimers. Although, these dendritic polymers are both synthetically and topologically different, their chemical properties are almost similar. In this regard, HPs are finding more scientific interest than dendrimers [1]. The advantages of HPs include: low entanglement, low solution and melt viscosity, good solubility, compact structure and large number of terminal functional groups. Initial research on HPs was focussed on synthesis, characterization and industrial applications such as processing of additives, highly efficient cross-linkers, reactive components in coating and resin formulations and molecular templates for the growth of inorganic molecules to produce nanomaterials. Recently, HPs found great potential in biomedical applications which has initiated the research on self assemblies. Self assembled HPs find application as drug and protein delivery agents, gene transfection, antimicrobial and antifouling materials, dental resins, cytomimic chemistry, bioimaging, biomineralization and tissue engineering [2]. Biodegradable HPs synthesized from renewables justify their sustainable development and improve their environmental adaptability.

Glycerol (G) is a tri-functional molecule possessing the minimum criteria for branching. It is a part of the metabolic system. This biomolecule finds great applications in food and cosmetic industry. But recent advancement of biodiesel technology generates excess amount of glycerol as compared to its usual consumption [3]. Although there are multiple ways for the valorisation of glycerol, polyesterification with diacids of renewable background such as succinic (SA) and adipic acid (AA) to generate hyperbranched ester architectures is highly promising. Carnahan and Grinstaff [4] have named dendrimers synthesized from G and SA as biodendrimers since the building blocks are known to be biocompatible or the polymers are degradable *in vivo* to natural metabolites. Dendritic architectures of G-SA polymer have already been employed for biomedical applications such as for covering the linear laceration wounds in eye treatment [5].

Polyesterification of glycerol with SA and AA has been reported in presence of homogeneous catalysts such as mineral acids and dibutyltin [6, 7]. Handling these air/

moisture sensitive catalysts and their intense corrosive nature has always been a big concern. Further, the polyesters prepared using dibutyltin catalysts have a DB of only 48 mol%, which is relatively low [6, 7]. Aprotic solvents like dimethyl formamide (DMF) and dimethyl sulfoxide (DMSO) have been employed to control the gelation phenomenon and to increase the DB [7]. However, the product oligomers were found difficult to separate from the reaction medium as the solvent DMF takes part in reaction with acid terminals of the branched oligomers [7]. Enzymes had also been employed to improve the DB by conducting reactions at ambient conditions but they needed longer reaction times (>48 h) [8]. Controlling the gelation phenomenon to improve DB at high conversions is an issue in these processes. A solid catalyst-based process has several engineering, environmental and economic advantages [9]. Solid catalyst is easy to handle during the polymerization and is less corrosive. In addition, the catalyst can be easily separated from the reaction mixture to generate pure polymers for speciality application.

Fe-Zn double-metal cyanides (Fe-Zn DMCs) are industrially well known catalysts for ring-opening polymerization of epoxides [10-14]. It has also shown amazing activity for esterification and transesterification reactions [15, 16]. This chapter discusses, for the first time, the application of Fe-Zn DMCs for the polyesterification of glycerol with SA and AA diacids. The DMC catalysts were prepared by using different complexing and co-complexing agents and by varying the mode of addition of reagents. In this chapter, Fe-Zn catalysts with differing structural and acidic properties are studied for the polyesterification reaction in detail and are found to be highly efficient in producing HPs of high DB and with controlled gelation. Three critical features of Fe-Zn DMC are found responsible for producing HPs with high DB at controlled gelation. They are Lewis acidity to initiate the reaction, hydrophobicity of surface to prevent deactivation due to water and micro-mesoporous framework to control the gelation phenomenon.

3.2. Experimental

Fe-Zn DMCs of varying chemical composition were synthesized and characterized by procedures reported in Chapter 2 (Sections 2.2.1.1 to 2.2.1.9 and Section 2.3). Nine different compositions of DMCs were prepared by changing the complexing agent (t-BuOH, MeOH and glycerol), using co-complexing agents with varying molecular weight (polyethylene glycol - PEG of molecular weights 300, 600, 1500 and 4000) and varying the mode of addition of reagents. Table 3.1 shows the nomenclature of catalysts and the type of complexing and co-complexing agents used in their synthesis. Among the catalysts investigated, Fe-Zn-4, Fe-Zn-5 and Fe-Zn-6 (Table 3.1) were prepared using the same stock

reagent solutions but with variation in the mode of addition of these reagent solutions. During the synthesis of Fe-Zn-5, solution 2 was added to solution 3 and this mixture was then added to solution 1 (Chapter 2, Section 2.2.1.6). While in the preparation of Fe-Zn-6, solution 3 was added to solution 1 and then, to this mixture solution 2 was added (Chapter 2, Section 2.2.1.7).

Table 3.1. Nomenclature of DMC catalysts and the complexing and co-complexing agents used in their synthesis.

Catalyst	Complexing agent	Molecular weight (M_n) of co-complexing agent, PEG
Fe-Zn-0	-	-
Fe-Zn-1	t-BuOH	300
Fe-Zn-2	t-BuOH	600
Fe-Zn-3	t-BuOH	1500
Fe-Zn-4	t-BuOH	4000
Fe-Zn-5	t-BuOH	4000
Fe-Zn-6	t-BuOH	4000
Fe-Zn-7	MeOH	4000
Fe-Zn-8	Glycerol	4000

The catalysts were characterized by the techniques described in Chapter 2 (Sections 2.3.1 to 2.3.7 and 2.3.9). Details of the reaction procedure and methods of product characterization were described in Sections 2.4.1 and 2.5.1.1 to 2.5.1.3, respectively.

3.3. Results and discussion

3.3.1. Structural characterization

3.3.1.1. XRD

Figure 3.1(a) shows the XRD patterns of Fe-Zn DMC catalysts prepared by different methods. Fe-Zn-0 prepared without using complexing and co-complexing agents showed reflections at 16.4°, 19.7°, 21.8°, 24.6° and 28.6° corresponding to (110), (200), (210), (211) and (221) planes of a cubic lattice [17]. XRD of other Fe-Zn DMC catalysts showed diffraction patterns similar to Fe-Zn-0 indicating that these catalysts were also crystallized in the same crystal symmetry. Composition of reagent solutions and mode of addition of reagents have a great influence on the position (that provides unit cell parameter, *a*) and peak width at half maximum (that provides the average crystallite size) of the reflections. Among

Fe-Zn-4, Fe-Zn-5 and Fe-Zn-6 (synthesized with same reactant solutions but with different mode of their addition) showed significant differences in the intensity of their reflections (Fig. 3.1(b)). The XRD of Fe-Zn-5 was more diffused than the other two indicating that it is composed of smaller crystallites. The crystallite size of Fe-Zn DMCs determined using the Debye-Scherrer formula followed the order: Fe-Zn-6 (59.5 nm) > Fe-Zn-4 (43.6 nm) > Fe-Zn-5 (33.7 nm). As the complexing agent was changed from t-BuOH (in Fe-Zn-4) to methanol (in Fe-Zn-7) and glycerol (in Fe-Zn-8), an increase in the crystallite size from 43.6 to 55.2 and 57.5 nm was observed (Table 3.2). The purpose of introducing co-complexing agent during the synthesis of DMC catalysts is to mimic the action of surfactants in mesoporous materials synthesis. Their special organization in solution can impart porosity in the catalysts apart from dispersing the nucleation points during the crystallization process. Hence, as the molecular weight of co-complexing agent was systematically increased, a linear decrease in crystallite size was observed for Fe-Zn-1, Fe-Zn-2, Fe-Zn-3 and Fe-Zn-4 (Table 3.2). The co-complexing agent has little influence on the unit cell parameter.

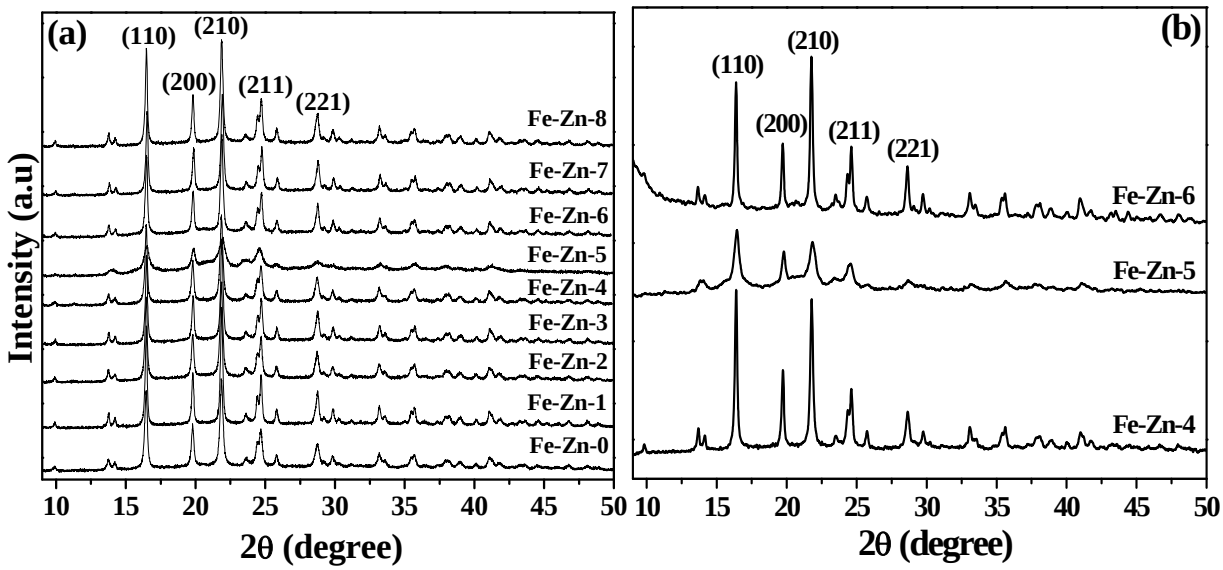

Fig. 3.1. XRD patterns of Fe-Zn DMC catalysts.

3.3.1.2. FTIR

Crystallization of DMC complexes involves complexation of Fe^{2+} and Zn^{2+} through CN bridging which was confirmed by the FTIR spectroscopy. Representative FTIR spectra of Fe-Zn-4, Fe-Zn-5 and Fe-Zn-6 are shown in Fig. 3.2. The precursor $K_4[Fe(CN)_6]$ showed a CN stretching band at 2039 cm^{-1}. This band for DMC appeared at 2096 cm^{-1}. A shift in band position to higher wavenumber confirms formation a CN bridging complex. The presence of a second metal in M-CN-M′ constrains the vibration of the CN group resulting in increase in

Table 3.2. Physicochemical characteristics of Fe-Zn DMC catalysts.

Catalyst	Structural properties			Overall acidity (mmol NH_3/g)	Elemental analysis (wt%)			Textural properties (N_2 physisorption)		
	Inter planar spacing (d_{200}; nm)	Unit cell parameter (*a*; nm)	Average crystallite size (nm)		C	H	N	S_{BET} (m^2/g)	Average pore diameter (nm)	Pore volume (cc/g)
Fe-Zn-0	0.448	0.900	51.2	3.52	17.5	1.6	19.8	40	7.4	0.074
Fe-Zn-1	0.448	0.896	52.8	3.87	18.3	1.7	20.2	24	9.1	0.055
Fe-Zn-2	0.449	0.898	49.6	4.82	18.5	1.9	21.8	53	5.1	0.067
Fe-Zn-3	0.449	0.899	47.5	5.30	18.6	1.8	21.5	47	4.5	0.053
Fe-Zn-4	0.450	0.900	43.6	7.10	17.8	1.9	21.0	52	2.5	0.030
Fe-Zn-5	0.448	0.896	33.7	8.23	21.9	2.5	18.5	160	6.4	0.150
Fe-Zn-6	0.450	0.900	59.5	3.14	19.2	2.0	20.2	37	3.7	0.060
Fe-Zn-7	0.449	0.899	55.2	3.30	18.7	2.0	21.6	51	6.6	0.083
Fe-Zn-8	0.449	0.894	57.5	4.28	18.1	1.9	21.8	18	12.7	0.058

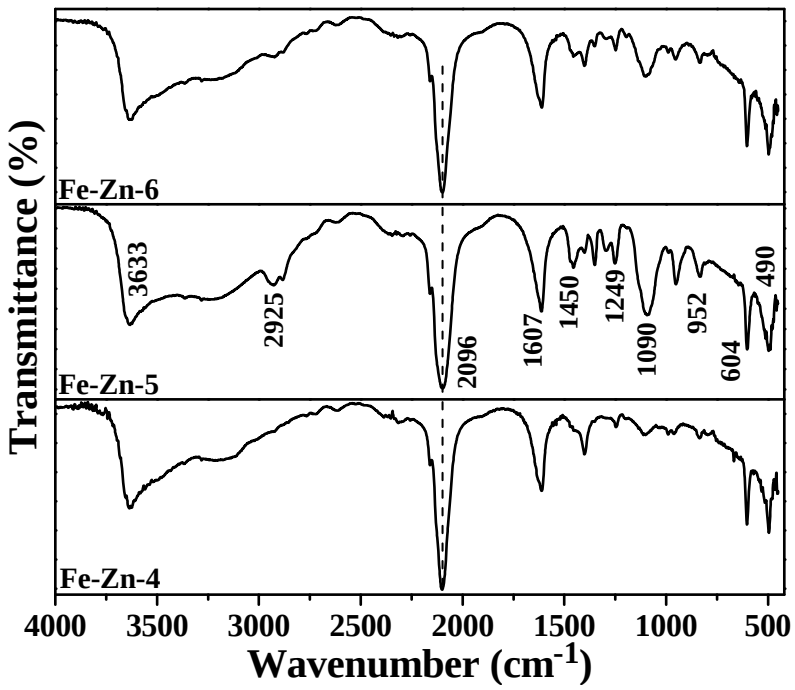

Fig. 3.2. Representative FTIR spectra of Fe-Zn-4, Fe-Zn-5 and Fe-Zn-6 catalysts.

stretching frequency. The coordinative behaviour of CN^- ligands to Fe^{2+} is σ bonding in nature. This bonding increases e^- density at Fe^{2+} which is then back donated to the antibonding molecular orbital of CN^- ligand. As a consequence, the N atom, now richer in e^- density is the new coordination site for Lewis acidic Zn^{2+} ions. Since these electrons are removed from the antibonding π* molecular orbital of CN^-, the bond strength increases and the stretching frequency shifts to higher wavenumbers. All the Fe-Zn DMC catalysts investigated showed the CN stretching band at nearly identical position indicating that the method of preparation employed in this study has little influence on the coordination behaviour of bridging CN^- ligands. The FTIR spectra of the complexes also confirmed the inclusion of t-BuOH in their structure. The band observed at 2925 cm^{-1} is assigned to anti-symmetric C-H stretching vibration, those at 1249 - 1450 cm^{-1} are due to symmetric and anti-symmetric C-H deformation and out-of-plane C_3C-O anti-symmetric stretching vibrations, and the band at 1090 cm^{-1} is assigned to rocking vibrations of $-CH_3$ group [16]. But the amount of complexing agent included in DMC complexes varied with the method of preparation and the mode of reagent addition. In case of catalysts prepared with the same reagents but with different mode of their addition, the amount of t-BuOH in the final composition decreased as follows: Fe-Zn-5 > Fe-Zn-6 > Fe-Zn-4. Further confirmation for this was obtained from the elemental analysis [Fe-Zn-5: 21.9 (%C), 2.5 (%H), 18.5 (%N); Fe-Zn-6: 19.2 (%C), 2.0 (%H), 20.3 (%N); Fe-Zn-4: 17.8 (%C), 1.9 (%H), 21.0 (%N)]. Table

3.2 lists the elemental compositions of all DMC catalysts investigated. Based on the findings, the generalized molecular formula of DMC catalysts investigated in this chapter is written as: $K_4Zn_4[Fe(CN)_6]_3.6H_2O.x$(t-BuOH) where x = 1 - 2. The CN moieties in the complexes are responsible their surface hydrophobicity. Studies of Satyarthi et al [17] established that if there is an option of aqueous and organic medium, DMC prefers to be in the aprotic, organic medium. These DMC complexes are in general hydrophobic. Surface hydrophobicity is a crucial parameter for reactions where water is the by-product (as in the case of esterification) as it prevents the surface active sites of the catalyst towards deactivation due to water.

3.3.1.3. N_2–physisorption

Method of preparation has greatly influenced the textural properties of DMC catalysts (Table 3.2). The adsorption isotherms of Fe-Zn-4, Fe-Zn-5 and Fe-Zn-6 are categorized into Type IV with H3 hysteresis loop (Fig. 3.3) indicating the presence of mesoporosity [18]. S_{BET} values of these catalysts decreased in the order: Fe-Zn-5 (160 m^2/g) > Fe-Zn-4 (52 m^2/g) > Fe-Zn-6 (37 m^2/g). Total pore volume varied in the order: Fe-Zn-5 (0.15 cc/g) > Fe-Zn-6 (0.06 cc/g) > Fe-Zn-4 (0.03 cc/g) and average pore diameter decreased in the order: Fe-Zn-6 (6.4 nm) > Fe-Zn-5 (3.7 nm) > Fe-Zn-4 (2.5 nm). In the case of Fe-Zn-4, the microporous area is nearly 74% of the total surface area (S_{BET} = 52 m^2 /g). The surface area, pore diameter and pore volumes of all other catalysts are provided in Table 3.2.

3.3.1.4. SEM

Morphology of Fe-Zn DMC complexes was identified from SEM (Fig. 3.4). Fe-Zn-0 prepared in the absence of complexing and co-complexing agents exhibited spherical particles. Fe-Zn-1, Fe-Zn-2, Fe-Zn-3 and Fe-Zn-4 prepared with same complexing agent but with PEG of different M_n are cubic in shape. Fe-Zn-5 and Fe-Zn-6 prepared by changing the modes of addition of reagents are spherical in shape. Fe-Zn-7 and Fe-Zn-8 synthesized with methanol and glycerol as complexing agent showed cube shaped particles. Thus, method of preparation of DMC complexes greatly influenced their morphology.

3.3.1.5. HRTEM

The presence of mesopores in DMC catalysts was further confirmed by high resolution imaging. HRTEM of Fe-Zn-4 indeed showed the presence of mesopores in the catalyst (Fig. 3.5). These mesopores are observed as tortuous in nature without any perfect ordering. It is presumed that the aggregation of co-complexing agent used in very high concentration during the synthesis would have helped in directing the formation of mesopores in the catalysts.

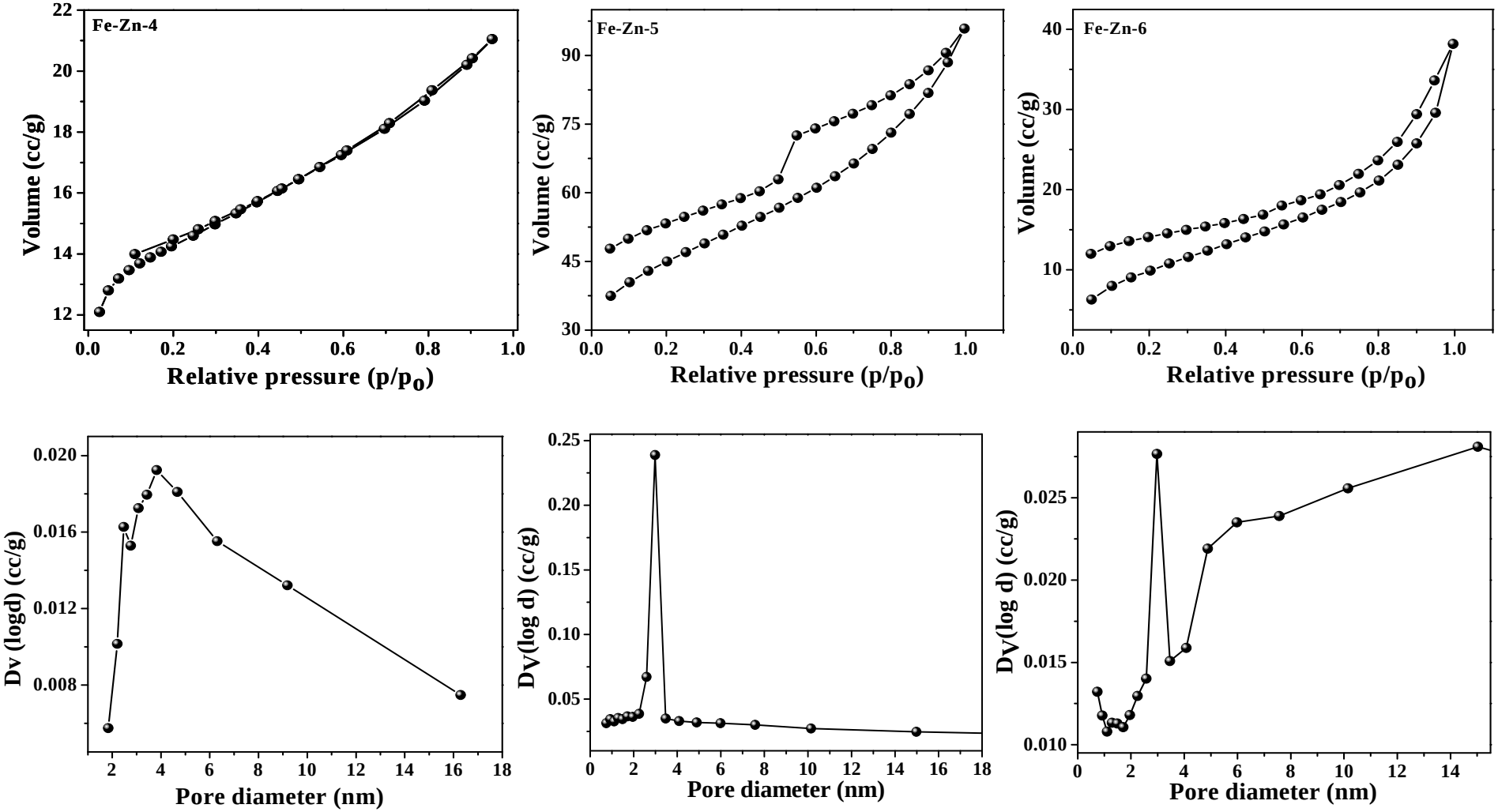

Fig. 3.3. N_2-physisorption isotherms (top) and pore size distributions (bottom) of Fe-Zn-4, Fe-Zn-5 and Fe-Zn-6.

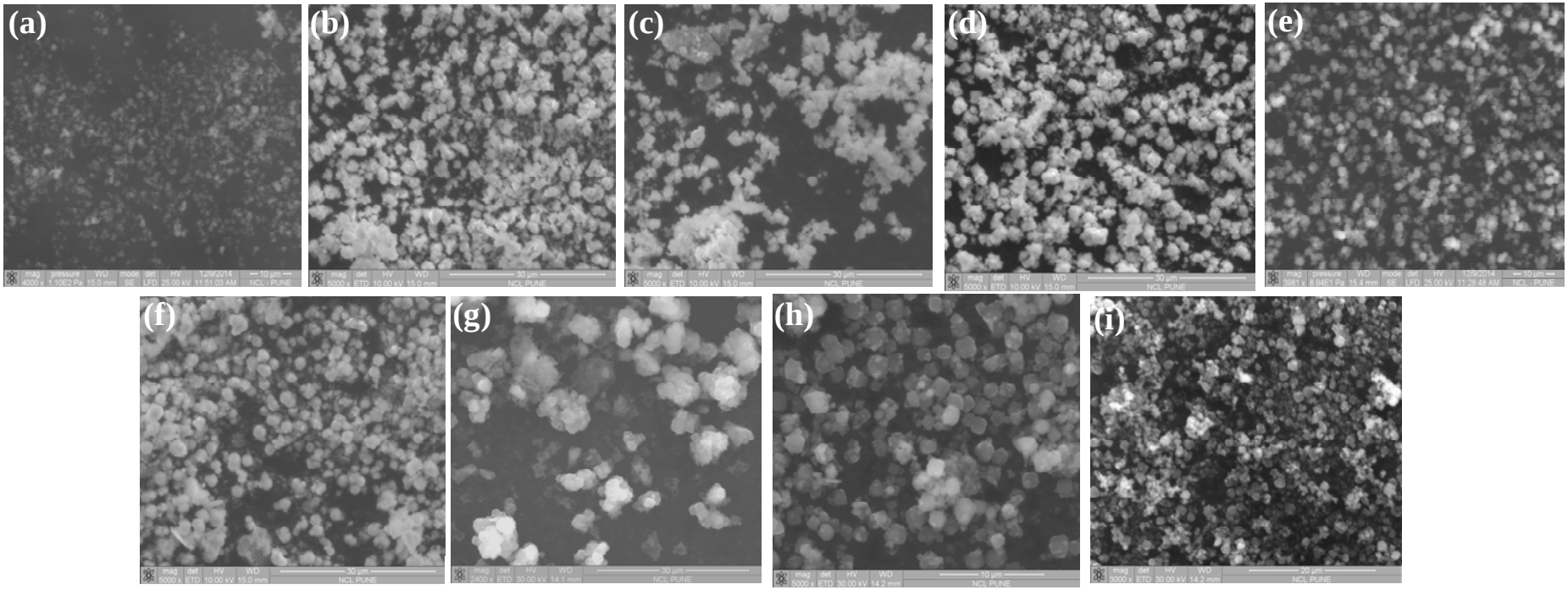

Fig. 3.4. SEM images of (a) Fe-Zn-0, (b) Fe-Zn-1, (c) Fe-Zn-2, (d) Fe-Zn-3, (e) Fe-Zn-4, (f) Fe-Zn-5, (g) Fe-Zn-6, (h) Fe-Zn-7 and (i) Fe-Zn-8.

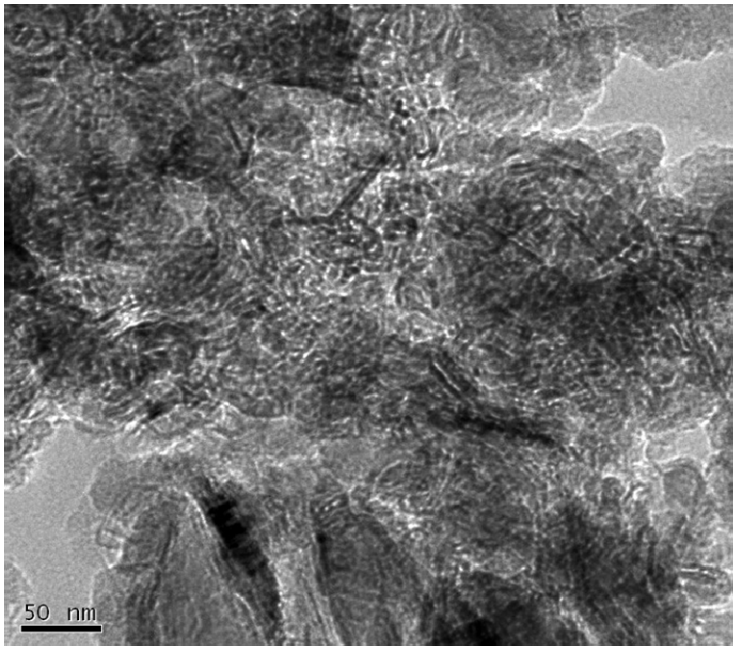

Fig. 3.5. HRTEM of Fe-Zn-4 showing mesopores.

3.3.1.6. DRIFT spectroscopy of adsorbed pyridine

The nature of acidic sites in DMC catalysts was differentiated by the DRIFT spectroscopy of adsorbed pyridine. Measurements conducted on Fe-Zn-4 revealed that the catalyst is mainly Lewis acidic in nature. The spectrum showed (Fig. 3.6) bands corresponding to Lewis acid sites at 1450, 1608 (C-C stretching vibration of coordinatively bonded pyridine, strong Lewis acid sites) and 1488 cm^{-1} (Lewis and Brönsted acid sites). Although the bands observed at 1541 and 1638 cm^{-1} are associated with Brönsted acid sites, their origin in DMC is intriguing. It could be probable that these band might have contribution from the -OH group associated with the complexing agent.

3.3.1.7. NH_3-TPD

The density of acid sites in DMC catalysts were quantified from NH_3-TPD measurements. The NH_3-TPD of Fe-Zn-4 depicted in Fig. 3.7 showed a broad distribution of acid sites in the desorption temperature of 100 - 200 °C. The unsymmetrical peak was then deconvoluted into three desorption peaks with peak maximum centred at 125, 150 and 192 °C. The first peak is attributed to desorption of physisorbed ammonia and the latter two are corresponded to ammonia desorbed from weak and strong acid sites. Overall acidity of the catalysts is given in Table 3.2. It is observed that the total acidity of Fe-Zn-1, Fe-Zn-2, Fe-Zn-3 and Fe-Zn-4 followed an inverse relation to their crystallite size variation.

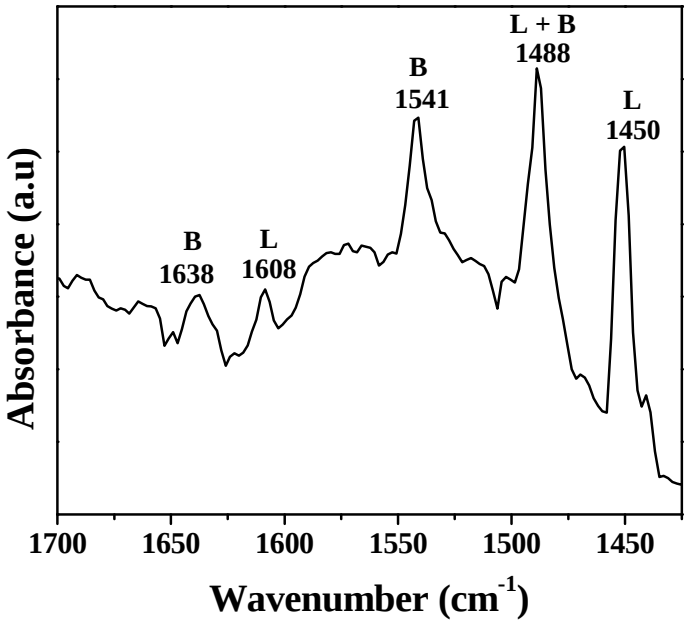

Fig. 3.6. Py-DRIFT spectrum of Fe-Zn-4 recorded at 150 °C.

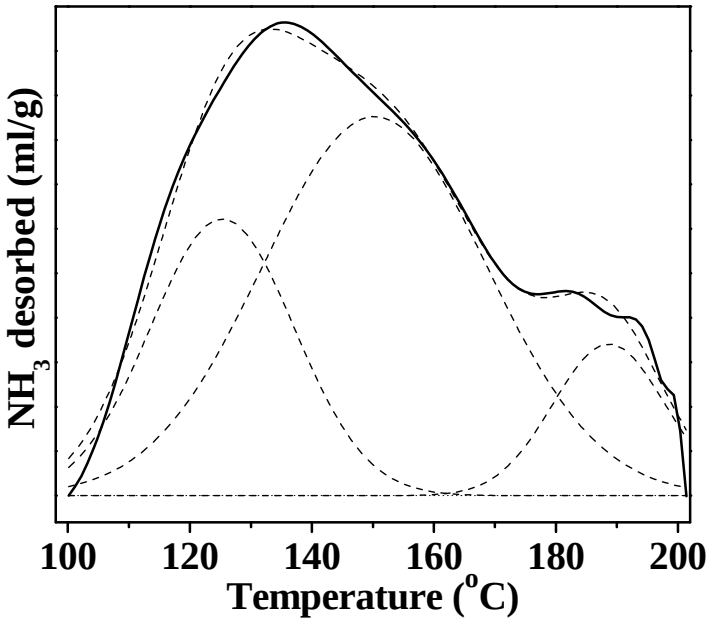

Fig. 3.7. NH_3-TPD profile of Fe-Zn-4.

By and large, the characterization studies established that the method of preparation of DMC catalysts has a marked influence on their physicochemical properties.

3.3.2. Catalytic activity

Table 3.3 lists the activity of Fe-Zn DMC catalysts for polyesterification of glycerol and succinic acid (Scheme 2.1 and Section 2.4.1). Since the topological characteristics of HPs are controlled by DB, the activity of the catalysts is expressed in terms of isolated yield and

DB of the polymer. DB was calculated by Frey's equation by substituting the integrated values of various branching segments obtained from inverse-gated ^{13}C NMR spectrum of the purified polymers. The equation and assignments of carbon signals of different connectivity are provided in Chapter 2 (Section 2.5.1.1).

Table 3.3. Catalytic activity of Fe-Zn DMC: Polyesterification of glycerol with succinic acid.

Catalyst	Isolated yield of G-SA (wt%)	Distribution of segments (mol%)[a]							Inherent viscosity (η; dl/g)[b]
		L_{13}	D	T_{12}	L_{12}	T_{13}	T_A	DB (mol%)	
Fe-Zn-0	53.8[c]	18.8	11.9	6.5	5.5	0.0	57.2	49.5[c]	0.039
Fe-Zn-1	52.3	18.6	9.2	7.6	5.0	0.0	59.7	43.8	0.048
Fe-Zn-2	63.4	19.4	11.8	6.3	5.4	0.6	56.5	48.8	0.038
Fe-Zn-3	66.2	19.3	12.3	5.9	5.0	0.0	57.5	50.3	0.033
Fe-Zn-4	76.2	18.5	15.3	4.8	5.6	0.5	55.3	55.9	0.037
Fe-Zn-5	75.7	18.9	9.8	7.3	5.3	0.7	58.0	44.6	0.044
Fe-Zn-6	70.6	17.9	8.5	8.2	5.6	0.0	59.9	42.0	0.045
Fe-Zn-7	71.5	18.0	8.9	7.9	5.3	0.0	59.9	43.2	0.064
Fe-Zn-8	71.4	17.5	9.4	8.2	5.4	0.0	59.4	45.0	0.044

Reaction conditions: Succinic acid (SA) = 1.733 g, glycerol (G) = 0.935 g, G : SA (molar ratio of functional groups) = 1:1, catalyst = 0.08 g, reaction temperature = 180 °C, reaction time = 1.5 h. [a]Calculated by integration of signals in inverse-gated and DEPT ^{13}C NMR spectra. [b]Estimated at 29 °C in THF. [c]Reaction time = 1.2 h.

Modification in synthesis of DMC catalysts by changing the complexing agent, co-complexing agent and mode of addition of reagents resulted variation in catalytic activity. By keeping the complexing agent the same and systematically increasing the molecular weight of co-complexing agent, the generated Fe-Zn-1, Fe-Zn-2, Fe-Zn-3 and Fe-Zn-4 catalysts showed a negligible change in unit cell parameter (0.896 nm), a decrease in crystallite size from 52.8 to 43.6 nm and an increase in total acidity from 3.87 to 7.10 mmol/g (Table 3.2). Isolated yield and DB of polymer followed a linear correlation with the total acidity and crystallite size of the catalysts as shown in Fig. 3.8[(a) and (b)]. Isolated yield and DB of HPs varied in direct proportion with the total acidity and in inverse proportion to the crystallite size of the DMC catalysts.

When DMC catalysts were prepared by keeping the co-complexing agent (PEG-4000) same and varying the complexing agent from t-BuOH to methanol and glycerol, the newly

formed catalysts (Fe-Zn-7 and Fe-Zn-8) showed a different trend in catalytic activity. The catalysts prepared using methanol (Fe-Zn-7) and glycerol (Fe-Zn-8) had bigger crystallites and lower acidity than Fe-Zn-4 (prepared using t-BuOH). This correlation between total acidity / crystallite size and isolated yield / DB is non-linear for Fe-Zn-4, Fe-Zn-7 and Fe-Zn-8 [Fig. 3.8 (c) and (d)]. DB portrayed a slightly exponential behaviour with increase in acidity. While isolated yield of the polymer was almost the same for Fe-Zn-7 and Fe-Zn-8, it was appreciably high for Fe-Zn-4. Even though the DB increased with increase in total acidity, the non-linear increase indicated that perhaps stronger acid sites in the catalysts would be the deciding factor of catalytic activity. In this regard, stronger acid sites in the catalysts were taken into consideration. Integration of deconvoluted peaks of NH_3- TPD gave the relative amount of stronger acid sites (at 192 °C) in DMC catalysts. Calculations showed that Fe-Zn-4 has the highest amount of strong acid sites (8.4 mol %) than Fe-Zn-7 (5.7 mol %) and Fe-Zn-8 (4.8 mol %). This clearly demonstrates the importance of stronger acid site in determining catalytic activity. Although Fe-Zn-8 has lesser fraction of strong acid sites, it has outnumbered Fe-Zn-7 mainly because of its higher amount of overall acidity. A plot of isolated yield and DB of the polymer versus the crystallite size also showed a non-linearity (Fig. 3.8 (d)). Isolated yield of the polymer showed a decreasing trend with increase in crystallite size. But the DB of the polymer decreased from Fe-Zn-4 to Fe-Zn-7 and then increased with Fe-Zn-8 as the crystallite size is increased. This behaviour shows that the crystallite sizes of the catalysts have little or insignificant effect on catalytic activity. Thus it can be concluded that one of the deciding factors for the catalytic activity is the percentage of stronger acid sites in the catalysts. To further confirm the effect of stronger acid sites on catalytic activity, polyesterification was carried out in presence of highly acidic Amberlyst-70. The reaction over Brönsted acidic Amberlyst-70 catalyst led to gelation within 20 minutes. A maximum attainable DB before the gelation was only 42 mol% indicating that too acidity (Brönsted sites) can trigger the gelation phenomenon much earlier during the polymerization. Hence, apart from stronger (Lewis) acid sites, the catalytic activity of DMC catalysts and their control on gelation are influenced also by other factors which will be discussed in the following section.

As the mode of addition of reagents was changed during the synthesis of Fe-Zn-4, the newly formed Fe-Zn-5 and Fe-Zn-6 showed difference in their textural and chemical properties. With these set of catalysts, the correlation of isolated yield and DB of the polymer with total acidity and crystallite size has also been attempted [Fig. 3.8 (e) and (f)]. In spite of having higher amount of total acid sites (8.23 mmol/g) and smaller crystallite

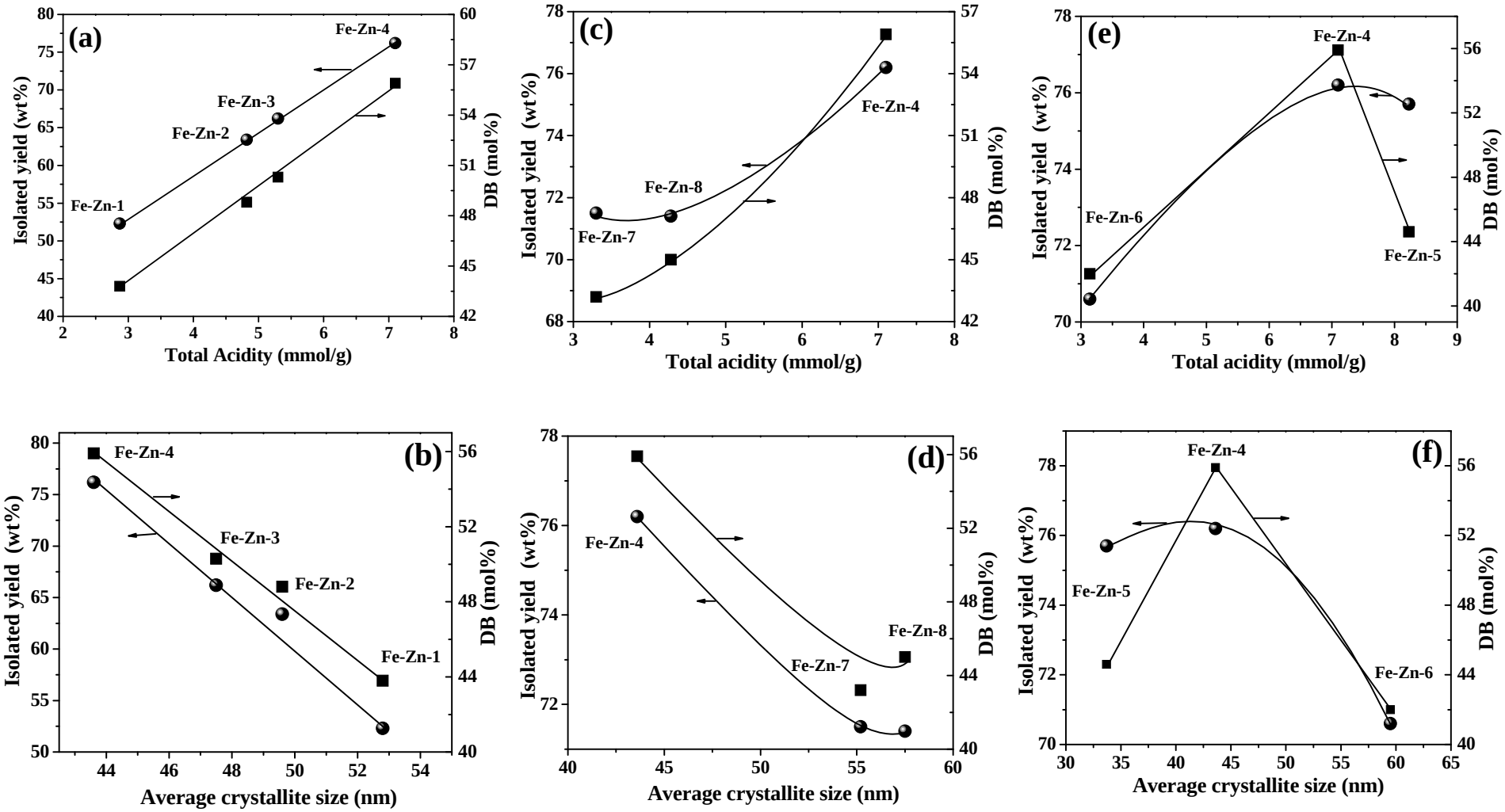

Fig. 3.8. Dependence of catalytic activity on total acidity (top) and average crystallite size (bottom) of Fe-Zn DMC catalysts.

size (33.7 nm), Fe-Zn-5 did not show the expected higher catalytic activity than Fe-Zn-4 (7.1 mmol/g and 43.6 nm respectively). This observation is contrary to the conclusions made above. Even Fe-Zn-0, possessing appreciable amount of acidity (3.52 mmol/g), did not show any control on gelation. Gelation was initiated at 1.2 h (isolated yield is 53.8 wt% and DB is 49.5 mol%) while it was not detected even at 1.8 h with Fe-Zn-4 catalyst. While Fe-Zn-0 was prepared with no complexing and co-complexing agents and is microporous in nature, Fe-Zn-4 (prepared in the presence of complexing and co-complexing agents) showed micro-mesoporous architecture. These observations rationalize that although acidic sites are important, surface architecture may also play a crucial role in controlling gelation and improving DB of the polymer. N_2 physisorption and HRTEM studies have revealed that Fe-Zn-4, Fe-Zn-5 and Fe-Zn-6 possess micro-mesoporous architecture. But the unprecedented activity of Fe-Zn-4 as compared to Fe-Zn-5 and Fe-Zn-6 needs special attention. This would be another deciding factor in explaining the catalytic activity of Fe-Zn DMCs. In this context a revisit to the nature of polymerization was attempted. Polyesterification is a condensation reaction which produces water as the byproduct. Water has detrimental effect on the stability of active acid sites. The fact that Fe-Zn-4 shows good conversion indicates that the active centres in it are stable towards water molecules. Water tolerance of the catalyst is represented by the hydrophobic nature of its surface. Water adsorption studies on Fe-Zn-4 and Fe-Zn-5 revealed that Fe-Zn-4 is more hydrophobic (15 wt% water loss) than Fe-Zn-5 (18 wt% water loss) (Fig. 3.9) and this could explain the high activity of Fe-Zn-4 over Fe-Zn-5 catalyst. Relatively high surface hydrophobicity of Fe-Zn-4 as compared to Fe-Zn-5 favours the reactant molecules to adsorb on the active site more strongly than water molecules. Hence, it is ascertained that Lewis acidity (to initiate the reaction), surface hydrophobicity (to stabilize the active centres) and micro-mesoporous architecture are the critical features of Fe-Zn DMC catalysts for producing hyperbranched polyesters with a high DB at controlled gelation. Further optimization of the reaction parameters was continued with Fe-Zn-4 catalyst. The reaction was performed with succinic acid and its higher homologue adipic acid. The efficiency of the catalyst is expressed in terms of isolated yield and DB of the polymers.

3.3.2.1. Effect of reaction temperature

The reactions were conducted at three different temperatures, 160, 180 and 190 °C. As the reaction temperature was increased from 160 to 180 °C, isolated yield of G-SA polymer increased from 61.5 to 76.2 wt% showing a rate enhancement of the reaction with temperature (Table 3.4). DB had also increased from 28.9 to 55.9 mol% with associated slight increase in inherent viscosity (η) from 0.019 to 0.037 dl/g. Further raise in temperature

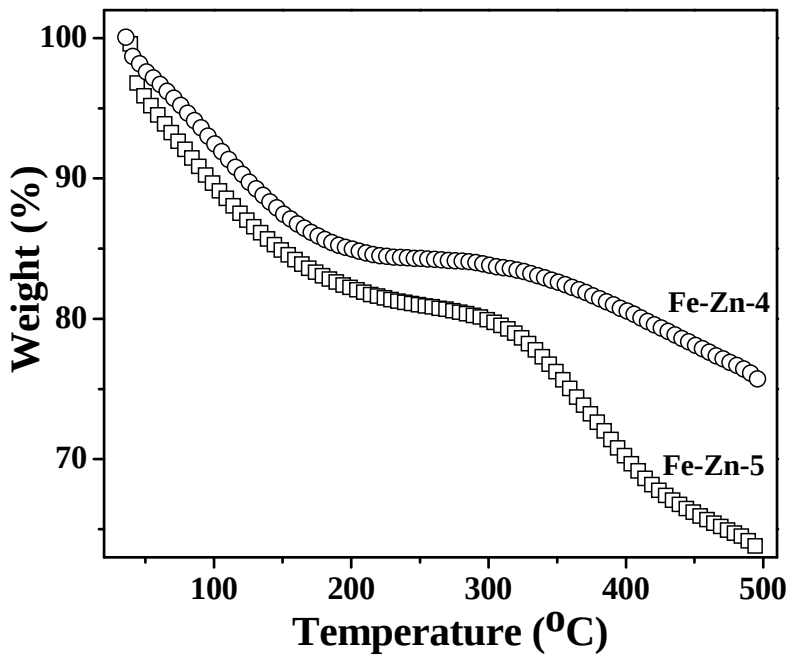

Fig. 3.9. Thermogravimetric analysis of Fe-Zn-4 and Fe-Zn-5.

to 190 °C showed a decrease in isolated yield of the polymer. This behaviour was identified due to the formation of anhydrides. The undesired side reaction caused low concentration of SA in the reaction medium and thereby leading to lower isolated yield of the polymer. The DB of the polymer at this temperature (56.4 mol%) is almost same as that at 180 °C but a slight increment in η was observed (0.043 dl/g). In case of G-AA polymer it was seen that the temperature has a positive effect on DB and isolated yield. Anhydride formation was not observed in G-AA polymerization even at 190 °C (Table 3.4). A linear increment of DB from 13.7 mol% to 58.6 mol% was noticeable as the temperature increased from 160 to 190 °C.

3.3.2.2. Effect of reaction time

Polyesterification with G/SA and G/AA monomers on Fe-Zn-4 catalyst showed nearly a linear increase in isolated yield of generated polymers with prolongation of the reaction time (Table 3.4). Isolated yield of G-SA polymer increased from 56.8 wt% to 80.2 wt% as the reaction time was extended from 1 to 2 h. Analogous to this trend, the DB of the polymer also showed an increment from 48.5 to 64 mol%. Apparently high viscosity values (0.05 dl/g) at 2 h indicated that few molecules were cross-linked. Maximum attainable DB of G-AA polymer was 56.2 mol% with an isolated yield of 88.7 wt% at the end of 2 h. Higher yield of product polymers indicated that gelation was not commenced even at longer reaction hours. However, gelation in G-SA polymerization was observed at 2.1 h and that for G-AA polymerization was commenced at 2.3 h.

Table 3.4. Effect of reaction parameters on the catalytic activity of Fe-Zn-4.

Reaction parameter	G-SA polymer			G-AA polymer		
	DB (mol%)[d]	Isolated yield (wt%)	η (dl/g)[e]	DB (mol%)[d]	Isolated yield (wt%)	η (dl/g)[e]
Effect of reaction temperature (°C)[a]						
160	28.9	61.5	0.019	13.7	76.9	0.046
180	55.9	76.2	0.037	38.3	84.6	0.050
190	56.4	52.6	0.043	58.6	76.2	0.070
Effect of reaction time (h)[b]						
1	48.5	56.8	0.024	17.8	76.5	0.047
1.5	55.9	76.2	0.037	38.3	84.6	0.050
2	64.0	80.2	0.050	56.2	88.7	0.068
Effect of molar ratio of reactants (G : Diacid)[c]						
1:1	55.9	76.2	0.037	38.3	84.6	0.046
1: 1.5	81.9	52.4	0.030	68.5	72.5	0.060
1 : 2	90.2	62.3	0.026	84.7	47.0	0.070

[a]Reaction conditions: glycerol : diacid acid functional groups molar ratio = 1:1, Fe-Zn-4 = 3 wt% of total reactants, reaction time = 1.5 h. [b]Glycerol: diacid acid functional groups molar ratio = 1:1, Fe-Zn-4 = 3 wt% of total reactants, reaction temperature = 1.5 h. [c]Reaction temperature = 180 °C, Fe-Zn-4 = 3 wt% of total reactants, reaction time = 1.5 h. [d]Estimated from inverse-gated and DEPT ^{13}C NMR spectra. [e]Values at 29 °C using THF as solvent.

3.3.2.3. Effect of molar ratio of reactants

Polyesterifications were performed at increasing concentration of diacid to monitor its effect on isolated yield and DB (Table 3.4). As the molar ratio was increased from 1 to 2, the DB of G-SA had increased from 55.9 to 90.2 mol%. The η of the polymer confirmed that even at a DB of 90.2 mol%, gelation was not commenced and the product was not a mixture of sol and gel. The viscosity values are in coherence with the reported values [19]. In the case of G-AA polymer, the DB value increased from 38.3 to 84.7% as the molar ratio of the reactants increased from 1 to 2. The DB has decreased with increase in the chain length of diacid. This behaviour is attributed to a combination of polar and steric influences of the α-substituent on the carboxylic acid group. The electron density at carboxylate group increases with the alkyl chain length (inductive effect) favouring initial protonation but the

electrophilicity of the carbonyl carbon decreases, disfavouring the subsequent alkoxy insertion. However, above C_4 chain length, electronic properties are not believed to have a significant effect. So variation in DB is attributed to steric factors only (diffusional limitations) [20]. The catalyst showed consistent activity in producing hyperbranched polyesters with diacids of different chain length.

3.3.3. Product characterization

3.3.3.1. 2D NMR

The through-bond connectivity in hyperbranched polyesters were confirmed by 2D spectral analysis. The details of the experimental procedure are given in chapter 2 (Section 2.5.1.1). Two different spectroscopic analyses viz., heteronuclear single quantum correlation (HSQC) and heteronuclear multiple bond correlation (HMBC) was used for the structural analysis of G-SA polymer (Fig. 3.10). HSQC provides the correlation between a carbon and hydrogen which are separated by single bond. HSQC spectrum of G-SA polymer confirmed the formation of a dendritic unit as the signal due to correlation between the secondary hydrogen of glycerol and the carbonyl carbon of acid was present. The correlations between linear and terminal fractions of the hyperbranched structure were also present in the spectrum confirming the formation of hyperbranched structures [7]. HMBC provides the correlation between a carbon atom and a hydrogen atom separated by three bonds. HMBC of G-SA (Fig. 3.10) showed correlations arising from carbonyl carbon of acid with the secondary hydrogen of glycerol confirming the formation a dendritic unit. Correlations corresponding to other segments were also visible in the spectrum confirming its presence [7].

3.3.3.2. MALDI-TOF

The nature of branched segments in the hyperbranched structures was identified with the help of MALDI-TOF spectrometry. The details of the experimental procedure are given in chapter 2 (Section 2.5.1.3). If branched products are formed as a result of esterification of primary and secondary hydroxyl groups of glycerol, the spectrum of tri-substituted oligomers will show characteristic ion masses that differ from those of linear di-substituted structures. MALDI spectrum of G-SA and G-AA polymer showed in Fig. 3.11 confirms the presence of branched segments. The possible branching segments of G-SA and G-AA polymers deduced from the spectra are given are given Table 3.5. The evidence of cross-linking was confirmed by the masses of some species differing in 18 Da indicating loss of water molecules. The spectra also confirmed the absence of any cyclic product during the polyesterification.

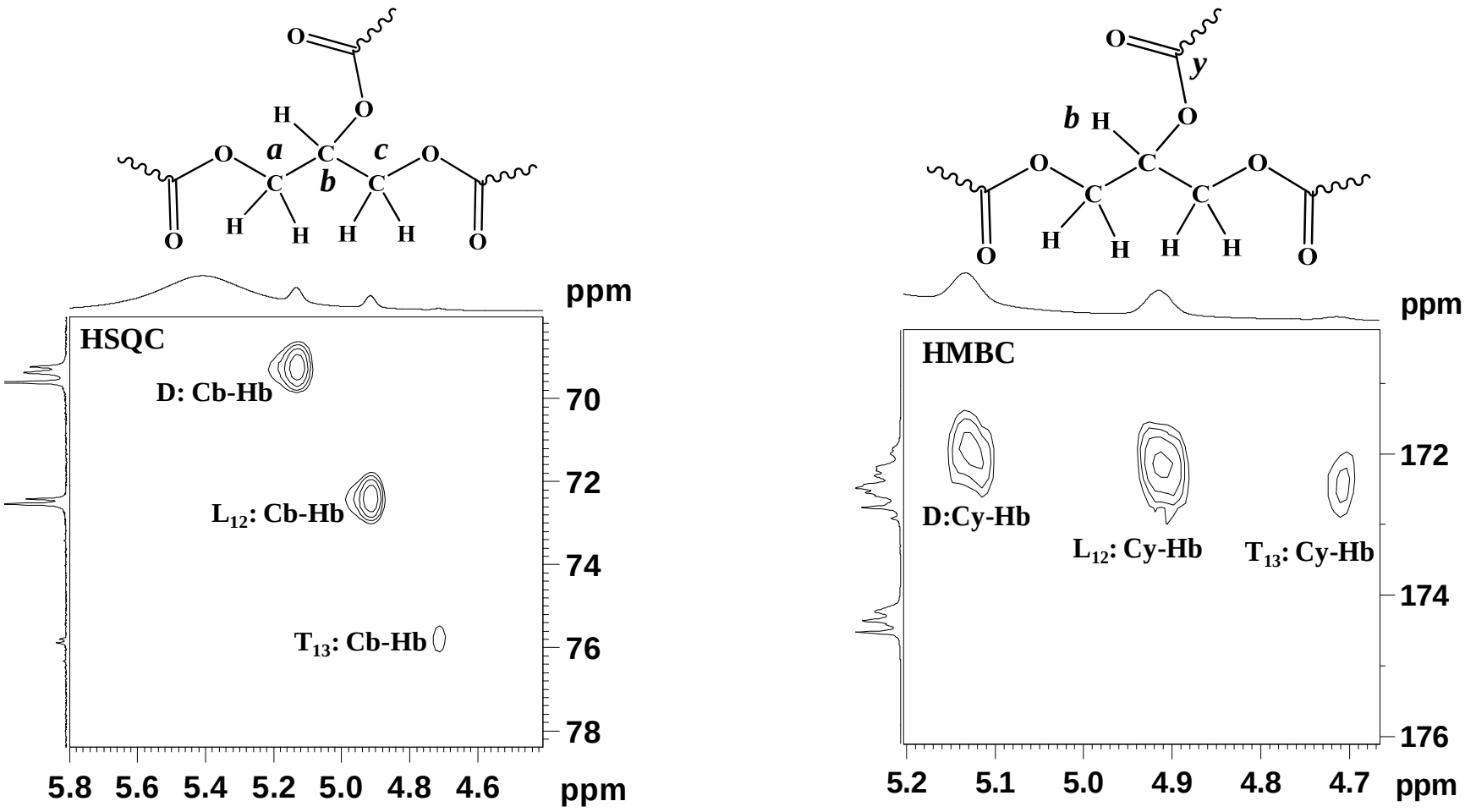

Fig 3.10. 2D NMR spectra of G-SA polymer.

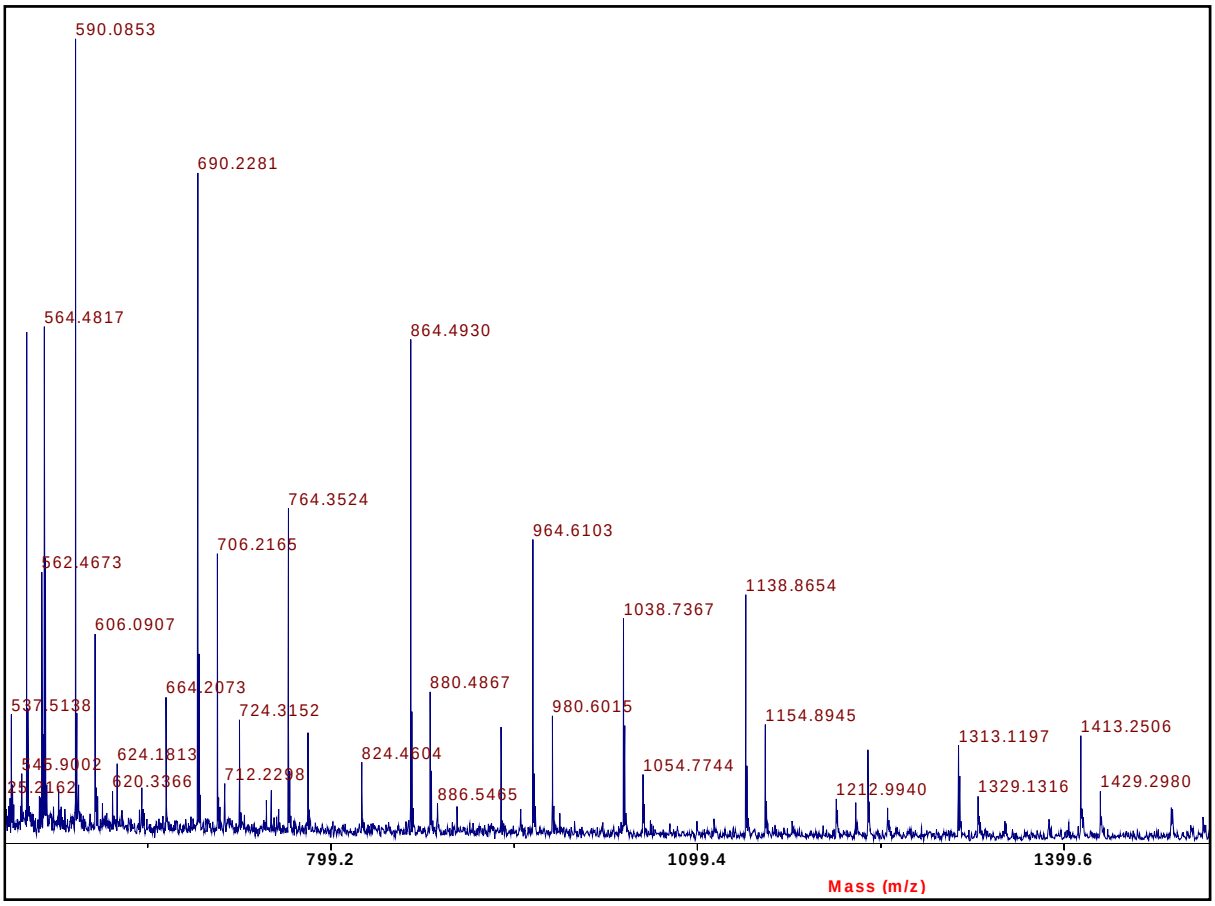

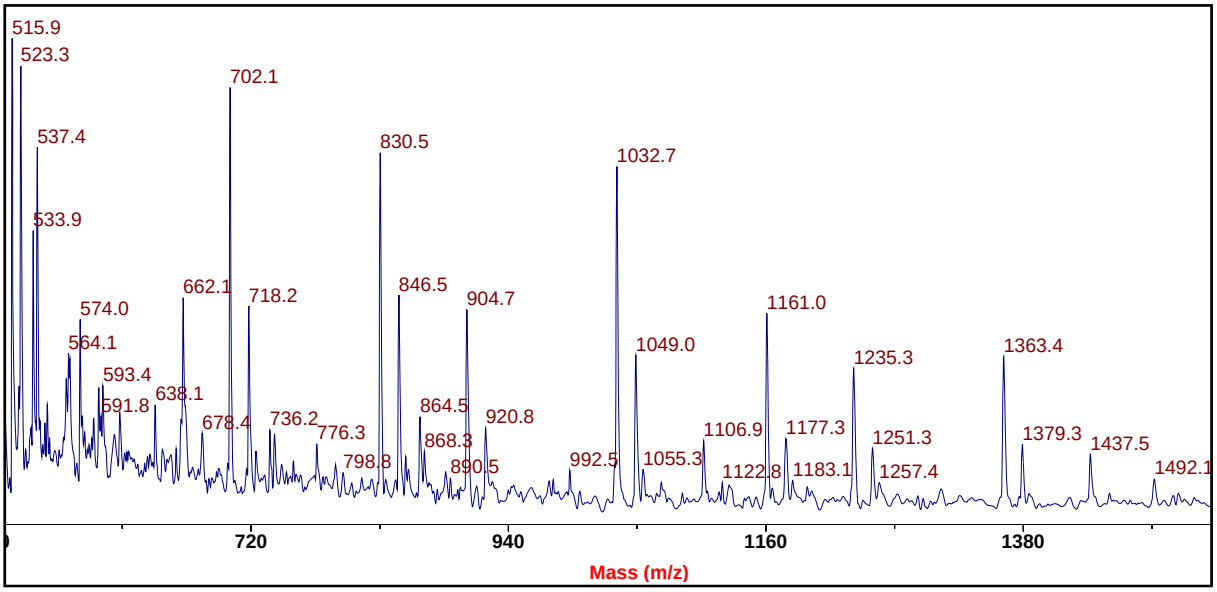

Fig. 3.11. MALDI-TOF spectra of G-SA (top) and G-AA (bottom) polymers.

Table 3.5. Suggested branched segments of G-SA and G-AA polymers.

Entry	Suggested branched segments	Succinic acid $(M+Na)^+$ $(M+K)^+$	Adipic acid $(M+Na)^+$ $(M+K)^+$
1	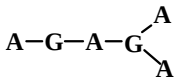	590.14 606.11	702.76 718.76
2	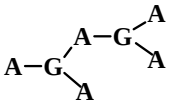	690.16 706.13	830.90 846.90
3	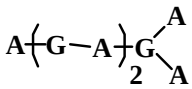	764.19 780.17	905.00 921.00
4	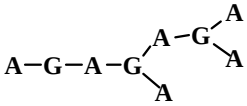	864.21 880.18	1033.14 1049.14
5	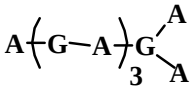	938.25 954.22	1107.24 1123.24
6	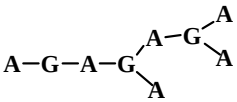	964.23 980.20	1161.28 1177.28
7	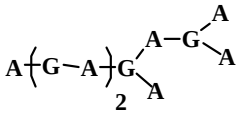	1038.26 1054.24	1235.38 1251.38
8	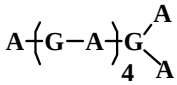	1112.30 1128.27	1329.48 1345.48

3.3.3.3. FTIR

FTIR spectra of the polymers confirmed the presence of ester linkages. The spectrum of G-SA polymer (Fig. 3.12) showed bands corresponding to ester linkages at 1735 and 1165 cm^{-1} due to antisymmetric and symmetric stretching vibrations. The band due to terminal acid groups of the branched structures appeared as a shoulder at 1730 cm^{-1}. The presence of C-H and O-H (terminal) stretchings in the polymer were visible by the bands at 2966 and 3490 cm^{-1}, respectively.

3.3.3.4. EDX

EDX analysis of G-SA polymer showed peaks corresponding to carbon and oxygen only. No peaks due to presence of elements like Fe, Zn and N were detected (Fig. 3.13). Thus, the purification process adopted involving centrifugation followed by filtration is efficient in removing all the catalyst particles from the polymer. Absence of above contaminants in the isolated polyester samples assures that the product is non-toxic and can be adopted for biomedical applications. This can be considered as one of the beneficial

features of solid catalysts in producing non-toxic, hyperbranched polyesters for speciality applications.

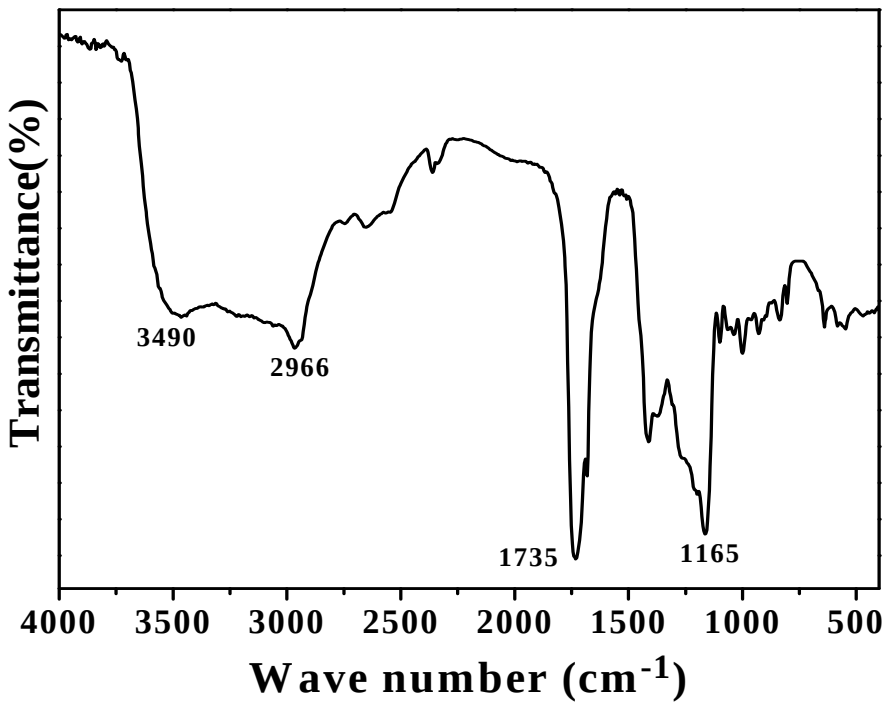

Fig. 3.12. FTIR spectrum of G-SA polymer.

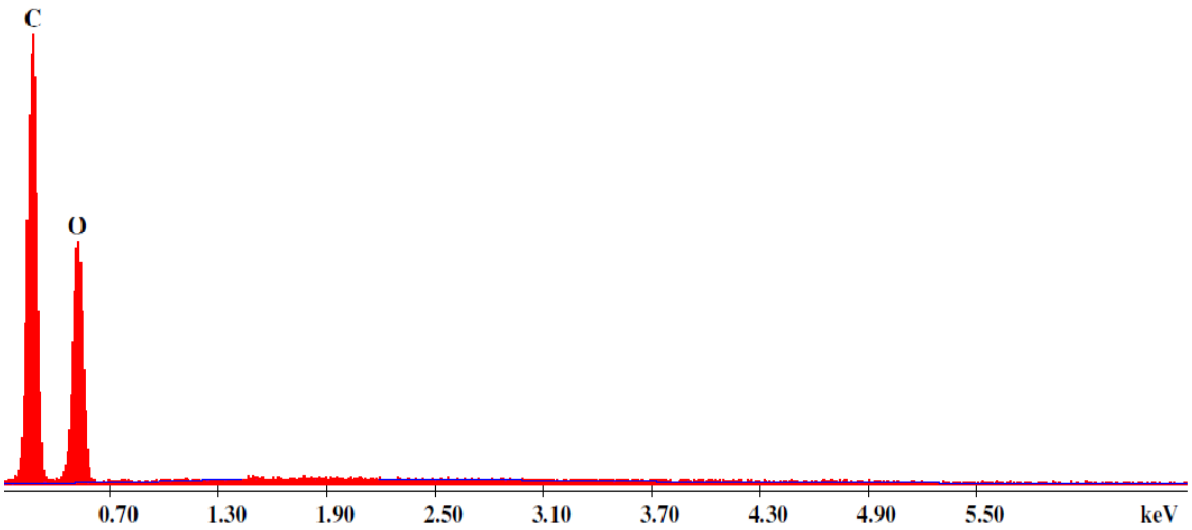

Fig. 3.13. EDX spectrum of G-SA polymer.

3.3.4. Catalyst reusability

Reusability of Fe-Zn-4 was confirmed in G-SA polymerization (G : SA functional group molar ratio = 1 : 1) conducted at 180 °C for 1 h. At the end of the reaction the catalyst was separated by centrifugation, dried and then reused. The catalyst was reused in ten

recycling experiments. Little decrease in activity was observed [DB = 48.5 (1st), 47 (2nd), 45.7 (5th) and 45.6 mol% (9th run)]. Fig. 3.14 shows the XRD and FTIR of Fe-Zn-4 after the 10th recycle. XRD confirmed the stability of the crystalline structure of the catalyst. While FTIR also confirmed the structural stability showing ν(CN) band at the same position as that of the fresh catalyst. The band at 1729 cm^{-1} indicates the presence of adsorbed SA molecule.

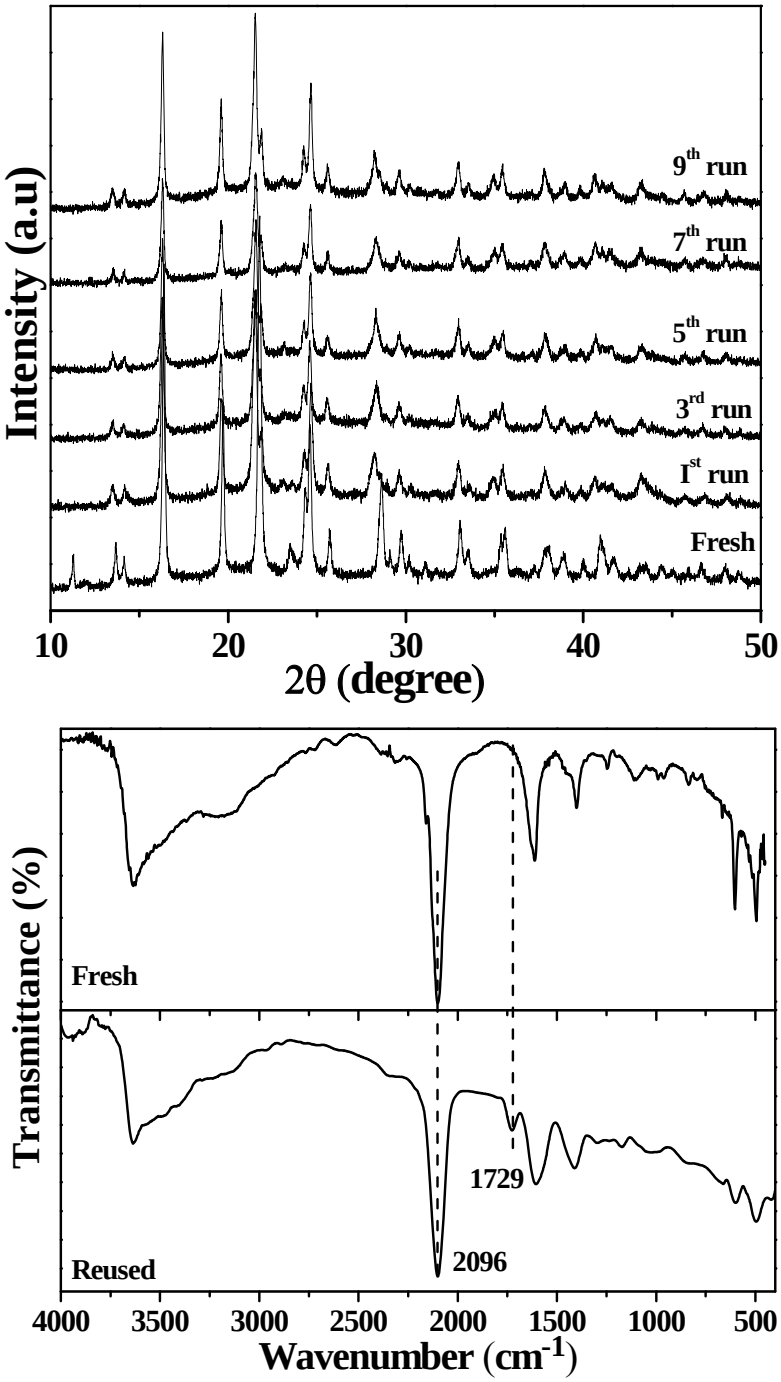

Fig. 3.14. XRD (top) and FTIR (bottom) of fresh and reused Fe-Zn-4.

3.3.5. Reaction mechanism

The exceptional activity of Fe-Zn DMC catalysts for the synthesis of hyperbranched polyesters at higher conversions and higher DB is expressed in terms of its reaction mechanism. It is intriguing that the catalyst was successful in producing hyperbranched polyesters with a DB as high as 90 mol% even without gelation. Therefore, the factors avoiding gelation were scrutinized in detail. It is documented that there are five critical features affecting the gelation phenomenon [1]. They are: (1) formation of reactive intermediates that resemble the AB_2 type monomers, (2) partial conversion of monomers, (3) slow addition of one monomer to another, (4) significant levels of cyclization reactions and (5) reactivity difference between identical functional groups within the molecule. If one or more of these factors arise, $A_2 + B_3$ (diacid + glycerol) polymerization will deviate from ideal cross-linking conditions and the polymerization will result in high molar mass hyperbranched structures. In the present study, the reactions yielded high conversions (~ 84 wt%; Table 3.4). Hence, the clause of partial conversion of reactant molecules to delay the gelation process is discarded. Again, the reaction was a batch process where slow addition of one monomer to another was not adopted, so that reason is also excluded. MALDI-TOF and 2D NMR have confirmed the absence of any cyclic compounds in the reaction mixture. Hence, the fourth point said above cannot be the reason for delayed gelation. Thus, the plausible reason for the delayed gelation phenomena at high DB (90 mol%) would be the formation of reactive intermediates that resembled AB_2 monomers (AB_2 polymerization does not lead to gelation, Chapter 1, Section 1.3.3). At the same time, the contribution from the reactivity difference between identical functional groups within the same molecule is also considered for better understanding of the reaction mechanism. Although glycerol is considered as a B_3 monomer, the -OH functional groups in it have different reactivity. Among the three -OH functionalities of glycerol, two are primary and one is secondary (B_2B'). The primary -OH group is slightly more reactive than the secondary and at the same time most of the dendrimeric molecules terminated in -OH functionalities would be rich in T_{12} fraction (the secondary and one primary -OH terminals) and this would be the other reason for delaying the cross-linking with another molecule. If the dendrimeric molecules are terminated with the T_{13} fraction (two primary -OH terminals) the cross-linking rate would be much faster than in the previous case. Indeed, higher concentration of T_{12} than T_{13} fraction was observed for the HPs produced using Fe-Zn DMC catalysts (Table 3.3).

It is proposed that in the first step of the catalytic cycle (Fig. 3.15) tetra coordinated Lewis acidic Zn^{2+} ions on the catalyst surface initiate the polymerization by activating the

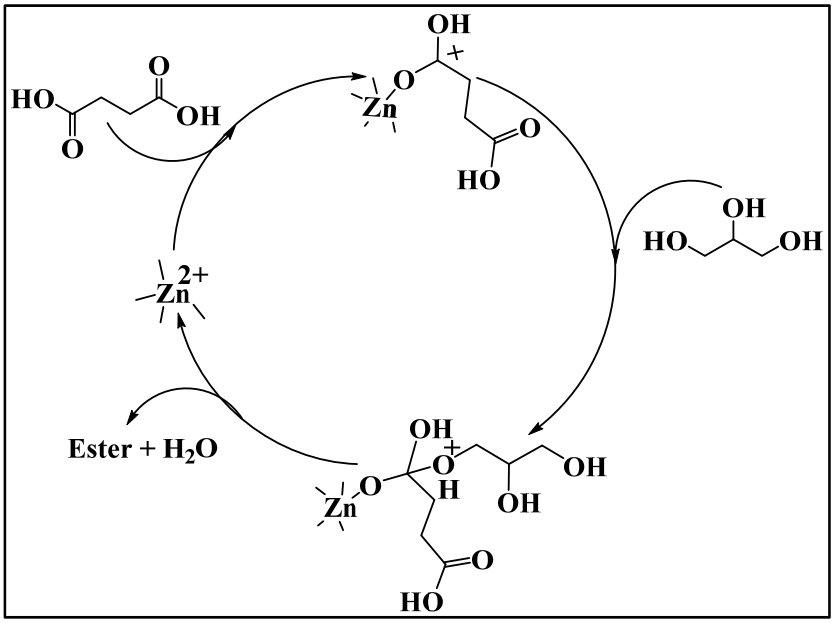

Fig. 3.15. Tentative reaction mechanism of polyesterification over Fe-Zn DMC catalyst.

carbonyl group of the diacid generating an electrophilic carbon centre. In the second step, the electrophilic carbon centre is attacked by nucelophilic -OH groups of glycerol forming the ester linkages and water molecules. Hydrophobic nature of surface active sites would enhance the sticking probability of reactant molecules than the water molecules and this would maintain the activity of the catalyst. Reactivity difference between the -OH groups of glycerol will preferentially generate the AB_2 intermediates. This is supported by the result of esterification of free fatty acids with methanol over Fe-Zn DMC [17] where monoesters were formed in the early stages of the reaction. Again, it is general in polyesterification reactions that the initial period of polymerization is the generation of dimers, trimers, tetramers and oligomers. During the course of the polyesterification, these oligomers will condense to form high molecular weight polymers. Micro-meso porous architecture on DMC would enhance the rate of formation of AB_2 monomers by reducing the diffusional limitation. Due to steric constraints further polymerization of these monomers will not continue inside the pores. So the initial time period of the reaction would be the generation of AB_2 type monomers and once these molecules are formed in large amount they will further undergo propagation step to form dendritic architectures at the external surface of the catalyst without meeting gelation (polymerization of AB_2 monomers will not lead to gelation, Chapter 1, Section 1.3.3). Although Fe-Zn-4 has relatively narrow pores (2.5 nm) than Fe-Zn-5 (3.7 nm) and Fe-Zn-6 (6.4 nm), this pore dimension seems good enough to form AB_2 intermediates. In addition to

that the reactivity difference between primary and secondary -OH groups on the terminals of hyperbranched molecules would also control the cross-linking rate.

3.4. Conclusions

Fe-Zn DMC catalysts have been used for the first time in the synthesis of hyperbranched polyesters from diacids (succinic and adipic acid) and glycerol based on A_2 + B_3 synthetic philosophy. A systematic investigation about the structural and textural features of the catalyst and product polymer through various characterization techniques confirmed that the DMC catalysts are highly efficient in producing hyperbranched polyesters in high yield with high DB without gelation. An increase in density of acid sites increased the rate of the reaction which is reflected on the yield and DB of the polymer. At the same time, stronger acid sites accelerated gelation rate as they can activate the condensation of secondary hydroxyl groups of one dendrimer molecule with carboxylic end of the other molecule. A unique combination of hydrophobicity that facilitates the adsorption of reactant molecules but not the by-product water, Lewis acidity that initiates the esterification reaction and micro-mesoporous architecture that controls the gelation found to be the critical features of Fe-Zn DMC catalyst (Fe-Zn-4), to divert the reaction mechanism from ordinary A_2 + B_3 type into an in-situ AB_2 type in producing hyperbranched polymers with controlled gelation.

3.5. References

[1] D. Yan, C. Gao, H. Frey, Hyperbranched Polymers, Synthesis Properties and Applications, John Wiley & Sons, New Jersey (2011) 1-27.

[2] H. Jin, W. Huang, X. Zhu, Y. Zhou, D. Yan, Chem. Soc. Rev. 41 (2012) 5986-5997.

[3] J.A. Melero, G. Vicente, G. Morales, M. Paniagua, J.M. Moreno, R. Roldán, A. Ezquerro, C. Pérez, Appl. Catal. A: Gen. 346 (2008) 44-51.

[4] M.A. Carnahan, M.W. Grinstaff, J. Am. Chem. Soc. 123 (2001) 2905-2906.

[5] N.R. Luman, T. Kim, M.W. Grinstaff, Pure Appl. Chem. 76 (2004) 1375-1385.

[6] J.F. Stumbé, B. Bruchmann, Macromol. Rapid Commun. 25 (2004) 921-924.

[7] V.T. Wyatt, G.D. Strahan, A. Nunez, J. Am. Oil Chem. Soc. 87 (2010) 1359-1369.

[8] A.S. Kulshresta, W. Gao, R.A. Gross, Macromolecules 38 (2005) 3193-3204.

[9] J.H. Clark, C.N. Rhodes, Clean Synthesis Using Porous Inorganic Solid Catalysts and Supported Reagents RSC Clean Technology Monograph, The Royal Society of Chemistry, Cambridge (2000).

[10] B. Le-Khac, W. Chester, US Patent No. 5,789,626 (1998).

[11] J. Hoffmann, S. Ehlers, B. Klinksiek, B. Klesczewski, C. Steinlein, L. Obendorf, H.

Pielartzik, J.F. Pazos, US Patent No. 20,020,198,278 A1 (2002).

[12] Y. Gu, X. Dong, Des. Monomers Polym. 16 (2013) 72-78.

[13] X. Sun, S. Chen, X. Zhang, G. Qi, Prog. Chem. 24 (2012) 1776-1784.

[14] Y. Gu, X. Dong, D.X. Sun, J. Macromol. Sci. A: Pure Appl. Chem. 49 (2012) 586-590.

[15] R. Srivastava, D. Srinivas, P. Ratnasamy, J. Catal. 241 (2006) 34-44.

[16] P.S. Sreeprasanth, D. Srinivas, P. Ratnasamy, Appl. Catal. A: Gen. 314 (2006) 148-159.

[17] J.K. Satyarthi, D. Srinivas, P. Ratnasamy, Energy Fuels 24 (2010) 2154-2161.

[18] R.R. Mather, Colloid Surf. 58 (1991) 401-407.

[19] M. Xu, X. Yan, R. Cheng, X. Yu, Polym. Int. 50 (2001) 1338-1345.

[20] C. Pirez, J.M. Caderon, J.P. Dacquin, A.F. Lee, K. Wilson, ACS Catal. 2 (2012)1607-1614.

Chapter - 4

Copolymerization of Cyclohexene Oxide and Carbon Dioxide over Co-Zn DMC Catalysts

4.1. Introduction

Global warming due to rising concentration of green house gas CO_2 has gained serious concerns among scientists, politicians and environmentalists. Enormous emission of CO_2 over 30 Gt/year from anthropogenic activities contributes by roughly 60% to global warming. CO_2 concentration in atmosphere is now close to 400 ppm which is significantly higher than the pre-industrial era (300 ppm). To alleviate global warming and its effect on environment, the Kyoto protocol had suggested 37 industrialized nations and the European Union to curtail CO_2 emission to a level of 5.2% in the period 2008-2012 [1]. Several key technologies and strategies were suggested thereafter as a remedy, of which the most important was the concept of CO_2 capture and utilization. Implementation of this concept relies on the exploitation of CO_2 as a C1 feedstock for the synthesis of chemicals and materials. Conversion of CO_2 to fuels and chemicals is a maturing research area in different countries. Among this, direct utilization of CO_2 through a low energy process involving epoxides to polycarbonates demonstrates a promising approach due to its long term fixation [2, 3]. Catalytic copolymerization of CO_2 with an epoxide was initially reported by Inoue in 1969 [4]. After this breakthrough, a number of catalyst systems were proposed for the efficient synthesis of polycarbonates, focussing on milder reaction conditions and maximum CO_2 incorporation [5]. Most often, depending on the reaction conditions and catalyst employed, the product takes form as either polycarbonate or polyethercarbonate [3]. Propylene oxide (PO) and cyclohexene oxide (CHO) are the usually exercised epoxides. The main challenges of copolymerization are the homopolymerization of epoxides and the formation of cyclic carbonates. Cyclic carbonate formation is more prominent with PO than with CHO due to the ring strain generated by the latter. Polycarbonates find increasing application as environmentally adaptable engineering thermoplastics, as resins and as packaging materials. Clean burning of poly(propylene carbonate) (PPC) and poly(cyclohexene carbonate) (PCHC) is an advantage to use as a binder for ceramics, as adhesives, propellants and for the lithographic application to generate capillary channels and pores. In addition, high glass transition temperature (T_g) of PCHC helps it for melt processing application [6].

Co-Zn double-metal cyanides (Co-Zn DMCs) are well known catalysts for the copolymerization of CHO and CO_2. Their activity improvements through various modifications are rich in literature. Yi et al [7] reported the initial detailed investigation on the copolymerization of CHO and CO_2 over nano-sized DMC and multi-metal cyanide

catalysts in 2004. The catalyst prepared by reverse emulsion method employing Igepal CA-520 (co-complexing agent) showed sizes in the range of 50-100 nm. The multi-metal cyanides were a hybrid of Fe and Co cyanides with Zn^{2+} and Y^{3+} metals. Polycarbonates produced by these catalysts were characterized with a number average molecular weight (M_n) of 5100 [polydispersity index (PDI) = 1.2] and with a maximum of 59 mol% CO_2 incorporation at a CO_2 pressure of 6.8 bar. During the same period, Chen et al [8] reported a highly active Co-Zn DMC catalyst prepared by using different complexing agents. The complexing agents were presumed to modify the electron density at the active centre. Among different complexing agents used tertiary butanol (t-BuOH) and 1-methyl-2-propanol gave the highest conversions of 94 and 86%, respectively with almost equal amount of CO_2 incorporation (44 mol%) over a reaction period of 2 h at 90 °C and 38 bar CO_2. T_g of the polymer obtained with t-BuOH as complexing agent with a weight average molecular weight (M_w) of 33061 (PDI = 1.94) was 109 °C. Kim et al [9] employed a series of Co-Zn DMCs prepared by changing the most important precursor of DMC synthesis, ZnX_2 (X = F, Cl, Br, I). Among these different zinc precursors, catalyst synthesized from ZnF_2 was not active whereas the maximum activity was obtained with $ZnCl_2$ and ZnI_2 precursors. Although the amount of CO_2 incorporated in the polymer was same (~ 53 mol%), the molecular weight obtained over $ZnCl_2$ was higher than that with ZnI_2 (89000 and 5100 with PDI of 1.7 and 1.2, respectively) at a reaction condition of 80 °C, 4 h and 9.6 bar of CO_2. Chen et al [10] have reported a novel DMC composed of Ni-Zn for the copolymerization. The catalyst with a molecular formula $Zn[Ni(CN)_4]$ produced 22.5 g-polymer/ g-catalyst with a CO_2 incorporation of 33 mol% but with extreme conditions of 140 °C, 30 bar CO_2 and a reaction time of 20 h. Lee et al [11] further continued to report the effect of co-complexing agent on catalytic activity. Various co-complexing agents such as poly(tetramethyleneether glycol), polypropylene glycol, polyethylene glycol, poly(ethylene oxide)-poly(propylene oxide)-poly(ethylene oxide) tri-block copolymer, and hyperbranched polyglycidol were used in the synthesis. Among them, DMC prepared with hyperbranched polyglycidol showed maximum incorporation of CO_2 (65 mol%) at 80 °C for 4 h and with 5 bar CO_2. This polycarbonate showed a T_g of 98.6 °C (M_n = 8500, PDI = 1.5) which is lower than the first report of Yan et al [7]. Dharman et al [12] reported a microwave assisted copolymerization over Co-Zn DMC to improve the initiation period of the catalyst. Microwave radiation was helpful in avoiding the induction period of the catalyst. The catalyst showed appreciable activity with a CO_2 incorporation of 75 mol%, M_n of 14500 and PDI of 1.5. In recent times, Sun et al [13] have reported the mechanism for CHO/CO_2 copolymerization through a combination of kinetic

study and electron spray ionization-mass spectrometry. These studies concluded that Zn-OH group in the DMC catalyst is the active centre for polymerization and ether fractions are formed at the early stages of initiation contributing to head groups of the polymer.

Although much attention was given in reporting a highly active DMC catalyst through various synthetic strategies and experimental techniques, a little awareness was paid to rationalise the key factors responsible for the catalytic activity. This chapter discusses the factors influencing the catalytic activity of Co-Zn DMC complexes for the copolymerization of CHO and CO_2. In the present study, Co-Zn DMCs were synthesized by different synthetic procedures, variation in the mode of addition of their reagents and without using a co-complexing agent. The molecular and crystal structures of catalysts were analyzed in detail by various physical, chemical and spectroscopic techniques. Structure-activity correlations revealed that high density and strength of Lewis acid sites, moderate crystallinity, low crystal symmetry (monoclinic/rhombohedral), Cl^- ions and coordinated t-BuOH control the catalytic activity of Co-Zn DMC in polycarbonate synthesis. CO_2 adsorption studies established that higher the host-guest interaction higher would be the catalytic activity and lower would be the induction period. Coordinated Cl^- ions increase the acid strength and thereby, improve the polar interaction between CO_2 and Zn^{2+} which would ultimately reduce or even avoid the induction period. Polycarbonates with CO_2 incorporation as high as 86 mol% and M_w of 20900 with a PDI of 1.8 were synthesized at complete conversion of CHO.

4.2. Experimental

Co-Zn DMC catalysts were synthesized and characterized by the procedures reported in Chapter 2 (Sections 2.2.2 and 2.3). Five different catalysts were prepared mainly by two synthesis procedures. Modifications in synthesis procedure were adopted by changing the mode of addition of reagents and avoiding the co-complexing agent. Co-Zn-0 was prepared by simple precipitation of catalyst precursors in the absence of complexing and co-complexing agents. Co-Zn-1 and Co-Zn-2 were prepared by the same synthesis procedure and with same composition of reagent solutions, but by varying the mode of addition of reagents (Chapter 2, Sections 2.2.2.2 and 2.2.2.3). During the synthesis of Co-Zn-1, each reagent solution such as solution 2 and solution 3 were added to solution 1 in their chronological orders. While in the synthesis of Co-Zn-2, solution 2 was added to solution 3 and this mixture was added to solution 1. Co-Zn-3 and Co-Zn-4 were prepared by a different synthesis procedure. The main modification in the synthesis procedures of Co-Zn-3 and Co-Zn-4 was the use of co-complexing agent in Co-Zn-3 and absence of it in Co-Zn-4 (Chapter 2, Sections 2.2.2.4 and 2.2.2.5). The catalysts were characterized by the techniques described

in Chapter 2 (Sections 2.3.1 to 2.3.6, 2.3.8 and 2.3.9). Details of reaction procedure and product characterization including the calculation of percentage incorporation of CO_2 in the polymer were described in Sections 2.4.2 and 2.5.2 of Chapter 2, respectively.

4.3. Results and discussion

4.3.1. Structural characterization

4.3.1.1. XRD

Figure 4.1 shows XRD patterns of Co-Zn DMC catalysts prepared by different procedures. Co-Zn-0 prepared in the absence of complexing and co-complexing agents showed XRD pattern composed of highly intense sharp peaks which could be indexed to a cubic phase (peak positions 2θ: 14.9°, 17.2°, 24.5°, 34.9°, 39.2° and 43.1°) [14]. Further, the XRD pattern confirmed the phase purity of the sample (as no additional peaks due to any other crystalline phase or impurity were observed). When the synthesis conditions were modified by introducing complexing and co-complexing agents, the newly formed Co-Zn-1 showed XRD peaks typical of the cubic phase (as observed for Co-Zn-0). Additional peaks at 2θ = 14.5°, 20.6° and 23.6° corresponding to a monoclinic phase were also observed for Co-Zn-1 [14]. Addition of complexing and co-complexing agents had greatly influenced the phase purity of Co-Zn-1. Further modification in the synthesis of Co-Zn-1 by keeping the composition of reagent solutions the same but changing the mode of their addition, produced Co-Zn-2. XRD Co-Zn-2 is similar to that of Co-Zn-1 confirming the co-existence of cubic and monoclinic phases in it composition. Relative crystallinity [15] of Co-Zn-1 and Co-Zn-2 were calculated by the integration of peak intensities in the range 12°- 40°. Percentage crystallinity was estimated with respect to Co-Zn-0 catalyst whose crystallinity was assumed as 100%. Addition of complexing and co-complexing agents significantly reduced the crystallinity of Co-Zn-1 to 85%. But modification in the synthesis of Co-Zn-1 by changing the mode of addition of reagents restored the crystallinity in Co-Zn-2 to 102%. Percentage contribution of monoclinic phase to total crystallinity in Co-Zn-1 and Co-Zn-2 showed greater contribution in Co-Zn-1 (19%) than in Co-Zn-2 (9%). Crystallite size calculation also indicated that Co-Zn-1 is composed of larger size monoclinic crystals than Co-Zn-2 (51 versus 35 nm, based on the peak at 23.6°). Crystallite size of cubic phase decreased in the order: Co-Zn-2 (87 nm) > Co-Zn-0 (70 nm) > Co-Zn-1 (68 nm). These analyses demonstrate that although the method of preparation of Co-Zn-1 and Co-Zn-2 are the same, a slight modification in the addition of reagents can impart significant changes in their crystallization behaviours.

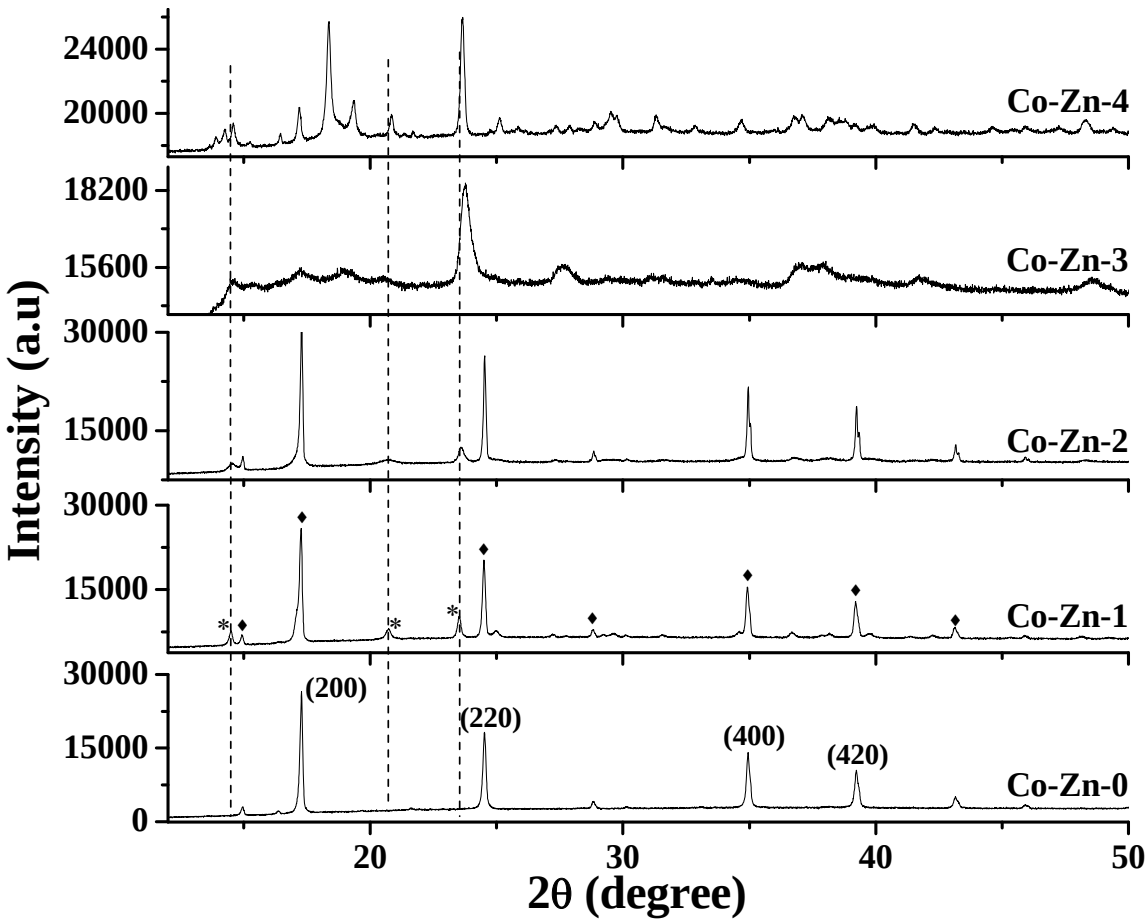

Fig. 4.1. XRD patterns of Co-Zn DMC complexes. Peaks due to cubic (♦) and monoclinic (*) phases are marked.

As the method of preparation of DMC catalysts was changed to synthesize Co-Zn-3 and Co-Zn-4, the produced catalysts showed XRD pattern entirely different from those of Co-Zn-1 and Co-Zn-2. Co-Zn-3 was synthesized in the presence of both complexing and co-complexing agents. As compared to Co-Zn-0, XRD pattern of this catalyst is highly amorphous. The dominant peak at 23.5° and the small peak at 14.5° correspond to the monoclinic phase. Percentage crystallinity of Co-Zn-3 was estimated to be 11% (entirely due to the monoclinic phase) and is substantially lower than that of Co-Zn-1. Crystallite size calculations showed an average size of 29 nm which is even lower than the monoclinic crystals observed in Co-Zn-2. Addition of co-complexing agent (PEG-4000) during the synthesis would have possibly assisted to disperse the nucleation points from crystal growth to generate the amorphous bulk structure. Modification in the synthesis of Co-Zn-3 without using the co-complexing agent restored the crystallinity in the catalyst. But the newly formed Co-Zn-4 showed XRD pattern with no resemblance to Co-Zn-0. The peak pattern shows few peaks corresponding to monoclinic phase (2θ at 14.6°, 17.1°, 20.8° and 23.7°) and some

additional peaks of a different crystalline phase with appreciable intensity. These additional peaks were then compared with those of the precursors ($K_3[Co(CN)_6]$ and $ZnCl_2$, Fig. 4.2 (a)) and ascertained that there were no retention of precursor impurities in Co-Zn-4. Percentage crystallinity of Co-Zn-4 was estimated to be 54% with crystals composed of average size 51 nm (2θ at 18.3°) which is significantly lower than Co-Zn-0 but considerably higher than Co-Zn-3. Modification in the synthesis of Co-Zn-3 has improved the crystallinity but reduced the phase purity.

Stability of different crystalline phases of DMC catalysts was analyzed by XRD after activation of the complexes at 180 °C for 2 h. No noticeable phase transformation was observed in Co-Zn-0, Co-Zn-1, Co-Zn-2 and Co-Zn-3 catalysts (Fig. 4.2 (b)). Thermal activation of these catalysts shows only a fortification in the intensities of diffraction peaks. But a significant phase transition was noticed in Co-Zn-4 catalyst (Fig. 4.2 (c)). The newly formed peak pattern in Co-Zn-4 with peak positions at 2θ = 9.8°, 14.3°, 16.4°, 19.6°, 21.6° and 24.8° shows correspondence to rhombohedral phase [16]. Structural transformation due to thermal activation in other materials has been reported due to the removal of water molecules. The framework collapses during water evaporation followed by temperature induced crystallization is the only probable reason for the phase transition in Co-Zn-4. Analysis of the catalyst after long activation times confirmed that the newly formed phase is sufficiently stable as it retains its structural integrity even after long activation times of 4 h. Altogether, XRD analysis has shown that the bulk structure and the extent of crystallization of Co-Zn DMC catalysts are highly influenced by the synthesis procedure.

4.3.1.2. FTIR

FTIR spectroscopy is the most commonly used characterization technique to verify C≡N bridging in DMCs. FTIR spectra of activated samples are shown in Fig. 4.3. The precursor complex, $K_3[Co(CN)_6]$ showed the ν(C≡N) band at 2119 cm^{-1}. This band appeared at higher wavenumbers ca., 2181 cm^{-1} for Co-Zn-0 synthesized in the absence of complexing and co-complexing agents. The shift to higher wavenumber is due to the back donation phenomenon. Cyanide ions coordinate to central Co^{3+} by σ-donation. The σ-bonding rises the electron density in d-band which eventually causes a back donation to 2pπ* antibonding molecular orbital of C≡N. The back donated electron density accumulates at the more electronegative N atom and transforms it to a new coordination site for Zn^{2+} ions. Since the electrons are removed from the antibonding molecular orbital during this bridging, the ν(C≡N) shifts towards higher wavenumber [17-18]. However, the extent of electron

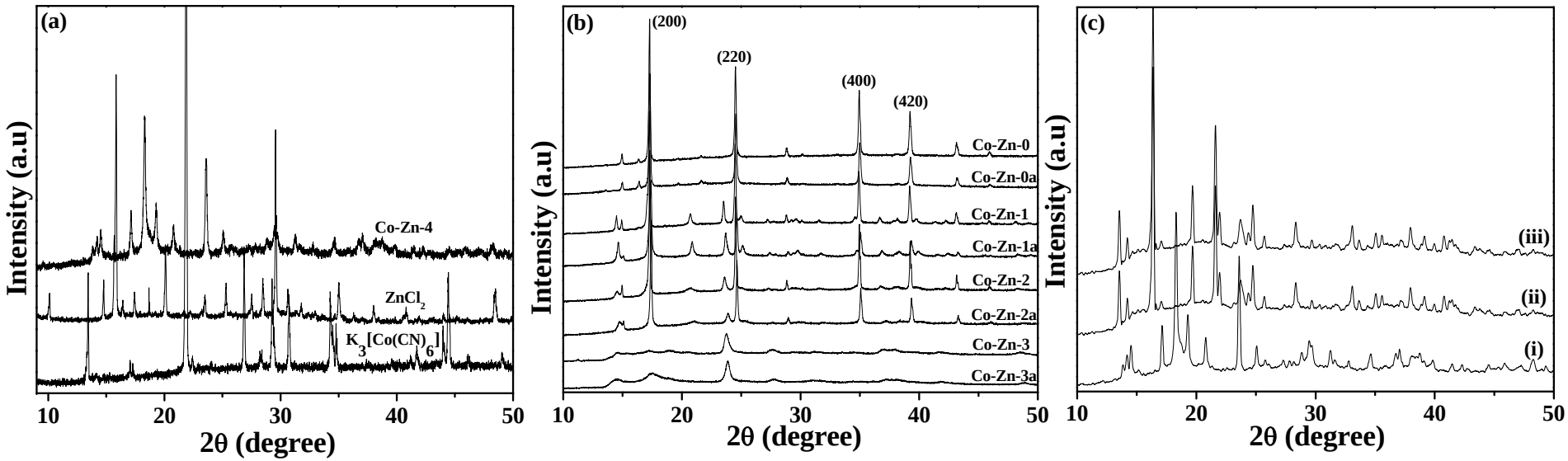

Fig. 4.2. XRD patterns: (a) Co-Zn-4, $ZnCl_2$ and $K_3[Co(CN)_6]$, (b) Co-Zn-x and Co-Zn-xa (before and after thermal activation, respectively, at 180 °C for 2 h) and (c) as-synthesized Co-Zn-4 (i), after thermal treatment at 180 °C for 2 h (ii) and after thermal activation at 180 °C for 4 h (iii).

donation from the N end of C≡N to Zn^{2+} depends on the strength of Lewis acidity at the Zn^{2+} centre. It can be increased by coordinated electron withdrawing groups such as Cl^- ions and contribute to band shift to higher wavenumbers [19]. The remaining bands in the spectrum of Co-Zn-0 are attributed to coordinated and H-bonded water molecules. The coordinated water molecules show a band at 3654 cm^{-1} while the H-bonded water shows a band at 3417 cm^{-1}. Band at 1609 cm^{-1} indicates the bending vibration of these water molecules. A small band at 452 cm^{-1} corresponds to ν(Co-C) vibrations and confirms the coordination of C≡N ligand through its C atom to the Co^{3+} ions [17-18].

Catalysts prepared in the presence of complexing and co-complexing agents showed C≡N stretching bands at same position as Co-Zn-0 confirming the cyano bridging during complexation (Fig. 4.3). In order to ensure the effect of complexing and co-complexing agent on the electronic properties of DMC complexes, the exact position and shape of C≡N band was studied in detail. The analysis revealed that C≡N stretching of all catalysts differs greatly in their position and multiplicity (Fig. 4.4 (left)). Co-Zn-1 and Co-Zn-2 showed three overlapping bands at 2174, 2191 and 2220 cm^{-1}. Co-Zn-3 exhibited ν(C≡N) at 2157, 2191 and 2220 cm^{-1}. Co-Zn-4 showed multiple bands at 2150, 2165, 2191, 2207 and 2220 cm^{-1}. Differences in IR band positions indicate the difference in the structure and bonding of the bridging cyanide groups. XRD showed cubic and monoclinic phases in Co-Zn-1 and Co-Zn-2. Percentage crystallinity calculations confirmed that Co-Zn-2 is dominant in cubic phase than Co-Zn-1. If the IR band at 2181 cm^{-1} is assigned to the cubic structure and that at 2191 cm^{-1} to monoclinic structure, the intensity ratio of cubic/monoclinic IR bands (I_{2181}) / I_{2191}) is higher for Co-Zn-2 than for Co-Zn-1 which confirms the conclusion drawn from the XRD. The band at 2191 cm^{-1} in Co-Zn-3 is relatively sharp and intense as compared to other DMCs due to the dominant monoclinic phase. The multiple ν(C≡N) bands in Co-Zn-4 indicate the presence of more than one type of crystalline phases/C≡N bondings, which is again in accordance with the XRD analysis. The decreased molecular symmetry and defect structure is expected to produce multiplicity in IR bands. IR Bands at 2157 and 2220 cm^{-1} are assigned to surface cyanide groups. These bands are less prominent in Co-Zn-0 than the rest of the complexes. Co-Zn-0 is monophasic (cubic) while the other catalysts (prepared in presence of complexing/co-complexing agents) are multi-phasic (cubic, monoclinic and rhombohedral). Monoclinic crystals are smaller in size (XRD) and therefore have more exposed surface C≡N groups. This is supported by the high intensity of 2157 and 2220 cm^{-1} bands in Co-Zn-4. In the cubic structure, Zn^{2+} has an octahedral geometry while in the monoclinic it has a

tetrahedral geometry [17]. The octahedral geometry has an average coordination of four C≡N ligands and two water molecules. Thermal activation removes the coordinated water molecules transforming the octahedral geometry to a pseudo tetrahedral geometry. Removal of coordinated water makes the Zn^{2+} centre more electrophilic and increases the σ-donation from C≡N ligand. This phenomenon also contributes to the shift in C≡N stretching towards higher wavenumbers.

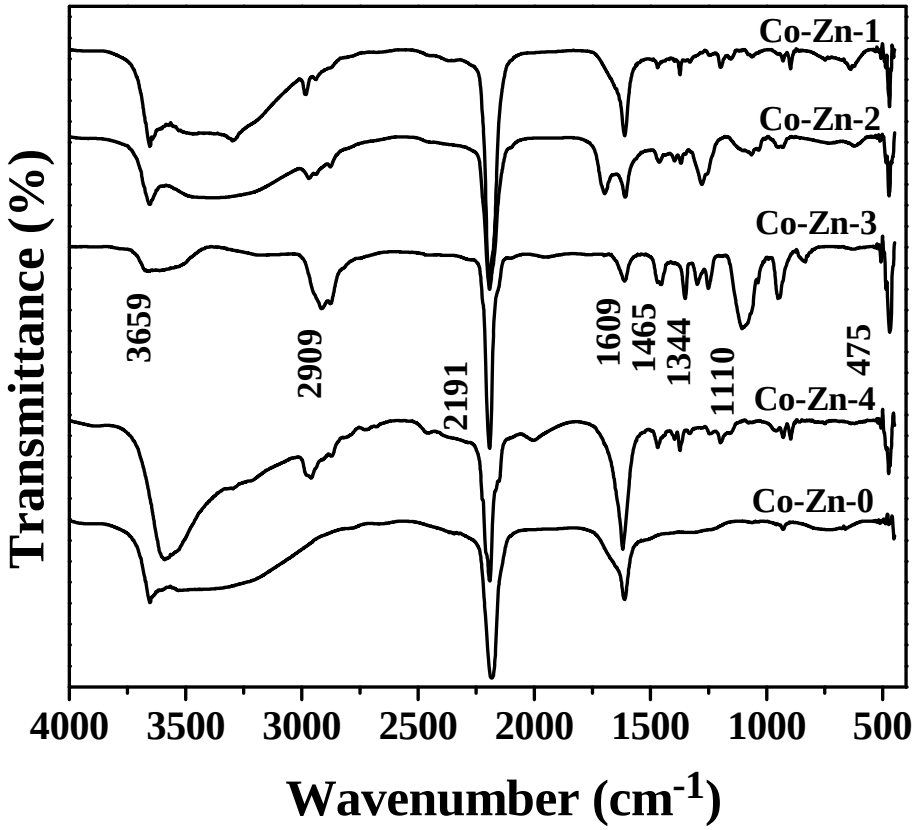

Fig. 4.3. FTIR spectra of Co-Zn DMC catalysts.

IR spectra of Co-Zn-1, Co-Zn-2, Co-Zn-3 and Co-Zn-4 synthesized in the presence of complexing and co-complexing agents confirmed the retention of t-BuOH in their structures (Fig. 4.3). This is verified by the presence of bands at 2909 cm^{-1} (CH stretch), 1465 cm^{-1} (CH scissoring), 1344 cm^{-1} (OH bending) and 1110 cm^{-1} (3°-C-O stretch). Co-Zn-3 showed more intense t-BuOH bands than Co-Zn-4. During the synthesis of Co-Zn-3, the catalyst was suspended twice in varying amounts of PEG-4000, t-BuOH and water mixtures before it was dried. Co-Zn-4 was also suspended twice but in the mixture having no PEG-4000. Hence, it can be concluded that apart from controlling the crystallite size and structure, the co-complexing agent (PEG-4000) enabled the retention of more amount of t-BuOH in Co-Zn-3.

Elemental analysis (C, H, N) of the complexes have also revealed the inclusion of complexing agent in varying amounts in DMC catalysts (Table 4.1).

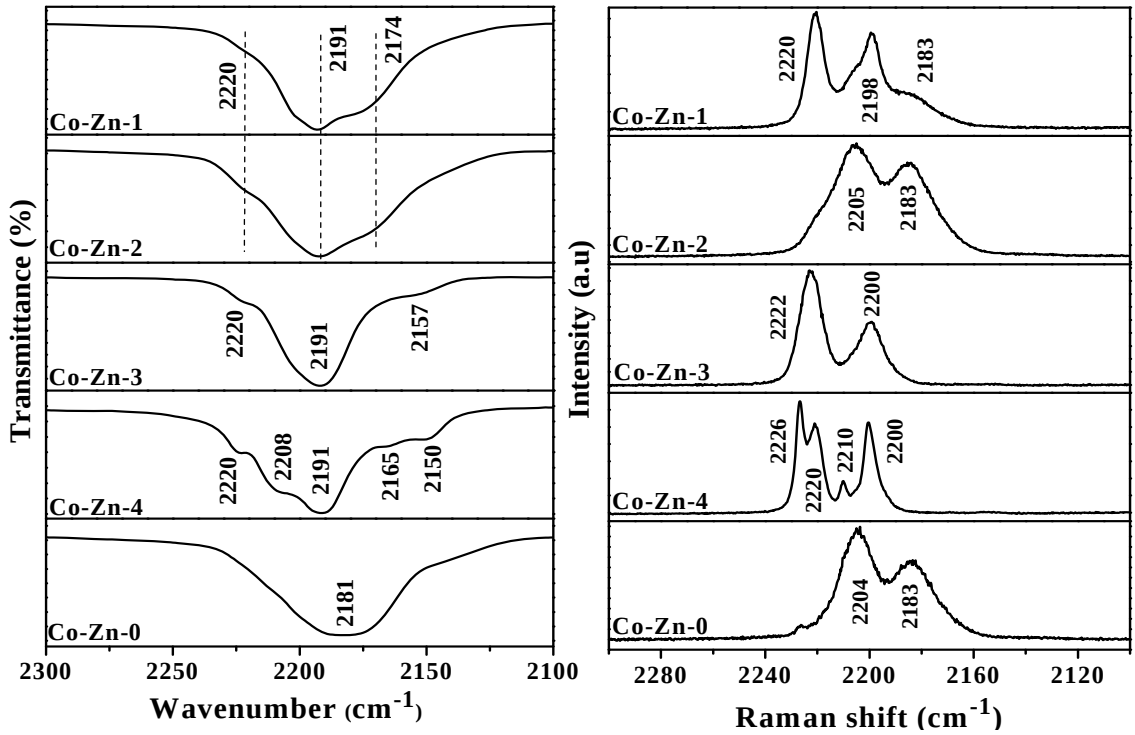

Fig. 4.4. FTIR (left) and FT-Raman (right) spectra in the ν(C≡N) region of DMC catalysts.

4.3.1.3. Raman spectroscopy

The multiplicity in C≡N stretching region of Co-Zn DMCs was further established by the Raman analysis (Fig. 4.4 (right)). Highly crystalline monophasic Co-Zn-0 showed two bands at 2183 and 2204 cm^{-1} and assigned to DMC with cubic symmetry. These bands for Co-Zn-1 and Co-Zn-2 were present at 2183 and 2198 cm^{-1}, and 2183 and 2205 cm^{-1}, respectively. An additional band at 2220 cm^{-1} in Co-Zn-1 designated the presence of a monoclinic phase. The intensity of this band is significantly low for Co-Zn-2 reassuring that Co-Zn-2 contains lesser amount of monoclinic phase than in Co-Zn-1. Co-Zn-3 shows an intense band at 2222 cm^{-1} corresponding to monoclinic phase and a band at 2200 cm^{-1} possibly due to some cubic phase. Co-Zn-4 shows multiple bands in the Raman spectra with two additional bands as compared to Co-Zn-3 at 2226 cm^{-1} and 2210 cm^{-1} indicating the presence of other crystalline phases. Raman spectra of the complexes confirmed the conclusions drawn from XRD and FTIR.

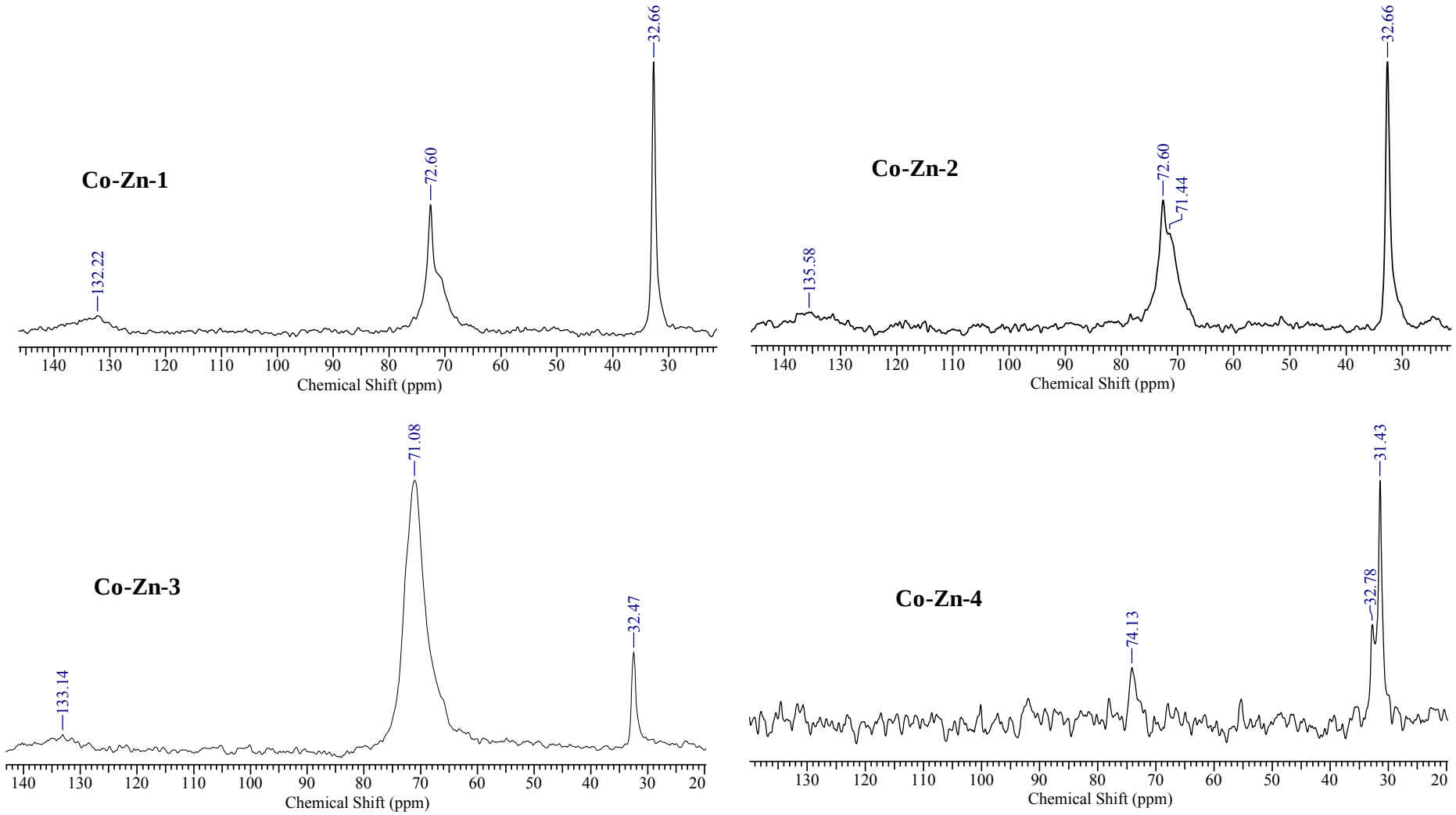

Fig. 4.5. CP-MAS spectra of Co-Zn DMC catalysts.

4.3.1.4. CP-MAS NMR

Presence of t-BuOH and its coordinative nature in DMC complexes was identified by ^{13}C CP-MAS NMR spectroscopy. The spectra shown in Fig. 4.5 confirm the presence of t-BuOH in the catalysts. t-BuOH in liquid state shows ^{13}C NMR signals corresponding to tertiary carbon and methyl groups at 68.8 and 32.0 ppm, respectively. These signals in Co-Zn DMC complexes appeared at 72.6 and 32.6 ppm, respectively. A downfield shift of these signals indicates their coordination to Zn^{2+} ions than their existence as weakly adsorbed species. NMR spectra also confirmed the bonding nature of CN ligand in DMC complexes. The precursor complex $K_3[Co(CN)_6]$ showed a signal related to cyanide groups at 102.6 ppm. This signal is down-field shifted to 132.2 ppm in Co-Zn DMCs implying the depletion of electron density in the anti-bonding π^* molecular orbital of CN due to its coordination to Zn^{2+} ions. This conclusion is in agreement with the bonding nature derived from the FTIR.

4.3.1.5. TG- FTIR

In situ TG-FTIR experiment was carried out to identify the desorption pattern of water and t-BuOH in DMC catalysts. The experiment was performed at increasing temperatures from 30 to 300 ^oC in DRIFT mode. TG-DRIFT of Co-Zn-1 (Fig. 4.6 (a)) at 30 ^oC shows evidence for zeolitic and H-bonded water molecules showing a band at 3300 cm^{-1} due to OH stretching vibration. This is supported by the band at 1609 cm^{-1} due to bending vibrations. The band at 3300 cm^{-1} showed a reduction in intensity when the temperature was raised to 100 ^oC (hold time = 30 min) indicating the first desorption during thermal treatment of DMC as the removal of zeolitic water molecules. This is supported by the gradual narrowing and disappearance of bending vibrations at 200 ^oC (stage I, 30 to 200 °C). The second desorption process is likely due to the simultaneous removal of coordinated water and t-BuOH up to 300 ^oC (stage II, 200 to 300 °C and above) as the spectrum at this temperature showed considerable decrease in the intensity of OH stretching at 3330 cm^{-1}; however the C-H stretching band due to t-BuOH was still visible at 2979 cm^{-1}.

4.3.1.6. TG

TG analysis of DMC catalysts under inert atmosphere shows different weight loss patterns as a function of decomposition temperatures (Fig. 4.6 (b)). With the assistance from TG-FTIR, three stages of weight loss were assigned. Stage I (40 - 180 °C) corresponds to desorption of zeolitic water molecules [17]. These water molecules were incorporated as solvent of crystallization and held to the lattice by H-bonding. Stage II (190 - 375 °C) corresponds to removal of coordinatively bound water and t-BuOH molecules. Stage III (400 - 850 °C) corresponds to the disintegration of cyanide moiety and collapse of framework.

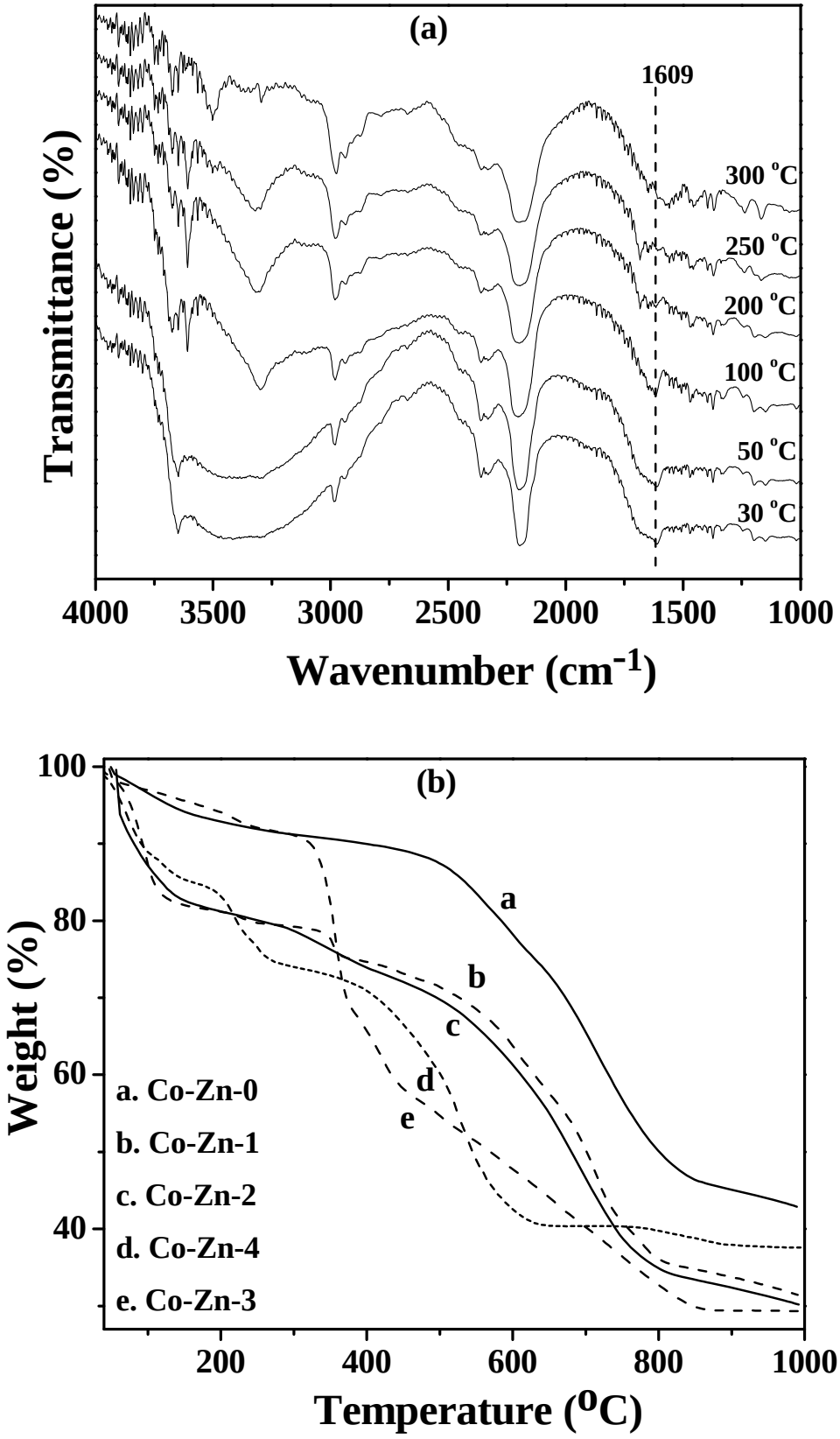

Fig. 4.6. (a) TG-FTIR of Co-Zn-1 at various temperatures and (b) TG curves of various Co-Zn DMC catalysts.

Table 4.1. Physicochemical properties of Co-Zn DMC catalysts.

Catalyst	Elemental composition (EDX, at %)			Crystalline phase [a] (size; nm)	N_2 physisorption analysis			Elemental analysis (wt %)			Total acidity (mmol NH_3/g)	% weight loss (TG)		
	Zn/Co	K	Cl		S_{BET} (m^2/g)	Average pore radius (nm)	Pore volume (cc/g)	C	H	N		I	II	III
Co-Zn-0	1.6	0.41	0.12	C (70)	895	1.3	0.592	20.2	0.9	24.0	2.16	6.9	2.8	45.2
Co-Zn-1	1.9	0.29	0.24	C (68) + M (51)	48	9.5	0.277	25.7	1.9	21.4	1.34	18.5	6.2	40.6
Co-Zn-2	1.6	0.19	0.17	C (87) + M (35)	486	2.1	0.518	23.9	1.5	22.9	1.79	18.0	6.9	41.5
Co-Zn-3	2.5	1.46	5.39	M (29)	48	10.3	0.251	25.7	2.2	14.8	1.40	5.4	24.7	36.8
Co-Zn-4	2.8	2.0	11.3	M (51) + R (44)	235	2.1	0.243	15.7	1.2	17.0	2.27	15.7	12.1	33.4

[a]C = cubic, M = monoclinic, R = rhombohedral and values in parenthesis represents average crystallite size calculated by Debye Scherer formula.

Weight loss above 850 °C corresponds to transformation of residual metals (Zn and Co) into spinel structures. Method of preparation and mode of addition of reagents greatly influenced the composition (water, t-BuOH and cyanide contents; Table 4.1) and thermal stability of DMC complexes. Co-Zn-0 prepared in the absence of complexing and co-complexing agent showed cyanide decomposition at 683 °C. This for Co-Zn-1, Co-Zn-2, Co-Zn-3 and Co-Zn-4 (prepared using complexing/co-complexing agents) occurred at lower temperatures of 670, 650, 602 and 519 °C, respectively (Fig. 4.6 (b)). The decrease in trend of decomposition temperature is correlated with the crystallinity and crystalline phase purity of complexes. XRD revealed that Co-Zn-0 is monophasic while Co-Zn-1 and Co-Zn-2 are biphasic. Co-Zn-3 is monophasic but less crystalline, while Co-Zn-4 is multiphasic and less crystalline. Co-Zn-0 showed a weight loss of 6.9% in stage I, 2.8% in stage II and 45.2% in stage III. These values confirm its molecular formula: $Zn_3[Co(CN)_6]_2.4H_2O$. The weight losses from other DMC complexes are reported in Table 4.1. Except for marginal change, the compositions of Co-Zn-1 and Co-Zn-2 were nearly the same. But Co-Zn-3 and Co-Zn-4 showed different compositions. Co-Zn-3 contained more amount of coordinated t-BuOH (also confirmed by FTIR) than the other complexes. Molecular formulae of Co-Zn-1, Co-Zn-2, Co-Zn-3 and Co-Zn-4 are expected to take a complex mixture of different forms such as $Zn_3[Co(CN)_6]_2.xH_2O$, $Zn_2[Co(CN)_6]OH.xH_2O$, $KZn[Co(CN)_6]$ and $Zn_3[Co(CN)_6]_2.mZnCl_2.xH_2O$ [20].

4.3.1.7. EDX

Elemental composition of DMC complexes was determined also by EDX. The percentage contribution of each element ca., Zn, Co, K and Cl ions is given in Table 4.1. Co-Zn-0 and Co-Zn-2 showed a Zn/Co ratio of 1.6 pointing to a molecular formula of $Zn_3[Co(CN)_6]_2.xH_2O$. Co-Zn-1 has a Zn/Co ratio of 1.9 forecasting a tentative molecular formula as $Zn_2[Co(CN)_6]OH.xH_2O$. All these three Co-Zn DMC catalysts have very low K^+ and Cl^- ions in their structures. On the contrary, Co-Zn-3 and Co-Zn-4 have shown significant amounts of K^+ and Cl^- ions in their composition. Further, Zn/Co ratio of these two systems are 2.5 and 2.8, respectively indicating that these are mixtures of $KZn[Co(CN)_6]$ and $Zn_3[Co(CN)_6]_2.mZnCl_2.xH_2O$.

4.3.1.8. DRIFT spectroscopy of adsorbed pyridine

The nature of acidic sites in DMC catalysts were differentiated by DRIFT spectroscopy of adsorbed pyridine. The spectra for Co-Zn-0 and Co-Zn-4 (at 180 °C) showed absorption bands corresponding to strong Lewis acid sites at 1452 and 1608 cm^{-1} and bands corresponding to weak Lewis acid sites at 1576 and 1493 cm^{-1} (Fig. 4.7 (a)). Absence of characteristic IR bands of H-bonded pyridine due to Brönsted acid sites at 1639 and 1545 cm^{-}

[1] ruled out their existence in Co-Zn DMC catalysts. Co-Zn-4 prepared in the presence of complexing agent showed an additional shoulder band at 1619 cm^{-1} indicating the presence of stronger Lewis acid sites.

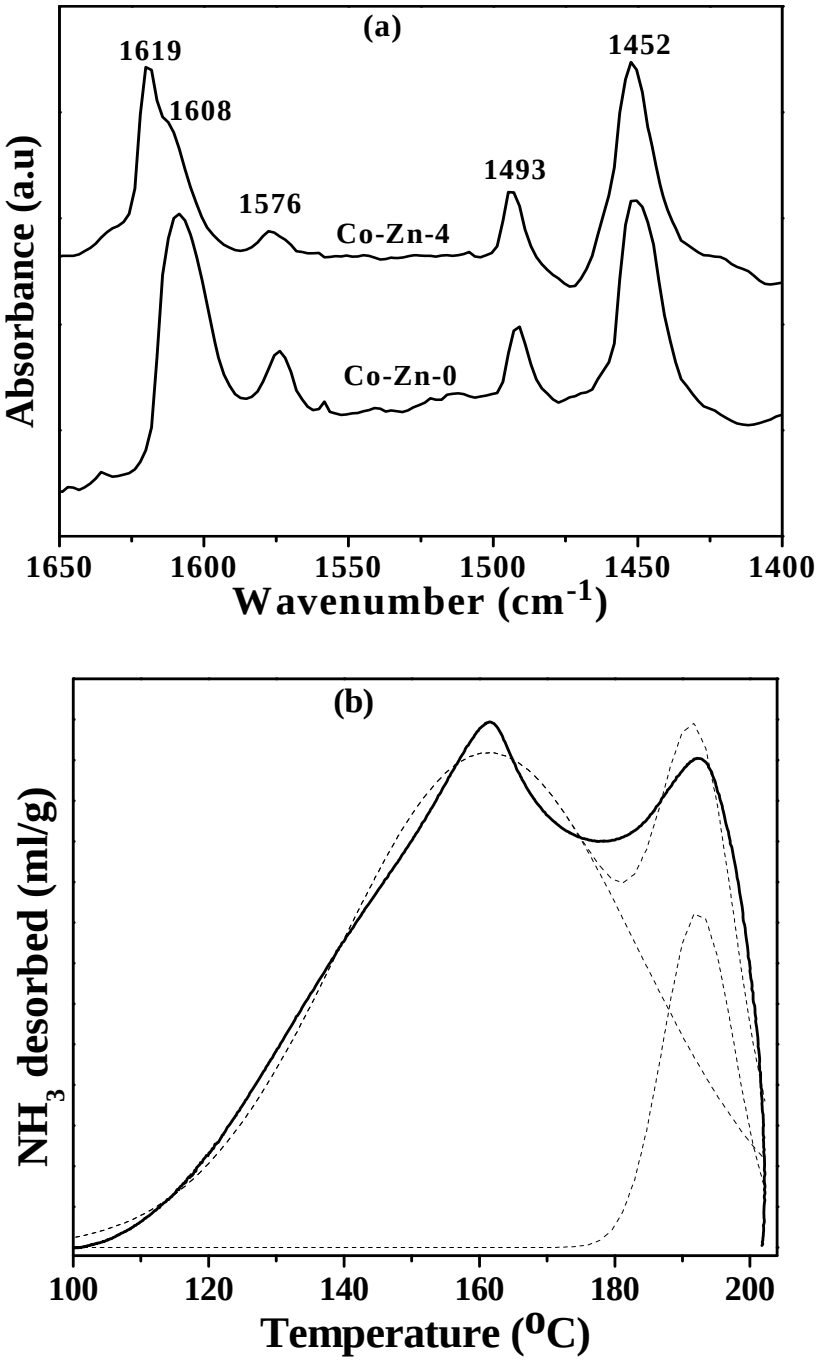

Fig. 4.7. (a) DRIFT spectroscopy of adsorbed pyridine and (b) NH_3-TPD of Co-Zn-4.

4.3.1.9. NH_3-TPD

Total amount of Lewis acidic sites in Co-Zn DMC catalysts were computed from temperature-programmed desorption of ammonia. Co-Zn-0 showed mainly a broad NH_3 desorption with a T_{max} at 160 °C. Other catalysts showed a bimodal distribution of acid sites representative of different strengths. The deconvoluted peak maxima observed at 160 °C and 193 °C for Co-Zn-4 were assigned to weak and strong acid sites, respectively (Fig. 4.7 (b)). The overall acidity of DMC catalysts decreased in the order: Co-Zn-4 (2.27 mmol/g) > Co-Zn-0 (2.16 mmol/g) > Co-Zn-2 (1.79 mmol/g) > Co-Zn-3 (1.40 mmol/g) > Co-Zn-1 (1.34 mmol/g).

4.3.1.10. SEM

Figure 4.8 shows the SEM images of Co-Zn DMC catalysts. Co-Zn-0 is composed of spherical particles of size less than 1μm. Co-Zn-1 is made up of particles with square pyramidal and flake geometries having sizes greater than 1 μm. Shapes of Co-Zn-2 DMC particles appeared similar to Co-Zn-1 but with large sizes (~ 4 μm). Image of Co-Zn-3 catalyst shows a situation where particles having geometry of flakes which are held together by amorphous particles. The combined sizes of these particles are over 6 μm. Particles of Co-Zn-4 appeared without any conventional morphology. The dimensions of these particles are in the range of 50 μm in length and 20 μm in width.

The characterization studies, thus, conclude that the method of preparation has a strong influence on the molecular and crystal structure of DMC complexes.

4.3.2. Catalytic activity

Table 4.2 shows the catalytic activity data of Co-Zn DMCs in the copolymerization of CHO and CO_2. Co-Zn-0 (prepared in the absence of complexing and co-complexing agent) was barely active for the copolymerization reaction. Co-Zn-1 (prepared in the presence of both complexing and co-complexing agents) yielded 1.6 g of polycarbonate having percentage CO_2 incorporation of 84 mol%. Co-Zn-2 (prepared using the same reagents that were used in the preparation of Co-Zn-1, but with difference in the mode of addition of reagents) exhibited complete conversion of epoxide with an isolated polycarbonate yield of 12.5 g and percentage CO_2 incorporation (in the polymer) of 80 mol%. Thus, method of preparation of Co-Zn DMCs has a definite influence on their catalytic activity. An increase in weight of polymer with respect to the weight of epoxide taken (9.7 g) undoubtedly reveals the incorporation of CO_2 units in the polymer matrix as polyether polyol formation doesn't increase the weight of product polymer. In contrast to Co-Zn-2, Co-Zn-1 resulted only little CHO conversion but with 84 mol% of carbonate unit incorporation. Subtle changes in

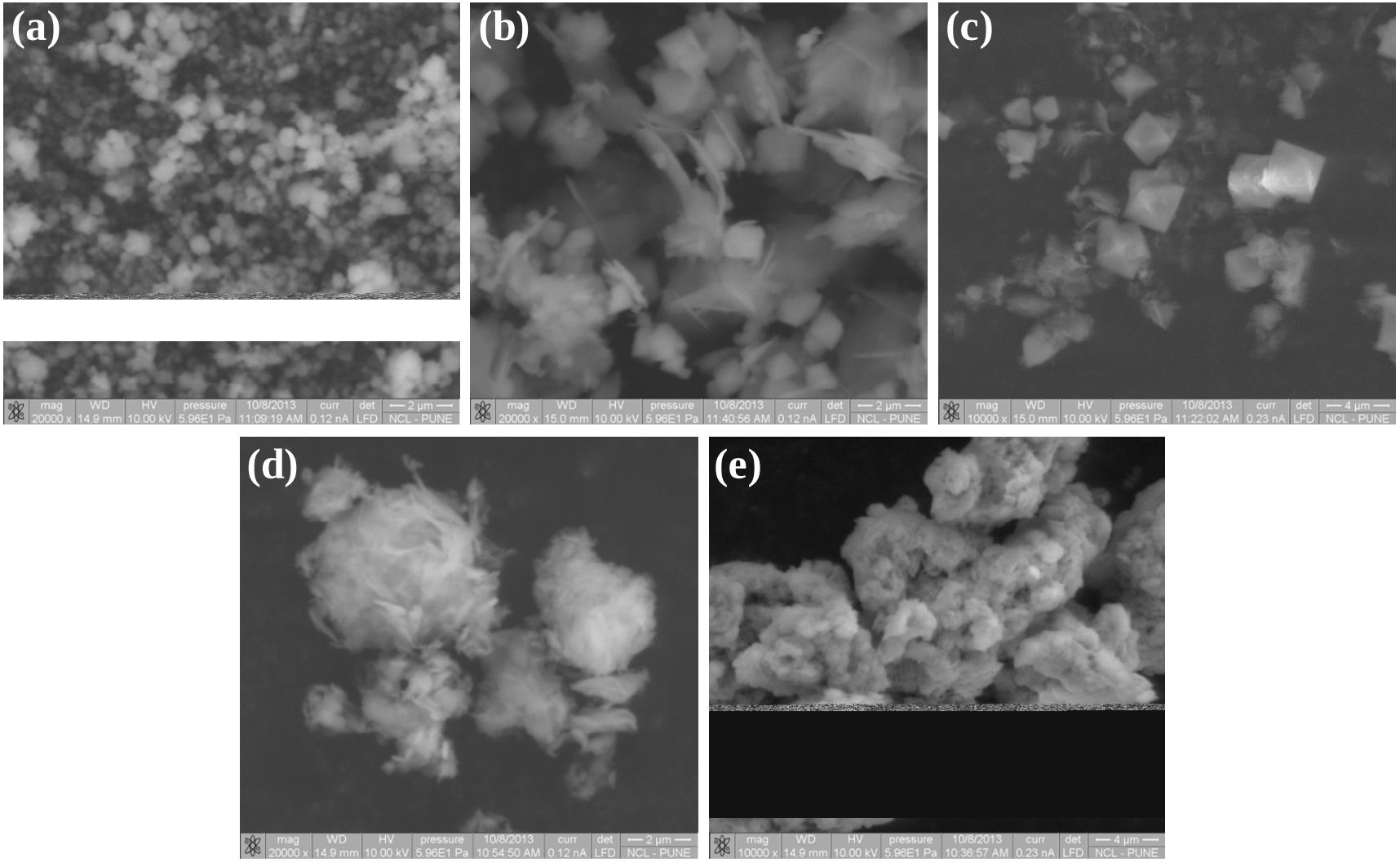

Fig. 4.8. SEM images of Co-Zn DMC catalysts: (a) Co-Zn-0, (b) Co-Zn-1, (c) Co-Zn-2, (c) Co-Zn-3 and (d) Co-Zn-4.

Table 4.2. Catalytic activity data of Co-Zn DMC in polycarbonates synthesis.[a]

Catalyst	Isolated yield of the polymer (g)	Productivity (g polymer/g catalyst)	MeOH insoluble part (wt%)	% Incorporation of carbonate unit (mol)[b]	M_w	PDI
Co-Zn-0	0.6	2.4	---	44[c]	24100	1.5
Co-Zn-1	1.6	6.4	9.6	84	15300	1.8
Co-Zn-2	12.5	50.0	77.4	80	14600	1.6
Co-Zn-3	3.8	15.2	38.2	64	14200	1.8
Co-Zn-4	13.2	52.8	77.6	86	20900	1.8
Co-Zn-4-1	12.2	48.8	68.0	86	22800	1.7
Co-Zn-4-2	3.3	13.2	45.5	80	17000	1.8

[a]Reaction conditions: CHO = 9.7 g, toluene = 8.7 g, catalyst = 0.25 g, P_{CO2} = 30 bar, reaction time = 11 h, reaction temperature = 75 °C. [c]Determined from ^{1}H NMR in $CDCl_3$, [c]Value corresponding to crude polymer without purification.

catalyst synthesis showed a significant influence on the catalytic activity of DMC complexes. Elemental analysis estimated that Co-Zn-1 has higher amount of complexing agent in its composition than Co-Zn-2 (Table 4.1). At the same time, Co-Zn-2 has higher amount of total acidity than Co-Zn-1. Hence, the difference in catalytic activity of Co-Zn-1 and Co-Zn-2 can be assigned to higher amount of total acidity and lower amount of t-BuOH. Although Co-Zn-0 has higher amount of total acid sites than Co-Zn-2, the former was weakly active than the latter. This is because Co-Zn-0 was composed of weak acid sites only (NH_3 desorption peak was centered at 160 °C) while Co-Zn-2 contained also the strong acid sites (NH_3-TPD peak at 193 °C). This point outs the requirement of stronger acid sites for catalytic activity.

Between Co-Zn-3 and Co-Zn-4 (synthesized by the same method but in the presence and absence of co-complexing agent) the latter showed superior activity to than the former (13.2 g polymer versus 3.8 g, 86 versus 64 mol% carbonate unit incorporation). Co-Zn-3 was mostly amorphous while Co-Zn-4 was crystalline with monoclinic/rhombohedral phases. Elemental analysis showed that Co-Zn-3 had higher amount of complexing agent and lower amount of total acidity than Co-Zn-4 (1.4 versus 2.27 mmol NH_3/g) (Table 4.1). This correlation between acidity and catalytic activity is similar to that found with Co-Zn-1 and Co-Zn-2 DMCs. Higher the total acidity and lower the complexing agent higher would be the catalytic activity. Although there have been reports relating the crystallinity of DMC catalysts with the catalytic activity revealing that amorphous structure is the active form [21], the

present study demonstrates that even a highly crystalline catalyst can initiate the polymerization. High catalytic activity shown by perfectly crystalline Co-Zn-2 make obvious that the structure alone is merely not the deciding parameter but complexing agent and acidity, in particular strong acid sites significantly influence the catalytic activity.

DMC catalysts have been known to show induction period in polyether polyol synthesis [22]. The pressure drop in the reactor was monitored at regular intervals of 30 min. Fig. 4.9 shows the pressure drop during polymerization as a function of reaction time. Pressure drop is a direct indication for the activity of Co-Zn DMC in polycarbonate synthesis. Co-Zn-0, Co-Zn-1 and Co-Zn-3 showed long induction periods (>7 h), while Co-Zn-2 exhibited an induction period of 2 h only. Interestingly, Co-Zn-4 showed no induction period. Reactants (CO_2 and CHO) got consumed in polymer formation from the very beginning itself. The *in situ* monitoring of CO_2 pressure in the reactor supports the superior catalytic activity of Co-Zn-2 and Co-Zn-4 as compared to other DMC catalysts. While behaviour of pressure drop with Co-Zn-2 was almost linear towards the completion of reaction time, it was exponential with Co-Zn-4. To understand the difference in activity behaviour of Co-Zn-2 and Co-Zn-4, variations in chemical composition were looked into. Co-Zn-4 contained significant amount of K^+ and $ZnCl_2$ in its chemical composition while these were negligible in Co-Zn-2 (Table 4.1). This observation points out that perhaps the excess $ZnCl_2$ in Co-Zn-4 would be the prime reason for the activation of CO_2 without any induction period. A replication of polycarbonate synthesis with neat $ZnCl_2$ showed no activity. This experiment clarified that excess $ZnCl_2$ in Co-Zn-4 exists as dispersed molecules. The direct dependence of dispersed $ZnCl_2$ on catalytic activity was further verified by a rational modification in preparation procedure of Co-Zn-4 to generate catalysts with varying amount of dispersed $ZnCl_2$. This was achieved by avoiding the second suspension in t-BuOH (which retains excess of $ZnCl_2$, designated as Co-Zn-4-1) and by introducing an additional water washing after ageing (which removes the excess $ZnCl_2$, designated Co-Zn-4-2) (Chapter 2, Sections 2.2.2.6 and 2.2.2.7). EDX analysis of the catalysts revealed that the contents of Zn/Co, K^+ and Cl^- vary in the order as Co-Zn-4 (2.8, 2.0, 11.3) > Co-Zn-4-1(2.1, 1.2, 10.6) > Co-Zn-4-2 (1.9, 0.8, 0.9). The total acidity followed the trend: Co-Zn-4 (2.27) > Co-Zn-4-1(2.29) > Co-Zn-4-2 (1.72). The catalytic activity (polymer productivity and CO_2 consumption) followed the same order as of their elemental contents and acidity (Table 4.2 and Fig. 4.9). Removal of K^+ and $ZnCl_2$ by an additional washing step (as in Co-Zn-4-2) led to induction period in the polymerization reaction (Fig. 4.9). These experiments confirm that small quantities of isolated $ZnCl_2$ species

in the structure of Co-Zn DMCs are essential in improving the catalytic activity and to avoid the induction period in the polymerization reaction.

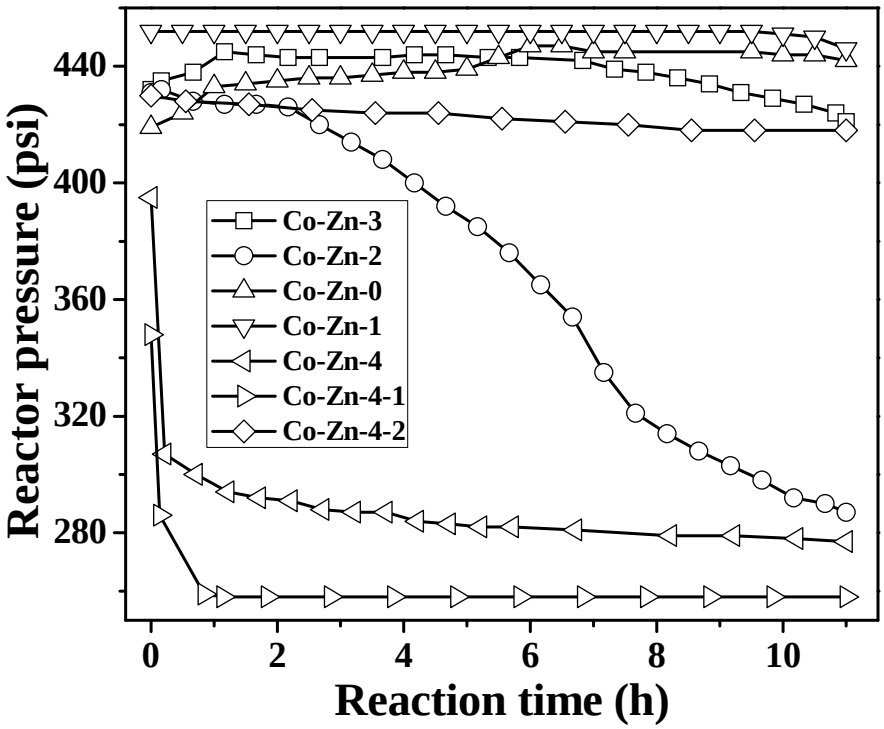

Fig. 4.9. Time on stream activity of Co-Zn DMC catalysts.

The remarkable activity of Co-Zn-4 towards CO_2 activation was further established by conducting the reaction in presence of N_2 instead of CO_2. The catalyst showed no activity in producing polyethers even after 11 h. But, when the catalyst was first suspended in toluene and activated in CO_2 (30 bar) for 2 h then CHO was added and pressurized with N_2, the reaction yielded poly(cyclohexene ether) in good amount (isolated yield = 8.6 g and CHO conversion = 88.7%). ^{1}H NMR of the polyether showed 15 mol% of CO_2 incorporation. This experiment suggests that the activation of CO_2 at Lewis acidic Zn^{2+} centre is the first and possibly the rate determining step in Co-Zn DMC catalyzed polycarbonates synthesis.

The interaction and the extent of adsorption of CO_2 molecules on catalyst surface were analyzed by CO_2 adsorption isotherms. Fig. 4.10 depicts the CO_2 adsorption isotherms of Co-Zn-1, Co-Zn-2 and Co-Zn-4. CO_2 adsorption was slightly higher for Co-Zn-4 than for Co-Zn-2. The adsorption capacity of Co-Zn-1 was lower than that of the other two. At lower pressures, guest-guest interactions are minimum and the slope of the isotherm can be taken as marker for predicting the strength of guest-host interactions [16]. The isotherm shows higher guest-host interactions in Co-Zn-4 and Co-Zn-2 than in Co-Zn-1. This can be correlated to

the catalytic activity (CO_2 activation/incorporation and induction period in the reaction). Further, the isotherms were analyzed using the Dubinin-Astakhove model [23].

$$a_{ad} = a_o \times e^{-\left[\frac{RT}{E} \times ln(P_r)^{-1}\right]^n}$$

where a_{ad} is the amount of CO_2 adsorbed at a relative pressure P_r ($P = P_{eq}/P_r$), a_o is the limiting amount filling of micropores, E is characteristic energy, n is heterogeneity parameter, R is universal gas constant and T is temperature. The characteristic energy, E indicates the average adsorption energy for CO_2 molecules on catalyst surface. It is high for the least active Co-Zn-1 catalyst (E = 6.98, 2.99 and 3.07 kcal/cm^3 for Co-Zn-1, Co-Zn-2 and Co-Zn-4, respectively). The value of a_o is also low for Co-Zn-1 (a_o = 0.628, 0.788 and 0.784 mmol for Co-Zn-1, Co-Zn-2 and Co-Zn-4, respectively). The parameter n is a measure of the heterogeneity of adsorption potential. Higher value for n corresponds to less heterogeneous adsorption potential (n = 10, 9 and 9 for Co-Zn-1, Co-Zn-2 and Co-Zn-4, respectively). Co-Zn-1 showed very long induction period (>11 h) and on prolonging the reaction to 24 h, it showed appreciable activity (polymer of yield 9.4 g with 66.8 mol% CO_2 incorporation). The long induction period of Co-Zn-1 in activating CO_2 molecules is due to the less guest-host interactions as revealed by the CO_2 adsorption isotherms.

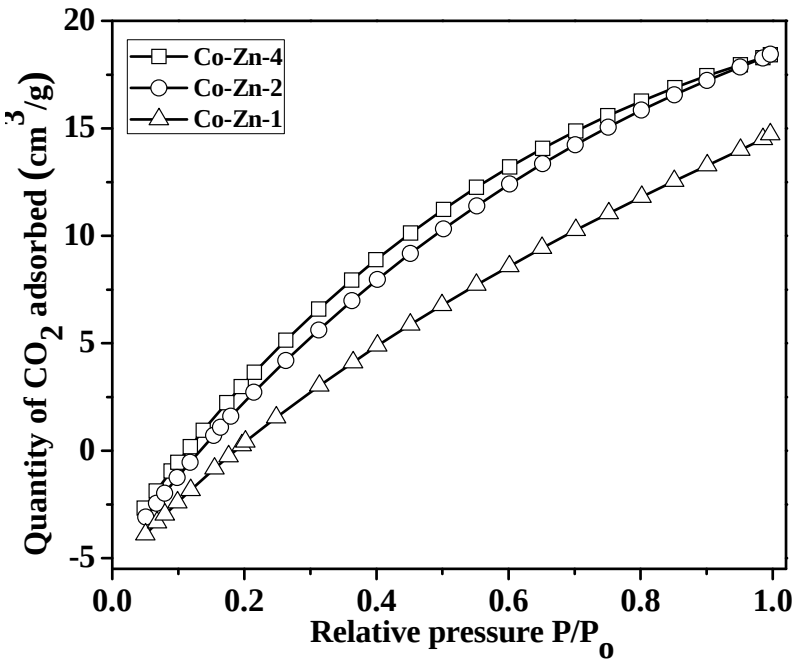

Fig. 4.10. CO_2 adsorption isotherms of Co-Zn-1, Co-Zn-2 and Co-Zn-4.

Optimization of reaction conditions was performed with the most active Co-Zn-4 catalyst. All the optimization studies were conducted over a reaction period of 11 h except for the pressure studies, in which the reaction was conducted for 5 h (Table. 4.3). The progress of reaction was examined in terms of pressure drop in the reactor at regular time intervals.

Table 4.3. Influence of reaction parameters on the catalytic activity of Co-Zn-4.

Reaction parameter	Isolated yield of the polymer (g)	Productivity (g polymer/g catalyst)	MeOH insoluble part (wt%)	% carbonate unit (mol)	M_w	PDI
Catalyst amount (g)						
0.250	13.3	53.2	77.6	85.3	20900	1.8
0.125	13.5	108.0	81.8	60.4	21600	2.2
0.100	13.3	133.0	90.0	85.1	17900	2.6
0.075	13.3	177.3	74.0	77.9	19500	2.3
0.025	3.4	136.0	66.7	83.3	17100	1.6
Effect of temperature (^oC)						
65	10.3	41.2	90.5	84.5	17200	2.4
75	13.3	53.2	77.6	85.3	20900	1.8
85	11.9	47.6	63.1	83.8	11800	2.3
Effect of pressure (bar)[a]						
30	9.7	38.8	77.9	83.0	22200	2.4
20	8.6	34.4	72.5	83.2	18300	2.0
10	5.1	20.4	71.0	69.1	15200	1.7
Effect of time (h)						
2	12.2	48.8	63.5	85.7	19700	2.2
11	13.3	53.2	77.6	85.3	20900	1.8

Reaction conditions: CHO = 9.7 g, toluene = 8.7 g, P_{CO2} = 30 bar, reaction time = 11 h, Co-Zn-4 = 0.25 g, reaction temperature = 75 °C. [a]Reaction time = 5 h.

4.3.2.1. Effect catalyst quantity

The isolated yield of crude polymer at the end of 11 h was nearly the same (13.3 g) irrespective of the amount of catalyst taken (0.075 - 0.25 g). But it affected the yield of methanol insoluble portion and the percentage incorporation of CO_2 (60.4 - 85.3 mol%; Table

4.3). Catalyst concentration had influenced the rate of reaction (pressure drop in the reactor) (Fig. 4.11 (a)). When the catalyst quantity was further reduced to 0.025 g, a significant decrease in isolated yield (3.4 g) of crude polymer was found. The rate of polymerization portrayed a direct dependence on the quantity of catalyst. High molecular weight polymers were formed at higher catalyst loading (M_w = 20900 and PDI = 1.8).

4.3.2.2. Effect reaction temperature

Influence of reaction temperature on the synthesis of PCHC over Co-Zn-4 revealed that 75 ^oC is ideal for producing higher molecular weight (M_w = 20900) polymer in higher isolated yield (13.3 g; Table 4.3). When the temperature was reduced to 65 °C, the catalyst showed an induction period (Fig. 4.11 (b)). Higher temperatures (85 °C) affected marginally the molecular weight (M_w = 11800) and PDI (2.3) of the polymer although the conversion and percentage incorporation of CO_2 was almost same as that at 75 °C (Table 4.3). High temperature can accelerate the chain transfer to water molecules. This will reduce the molecular weight and increase the PDI.

4.3.2.3. Effect reaction pressure

CO_2 pressure in the reactor has a positive effect on the isolated yield, percentage incorporation of CO_2 and molecular weight of the polymer (Table 4.3). They increased with increase in reactor pressure. A pressure of 30 bar was essential to maintain high isolated yield and percentage incorporation of CO_2 in the polymer. CO_2 pressure was found to have no effect on the initial activity of catalyst as the catalyst did not demonstrate any induction period (Fig. 4.11 (c)).

4.3.2.4. Effect reaction time

When the reaction time was 2 h, the isolated yield of the polymer obtained (12.2 g) was lower than that at 11 h (13.3 g, Table 4.3). Also the methanol insoluble fraction was lower at shorter reaction times. Low molecular weight polymers were produced at shorter reaction times. However, the percentage incorporation of CO_2 in the polymer was nearly the same (85 mol%) regardless of the molecular weights.

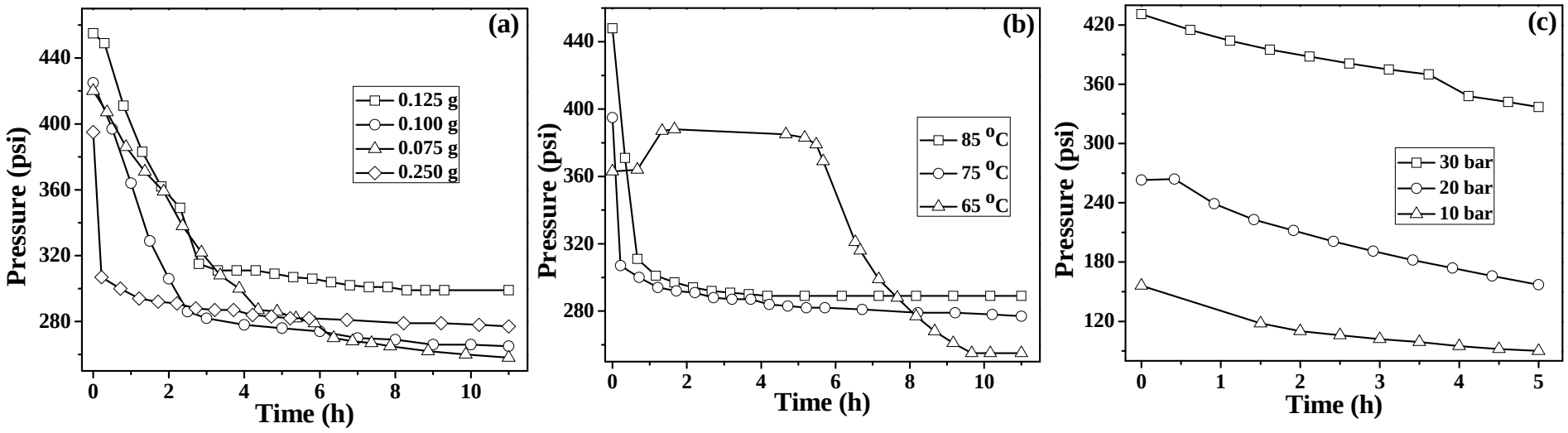

Fig. 4.11. Effect of reaction parameters on the induction period of Co-Zn-4: (a) catalyst quantity, (b) reaction temperature and (c) reaction pressure.

4.3.3. Product characterization

4.3.3.1. ^{13}C NMR

Tacticity pattern of PCHC synthesized over Co-Zn-4 was analyzed by ^{13}C NMR spectroscopy recorded at 500 MHz in inverse-gated mode. The spectrum of PCHC in the carbonyl region (Fig. 4.12) indicated different regio connections around the carbonate group [24]. Isotatic region in the polymer showed a signal at 153.79-154.23 ppm corresponding to carbonyl carbons of m-centered tetrad (mmm/mmr/rmr). While syndiotatic isomers showed signals at 153.14 - 153.28 ppm, corresponding to the r-centred tetrads (rrr/rrm/mrm) [25]. Percentage of isotacticity in the polymer was estimated to be 63.2 mol% and suggests that Co-Zn DMC catalysts do not show any selectivity to a preferred configuration.

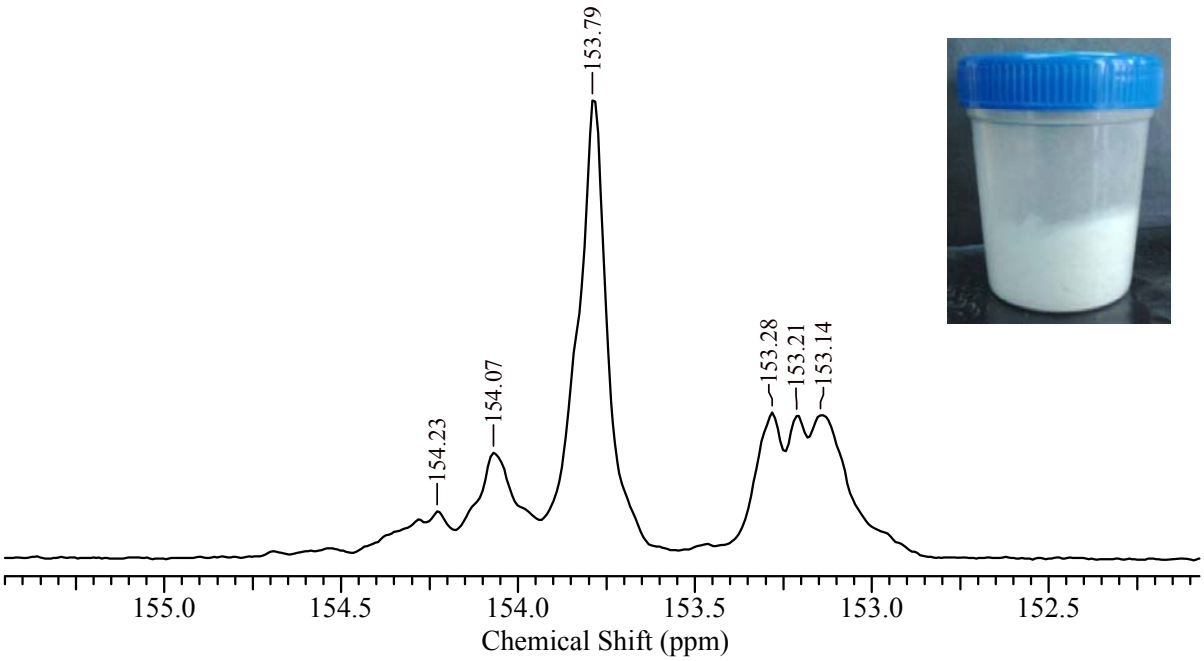

Fig. 4.12. Inverse-gated ^{13}C NMR spectrum of PCHC synthesized over Co-Zn-4. Inset shows the polymer produced.

4.3.3.2. FTIR

The FTIR spectrum of the polycarbonate (Fig. 4.13) showed a band at 1745 cm^{-1} corresponding to stretching vibration of the carbonyl group. The band at 2918 cm^{-1} corresponds to CH stretching vibration. Bands at 970 and 1250 cm^{-1} correspond to C-O stretching vibrations. The band at 770 cm^{-1} was ascribed to bending vibrations of terminal OH groups and a weak band at 3650 cm^{-1} corresponds to the stretching vibrations of OH. Absence of a band at 1800 cm^{-1} confirms the absence of cyclic carbonate in the product polymer.

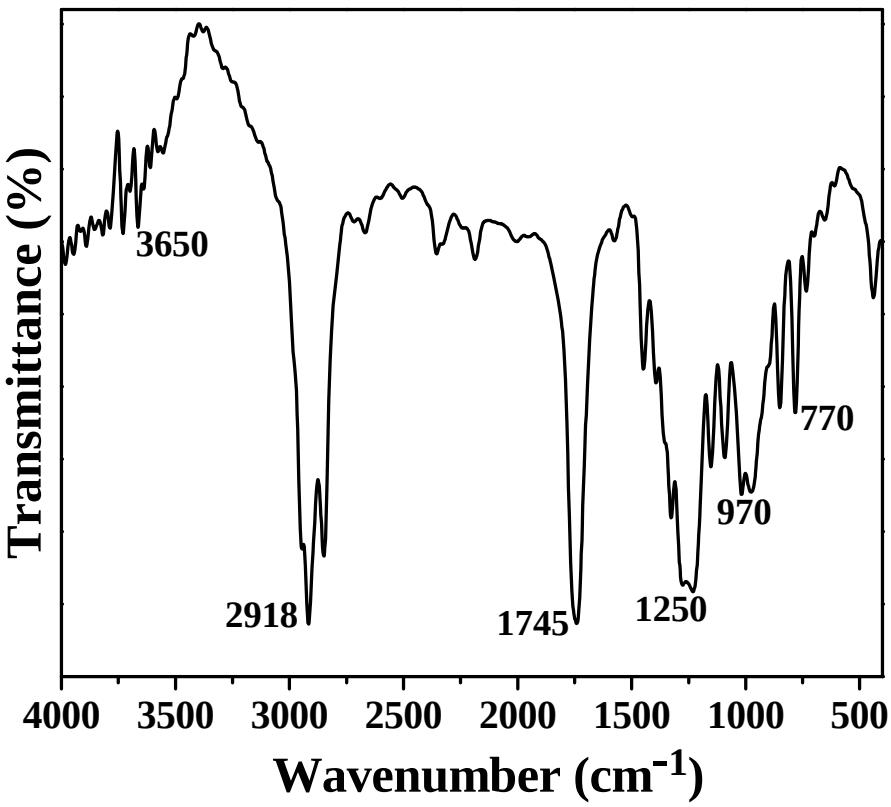

Fig. 4.13. FTIR spectrum of PCHC.

4.3.3.3. TG

TG analysis of PCHC under N_2 atmosphere showed two weight losses (Fig. 4.14 (a)). The first loss (9.4 wt%) occurred at 200 °C while the second (90.6 wt%) occurred at 286 °C. The first weight loss is due to the decomposition of ether fractions in PCHC. The second weight loss in the polymer corresponds to decomposition of carbonate fractions.

4.3.3.4. DSC

T_g of PCHC was calculated from the DSC analysis conducted under N_2 atmosphere. Fig. 4.14 (b) shows DSC of PCHC recorded from -80 to 145 °C. The thermogram shows two glass transitions, one at 42 °C and other at 96.7 °C due to polyether and polycarbonate regions respectively.

4.3.3.5. XRD

Powder XRD of PCHC in the range 10- 60° indicated that the polymer is amorphous in nature (Fig. 4.14 (c)). However a broad intense peak observed at 17.7° points out some local, short-range ordering in the polymer.

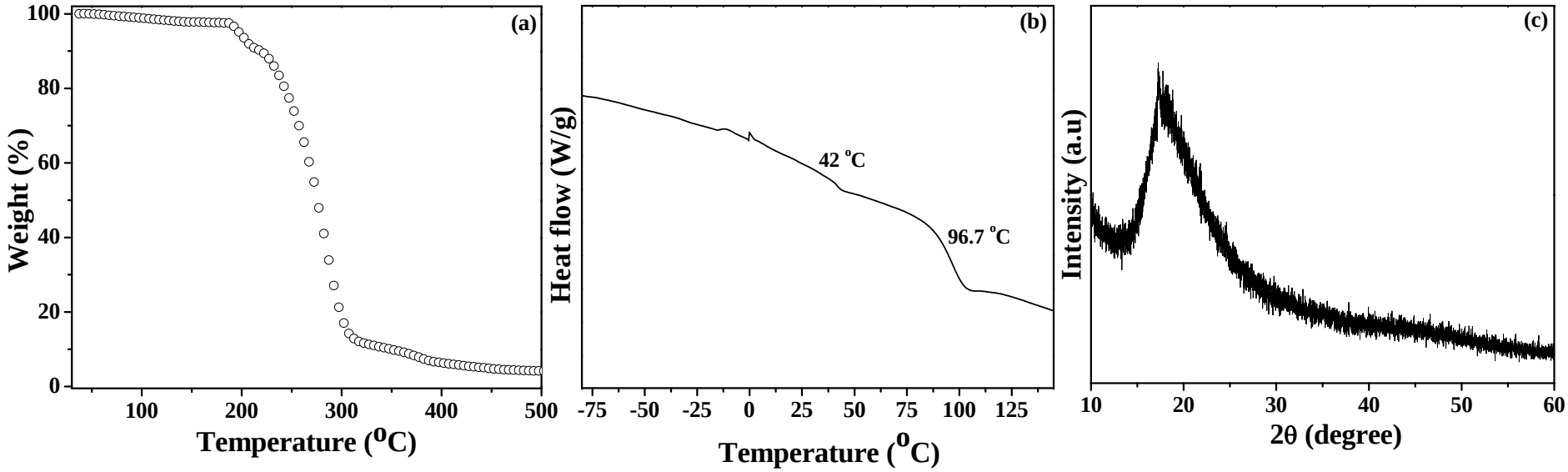

Fig. 4.14. (a) TG, (b) DSC and (c) XRD of PCHC.

4.3.4. Catalyst reusability

The stability of Co-Zn-4 was investigated in a reusable study. After the reaction (2 h), the catalyst was separated by centrifugation. It was extensively washed with toluene and then, charged into the reactor for further run. Isolated yield of the polymer was 12.2 and 12.1 g in the 1st and 2nd runs, respectively. XRD revealed some loss in crystallinity and structure of the catalyst (Fig. 4.15). On use, the catalyst broke down to smaller particles and a decrease in average crystallite size from 44 to 20.7 nm was observed.

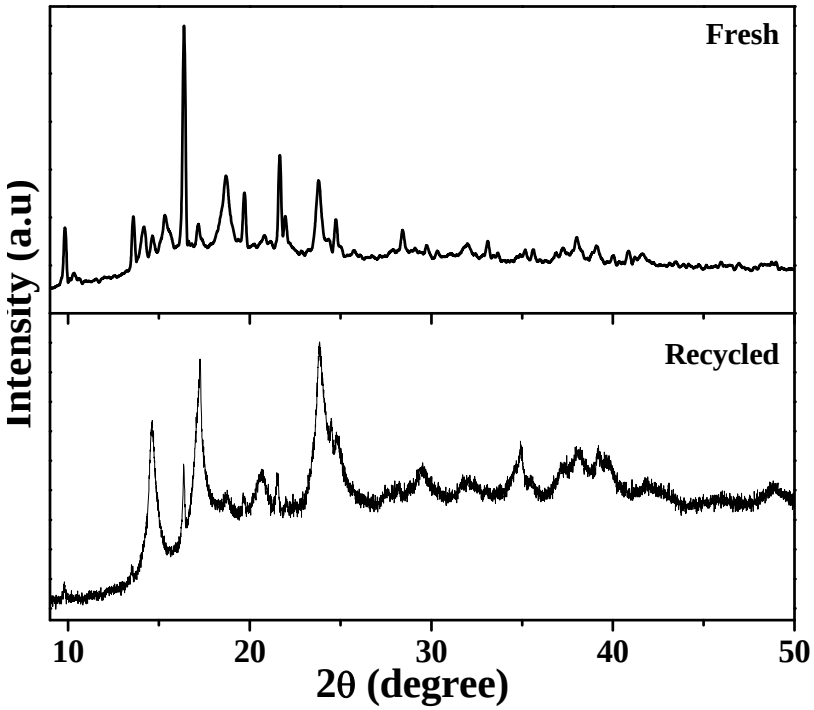

Fig. 4.15. XRD of fresh and recycled Co-Zn-4.

4.3.5. Structure activity correlations

4.3.5.1. Structure of DMC complexes

Hexacyanometallates are molecular materials formed by the assembling of octahedral $[M'(CN)_6]$ blocks connected through a transition metal (M^{n+}) (M′ and M are Co and Zn in the present study). Zn^{2+} coordinates to the N ends of the neighbouring blocks. In the cubic system of Co-Zn-0 $\{Zn_3[Co(CN)_6]_2.xH_2O$; unit cell parameter a = 1.02632(1) nm$\}$, Co is octahedrally coordinated by C atoms of six CN ligands and the 12N ends are shared by only three Zn atoms. So each Zn atom gets an average coordination of 4N ends [17, 26-28]. This leads to $1/3[Co(CN)_6]^{3-}$ site vacancies in the crystal structure. These vacancies are responsible for the network of pores of 0.85 nm of diameter interconnected through small windows of 0.45 nm. The vacant sites are generally filled by water molecule/complexing

agent ions and can be removed by thermal treatment to generate coordinatively unsaturated sites for catalytic activity. Other than cubic structure, these complexes are known to crystallize in rhombohedral (unit cell parameters: a = b = 1.24847(3) nm and c = 3.2756(1) nm, [17]) and monoclinic phases. Based on density functional calculations, Wojdel et al [29] proposed a tetrahedral coordination for Zn in monoclinic phase. Method of preparation greatly influenced the structure of DMC complexes. Co-Zn-0 prepared without using complexing and co-complexing agents had a molecular formula of $Zn_3[Co(CN)_6]_2.xH_2O$ and cubic structure. Co-Zn-1 and Co-Zn-2 prepared in presence the of complexing and co-complexing agents crystallized in both cubic and monoclinic structures. Co-Zn-3 and Co-Zn-4 prepared with different procedures have compositions of $KZn[Co(CN)_6]$ and $Zn_3[Co(CN)_6]_2.mZnCl_2.xH_2O$. While Co-Zn-3 was nearly amorphous, Co-Zn-4 contained monoclinic/rhombohedral phases. In polycarbonates synthesis, it is found that low symmetry monoclinic/rhombohedral structures (Co-Zn-4 and Co-Zn-2) are more active than the cubic structure. Further, certain amount of crystallinity is essential for high polymer productivity. The density and more particularly, the strength of acid sites are other crucial parameters for the improved catalytic activity. Presence of Cl^- ions in the structure in the form of dispersed $ZnCl_2$ species are essential for eliminating the induction period. Co-Zn-4 having all the above features represents the most efficient catalyst for the co-polymerization of CO_2 and CHO. This study also demonstrates that a highly efficient polymerization catalyst can be synthesized even without using a co-complexing agent.

4.3.5.2. Reaction mechanism

In principle, alternative co-polymerization of CO_2 and CHO can be initiated by activation of either CHO or CO_2 at the Lewis acidic, tetra-coordinated Zn^{2+} centres [30, 31]. Dharman et al [12] reported the initiation by CHO activation. However, in the present study points out that the polymerization gets initiated by CO_2 activation and it is the rate determining step. In the reaction mechanism showed in Fig 4.16, copolymerization is initiated by activation of CO_2 through coordination of its oxygen to Zn^{2+} active centre. In the next step, the activated CO_2 facilitates the ring-opening of CHO forming Zn-alkoxy and carbonate bonds. The polymer grows in size by alternating addition of monomers to the active centre and the active centre shifts its nature from metal carbonate to metal alkoxide, simultaneously. Polymerization is terminated by water molecules present in trace quantities in the feed [31].

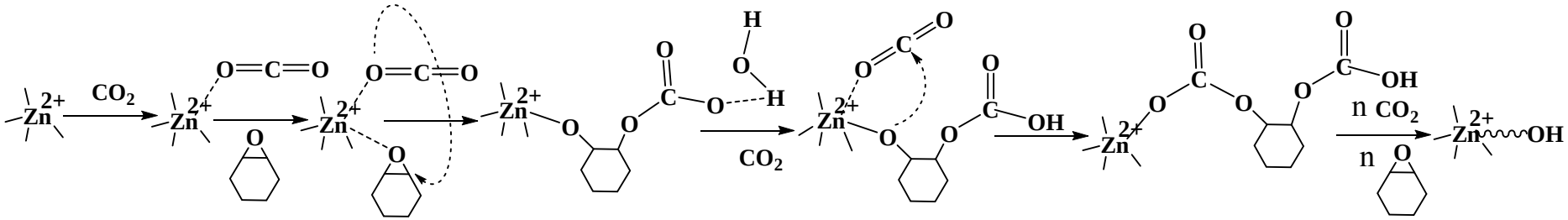

Fig. 4.16. Reaction mechanism for copolymerization of CHO and CO_2 over Co-Zn-4.

4.4. Conclusions

The influence of method of preparation of Co-Zn DMC catalysts on their catalytic activity for co-polymerization of CHO and CO_2 revealed that a highly active catalyst with no induction period can be synthesized even without using a co-complexing agent. Method of preparation of DMC complexes showed great influence on molecular structure, crystallinity and crystal structure. Density and strength of acid sites, low crystal symmetry (monoclinic/rhombohedral), moderate crystallinity, coordinated t-BuOH (complexing agent) and dispersed Cl^- ions in the structure are the critical parameters of Co-Zn DMCs responsible for high activity in copolymerization. CO_2 adsorption studies demonstrated that higher the guest-host interaction higher would be the catalytic activity and lower would be the induction period. Stronger acid sites in catalysts are conducive in improving the guest-host interactions. Cl^- ions in the catalyst structure avoided induction period by increasing acidity of the catalyst and thereby, improving the guest-host interactions. Altogether, this study lays the basis for future efforts in rational design of highly active DMC catalyst for the copolymerization of CO_2 and CHO through modification of these critical parameters.

4.5. References

[1] C.H. Huang, C.S. Tan, Aerosol Air Qual. Res. 14 (2014) 480-499.

[2] N. Assen, A. Bardow, Green Chem. 16 (2014) 3272-3280.

[3] J. Langanke, A. Wolf, J. Hofmann, K. Böhm, M.A. Subhani, T.E. Müller, W. Leitner, C. Gürtler, Green Chem. 16 (2014) 1865-1870.

[4] S. Inoue, H. Koinuma, T. Tsuruta, Makromol. Chem. 130 (1969) 210-220.

[5] M.R. Kember, A. Buchard, C.K. Williams, Chem. Commun. 47 (2011) 141-163.

[6] X.B. Lu, D.J. Darensbourg, Chem. Soc. Rev. 41 (2012) 1462-1484.

[7] M.J. Yi, S.H. Byun, C.S. Ha, D.W. Park, I. Kim, Solid State Ionics 172 (2004)139-144.

[8] S. Chen, G.R. Qi, Z.J. Hua, H.Q. Yan, J. Polym. Sci. 42A (2004) 5284-5291.

[9] I. Kim, M.J. Yi, K.J. Lee, D.W. Park, B.U. Kim, C.S. Ha, Catal. Today 111 (2006) 292-296.

[10] S. Chen, Z. Xiao, M. Ma, J. Appl. Polym. Sci. 107 (2008) 3871-3877.

[11] I.K. Lee, J.Y. Ha, C. Cao, D.W. Park, C.S. Ha, I. Kim, Catal. Today 148 (2009) 389-397.

[12] M.M. Dharman, J.Y. Ahn, M.K. Lee, H.L. Shim, K.H. Kim, I. Kim, D.W. Park, Green Chem. 10 (2008) 678-684.

[13] X.K. Sun, X.H. Zhang, R.J. Wei, B.Y. Du, Q. Wang, Z.Q. Fan, G.R. Qi, J. Polym. Sci.

Part A: Polym. Chem. 50 (2012) 2924- 2934.

[14] A. Peeters, P. Valvekens, R.P. Ameloot, G. Sankar, C.E.A. Kirschhock, D.E. De Vos, ACS Catal. 3 (2013) 597-607.

[15] K. Tarach , K.G. Marek, J. Tekla, K. Brylewska, J. Datka, K. Mlekodaj, W. Makowski, M.C.I. Lopez, J.M. Triguerob, F. Rey, J. Catal. 312 (2014) 46-57.

[16] C.P. Krap, B. Zamora, L. Reguera, E. Reguera, Micropor. Mesopor. Mater. 120 (2009) 414-420.

[17] J.R. Hernádez, E. Reguera, E. Lima, J. Balmaseda, R.M. Garcìa, H. Madeira, J. Phys. Chem. Solids 68 (2007) 1630-1642.

[18] M. Avila, L. Reguera, J.R. Hernández, J. Balmaseda, E. Reguera, J. Solid State Chem. 181 (2008) 2899-2907.

[19] X.H. Zhang, Z.J. Hua, S. Chen, F. Liu, X.K. Sun, G.R. Qi, Appl. Catal. A: Gen. 325 (2007) 91-98.

[20] J. Kuyper, G. Boxhoorn, J. Catal. 105 (1987) 163-174.

[21] B.L. Khac, W. Chester, US Patent No. 5,589,431 (1996).

[22] S. Lee, S.T. Baek, K. Anas, C.S. Ha, D.W. Park, J.W. Lee, I. Kim, Polymer 48 (2007) 4361-4367.

[23] M.M. Dubinin, D.A. Cadenheat (Ed.), Progress in Surface Science and Membrane Science, Academic Press, New York (1975).

[24] M. Chen, N.A. Darling, E.B. Lobkovsky, G.W. Coates, Chem. Commun. 2000 (2000) 2007-2008.

[25] K. Nakano, K. Nozaki, T. Hiyama, Macromolecules 34 (2001) 6325-6332.

[26] D.F. Mullica, W.O. Milligan, G.W. Beall, W.L. Reeves, Acta Crystallogr. 34B (1978) 3558-3561.

[27] J. Roque, E. Reguera, J. Balmaseda, J.R. Hernández, L. Reguera, L.F.D. Castillo, Micropor. Mesopor. Mater. 103 (2007) 57-71.

[28] J. Balmaseda, E. Rguera, J.R. Hernándes, L. Regurea, M. Autie, Micropor. Mesopor. Mater. 96 (2006) 222-236.

[29] J.C. Wojdel, S.T. Bromley, F. Illas, J.C. Jansen, J. Mol. Model. 13 (2007) 751-756.

[30] X.K. Sun, X.H. Zhang, F. Liu, S. Chen, B.Y. Du, Q. Wang, Z.Q. Fan, G.R. Qi, J. Polym. Sci. Part A: Polym. Chem. 46 (2008) 3128-3139.

[31] X.K. Sun, X.H. Zhang, R.J. Wei, B.Y. Du, Q. Wang, Z.Q. Fan, G.R. Qi, J. Polym. Sci. Part A: Polym. Chem. 50 (2012) 2924-2934.

Chapter - 5

Copolymerization of Propylene Oxide & CO_2 and Terpolymerization of Propylene Oxide, Cyclohexene Oxide & CO_2 over Co-Zn DMC Catalysts

5.1. Introduction

Copolymerization of propylene oxide (PO) and CO_2 is one of the most studied reactions for the fixation of green house CO_2 in polymeric materials. Other than the efficient utilization of CO_2, interest in this topic was further accelerated by features like sustainability through CO_2 utilization, excellent mechanical properties the polymer (good elasticity and tensile strength) and biodegradability [1]. Initial attempts to polymerize CO_2 with an epoxide in presence of an alkali envisaged that the copolymerization can be successfully initiated by activation of CO_2 on transition metals in catalytic amounts [2, 3]. Several heterogeneous and homogeneous catalysts were subsequently proposed for the copolymerization [4-8]. Homogeneous catalysts dominated the field due to interests in mechanistic aspects of the reaction. Most efficient homogeneous catalyst reported until now is based on a cobalt salen complex containing pendant quaternary ammonium salts [Turnover frequency (TOF) = 3300 h^{-1}, number average molecular weight (M_n) = 71000, polydispersity index (PDI) = 1.25, selectivity towards polycarbonate formation = 94%] [9]. Although heterogeneous catalysts like zinc glutarate had shown good polycarbonate selectivity (> 99% MeOH insoluble portion) and appreciable molecular weight (M_n = 143000, PDI = 2.4), they suffer from low productivity (64-70 g polymer/g catalyst) [10]. In spite of the advantages like simple catalyst synthesis and easy handling and separation, research on heterogeneous catalysts has received less attention than the homogeneous catalysts.

Double-metal cyanide complexes (DMCs) are industrially well recognised heterogeneous catalysts for the homopolymerization of PO [11, 12] and its copolymerization with CO_2. Details on the historical developments of DMC catalyzed PO/CO_2 copolymerization are given in Chapter 1 (Section 1.5.3.1). Recently, Langanke et al [13] demonstrated the use of polyethercarbonate polyols synthesized from PO and CO_2 as a substitution to polyether polyols for commercial polyurethane application using a Co-Zn DMC catalyst. Recently, BASF has commercialized this technology. Life cycle assessment studies [14] conducted on polyethercarbonate polyols prepared over this DMC catalyst concluded that compared to the production of conventional polyether polyols, synthesis of polyols with 20 wt% CO_2 allows green house CO_2 reduction up to 11–19%. This is equivalent to roughly 3 kg of CO_2 emission reduction per kg of CO_2 utilized. The impact of reduction increases with further increase in CO_2 content in the polyols [14]. These studies demonstrate the convenience of poly(propylene carbonate) (PPC) with varying CO_2 content for a variety of industrial applications.

Given that, there is a large array of literature existing on the technical and economical commercialization of DMC catalysts and various methods to improve their activity for PPC synthesis, a deep insight to the structural aspects of the catalyst and its correlation to competitive homopolymerization and cyclic carbonate formation as compared to copolymerization is lacking. This chapter forms an extension to Chapter 3 where the catalysts used in Chapter 3 are extended to the more challenging copolymerization of PO/CO_2 to draw some insight about the behaviour of catalysts and to compare the reactivity of two structurally and chemically different epoxides towards the same set of DMC catalysts. Later sections of the chapter discuss a further more challenging terpolymerization of PO, cyclohexene oxide (CHO) and CO_2 and a correlation of the structure and composition of terpolymers with the physicochemical properties of catalysts. Structure-activity correlations and reaction mechanism studies revealed that DMC catalysts behave differently in these two reactions media. All the DMC catalysts were equally productive for the PO/CO_2 copolymerization due to the high reactivity of PO. However, they have shown difference in selectivity towards the amount of CO_2 incorporated in the copolymer. Among the catalysts prepared by same method but with a different mode of addition of reagents, Co-Zn-2 was highly selective than Co-Zn-1. On the contrary, the catalysts prepared by a different method with and without using a co-complexing agent showed similar activities and selectivities (Co-Zn-3 and Co-Zn-4 respectively). Disparities in their structural and acidic properties appeared trivial in differentiating their activity towards PO/CO_2 copolymerization. These catalysts incorporating excess amount of K^+ and Cl^- ions in their structures are found to be highly favourable for the side product cyclic carbonate production. Time on stream activity studies showed that DMC catalysts behaved differently towards new monomers PO and CO_2 and their induction period changed from that observed with CHO and CO_2 monomers. The pressure rise spots in the graph also gave information about the successive addition of PO towards polyether formation. Structure-activity correlations of DMC catalysts for the copolymerization of PO/CO_2 revealed that Co-Zn-2 with cubic crystal structure and with less monoclinic phase impurities is highly selective for polycarbonate formation than those with other crystal structures. This conclusion is different from that for CHO/CO_2 copolymerization where it was concluded that DMC catalyst with monoclinic/rhombohedral crystal structures (Co-Zn-4) is highly active and selective for the copolymerization than the DMC catalyst with cubic structure (Co-Zn-2). Activity studies of DMC catalysts for the terpolymerization of PO, CHO and CO_2 showed a combined behaviour of PO/CO_2 and CHO/CO_2 copolymerizations. The catalysts showed variation in the yield of isolated polymer as observed for CHO/CO_2

copolymerization. ^{1}H NMR and DSC analysis revealed that Co-Zn-1 has produced a block copolymer, Co-Zn-2 gave a nearly alternating terpolymer with more PPC fractions in its composition, Co-Zn-3 has generated a mixture of block and terpolymer and Co-Zn-4 has produced a highly alternating terpolymer with equal fractions of PPC and poly(cyclohexene carbonate) (PCHC).

5.2. Experimental

Five different variations of Co-Zn DMC catalysts were synthesized by procedures reported in Chapter 2 (Section 2.2.2). Co-Zn-0 was prepared in the absence of complexing and co-complexing reagents. Co-Zn-1 and Co-Zn-2 were prepared in presence of complexing and co-complexing agents, but with a difference in the mode of addition of reagent solutions (Sections 2.2.2.2 and 2.2.2.3). During the synthesis of Co-Zn-2, solution 2 was added to solution 3 and this mixture was added to solution 1, whereas in the synthesis of Co-Zn-1 sequential addition of solution 2 and solution 3 to solution 1 was followed. The catalysts Co-Zn-3 and Co-Zn-4 were prepared with and without using a co-complexing agent, respectively (Sections 2.2.2.4 and 2.2.2.5). The experimental techniques used for the characterization of these catalysts are described in Chapter 2 (Sections 2.3.1 to 2.3.6, 2.3.8 and 2.3.9). The detailed procedure for the copolymerization and product characterization involving the calculation of percentage incorporation of CO_2 in the polymer and the estimation of wt% of cyclic propylene carbonate (PC) are presented in Sections 2.4.3 and 2.5.2 of Chapter 2, respectively.

5.3. Results and discussion

5.3.1. Structural characterization

Structural analysis of DMC catalysts through various characterization techniques is already discussed in detail in Chapter 4 (Section 4.3.1). Co-Zn-0 has a cubic structure. Co-Zn-1 and Co-Zn-2 have a dominant cubic structure but with some monoclinic phase (XRD). They however, differ in their crystallinity. Co-Zn-1 was less crystalline (but had higher amount of monoclinic phase) than Co-Zn-2. Within the catalysts prepared by same method but with and without using co-complexing agent, the one prepared with co-complexing agent (Co-Zn-3) was highly amorphous while Co-Zn-4 (prepared without a co-complexing agent) was less amorphous and had monoclinic and rhombohedral phases. FTIR spectra of these catalysts confirmed the formation and cyanide bridging between Co and Zn ions. Raman spectra had also confirmed the presence of multiple phases of DMC complex as the XRD did. Acidity measurements (with pyridine as probe molecule) revealed that Co-Zn DMCs are Lewis acidic. Total acidity of these catalysts (NH_3-TPD) decreased in the order: Co-Zn-4

(2.27 mmol/g) > Co-Zn-0 (2.16 mmol/g) > Co-Zn-2 (1.79 mmol/g) > Co-Zn-3 (1.40 mmol/g) > Co-Zn-1 (1.34 mmol/g). Co-Zn-3 and Co-Zn-4 contained excess amount of K^+ and Cl^- ions in their composition while these contents were negligible for Co-Zn-1 and Co-Zn-2. Co-Zn-0 and Co-Zn-2 showed a Zn/Co ratio of 1.6 pointing to a molecular formula of $Zn_3[Co(CN)_6]_2.xH_2O$. Co-Zn-1 had a Zn/Co ratio of 1.9 corresponding to a molecular formula: $Zn_2[Co(CN)_6]OH.xH_2O$. Zn/Co ratios of Co-Zn-3 and Co-Zn-4 were 2.5 and 2.8, respectively indicated a mixture of complexes with molecular formula: $KZn[Co(CN)_6]$ and $Zn_3[Co(CN)_6]_2.mZnCl_2.xH_2O$.

5.3.2. Catalytic activity

Table 5.1 lists the catalytic activity data of Co-Zn DMC complexes for the copolymerization of PO and CO_2. Co-Zn-0 synthesized without using complexing and co-complexing agents is not active for this polymerization reaction. But this complex showed a little activity for the copolymerization of CHO/CO_2 (isolated yield of the polymer was 0.6 g, Table 4.2). Though it exhibited very little activity for CHO/CO_2, the percentage incorporation of CO_2 in the polymer was 44 mol% and suggests it does activate CO_2 in the CHO/CO_2 reaction medium (75 °C). In the present case (PO/CO_2), the same catalyst is inert even at a higher temperature (85 °C). Good coordinating ability of CHO induced by the +I effect of cyclohexane ring is the probable reason for the milder activity of Co-Zn-0 in CHO/CO_2 copolymerization. As observed in CHO/CO_2 copolymerization (Chapter 4), Co-Zn-1 and Co-Zn-2 (prepared in the presence of complexing and co-complexing agents but following different methods) showed higher polymerization activity than Co-Zn-0 for PO/CO_2 copolymerization. The essentiality of complexing agent in inducing activity in Co-Zn DMC for copolymerization of an epoxide with a highly stable CO_2 is thus justified. With Co-Zn-1 and Co-Zn-2, the isolated yield of crude PO/CO_2 polymer was nearly the same (9.3 g and 9.4 g, respectively; Table 5.1). But in CHO/CO_2 copolymerization, these catalysts showed a significant difference in their activity; isolated yield of crude PCHC was 1.6 g with Co-Zn-1 while it was 12.5 g with Co-Zn-2 catalyst. Thus the difference in sensitivity towards epoxides (CHO or PO) of these catalysts is worth noting. In the case of PO/CO_2 copolymerization, higher reactivity of PO monomer masked the influence of structure of the catalyst. Nevertheless, the selectivity of the catalysts in terms of percentage incorporation of CO_2 in the crude polymer was different, with Co-Zn-2 being more selective in incorporating almost double the amount of CO_2 in the polymer compared to Co-Zn-1 (39.8 versus 19.5 mol%, Table 5.1). On solvent purification, it was found that the yield of methanol insoluble portion of the PO/CO_2 copolymer was higher (23.2 wt%) over Co-Zn-2 than over Co-Zn-1 (5.8

wt%). Fraction of CO_2 incorporation (F_{CO2}) in the methanol insoluble portion of copolymer was 54.3 and 57.8 mol% over Co-Zn-1 and Co-Zn-2, respectively. This trend was similar also for CHO/CO_2 copolymerization where Co-Zn-2 dominated in precipitating an appreciably higher amount of methanol insoluble fraction (77.4 wt%) than Co-Zn-1 (9.6 wt%); F_{CO2} was ~ 80 mol% (Table 4.2).

Table 5.1. Catalytic activity of Co-Zn DMCs for PO/CO_2 copolymerization.

Catalyst	Isolated yield (g)	Crude fraction				MeOH insoluble fraction		
		F_{CO2} (mol %)[a]	PC (wt %)[a]	M_w	PDI	Yield (wt %)	F_{CO2} (mol %)[a]	PC (wt %)[a]
Co-Zn-0	0.0	----	----	----	-----	----	----	----
Co-Zn-1	9.3	19.5	7.7	16200	2.84	5.8	54.3	25.5
Co-Zn-2	9.4	39.8	17.8	21100	3.60	23.2	57.8	31.9
Co-Zn-3	9.5	29.0	30.8	15200	4.60	5.8	65.6	5.8
Co-Zn-4	9.2	30.9	27.0	15800	3.13	15.7	58.4	4.3

Reaction conditions: PO = 8.34 g, toluene = 8.7 g, catalyst = 0.25 g, P_{CO2} = 30 bar, reaction time = 11 h, reaction temperature = 85 °C. [a]Calculated from ^{1}H NMR of PPC in $CDCl_3$.

A comparison of the CO_2 incorporation in PCHC and PPC showed that the F_{CO2} content in PPC (54 mol%) is considerably lower than in PCHC (80 mol%). The lower selectivity of DMC catalysts towards CO_2 incorporation in PO/CO_2 is due to the high homopolymerization tendency of PO and cyclic carbonate (PC) formation. Cyclic carbonate formation was thermodynamically forbidden in CHO/CO_2 copolymerization due to crowd strain while it is highly favoured in PO/CO_2 copolymerization due to least ring strain. Co-Zn-1 had produced 7.7 wt% of undesired cyclic propylene carbonate. This was higher (17.8 wt%) over Co-Zn-2. NMR spectra of purified polymers showed retention of PC in varying amount as it was not completely removed from the elastomeric polymer during solvent evaporation because of its high boiling point (242 °C). In view of this, the comparison of PC formation in crude polymer would be an appropriate method to express the selectivity of catalysts towards polycarbonate formation.

Catalytic activities of Co-Zn-3 and Co-Zn-4 prepared by same synthetic procedure but with and without using co-complexing agent indicated that both the catalysts are equally active in copolymerizing PO and CO_2. The isolated yield of crude polymer with Co-Zn-3 and Co-Zn-4 was nearly the same as that obtained with Co-Zn-1 and Co-Zn-2 catalysts (~ 9.3 g,

Table 5.1). F_{CO2} (crude polymer) and yield of PC were nearly the same for Co-Zn-3 and Co-Zn-4 (Table 5.1). However, the yield of methanol insoluble fraction was higher with Co-Zn-4 (15.7 wt%) than with Co-Zn-3 (5.8 wt%); F_{CO2} (methanol insoluble portion) was 65.6 mol% with Co-Zn-3 and 58.4 mol% with Co-Zn-4. Comparison of the catalytic activities of Co-Zn DMC catalysts for PO/CO_2 copolymerization indicated that Co-Zn-2 is highly selective in producing PPC with high isolated yield, high F_{CO2} and low cyclic carbonate selectivity.

Monitoring the pressure drop at regular time intervals provided an indication about the induction period of catalysts in activating the monomers. Fig. 5.1 depicts the pressure drop in the reactor during copolymerization of PO and CO_2. DMC catalysts are known to show induction periods for the homopolymerization of PO [15]. Induction period is visible (Fig. 5.1) also for copolymerization of PO and CO_2. Co-Zn-0 was inactive for the copolymerization and the pressure graph shows no drop along the reaction time. Co-Zn-1 showed a long induction period (>8 h). This is in accordance with the less amount of CO_2 incorporation in the generated polymer. Co-Zn-2 displayed an induction period of 2 h. Co-Zn-3 exhibited an induction period of 1.3 h while it was zero hours for Co-Zn-4 catalyst. A sudden decrease in reactor pressure over Co-Zn-4 was seen in the early 3 hours of the reaction and remained steady towards the end of the reaction. This behaviour of Co-Zn-4 is similar that observed even in CHO/CO_2 copolymerization (Fig. 4.9) where the catalyst showed a sudden decrease in CO_2 pressure within 2 hours of the reaction and remained steady thereafter. All the DMC catalysts except Co-Zn-4 showed long induction period for CHO/CO_2 copolymerization (Fig. 4.9). However, in PO/CO_2 copolymerization, Co-Zn-3 showed only a little induction period as compared to that observed in CHO/CO_2 copolymerization (1.3 versus 7 h). The induction period of Co-Zn-2 is nearly the same in both the polymerizations. Induction period of Co-Zn DMCs in PO/CO_2 copolymerization decreased in the order: Co-Zn-0 > Co-Zn-1> Co-Zn-2 > Co-Zn-3 > Co-Zn-4.

Figure 5.1 indicates an unusual pressure rise during the course of the reaction. Such behaviour was not observed in CHO/CO_2 copolymerization where the reactor pressure was either steady or decreased (Fig. 4.9). Copolymerization of PO and CO_2 is exothermic but it is less exothermic compared to homopolymerization (PO ring opening is exothermic in nature). During the copolymerization, heat liberated by ring opening of epoxide provides the necessary energy for CO_2 activation and maintains the reaction temperature. A great percentage of ether linkages are present in the produced polymers (< 40 mol%, Table 5.1). So the pressure rise observed in Fig 5.1 can be assigned to polyether formation period. This information would be helpful in predicting the chain propagation during polymerization. The

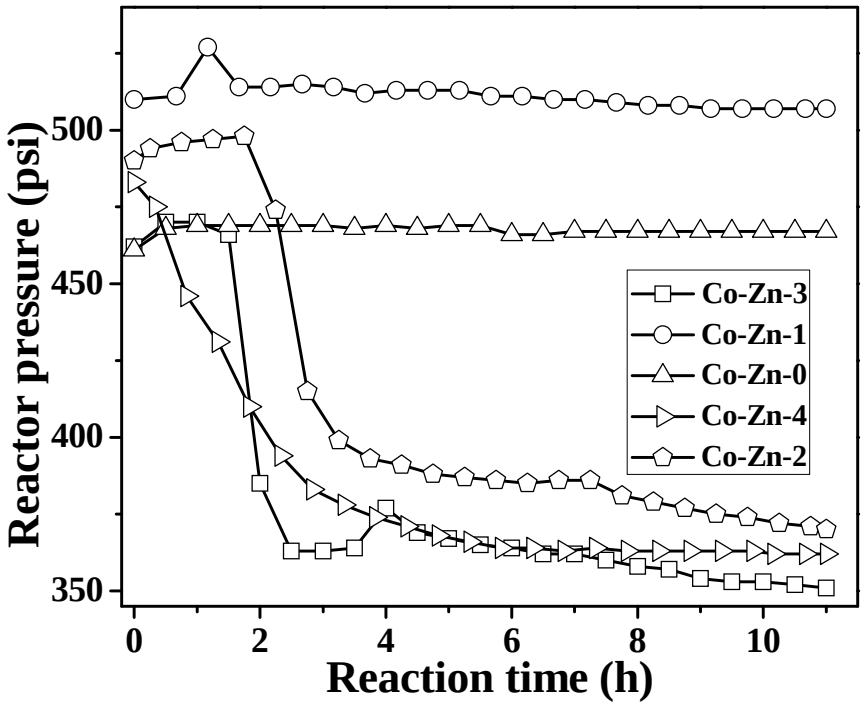

Fig. 5.1. Time on stream activity of Co-Zn DMCs for the copolymerization of PO and CO_2.

rise in pressure was observed at 1.2 h with Co-Zn-1 designating that ether formation is the first step in the catalytic cycle of Co-Zn-1. The gradual or rather minimal pressure drop indicated that CO_2 molecules are not incorporated easily due to competitive adsorption from PO. Co-Zn-1 is more active towards homopolymerization of PO than copolymerization with CO_2. It is evident from the fact that the amount of CO_2 incorporated in the polymer obtained over Co-Zn-1 was only 19.5 mol% (Table 5.1). The same pressure rise was observed for Co-Zn-3 at 4 h but it occurred after the initial pressure drop. So for Co-Zn-3, it is clear that the polymerization is initiated by the coordination of CO_2 molecules than epoxide and PO homopolymerization triggers at CO_2 saturation pressure. Same behaviour was observed for Co-Zn-2 but at a longer reaction time of 7.3 h. This propagation pattern of reactants was not observed for Co-Zn-4 catalyst where CO_2 molecules were incorporated in the beginning of the reaction and the extent of ether fraction is expected to be limited by the occasional incorporation of CO_2 in the polymer. Altogether, the pressure drop monitoring has helped to determine the moment of activity of DMC catalysts and their initiation modes during PO/CO_2 copolymerization. It may be noted that pressure rises observed were not spurious but were observed in all repeated experiments.

5.3.2.1. Structure-activity correlations

Characterization studies have shown that Co-Zn-0 is cubic with a molecular formula $Zn_3[Co(CN)_6]_2.xH_2O$. Addition of complexing and co-complexing agents reduced the crystal symmetry in Co-Zn-1 and Co-Zn-2 as additional monoclinic phase was observed along with the dominant cubic phase. Contribution of this monoclinic phase was high in Co-Zn-1 than in Co-Zn-2. Activity studies established that the presence of complexing agent is essential in inducing activity to catalysts. Co-Zn-2 was highly active and selective in incorporating CO_2 in the polymer whereas Co-Zn-1 was active but less selective in CO_2 activation. Higher amount acid sites and lower amounts of monoclinic phase and complexing agent are the key features of Co-Zn-2 to be selective for the copolymerization. Co-Zn-3 and Co-Zn-4 prepared by a different procedure in the presence and absence of complexing agent showed mixed compositions of $KZn[Co(CN)_6]$ and $Zn_3[Co(CN)_6]_2.mZnCl_2.xH_2O$. While Co-Zn-3 was nearly amorphous, Co-Zn-4 contained monoclinic/rhombohedral phases. Co-Zn-4 gave higher amount of methanol insoluble fraction than Co-Zn-3. However, the CO_2 incorporation with Co-Zn-3 was slightly higher than with Co-Zn-4. As compared to Co-Zn-1 and Co-Zn-2, these two catalysts showed very little or no induction period in copolymerization reaction. This is due to the high host-guest interaction between the catalyst and CO_2 (Fig. 4.10). Elemental analysis revealed that these catalysts have excess amount of Zn^{2+}, Cl^- and K^+ ions in their structures and copolymerization of CHO/CO_2 established that dispersed $ZnCl_2$ is conducive in improving the host-guest interactions. The presence of excess alkali metal in the catalysts is responsible for the low selectivity towards polycarbonate formation but high selectivity towards cyclic carbonate formation as it can favour the cyclic product by backbiting phenomenon.

Although Co-Zn-4 showed no induction period in initiating the polymerization, the catalyst was found to be less selective in incorporating CO_2 in the polymer than forming the undesired cyclic carbonate. Co-Zn-2, on the other hand, had shown an induction period of 2 h in the reaction. The catalyst was equally active but highly selective in forming polycarbonate than cyclic carbonate. The catalyst had also yielded higher amount of methanol insoluble fraction than Co-Zn-4. While the catalysts with monoclinic/rhombohedral phases and with higher amount of acid sites are active for the copolymerization of CHO/CO_2, those catalysts with cubic phase and higher amount of acid sites are active and selective for PO/CO_2 copolymerization.

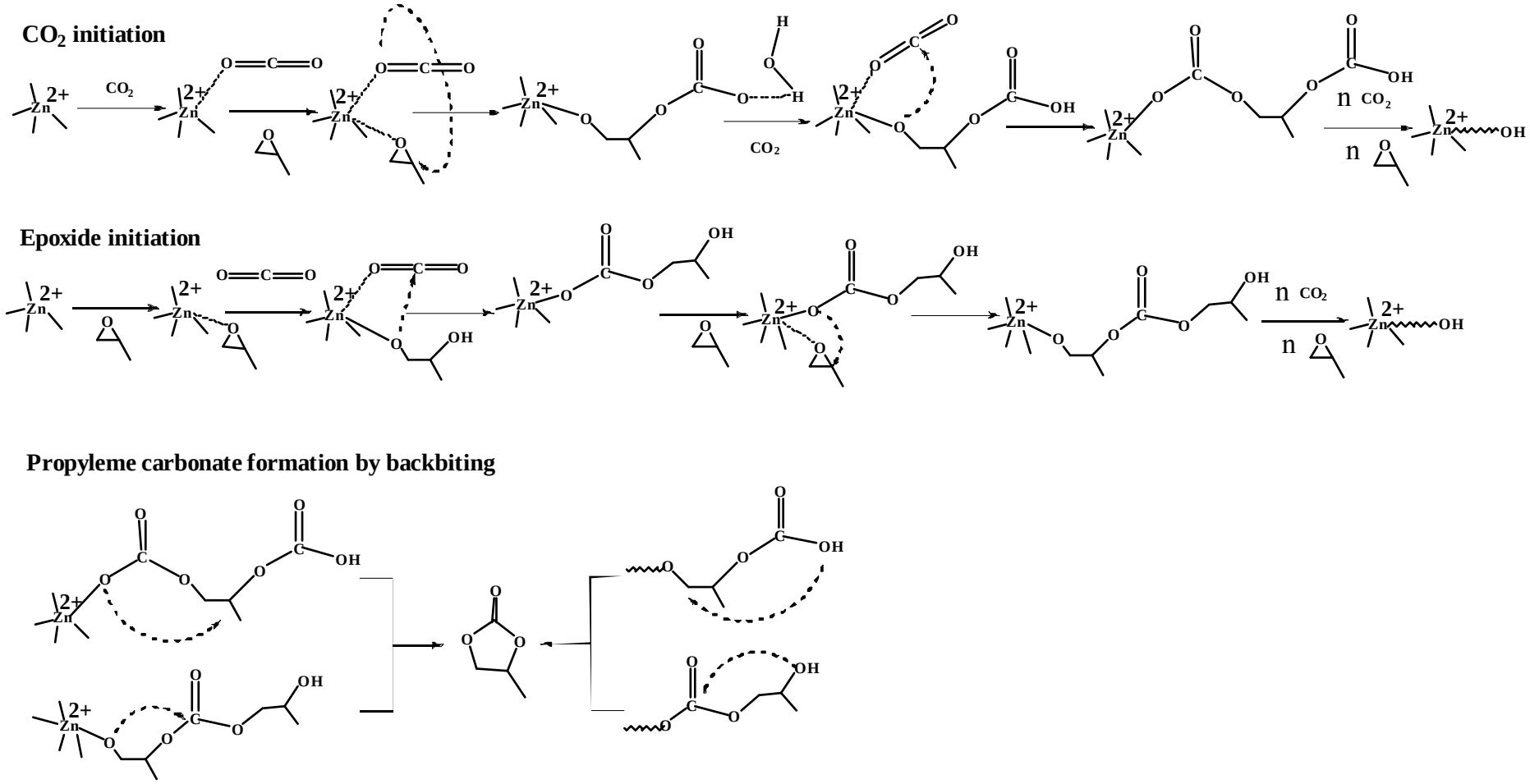

Fig. 5.2. Tentative reaction mechanism for copolymerization of PO and CO_2.

5.3.2.2. Reaction mechanism

Alternative co-polymerization of CO_2 and PO can get initiated by activation of either of the monomers at Zn^{2+} active centre. Based on the conclusions derived from time on stream activity graph, both ways are possible on DMC catalysts. A tentative mechanism for the initiation and propagation of the polymer by both ways is shown in Fig. 5.2. Initiation on Co-Zn-4 is expected to proceed through CO_2 activation, while on Co-Zn-1, it proceeds through PO activation. Propagation of polymer will continue by the uneven addition of both monomers with preference to successive addition of PO. Water present in trace quantities will be responsible for the chain transfer reactions (termination). Formation of undesired cyclic carbonate by backbiting reaction can occur either from a dead polymer or from a growing polymer. Backbiting through epoxide initiation and carbonate initiation are shown in the mechanism. Alkali metals are expected to accelerate the backbiting in dead polymer by ionising the terminal OH functionalities of carbonate and alcohol groups [17].

5.3.3. Product characterization

5.3.3.1. ^{13}C NMR

Regio connectivity in purified PPC was analyzed from ^{13}C NMR spectra of the polymer in inverse-gated mode. The carbonate region of PPC obtained over Co-Zn-2 is shown in Fig. 5.3. Multiplicities in the spectrum indicate the different connectivity around the carbonate unit. The spectrum showed signals due to head-to-head (HH), head-to-tail (HT) and tail-to-tail (TT) tacticity patterns at 153.69-154.0, 154.20-154.66 and 154.87 ppm, respectively [18]. Relative distribution of these segments by integration showed 76.1 mol% HT preferences (isotactic segments). HH connections contributed 18.5 mol% while TT fraction contributed only 5.4 mol%.

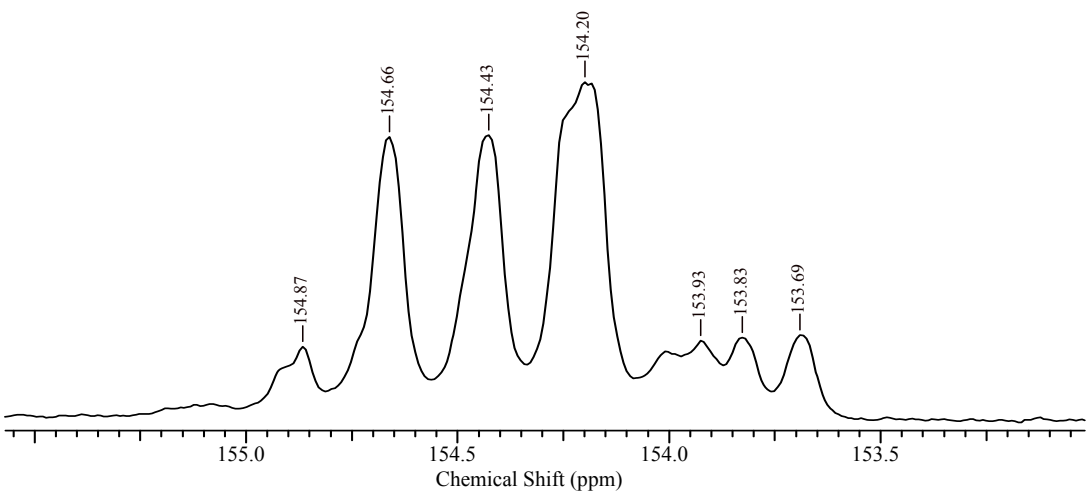

Fig. 5.3. Inverse-gated ^{13}C NMR spectrum of PPC synthesized over Co-Zn-2.

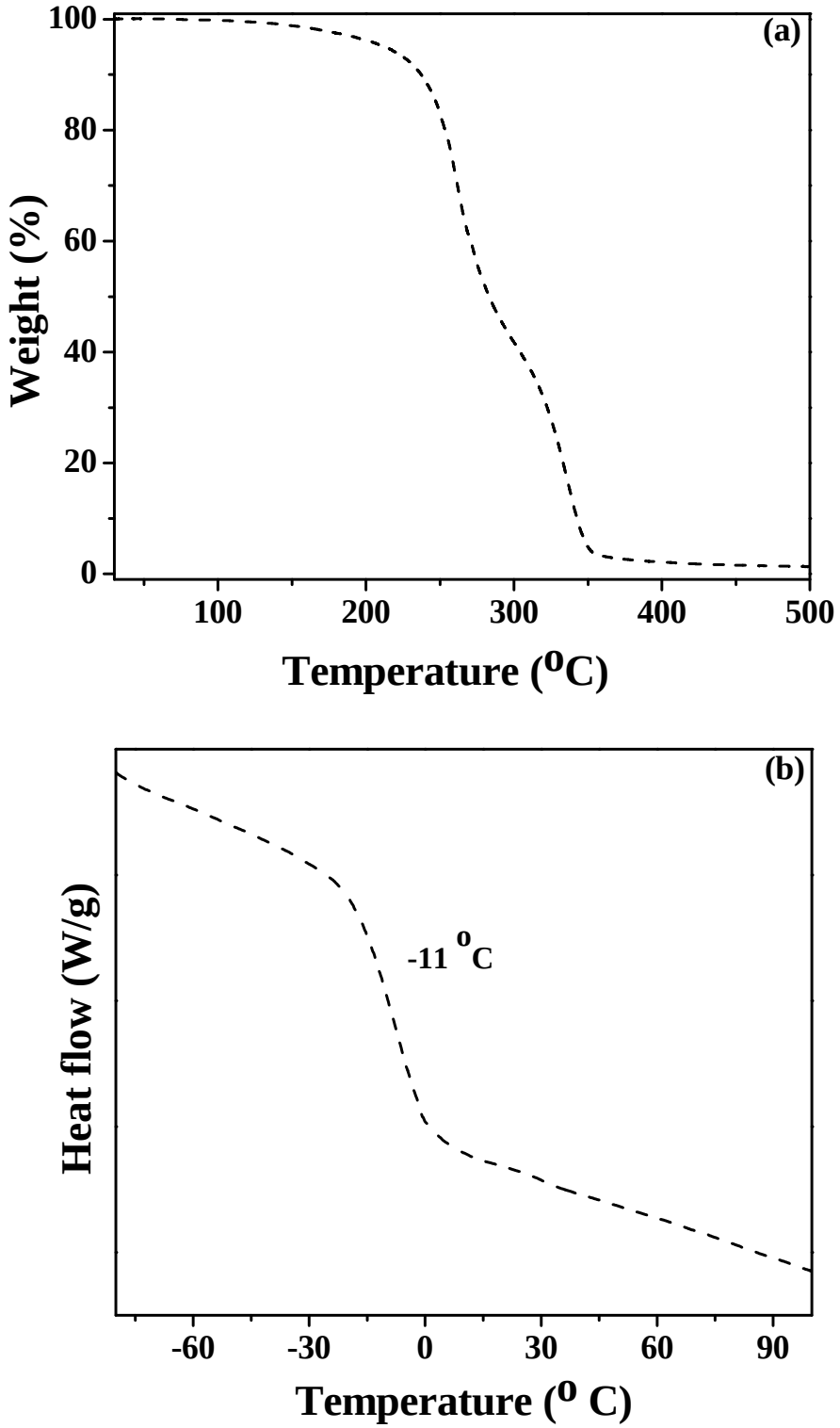

Fig. 5.4. (a) TG and (b) DSC of PPC synthesized over Co-Zn-2.

5.3.3.2. TG

Thermal analysis of purified PPC under inert atmosphere showed two weight loss regions (Fig. 5. 4 (a)). The first weight loss occurred at 263 °C is due to decomposition in carbonate region in the polymer and it contributed 52 wt%. The second weight loss occurred at 338 °C corresponds to the decomposition in ether regions in the polymer and contributed 48 wt%. No residual weight was observed in the thermogram indicating clean burning of polymer with no catalyst impurities.

5.3.3.3. DSC

DSC analysis of purified PPC was recorded from -80 to 145 °C under nitrogen atmosphere. DSC of the polymer showed (Fig. 5.4 (b)) a single glass transition (T_g) at -11° C in accordance with the higher amount of ether fractions.

5.4. Conclusions

Copolymerization of PO and CO_2 over Co-Zn DMC catalysts prepared by different synthetic procedures and their modifications have shown that structural and chemical properties of catalysts have influence on the isolated yield of the methanol insoluble portion of the polymer and on the selectivity of catalysts towards CO_2 activation / incorporation for polycarbonates and cyclic carbonate formation. Among different DMC catalysts, Co-Zn-2 with high crystallinity and high cubic phase purity showed good selectivity towards polycarbonates. Higher amount of acid sites were helpful in increasing the host-guest interactions in the catalyst which were responsible for the activation/ incorporation of CO_2 in the polymer. Co-Zn-4 was found to less selective for polycarbonates synthesis. Lower crystal symmetry (monoclinic/rhombohedral) and excess amount of alkali metal are the critical features of Co-Zn-4 that led to reduced selectivity towards polycarbonate formation. Structure-activity correlations revealed that Co-Zn DMC catalysts having cubic structure, higher amount of acid sites and lesser amount alkali impurity are highly active and selective for PO/CO_2 copolymerization.

5.5. Terpolymerization of CHO, PO and CO_2

Terpolymerization is the polymerization of three monomers. It is a well practiced technique to create novel polymeric materials and to improve the properties of a copolymer by introducing structure reinforcing molecules. Challenges and complexities of a given type of polymerization increase with increase in number of monomers: terpolymerization (3 monomers) > copolymerization (2 monomers) > homopolymerization (single monomer). Bulk applications of polycarbonates are entirely based on their mechanical and thermal

properties. These properties are highly desirable in PPC than PCHC. But low T_g of PPC (30-40 °C) as compared to PCHC (100 - 120 °C) hampers its broad utility. Terpolymerization of PO, CHO and CO_2 can improve the T_g. But the concept is more challenging due to difference in reactivity of PO and CHO which can lead to different side reactions such as individual copolymerization of PO/CO_2 and CHO/CO_2, homopolymerization of PO, formation of block copolymers and cyclic carbonates. This makes very hard to control the composition of terpolymer produced. Some successful design of homogeneous single-site catalysts have been reported for the synthesis of a nearly alternating terpolymer of PO, CHO and CO_2 [19-21], but reports on solid catalysts are scarce [22-24] due to multiple sites of varying activity on their surface. Having shown that Co-Zn DMCs are active for individual copolymerization of PO/CO_2 and CHO/CO_2, their efficiency in terpolymerizing PO, CHO and CO_2 is discussed in this section of this chapter. Although there are plentiful reports on individual copolymerization of PO and CHO with CO_2 over DMC catalysts, their application on terpolymerization and the structure of polymer generated is not documented in the literature so far. This section of present chapter discusses the structure-activity correlations of Co-Zn DMCs for the terpolymerization PO, CHO and CO_2.

5.5.1. Catalytic activity

Table 5.2 lists the catalytic activity data of Co-Zn DMC complexes for the terpolymerization of PO, CHO and CO_2. Co-Zn-0 synthesized in the absence of complexing agent displayed no activity for the polymerization. Co-Zn-1 and Co-Zn-2 synthesized in presence of complexing and co-complexing agents showed good activity with isolated yields of 10.7 g and 13.0 g, respectively. This activity behaviour is similar to that observed in copolymerizations and reconfirms that introduction of complexing agent is vital in inducing activity to DMC catalysts. Co-Zn-1 was weakly active in CHO/CO_2 copolymerization. However, it was equally active as Co-Zn-2 in PO/CO_2 copolymerization. Performance of Co-Zn-1 has improved in terpolymerization similar to that in PO/CO_2 copolymerization but is still lower as compared to Co-Zn-2. Similar behaviour was found also in CHO/CO_2 copolymerization. Co-Zn-2 was highly active in both the copolymerizations and appeared the same in terpolymerization as well. On purification of the terpolymer, Co-Zn-1 yielded 59 wt% of methanol insoluble fraction while Co-Zn-2 precipitated 91.5 wt% (Table 5.2). Purified terpolymer obtained over Co-Zn-2 incorporated 77.3 mol% CO_2 whereas it was only 56 mol% over Co-Zn-1. These values are higher than those observed for PO/CO_2 copolymers but lower than for CHO/CO_2 copolymers. The presence of PO can facilitate the side product cyclic carbonate (PC) formation. NMR analysis of the crude polymer showed 7.9 wt% of PC

Table 5.2. Catalytic activity of Co-Zn DMCs for the terpolymerization of PO, CHO and CO_2.

Catalyst	Isolated yield (g)	MeOH insoluble fraction (wt%)	% incorporation of CO_2 (mol%)[a]			PC (wt%)[a]	Nature of polymer	M_w	PDI	T_g (°C)
			total	PPC	PCHC					
Co-Zn-1	10.7	59.0	56.0	51.4	48.6	7.9	Block polymer	21800	2.93	44.4, 28.5
Co-Zn-2	13.0	91.5	77.3	59.4	40.5	10.7	Terpolymer	46900	4.89	58.2
Co-Zn-3	12.3	60.3	78.9	56.8	43.2	16.4	(Ter + Block) polymer	34900	3.07	60.7, 26.0
Co-Zn-4	11.7	63.1	75.5	53.0	47.0	19.4	Terpolymer	22700	2.97	55.0

Reaction Conditions: CHO: PO = 1: 1 (mol). CHO = 5.6 g, PO = 3.5 g, catalyst = 0.226 g, toluene = 8.7 g, P_{CO2} = 30 bar, reaction temperature = 85 ^{o}C, reaction time = 11 h. [a]Calculated from ^{1}H NMR of polymer in $CDCl_3$.

over Co-Zn-1 and 10.7 wt% over Co-Zn-2. This trend is in accordance with the higher incorporation of CO_2 during terpolymerization analogues to PO/CO_2 copolymerization. However, its amount is significantly lower than that produced during PO/CO_2 copolymerization (7.7 and 17.8 wt%, respectively for Co-Zn-1 and Co-Zn-2 in PO/CO_2 copolymerization, Table 5.1) indicating presence of an additional monomer (CHO) can reduce the side product during terpolymerization. Altogether, Co-Zn-2 has shown good activity over Co-Zn-1 in CHO/CO_2 and PO/CO_2 copolymerizations and inherited the same activity trend in terpolymerization too. Percentage distribution of carbonate regions due to PPC and PCHC units in the terpolymer showed an equal contribution from PPC and PCHC over Co-Zn-1 in accordance with the epoxide feed ratio while it was uneven over Co-Zn-2 catalyst (59.4 mol% of PPC units and 40.5 mol% of PCHC units, Table 5.2). Although Co-Zn-2 was highly active and selective for the terpolymerization, it exhibited a low compositional control of carbonate units in the terpolymer. This selectivity shift towards higher amount of PPC units in the terpolymer can be correlated to its high activity towards PO/CO_2 copolymerization as revealed from the previous sections.

As in the case of PO/CO_2 copolymerization, the activities of Co-Zn-3 and Co-Zn-4 appeared similar in terpolymerization as well. The values of their isolated yield, methanol insoluble fraction and % incorporation of CO_2 are in close limits. These catalysts showed marginal difference in their activities during CHO/CO_2 polymerization where Co-Zn-4 always dominated Co-Zn-3 (Table 4.2). Selectivity of catalysts for incorporating CO_2 in terpolymers (~ 75 mol%) revealed that Co-Zn-4 incorporated higher amount of CO_2 in terpolymer as compared to that in PO/CO_2 copolymers but a lower amount as compared to CHO/CO_2 copolymers. Extension of this comparison showed that Co-Zn-3 incorporated higher amount of CO_2 in terpolymer than both PO/CO_2 and CHO/CO_2 copolymers. The amount of cyclic carbonate produced during terpolymerization over Co-Zn-3 and Co-Zn-4 is 16.4 and 19.4 wt%, respectively which is significantly lower than that produced during PO/CO_2 copolymerization (~ 30 wt%, Table 5.1). However, the trend appears to be the same as was in PO/CO_2 copolymerization. Percentage contribution of PPC and PCHC units in the terpolymer revealed that Co-Zn-4 showed compositional control of PPC and PCHC in the terpolymer (53 : 47) with respect to the molar ratio of epoxides taken. The catalyst is efficient in distributing equally the PPC and PCHC units in terpolymer. Co-Zn-3 showed slightly off equal distribution of these segments and had incorporated higher amount of PPC units (56.8 : 43.2). Structural disparities between Co-Zn-3 and Co-Zn-4 appeared to be insignificant in correlating catalytic activities. Therefore, their equivalent activity can be assigned to the

molecular formulae (mixtures of $KZn[Co(CN)_6]$ and $Zn_3[Co(CN)_6]_2.mZnCl_2.xH_2O$) constituting excess amount of Zn^{2+}, Cl^- and K^+ contents.

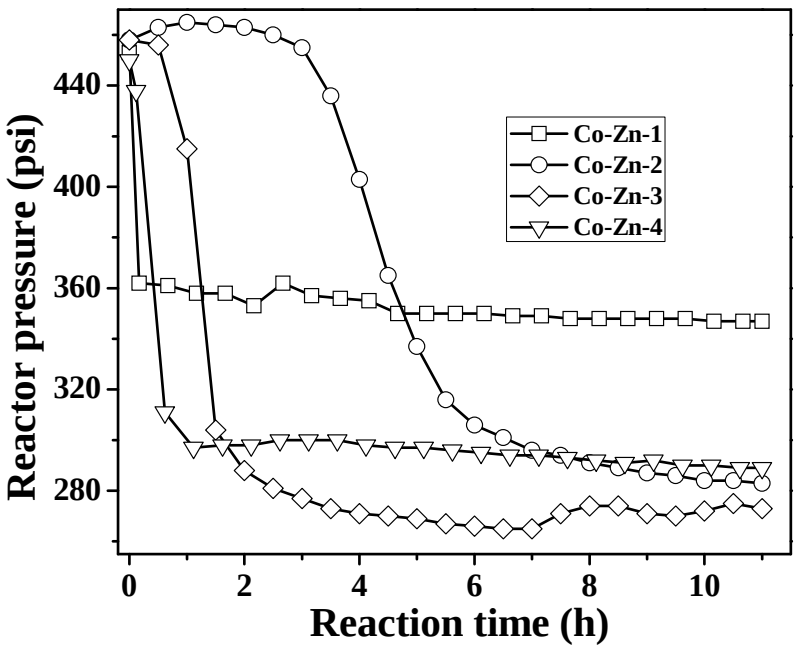

Fig. 5.5. Time on stream activity of Co-Zn DMCs for the terpolymerization.

Figure 5.5 shows the time on stream activity of Co-Zn DMCs for CO_2 activation/ incorporation during terpolymerization. Co-Zn DMCs have shown induction period during copolymerizations and it varied depending on the epoxide used (Fig. 4.9 and Fig. 5.1). Co-Zn-1 had shown an induction period of more than 7 h in CHO/CO_2 and PO/CO_2 copolymerizations but is instantly active in terpolymerization. The pressure drop in Co-Zn-1 was sudden and fast (0.2 h) and thereafter remained steady towards the end of reaction. Co-Zn-2 had shown induction period of 2 h during copolymerizations and 2.5 h in terpolymerization. Even the pressure drop fall was similar in copolymerization and terpolymerization. Co-Zn-3 had shown an induction period of more than 7 h in CHO/CO_2 copolymerization and 1.3 h in PO/CO_2 copolymerization, but in terpolymerization it is only 0.5 h. Co-Zn-4 was an instantly active catalyst in each copolymerization and appeared to be same in terpolymerization too. The time on stream activity graph also evidenced pressure rise spots similar to those observed in PO/CO_2 copolymerization due to successive addition of PO in large numbers. Pressure rise during terpolymerization over Co-Zn-1 was noticed at 2.5 h while it was at 1.2 h in PO/CO_2 copolymerization. Co-Zn-2 did not show any pressure rise spot during terpolymerization. A successful alternative addition of three monomers is thus expected to proceed on Co-Zn-2. Co-Zn-3 showed successive addition of epoxides at 7.5 h,

identical to that observed in PO/CO_2 copolymerization. Co-Zn-4 was an efficient catalyst in alternating addition of monomers in CHO/CO_2 and PO/CO_2 copolymerizations where this catalyst did not show any pressure rise during the long reaction hours and remained the same in presence of both the epoxides. High tendency for homopolymerization during terpolymerization is triggered by the high reactivity of PO. Since the hot spots in the reactor were monitored after initial pressure drop, all DMC catalysts indicated their preference to terpolymerization by CO_2 initiation.

5.5.2. Product characterization

5.5.2.1. ^{1}H NMR

^{1}H NMR spectroscopy was the prime tool in calculating the amount of carbonate unit in copolymers. In terpolymerization, additionally, the NMR spectral analysis helped to differentiate the connection patterns of PO and CHO in the product polymer. Activity studies revealed that the catalysts are sufficiently active for the terpolymerization. Rudimentary calculations of CO_2 incorporation in the polymer confirmed the formation of polycarbonates. However, the difficulties in getting an alternating terpolymer over individual copolymers or block copolymers during terpolymerization are not yet addressed. This section of the chapter discusses the structure of terpolymers obtained over each Co-Zn DMC in detail to differentiate their activity for copolymerization and terpolymerization. Fig 5.6 shows the ^{1}H NMR spectra of terpolymers obtained over Co-Zn DMC catalysts. The figure also incorporates a spectrum of physical blend of PPC and PCHC (Fig. 5.6 (a)) for comparison to differentiate copolymers, block-copolymers and terpolymers. NMR spectrum of physical blend shows signals corresponding to carbonate region of PPC at 5.0, 4.8 and 4.04- 4.27 ppm and signals corresponding to carbonate region of PCHC at 4.6 ppm. Ether fractions of both copolymers appeared as a merged signal at 3.43 - 3.70 ppm. The terpolymer obtained over Co-Zn-1 (Fig.5.6 (b)) shows signals at above positions indicating the existence of both copolymers. Copolymerization of CHO/CO_2 resulted solid polycarbonate after purification while copolymerization of PO/CO_2 produced an elastomer after purification. The terpolymer obtained after purification is entirely a white solid where no elastomeric fractions are segregated. This point rules out the possibility of individual copolymers in the purified polymer. The confirmation from NMR for this purified polymer has PPC unit indicates that the PPC units are a part of the terpolymer. In comparison with the physical blend, the terpolymer obtained over Co-Zn-1 showed all the multiplicities of signals due to carbonate and ether regions of PPC and PCHC. Taken together all the above discussions, the similarity of terpolymer with physical blend does not mean that the terpolymer is composed of

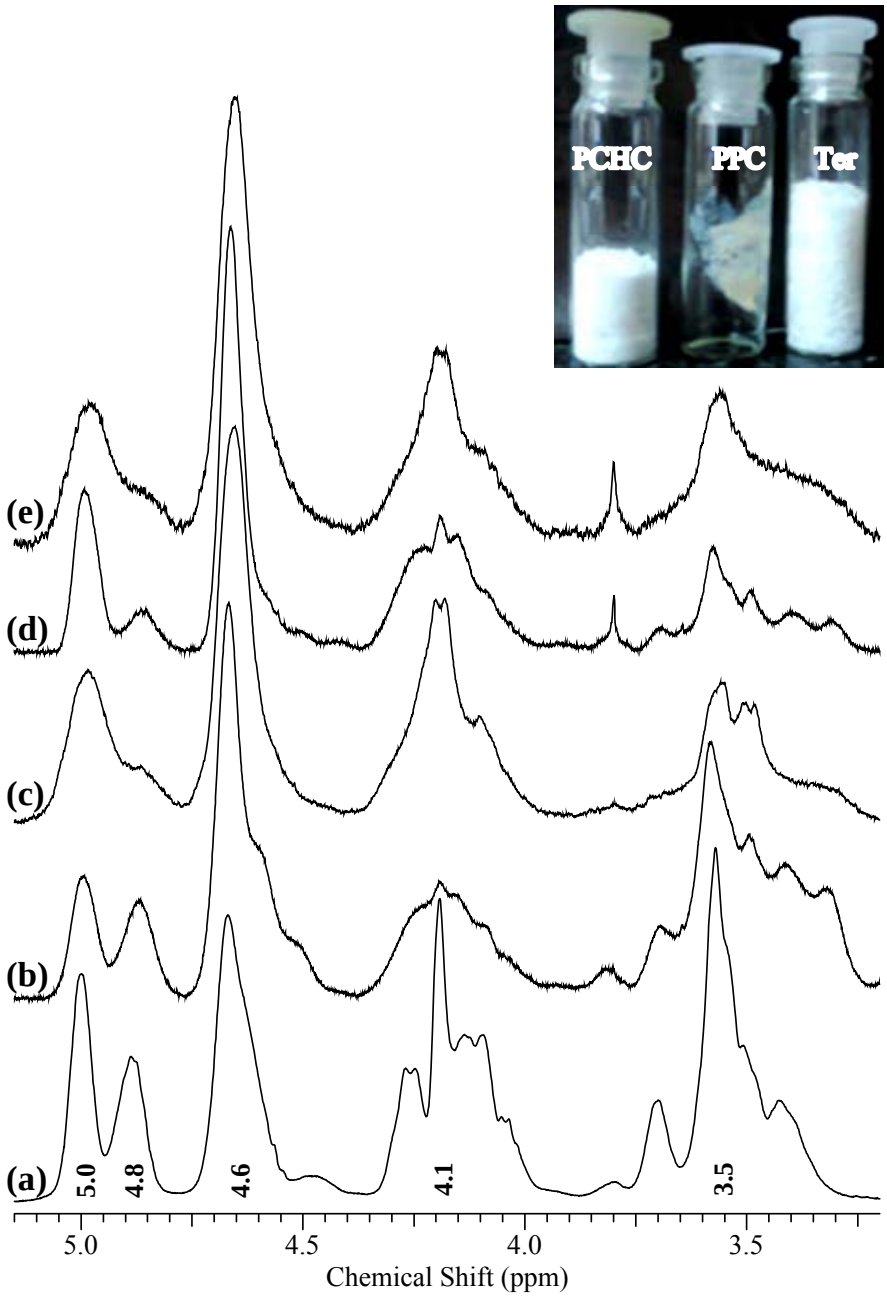

Fig. 5.6. ^{1}H NMR spectrum of terpolymers obtained over Co-Zn DMCs in the carbonate and ether regions. (a) PPC + PCHC and polymers obtained using (b) Co-Zn-1, (c) Co-Zn-2, (d) Co-Zn-3 and (e) Co-Zn-4. Inset shows produced polycarbonates.

individual copolymers but is made up of a block copolymer of PPC and PCHC. Block copolymers are expected to give a NMR spectrum similar to physical blend as the block length is enough to project the spectrum as that of individual copolymers. NMR spectrum of the terpolymer obtained over Co-Zn-2 (Fig. 5.6 (c)) evidenced the presence of carbonate units from both epoxides. However, in spite of showing signals at similar positions of physical blend, some major changes in signal intensities were observed. The carbonate signal due to

PPC units at 5.0 and 4.8 ppm appeared as almost merged and the multiplicities at 4.04-4.27 ppm were reduced indicating a different environment of PPC units in the terpolymer than in the physical blend of copolymers. A straight conclusion based on the observations including, that the purified terpolymer is solid and devoid of elastomeric fraction and the apparent reduction in intensity of 4.8 ppm signal and its merging with 5.0 ppm signal confirmed that the terpolymer is not a block copolymer but mostly composed of a nearly alternating terpolymer of both epoxides.

The terpolymer obtained using Co-Zn-3 DMC catalyst (Fig. 5.6 (d)) can be easily categorised into a block copolymer as it showed resemblance to the terpolymer obtained over Co-Zn-1. The intensity of carbonate signal due to PPC fraction in the terpolymer was low as compared to that obtained over Co-Zn-1 suggesting some alternating sequence of epoxides in the terpolymer. Terpolymer produced over Co-Zn-3 can be assumed as a mixture of block copolymers with a little fraction of alternating sequence. Terpolymer produced by Co-Zn-4 appeared similar to that obtained over Co-Zn-2, implying that the product is nearly an alternating terpolymer of both the epoxides (Fig. 5.6 (e)). However a close inspection of the multiplicities of carbonate and ether signals of Co-Zn-4 and Co-Zn-2 indicated that the alternating nature of epoxides in the terpolymer produced by Co-Zn-4 is more uniform than that produced by Co-Zn-2. This is more visible in the ether region of terpolymers where the terpolymer obtained from Co-Zn-2 shows multiplicities in their peaks whereas that produced from Co-Zn-4 is more like a single peak. ^{1}H NMR analysis of terpolymers produced by different Co-Zn DMC catalysts confirmed the incorporation of both epoxides in a single polymer chain. It ruled out the co-existence of individual copolymers. Co-Zn-1 has produced a block copolymer, Co-Zn-2 resulted in a nearly alternating terpolymer, Co-Zn-3 yielded a mixture of block copolymer and a terpolymer and Co-Zn-4 gave a highly alternating terpolymer.

5.5.2.2. DSC

Existence of block and terpolymers in Co-Zn DMC catalyzed terpolymerization was further confirmed by DSC analysis of purified product polymers in the temperature range -80 to 120 °C (Fig. 5.7). A perfectly alternating terpolymer is expected to give single T_g in the thermogram. While a block polymer will give more than one T_g. DSC of terpolymer produced over Co-Zn-1 showed two T_gs, one at 28.5 °C and another at 44.4 °C indicating the existence of different chemical compositions in the terpolymer (Fig. 5.7 (a)), probably due to a block copolymer as revealed from NMR. In addition to that, the thermogram showed minor yet considerable disturbance at -15 °C suggesting the existence of PPC blocks. Overall the

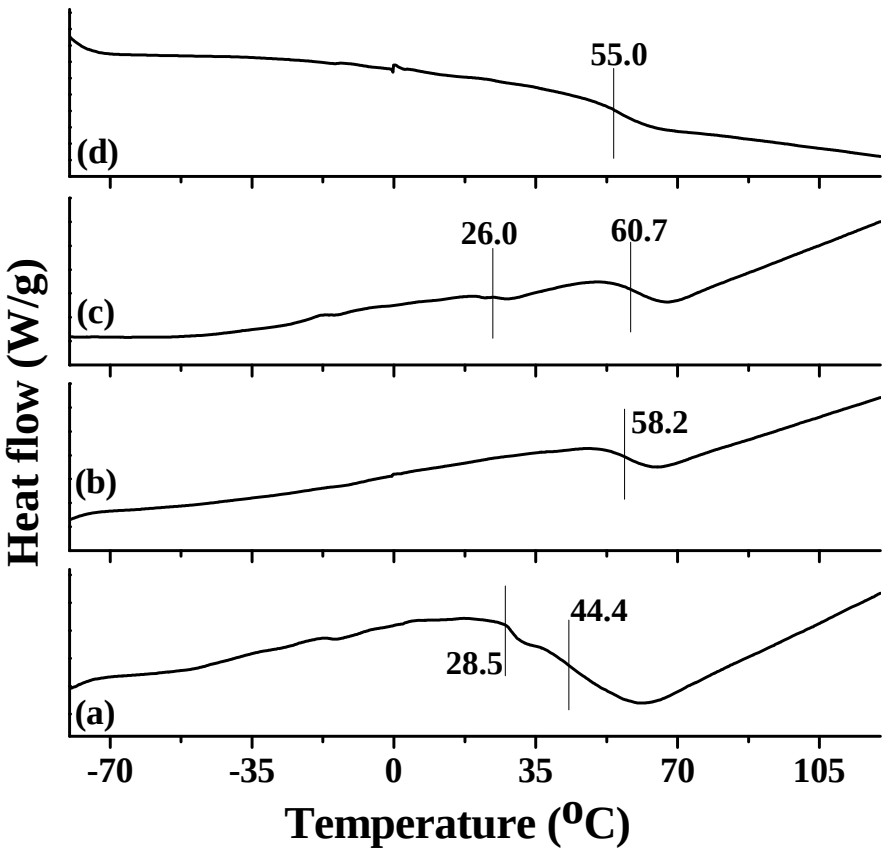

Fig. 5.7. DSC of terpolymers produced over (a) Co-Zn-1, (b) Co-Zn-2, (c) Co-Zn-3 and (d) Co-Zn-4.

DSC of terpolymer revealed a non-homogeneous distribution in the polymer chain. DSC of terpolymer produced over Co-Zn-2 revealed only one T_g at 58.2 °C (Fig. 5.7 (b)) implying the existence of a nearly alternating arrangement of epoxides around the carbonate units in the terpolymer. This observation is supportive to the conclusion drawn from NMR. DSC of terpolymer produced by Co-Zn-3 shows multiple T_gs (26.0 and 60.7 °C) indicating non-homogeneity in the polymer chain (Fig. 5.7 (c)) due to dominant block structure. Similar to Co-Zn-2, the terpolymer produced over Co-Zn-4 showed single T_g at 55 °C confirming a nearly alternating nature of PO and CHO around the carbonate unit (Fig. 5.7 (d)). Method of preparation of DMC catalysts has greatly influenced the architecture and composition of the terpolymer produced.

5.5.2.3. ^{13}C NMR

Tacticity patterns of PPC and PCHC units in the terpolymers were analyzed by inverse-gated ^{13}C NMR spectroscopy in the carbonate region. The spectra of terpolymers produced over different DMC catalysts were compared with their physical blend (Fig. 5.8). PPC showed carbonate signals at 153.69 -154.01, 154.20-154.66 and 154.87 ppm

corresponding to HH, HT and TT tacticity (Fig. 5.3). PCHC showed signals at 153.14-153.28 ppm due to syndiotactic isomers (r-centred tetrads: rrr/rrm/mrm) and 153.80-154.23 ppm corresponding to isotactic isomers (m-centred tetrads: mmm/mmr/rmr) (Fig. 4.12). All these signals are present in the physical blend of the polymers (Fig. 5.8 (a)) and in terpolymers. However the terpolymers showed an additional signal at 153.55 ppm indicating the regioselective connection of CHO and PO around the carbonate unit [25] which was absent in the physical blend confirming the alternative nature of monomers.

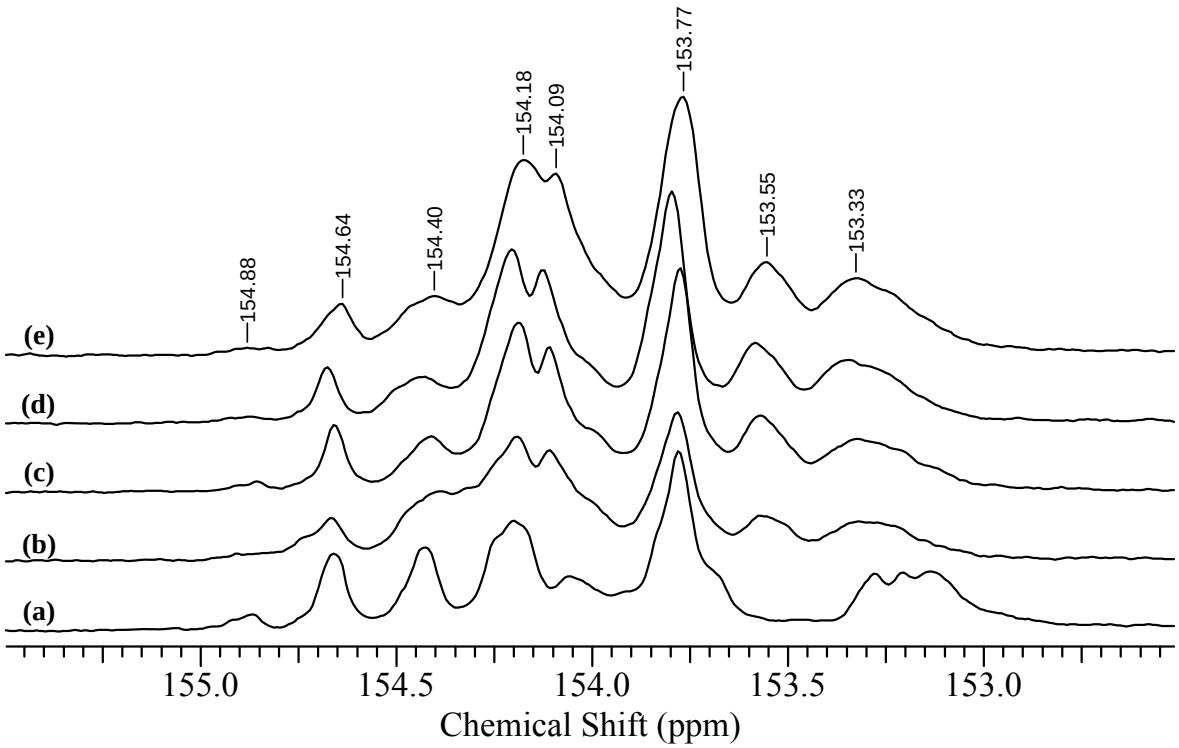

Fig. 5.8. Inverse-gated ^{13}C NMR spectra of (a) physical blend and terpolymers synthesized over (b) Co-Zn-1, (c) Co-Zn-2, (d) Co-Zn-3 and (e) Co-Zn-4.

5.5.2.4. TG

Fig. 5.9 shows TG of terpolymers synthesized over Co-Zn DMC catalysts. Terpolymers obtained over Co-Zn-1 and Co-Zn-2 showed a single weight loss at 285 and 277 °C, respectively, which was close to the decomposition temperature of PPC (263 °C) and PCHC (286 °C). Terpolymers synthesized over Co-Zn-3 and Co-Zn-4 showed two weight losses. The first weight loss of terpolymer obtained over Co-Zn-3 was observed at 208 °C and contributed 15.8 wt% and the second loss was observed at 300 °C and contributed 84.2 wt%. The first weight loss in Co-Zn-4 catalyzed terpolymer was observed at 207 °C

contributing 6.2 wt% and the second at 292 °C contributing 93.8 wt%. No residual weight was observed in the thermogram indicating the clean burning of polymer with no catalyst impurities.

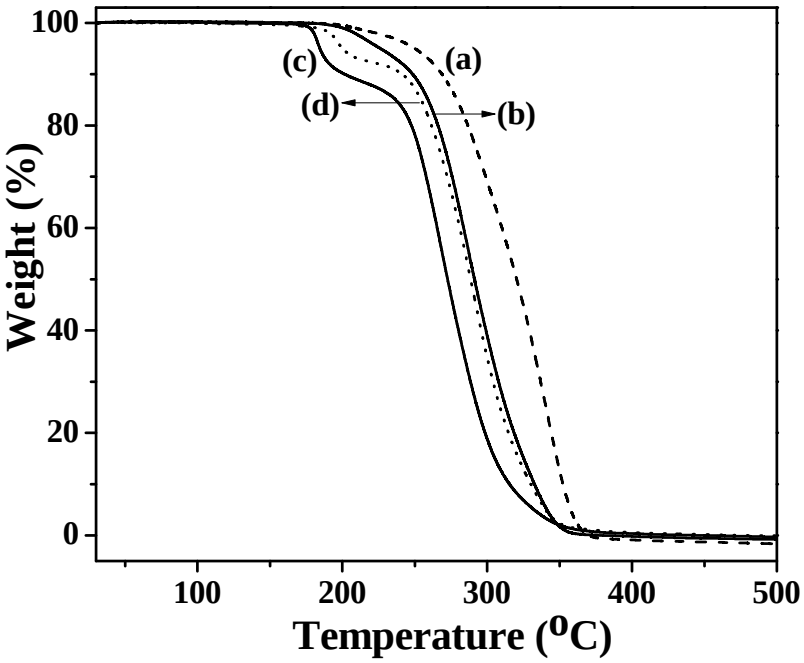

Fig. 5.9. TG of terpolymers synthesized over (a) Co-Zn-1, (b) Co-Zn-2, (c) Co-Zn-3 and (d) Co-Zn-4.

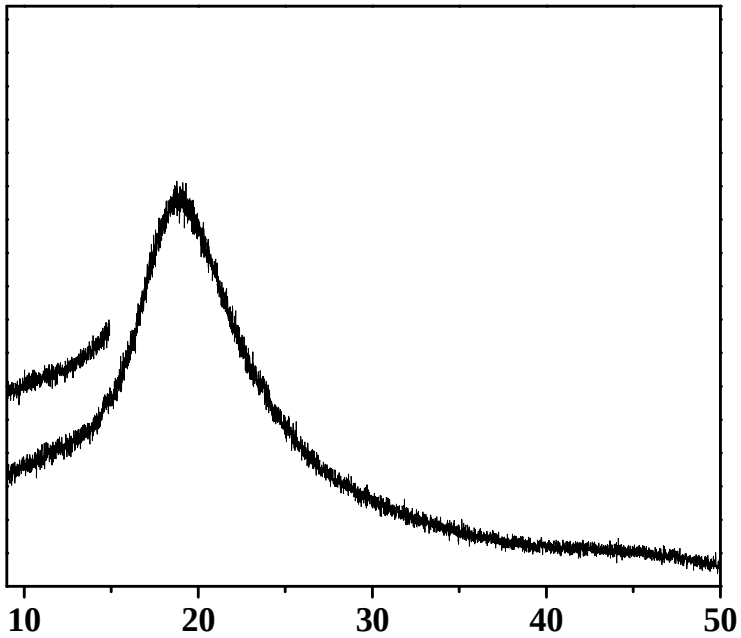

5.5.2.5. XRD

XRD of terpolymers showed a broad peak at 2θ = 18.8° (Fig. 5.10). PCHC showed this peak at 2θ = 17.7°. The shift in XRD peak for terpolymers in comparison with PCHC suggests a difference in configuration of PCHC units in terpolymers as confirmed by ^{13}C NMR spectroscopy.

5.5.3. Effect of reaction parameters

Among the different Co-Zn DMC catalysts the characterization studies have shown that Co-Zn-4 produced a terpolymer with an alternating connection of epoxides around the carbonate unit in equal compositions. Although Co-Zn-2 produced nearly an alternating terpolymer, the composition of the terpolymer was different from the epoxide feed ratio. Additionally, the molecular weight distribution over Co-Zn-2 was considerably higher than on Co-Zn-4 (4.89 versus 2.97, Table 5.2). Hence, parameter optimization studies were undertaken with Co-Zn-4 DMC catalyst.

5.5.3.1. Effect of reaction temperature

As the reaction temperature was raised from 75 to 85 °C, the isolated yield of terpolymer remained the same (11.7 g, Table 5.3). However, the methanol insoluble fraction and the amount of CO_2 incorporation in terpolymers decreased from 74.1 to 63.1 wt% and 83.8 to 75.5 mol%, respectively. Percentage distribution of PPC and PCHC in the terpolymer revealed a little deviation from equimolar distribution of both fragments (55.9 and 44.1 mol% of PPC and PCHC at 75 °C as compared to 53 and 47 mol% at 85 °C). The reaction showed an induction period of 1 h at lower temperature of 75 °C (Fig. 5.11 (a)). Induction period was not observed at 85 °C. A further increase in temperature to 95 °C resulted almost same yield of isolated polymer. But both the methanol insoluble fraction and CO_2 incorporation were reduced to 36 wt% and 72.3 mol%, respectively. Percentage distribution of PPC and PCHC were found to be the same as that at 85 °C (53.5 and 46.5 mol%, respectively, Table 5.3) and the catalyst did not show any induction period (Fig. 5.11 (a)). The effect of temperature on the side reaction to cyclic carbonate formation was found to be independent and remained approximately 19 wt% at all temperatures. A rise in reaction temperature (from 75 to 95 °C) was found to decrease both M_w and PDI of terpolymers from 29000 to 20500 and 3.16 to 2.43, respectively.

5.5.3.2. Effect of reaction pressure

CO_2 pressure was found to induce a positive effect on isolated yield, methanol insoluble fraction and incorporation of CO_2 in the terpolymer (Table 5.3). As the pressure was increased from 10 to 20 bar and finally, to 30 bar, the isolated yield increased from 10

Table 5.3. Effect of reaction parameters on catalytic activity of Co-Zn-4 during terpolymerization.

Parameter	Isolated yield (g)	MeOH insoluble part (wt%)	% incorporation of CO_2 (mol%)			PC (Wt%)	M_w	PDI
			total	PPC	PCHC			
Effect of reaction temperature (^oC)								
75	11.8	74.7	83.8	55.9	44.1	19.1	29000	3.16
85	11.7	63.1	75.5	53.0	47.0	19.4	22700	2.97
95	11.4	36.0	72.3	53.5	46.5	20.9	20500	2.43
Effect of pressure (bar)								
10	10.0	11.8	60.1	52.7	47.3	13.5	14700	2.48
20	11.5	41.8	65.7	45.1	54.9	20.1	20800	2.81
30	11.7	63.1	75.5	53.0	47.0	19.4	22700	2.97
Effect of catalyst quantity (g)								
0.226	11.7	63.1	75.5	53.0	47.0	19.4	22700	2.97
0.113	11.8	54.4	80.2	55.5	44.5	17.9	22300	2.58
0.083	12.7	51.7	85.0	58.1	41.9	20.1	23200	2.83
Effect of reaction time (h)								
1	9.5	16.0	60.8	52.0	48.0	20.6	13600	2.77
11	11.7	63.1	75.5	53.0	47.0	19.4	22700	2.97
Effect of molar ratio of PO (mol%)[a]								
80	10.0	20.3	78.1	79.4	20.5	31.1	27000	2.59
66	10.7	36.3	70.9	64.5	35.5	30.7	20000	2.31
57	11.3	46.4	81.4	59.8	40.2	27.6	23600	2.39
50	11.7	63.1	75.5	53.0	47.0	19.4	22700	2.97
43	10.7	60.9	77.3	45.0	54.9	17.9	14100	2.07
33	12.4	81.1	82.0	38.9	61.0	12.7	22700	2.56
20	12.7	80.0	77.0	25.7	74.2	11.7	15800	2.94

Reaction conditions: CHO: PO = 1:1, Co-Zn-4 = 0.226 g, toluene = 8.7 g, reaction time = 11 h, reaction temperature = 85 °C, P_{CO2} = 30 bar.[a]PO (mol%) = [PO/(PO + CHO)] x100, Co-Zn-4 = 2.5 wt% with respect to the highest amount of monomer.

g to 11.5 g and 11.7 g, methanol insoluble fraction increased from 11.8 wt% to 41.8 wt% and 63.1 wt% and percentage incorporation CO_2 increased from 60.1 mol% to 65.7 mol% and 75.5 mol%, respectively. An increase in pressure caused an increase in CO_2 incorporation in the terpolymer which was accompanied by an increase in isolated yield and methanol insoluble fractions. However, percentage distribution of PPC and PCHC in the terpolymer did not follow a trend with increase in reaction pressure. It was equimolar at 10 and 30 bar pressures. Cyclic carbonate production was less at 10 bar CO_2 pressure (13.5 wt%) and was levelled off to 20 wt% at 20 and 30 bar pressures. M_w of terpolymers increased from 14700 to 22700 as the pressure was increased from 10 to 30 bar. This is in accordance with the high amount of CO_2 incorporation in the polymer. Time on stream activity of the catalysts at different pressures disclosed no induction period in the reaction (Fig. 5.11 (b)).

5.5.3.3. Effect of catalyst quantity

As the amount catalyst was reduced from 0.226 to 0.113 g, isolated yield of the terpolymer remained the same at 11.7 g (Table 5.3). But the methanol insoluble fraction decreased from 63.1 to 54.4 wt%. CO_2 incorporation in the polymer showed an increment from 75.5 to 80.2 mol% and the amount of cyclic carbonate reduced from 19.4 to 17.9 wt%. M_w of terpolymer was almost same (~ 22000) but PDI has dropped from 2.97 to 2.58. Percentage contribution of PPC and PCHC in the terpolymer showed an inclination to PPC formation at lower catalyst loadings (55.5 mol%). A further decrease in catalyst quantity showed an increase in the amount of isolated yield of the polymer (12.7 g), a decrease in methanol insoluble fraction (51.7 wt%), an increase in CO_2 incorporation (85 mol%) and cyclic carbonate formation (20.1 wt%). M_w of the terpolymer also showed a slight increment to 23200 (PDI = 2.97). Composition of PPC and PCHC in the terpolymer showed an uneven distribution where PPC dominated PCHC (58.1 versus 41.9 mol%). Interestingly, the catalyst did not show induction period for the initiation (Fig. 5.11 (c)) signifying that the high activity is inherent of the catalyst not to the amount of it.

5.5.3.4. Effect of reaction time

When terpolymerization was quenched after 1 h an overall decrease in isolated yield (from 11.7 g to 9.5 g), methanol insoluble fraction (from 63.1 to 16.0 wt%) and the percentage of CO_2 incorporation (from 75.5 to 60.8 mol%) in the terpolymer was observed (Table 5.3) as compared to the 11 h reaction. A slight increase in cyclic carbonate was also observed (from 19.4 to 20.6 wt%). However, the percentage distribution of PPC and PCHC in the early hours of the polymerization was equimolar representative of an alternating nature of epoxides in the terpolymer.

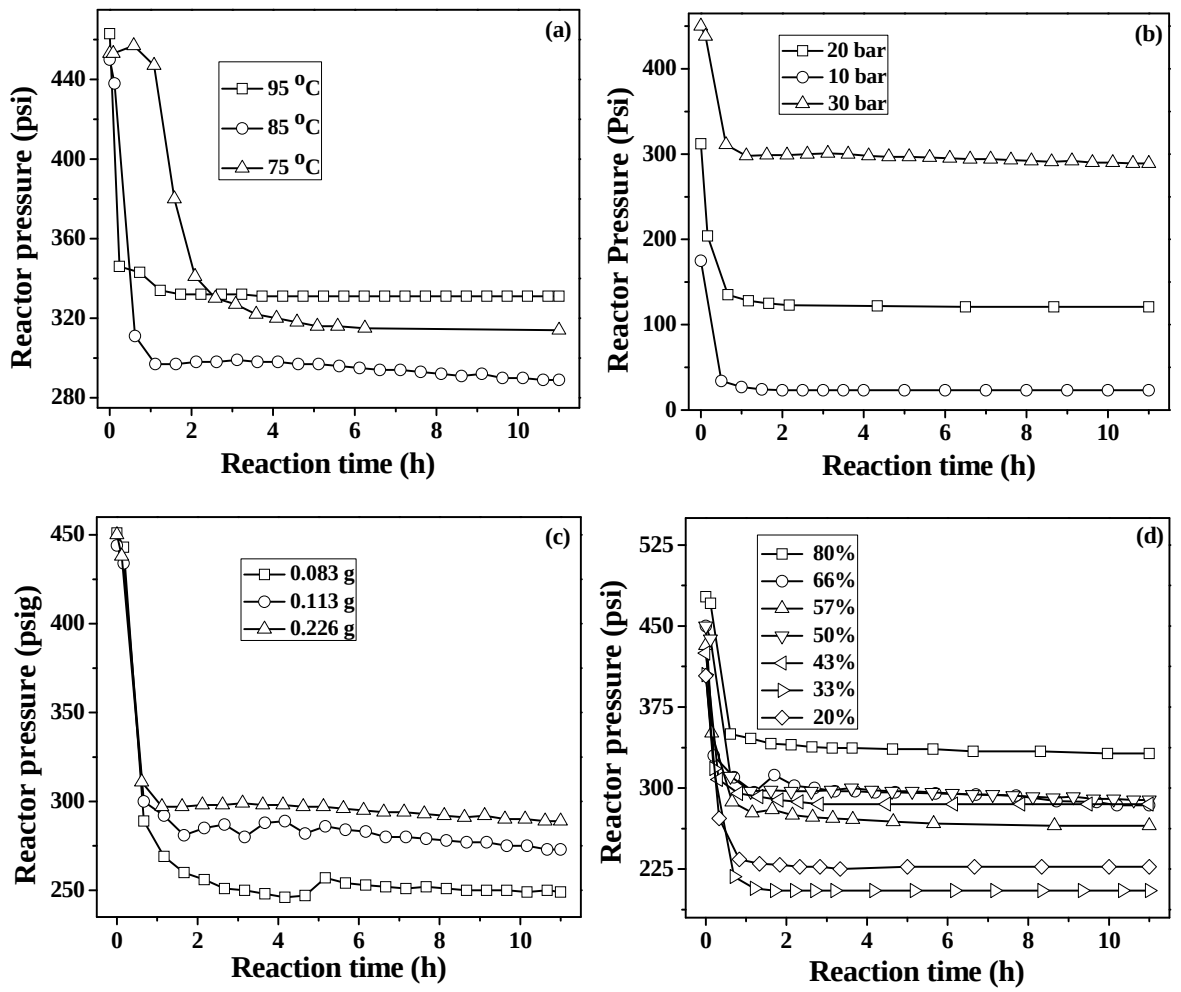

Fig. 5.11. Effect of reaction parameters on induction period of Co-Zn-4: (a) temperature, (b) CO_2 pressure, (c) catalyst quantity and (d) mol% of PO.

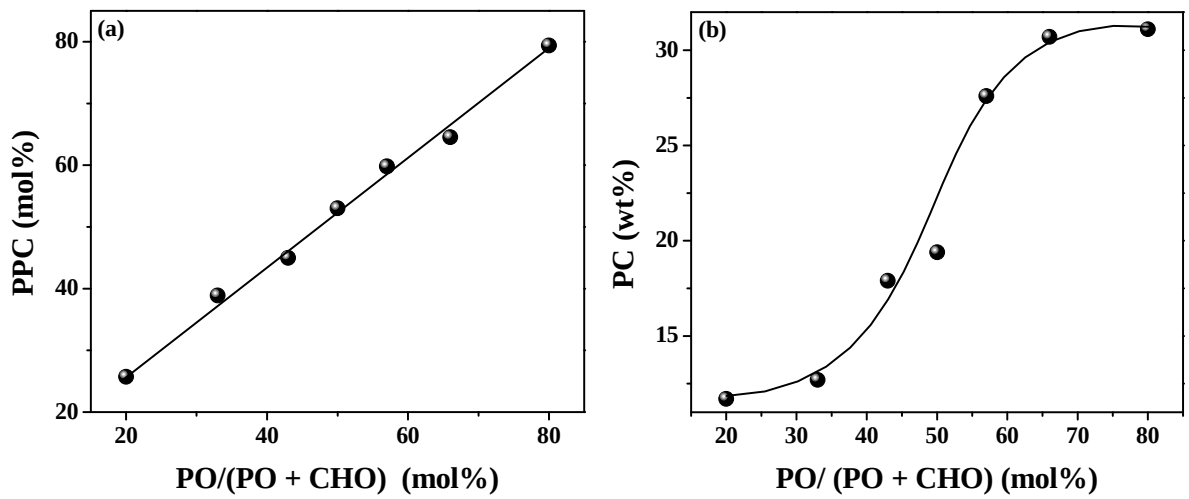

Fig. 5.12. (a) Effect of mol% of PO on output mol% of PPC and (b) wt% of PC produced.

5.5.3.5. Effect of molar ratio of epoxides

Molar ratio of PO and CHO were varied during the terpolymerization to examine the efficiency of Co-Zn-4 to maintain the composition of PPC and PCHC in the terpolymer with respect to the input ratio. The mol% PO in total epoxides was varied from 80 to 20 mol%. As the mol% of PO was decreased, the isolated yield of the terpolymer was gradually increased from 10 to 12.7 g. This increment can be assigned to the higher amount of PCHC fraction in the terpolymer whose unit formula molecular weight is higher than PPC formula unit. Analogous to this, the methanol insoluble fraction also increased from 20.3 to 80 wt% with increase in CHO mol% in the feed. Percentage of CO_2 incorporation showed no apparent trend with decreasing mol% of PO in the monomer feed. The overall variation was from 70 to 82 mol%. Most importantly, the percentage distribution of PPC and PCHC in the terpolymer followed the same ratio as the input ratio of PO. A plot of input PO mol% versus output PPC mol% revealed a linear relationship (Fig 5.12 (a)). This shows the efficiency of Co-Zn-4 in controlling the composition of PPC and PCHC in the terpolymer with respect to their monomer composition. The amount of PC produced over different mol% of PO showed an increasing trend with increasing amount of PO and levelled off at higher values (Fig. 5.12 (b)). The variation in M_w of the terpolymers did not show any trend with varying molar ratio of the epoxides. Overall it varied from 14100 to 27000 (PDI is between 2.01 and 2.97). The catalyst did not show any induction period with variation in the monomer feed (Fig. 5.11 (d)).

5.5.4. Reaction mechanism

Figure 5.13 shows a tentative mechanism for terpolymerization of PO, CHO and CO_2 over Co-Zn DMC catalyst. Time on stream activity of catalysts have shown that the polymerization is initiated by the activation of CO_2 at the tetra-coordinated, Lewis acidic Zn^{2+} active centers by coordination through its oxygen atom. This coordination transforms the active centre to a monodentate carbonate species. In the next step, PO is activated at the same Zn^{2+} site. The activated CO_2 facilitates ring-opening followed by its insertion in the epoxide (PO) forming an alkylene carbonate linkage. Subsequent insertion of another CO_2 molecule and CHO results in the formation of a terpolymer repeating unit. Alternative addition of these monomers in the propagation step results the desired polymer chain. Water (present in trace quantities in the feed) is responsible for chain termination and active site regeneration. Formation of undesired cyclic carbonate (PC) by backbiting reaction can occur either from a dead polymer or from a growing polymer (Fig. 5.2). Alkali metals are expected to accelerate the backbiting in dead polymer by ionising the terminal -OH functionalities of

carbonate and alcohol groups. Simultaneous addition of PO or CHO or both lead to ether linkages in the polymer.

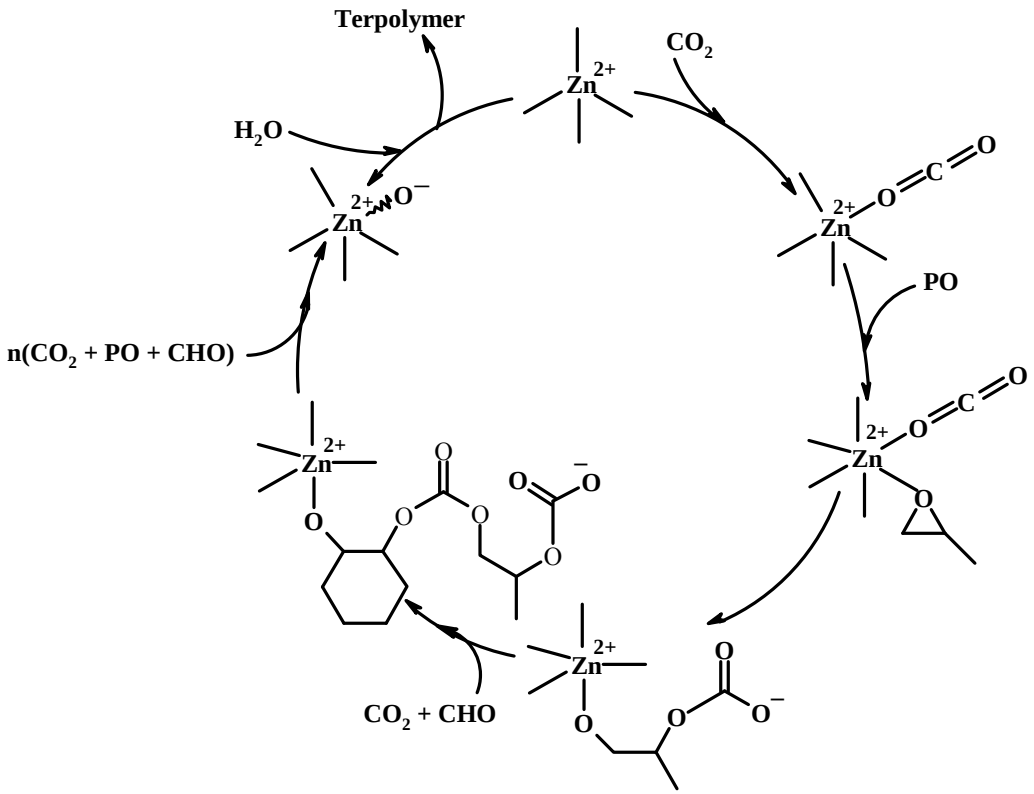

Fig. 5.13. Tentative reaction mechanism for terpolymerization of PO, CHO and CO_2.

5.6. Conclusions

Terpolymerization is one of the ways to improve the thermal and mechanical properties of PPC and PCHC copolymers. The concept is more challenging due to the high reactivity of PO and high coordination ability of CHO which would result individual copolymerizations in the reaction medium. This competing reaction would make difficult to manipulate the composition of PPC and PCHC in resulting terpolymers. Having shown that the same set of Co-Zn DMCs can catalyze the copolymerization of CHO/CO_2 and PO/CO_2, their efficiency for a more challenging terpolymerization of CHO/PO/CO_2 was attempted. Method of preparation of DMC catalysts has a great influence on their physicochemical properties. Structure-activity correlations in Co-Zn DMC catalyzed copolymerization of CHO/CO_2 revealed that catalyst with monoclinic/rhombohedral crystal structures are highly active and selective than with cubic structure. Stronger acid sites created by the excess amount of Cl^- ions coordinated to Zn^{2+} active centre increased the host-guest interactions and this in turn eventually removed the induction period for initiation. In the contrary, structure-

activity correlations on PO/CO_2 copolymerization revealed that the DMC catalyst with cubic structure is more active and selective than the catalyst with the monoclinic/rhombohedral crystal structures. The catalyst produced less amount of cyclic carbonate by-product and higher amount of CO_2 incorporation in the copolymer. Terpolymerization revealed an inherited combination effect of individual copolymerizations in the activity behaviour. Co-Zn-4 was an instantly active catalyst for the terpolymerization, an inherited property from individual copolymerization. Co-Zn-2 showed an induction period of about 2 h for initiation in terpolymerization similar to copolymerizations. Polymers produced by these catalysts showed single T_g in DSC confirming the formation of an alternating terpolymer. Co-Zn-1 and Co-Zn-3 showed multiple T_gs in DSC indicating block copolymer formation. Among Co-Zn-2 and Co-Zn-4, the latter showed good compositional control of PPC and PCHC fractions in the terpolymer with respect to the input ratio of epoxides than the former. A broad distribution of molecular weights for polymers over Co-Zn-2 than Co-Zn-4 was noted. Although, DMC catalysts are known for copolymerization of PO/CO_2 and CHO/CO_2 monomers, their application to terpolymerization is not documented well in literature. This study of Co-Zn DMC catalysts for terpolymerization provides a fundamental understanding of the behaviour of DMC catalysts for polycarbonate synthesis in different reaction media to assist a rational modification of their critical properties towards the design of highly efficient DMC catalysts.

5.7. References

[1] J. Xu, E. Feng, J. Song, J. Appl. Polym. Sci. 131 (2014) 39822-39838.

[2] H.C. Stevens, US Patent No. 3,248,415 (1966).

[3] G.A. Luinstra, Polym. Rev. 48 (2008) 192-219.

[4] G.W. Coates, D.R. Moore, Angew. Chem. Intd. Ed. 43 (2004) 6618-6639.

[5] X.B. Lu, D.J. Darensbourg, Chem. Soc. Rev. 41 (2012) 1462-1484.

[6] M.R. Kember, A. Buchard, C.K. Williams, Chem. Commun. 47 (2011) 141-163.

[7] P.P. Pescarmona, M. Taherimehr, Catal. Sci. Technol. 2 (2012) 2169-2187.

[8] D. Darensbourg, S.J. Wilson, Green Chem. 14 (2012) 2665-2671.

[9] E.K. Noh, S.J. Na, S. Sujith, S.W. Kim, B.Y. Lee, J. Am. Chem. Soc. 129 (2007) 8082-8083.

[10] M. Ree, J.Y. Bae, J.H. Jung, T.J. Shin, J. Polym. Sci. Part A: Polym Chem. 37 (1999) 1863-1876.

[11] B.L. Khac, W. Chester, US Patent No. 5,536,883 (1996).

[12] X.H. Zhang, Z.J. Hua, S. Chen, F. Liu, X.K. Sun, G.R. Qi, Appl. Catal. A: Gen. 325 (2007) 91-98.

[13] J. Langanke, A. Wolf, J. Hofmann, K. Böhm, M.A. Subhani, T.E. Müller, W. Leitner, C. Gürtler, Green Chem. 16 (2014) 1865-1870.

[14] N.V.D. Assen, A. Bardow, Green Chem. 16 (2014) 3272-3280.

[15] B.L. Khac, W. Chester, US Patent No. 5,589,431 (1996).

[16] PU Magazine 10 (2013) 236-240.

[17] X.H. Zhang, R.J. Wei, X.K. Sun, J.F. Zhang, B.Y. Du, Z.Q. Fan, G.R. Qi , Polymer 52 (2011) 5494-5502.

[18] M.H. Chisholm, D.N. Llobet, Z. Zhou, Macromolecules 35 (2002) 6494-6504.

[19] L. Shi, X.B. Lu, R. Zhang, X.J. Peng, C.Q. Zhang, J.F. Li, X.M. Peng, Macromolecules 39 (2006) 5679-5685.

[20] H. Li, Y. Niu, Polym. J. 43 (2011) 121-125.

[21] W.M. Ren, X. Zhang, Y. Liu, J.F. Li, H. Wang, X.B. Lu, Macromolecules 43 (2010) 1396-1402.

[22] L. Lu, K. Huang, J. Polym. Sci. Part A: Polym. Chem. 43 (2005) 2468-2475.

[23] P.F. Song, M. Xiao, F.G. Du, S.J. Wang, L.Q. Gan, G.Q. Liu, Y.Z. Meng, J. Appl. Polym. Sci. 109 (2008) 4121-4129.

[24] X.K. Sun, X.H. Zhang, S. Chen, B.Y. Du, Q. Wang, Z.Q. Fan, G.R. Qi, Polymer 51 (2010) 5719-5725.

[25] D.A. Darensbourg, M.W. Holtcamp, Macromolecules (1995) 28 7577-7579.

Chapter - 6

Summary and Conclusions

In recent years, the cost of petroleum based polymers has gone up sharply as a result of surge in crude oil prices (which appear to remain at a historically high level for some time to come). Biodegradable polymers have emerged as a new field of immense research interest in both academia and industry. Although biodegradable polymers have been started to produce in commercial scale only for a decade now, they have already found huge reception in different areas such as food packaging, bags and sacks, loose-fill packaging, agricultural film and as many niche market products. There is a growing trend for brand owners and retailers to utilize the potential marketing benefits of "green" or "sustainable" packaging as consumers become more and more concerned about the development of sustainable technologies, reduction in CO_2 emissions and conservation of the earth's fossil resources. The use of efficient and selective catalysts for the synthesis of biodegradable polymers is vital for their sustainable growth in polymer industry. A variety of homogeneous catalysts have found dominant role for their synthesis. Although heterogeneous catalysts are inferior in activity and selectivity compared to homogeneous catalysts, some promising results and commercialization have started to emerge. Application of solid catalysts in polymerization has advantages of unproblematic handling, effortless separation, less moisture sensitivity and reduced corrosive behaviour. But an in depth knowledge of the mechanism of polymerization would be complicated to visualize due to poorly defined active sites. However, this issue can be solved to a great extent by the extensive characterization of catalysts through various physicochemical and spectroscopic characterization techniques. Comprehensive structural analysis of the catalysts could help suggesting structure-activity correlations and facilitate a rational modification of their critical structural features for improved activities. The work presented in this thesis has successfully executed this concept for the synthesis of two families of aliphatic biodegradable polymers viz., hyperbranched polyesters and polycarbonates over industrially well known DMC catalysts.

Chapter 1 of the thesis presented a general introduction to biodegradable polymers, their degradation mechanism and their synthesis from renewable monomers. The chapter also introduced hyperbranched polymers, a brief history of them, their synthetic methodology, conventional catalysts for their synthesis and their applications in various fields. It discussed CO_2 utilization and its efficient fixation in polymers through copolymerization with epoxides. A brief history of aliphatic polycarbonates, catalysts employed in their synthesis, their physical and thermal properties and applications were also included. Discussion on DMC catalysts, their historical structural evolution and diverse applications was presented. Finally, the scope and objective of the work were discussed.

Fe-Zn and Co-Zn DMC catalysts were prepared in the presence of t-BuOH (complexing agent) and PEG (co-complexing agent). Apart from changing complexing agent (from t-BuOH to methanol and glycerol) and co-complexing agent (to PEG of varying molecular weight) the synthesis conditions were also modified by varying the mode of addition of precursor solutions. A detailed methodology for their synthesis and the experimental techniques adopted for their characterization are provided in **Chapter 2**. This chapter also discussed the details of reaction procedure, purification of product polymer and then its characterization methods. The principles of characterization techniques used were briefly discussed.

Chapter 3 reported the synthesis of aliphatic hyperbranched polyesters from renewable monomers - glycerol and diacids (succinic and adipic acid) over Fe-Zn DMC catalysts. Hyperbranched polymers are randomly branched polymeric architectures showing properties similar to dendrimers. Their attractive features like highly branched topological structure, adequate spatial cavities, numerous terminal functional groups and convenient synthetic procedures distinguish them from the available polymers such as linear, branched, and cross-linked polymers. They exhibit unique advantages in biological and biomedical systems and find potential applications such as coatings, resins, polymer additives and cross-linkers, nanoreactors and nanocapsules, multifunctional platforms, etc. Currently, they are synthesized using homogeneous catalysts. Taking advantages of heterogeneous catalysts, a Fe-Zn DMC catalyst was used in this chapter for their synthesis, for the first time. Fe-Zn DMC with various compositions were synthesized by changing the complexing (t-BuOH, MeOH and glycerol) and co-complexing agents (PEG of M_n = 300, 600, 1500, 4000) and by varying the mode of addition of reagent solutions. Activity studies pointed out a direct relationship between total acidity of the catalysts with isolated yield of the polymer and its degree of branching (DB). More precisely, stronger acid sites were found essential for higher conversions. However, acidity alone was not the parameter that determined the isolated yield and DB of the polymer, the textural properties of the catalyst especially the micro/mesopores and hydrophobicity of the catalyst surface were also essential in controlling the gelation phenomenon and maintaining the activity. Control on gelation is crucial in polymerization of type A_2 + B_3 to yield high DB at higher conversions. Structure-activity correlations of Fe-Zn DMC catalysts revealed that there are three essential structural features that cannot be avoided while explaining their high activity during polyesterification. They are Lewis acidity to initiate the polymerization, micro/mesoporous architecture to control the gelation by diverting the reaction mechanism from A_2 + B_3 to an *in situ* AB_2 type, and hydrophobicity of

surface to maintain the activity of the catalyst from water deactivation. Studies showed hyperbranched polyesters with DB as high as 90 mol% can be prepared on these catalysts at high conversions without gelation.

Chapter 4 investigated the atom-efficient chemical transformation of green house CO_2 to environmentally adaptable and biodegradable polymeric materials through copolymerization with an epoxide (cyclohexene oxide; CHO) over Co-Zn DMC catalysts. CO_2 is abundant and renewable. Although CHO is now petroleum derived, a new pathway for CHO from cyclohexadiene (a by-product of oleochemical metathesis reaction) has been realized and transforms it into a renewable feedstock. DMC is known to catalyze the copolymerization. However, a detailed understanding of the critical features of the catalyst that control the activity, selectivity and induction period is not known. Co-Zn DMC catalysts of the present study were prepared in the presence of complexing (t-BuOH) and co-complexing agent (PEG- 4000). Two different synthesis procedures and their modification through changing the mode of addition of reagents and avoiding the co-complexing agent were employed to produce chemically and structurally different Co-Zn DMC catalysts. XRD of the catalysts indicated that they had cubic, monoclinic and rhombohedral crystal structures depending on the synthesis procedure. Activity studies displayed good productivity and selectivity for the catalyst having monoclinic/rhombohedral structure. This catalyst was prepared without using a co-complexing agent. Co-Zn DMC possessing this structure had large amount of stronger acid sites. Interestingly, it did not show induction period for the activation of CO_2 and epoxide and to co-condense them. EDX analysis of this catalyst disclosed an excess amount of K^+ and Cl^- in its structure. CO_2 adsorption studies on DMC catalysts pointed out that higher the host-guest interaction, higher would be the catalytic activity and lower would be the induction period. Chloride ion in the catalyst structure improved the Lewis acidity and thereby improved the host-guest interaction and reduced the induction period. Structure-activity correlations concluded that Co-Zn DMC with low crystallinity, lower crystal symmetry, higher amount of strong acid sites, lower amount of complexing agent and dispersed Cl^- ions are instantly active in copolymerization of CO_2 and CHO. Polycarbonates with CO_2 incorporation as high as 86 mol%, M_w of 20900 and PDI of 1.8 were prepared at complete conversion of CHO.

Chapter 5 presented the application of the above set of Co-Zn DMC catalysts for the copolymerization of CO_2 with a structurally different and more challenging epoxide, propylene oxide (PO) and the terpolymerization of CHO, PO and CO_2. Although, the PO monomer is petroleum derived, it can also be synthesized from glycerol in a sustainable way

to make it renewable. The copolymerization is more challenging due to the homopolymerization of PO and formation of undesired cyclic carbonate (competing parallel reactions). Activity studies have shown that unlike CHO/CO_2 copolymerization, the most active catalyst for PO/CO_2 copolymerization is the one possessing good crystallinity, high crystal symmetry (cubic phase), higher acidity, lower amount of alkali ions and lesser amount of complexing agent in its composition. Catalyst with these properties was more selective towards polycarbonates (M_w = 21100, PDI = 3.60) than cyclic carbonate. Structure-activity correlations concluded that the properties of the catalyst for high activity and selectivity depend upon the monomers (CHO and PO) even though the type of polymerization is the same.

Later sections of Chapter 5 discussed the extension of these Co-Zn DMC catalysts for the terpolymerization of PO, CHO and CO_2. Terpolymerization represents one of the ways to improve the thermal and physical properties of PPC and PCHC polymers. However, it is more challenging owing to the high reactivity of PO and high coordinative nature of CHO which makes difficult to control the composition of the individual PPC and PCHC units in the terpolymer. Activity studies have shown that each DMC catalyst behaved differently towards the terpolymerization as they produced different polymer architectures such as block copolymers, mixture of block and terpolymers and alternating terpolymers. The most efficient catalyst for producing an alternating terpolymer was the one whose properties were similar to that of the CHO/CO_2 copolymerization catalyst (M_w = 22700, PDI = 2.97, T_g = 55 ^oC). The catalyst showed a good control on the composition of PPC and PCHC units in the terpolymer with respect to the molar ratio of PO and CHO taken. This catalyst showed no induction period in the terpolymerization reaction. The catalyst which was highly active and selective in PO/CO_2 copolymerization was also active even in the terpolymerization reaction, but it showed an induction period of 2 h and has less control on PPC and PCHC units in the terpolymer. Terpolymer produced by this catalyst contained more PPC units than PCHC units (M_w = 46900, PDI = 4.89, T_g = 58.2 °C).

By and large this thesis reports the structure-activity correlations in DMC catalyzed synthesis of two families of biodegradable polymers viz., 1) Fe-Zn DMC catalyzed hyperbranched polyesters (from glycerol and diacids) and 2) Co-Zn DMC catalyzed copolymerization of CO_2 and PO/CHO. Critical features of DMC catalysts for their high activity/selectivity towards each polymerization were confirmed through detailed characterization. This study advances the knowledge on DMC catalyzed polymerizations and contributes to the area of green and sustainable chemistry.

List of Publications

1. Novel Application of a Fe-Zn Double- Metal Cyanide Catalyst in the Synthesis of Biodegradable, Hyperbranched Polymers
   Joby Sebastian and D. Srinivas
   Chem. Comm. 47 (2011) 10449-10451.

2. Influence of Method of Preparation of Solid, Double- Metal Cyanide Complexes on their Catalytic Activity for Synthesis of Hyperbranched Polymers
   Joby Sebastian and D. Srinivas
   Appl. Catal. A: Gen. 464 (2013) 51-60.

3. Solid, Double- Metal Cyanide Catalysts for the Synthesis of Hyperbranched Polyesters and Aliphatic Polycarbonates
   Joby Sebastian and D. Srinivas
   J. Chem. Sci. 126 (2014) 499-509.

4. Effects of Method of Preparation on Catalytic Activity of Co-Zn Double- Metal Cyanide Catalysts for Copolymerization of CO_2 and Epoxide
   Joby Sebastian and D. Srinivas
   Appl. Catal. A: Gen. 482 (2014) 300-308.

5. Structure- Induced Catalytic Activity of Co-Zn Double- Metal Cyanide Complexes for Terpolymerization of Propylene Oxide, Cyclohexene Oxide and CO_2
   Joby Sebastian and D. Srinivas
   RSC Adv. 5 (2015) 18196-18203.

Patent

1. Process for Preparing Hyperbranched Polyesters.
   Darbha Srinivas and **Joby Sebastian**
   US 2013/0331542 A1,
   CN103476824A,
   EP2678370A1,
   WO2012114357A1,
   WO2012114357A8.